The Institute of Paper Science and Technology

Atlanta, Georgia

Doctoral Dissertation Reprint

FIBER-FIBER BOND STRENGTH: A STUDY OF A LINEAR ELASTIC MODEL STRUCTURE

A thesis submitted by

Alan F. Button

B.S. 1967, The Pennsylvania State University

M.S. 1972, The Pennsylvania State University

M.S. 1975, Lawrence University

in partial fulfillment of the requirements
of The Institute of Paper Chemistry
for the degree of Doctor of Philosophy
from Lawrence University,
Appleton, Wisconsin

June, 1979

TABLE OF CONTENTS

ABSTRACT

Fiber-fiber wood bond strength has been treated in the paper industry as being independent of the geometrical and mechanical properties of the bonded structure. In this research, the fiber-fiber bond is considered to be not only the bonded interface region usually considered, but also the fiber segments extending from that interface. In addition, the failure of the fiber-fiber bond is examined in terms of continuum fracture mechanics theory.

An experimental program was developed in which the relation between structural and material parameters and fiber-fiber bond behavior was examined. Rectangular cross section cellophane fibers, bonded in a single lap joint configuration, were employed to study the effects of fiber width, fiber thickness, fiber axial modulus, and bond length on bond strength (failure load/bond area) in symmetric and asymmetric bonded structures.

A linear elastic theoretical model of the experimental structures was developed using a finite element structural analysis program (SAP IV) and continuum fracture mechanics theory.

The combined experimental and theoretical results provided clear evidence that the strength of the experimental structures was dependent on a variety of parameters. Bond length was found to have a strong influence on bond shear strength. As bond length increased bond shear strength decreased. Increased fiber thickness decreased the nominal axial stress at failure (the failure load/fiber cross-sectional area). Increased fiber axial modulus resulted in an increase in the nominal axial stress at failure. Asymmetries in dimensions or in modulus produced decreased bond shear strength. The fracture toughness of the cellophane fiber lap joint interface was estimated from the experimental data to be 5466/erg/cm^2.

The theoretical model predicted, using the estimated fracture toughness, the strength of all cellophane lap joint configurations to within ± 30%. The ratio of the experimental nominal axial stress at failure results to the model predictions had an average value of 1.02 and a coefficient of variation of 13.2%.

It was concluded that the experimental structures failed in a manner consistent with linear elastic fracture mechanics. Some preliminary experimental evidence was found for the applicability of fracture mechanics theory to the failure of wood fiber lap joints.

INTRODUCTION AND OBJECTIVES

It is quite apparent that fiber-fiber bond behavior is only partially understood. Virtually every researcher investigating the interrelations of paper structure and mechanical properties has been limited to extreme case assumptions because quantitative information about fiber bonds is inadequate. Van den Akker[1] assumed rigid connections at the bonds. Perkins[2] developed a theory and examined it at two extremes (totally flexible or totally rigid bonds) because there was no fiber bond modulus information. Dodson,[3] in his survey of paper mechanics, provided this assessment:

> "At the moment (1974), we have neither a theory of one fibre-to-fibre bond in terms of the molecular mechanics of hydrogen bridges nor a deep enough theory of paper in terms of fibre and bond mechanics."

This research differs in two principal ways from previous fiber-fiber bond model investigations. First, all previous experimental studies have focused exclusively on the interfacial surface and the apparent strength of the bonds across that interface. In this thesis we consider the fiber-fiber bond to consist of the bonded interface region and the fiber segments which extend from that interface. The fiber-fiber bond thus becomes a structural entity as shown in Fig. 1. Second, the previous investigators did not invoke failure theories to explain fiber-fiber bond strength. The sharp structural discontinuities evident in Fig. 1, in particular, and fiber-fiber bonds, in general, suggest that fracture mechanics theories may apply. Therefore, in this thesis, fiber-fiber bond failure is examined in terms of continuum fracture mechanics theory.

The fiber-fiber bond structure is considered analogous to an adhesive joint, where the fibers are self-bonding adherends. From studies of adhesive

joint behavior, two general categories of parameters, which determine joint strength, have emerged. The first group consists of adhesive related properties (i.e., adhesive stiffness, ability to bond to the adherends, and bond defects). A variety of structural parameters and their interaction with the adherends and adhesive form the second group. On this basis, the stress distribution in and around the interface region is likely to be complicated by factors (fiber dimensions and stress/strain properties, bond configuration, and mode of fiber loading) and have little direct connection to the intrinsic bonding capabilities of the fibers. It is this group of structural parameters that will be investigated in this research.

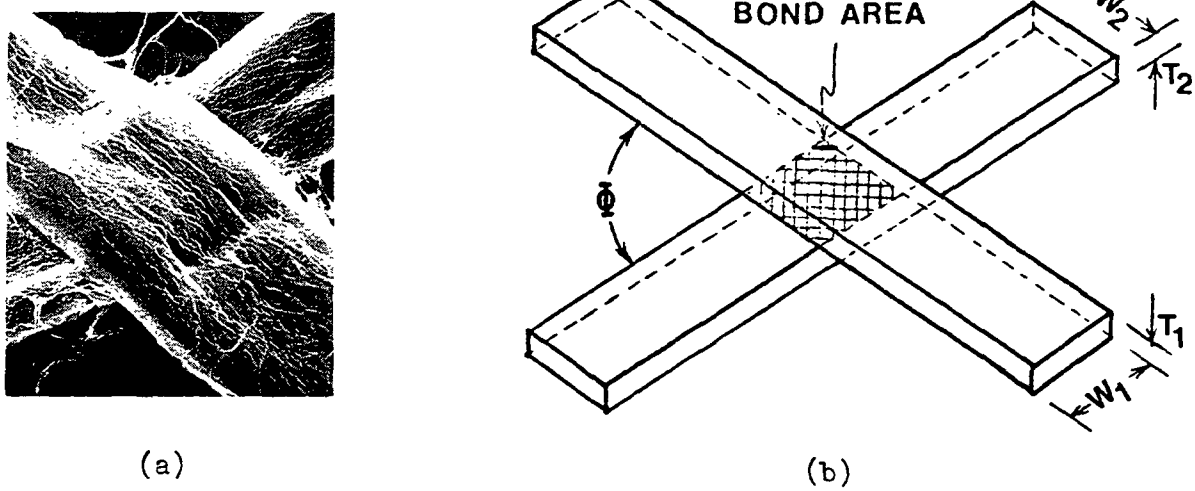

Figure 1. Representations of a fiber-fiber bond, where (a) is a scanning electron micrograph of two bonded wood fibers, and (b) is a schematic of the general bond structure.

Two thesis objectives were established. An experimental study of structural and material parameter effects on the strength of fiber-fiber bond model structures was the first objective. The second was to develop a theoretical

model to predict the deformations, stresses, and strength of these experimental structures.

The thesis is organized around these two objectives. Reviews of the pertinent fiber-fiber bond and adhesive joint literature precede the Experimental Program, which includes the results of structural and material parameter studies of a fiber-fiber bond model. The Theoretical Program contains the development of a linear elastic model of the experimental structures. Following the discussion of the general behavior and predictions of the model, the Theoretical Program concludes with a direct comparison between the experimental results and the model predictions.

LITERATURE REVIEW

A five-part literature review is presented, beginning with extensive coverage of fiber-fiber bonds in paper. The second part focuses exclusively on the results from investigations of model structures of the fiber-fiber bond. Adhesive joint behavior, with particular emphasis on the analysis of single lap joints, is reviewed in the third portion. The basic concepts of continuum fracture mechanics are outlined in the fourth part. A brief introduction to the finite element method concludes the review of the literature.

A broad view of the fiber-fiber bond literature provides a basis for viewing the succeeding literature and this research. The first part begins with a summary of the properties of wood fibers which leads into a discussion of the nature, formation and extent of the bonding between fibers. The results of the lone study of fiber-fiber bonds under load are reported. A discussion of the various approaches to the measurement of fiber-fiber bond strength and the interpretation of the bond strength results in light of fracture mechanics theory conclude the first section.

The second portion of the literature review is primarily a summary of the bond shear strengths obtained from studies of model structures of fiber-fiber bonds. The similarity of the models and the variability of the data are discussed. Several investigations in which only cellophane film was used are mentioned immediately before the bond deformation study is reviewed. A brief assessment of the inherent assumptions in these experimental models completes the second portion of the literature review.

A third part contains the adhesive joint literature presentation which is focused on experimental and theoretical studies of lap joint behavior (stresses

and strength). Included in the discussion is a brief summary of the types of adhesive joints and adhesive strength tests. Both continuum fracture mechanics theory and finite element stress analysis techniques have been used in investigations of adhesive joints. These analysis techniques are presented without immediate elaboration, because these two subjects are covered in the final two parts of this review.

In the fourth part, the basic concepts in the continuum approach to fracture begin with A. A. Griffith's classical work.[4] Irwin's[5] development of stress intensity factors and eventual demonstration of the equivalence of that approach to Griffith's energy criteria follow. The microscopic and molecular theories of fracture are not reviewed. Much of the literature in continuum theory is based on elasticity theory. This theory is developed in Appendix III specifically as it relates to an orthotropic elastic material.

The final portion of the literature review introduces the general concepts upon which finite elements are based. A brief summary of the different types of finite element models is included. The basic equations underlying the direct displacement method (the most widely used) are developed and presented in Appendix I. A brief discussion of the displacement functions assumed for various finite element formulations are also included in Appendix I.

FIBER-FIBER BONDS IN PAPER

In the context of this thesis fiber-fiber bonds are defined as consisting of both the bonded interfacial region and portions of fibers extending away from that interface to the points of loading. This definition casts fiber-fiber bonds as a structure potentially subject to the same analyses as any other

structure. It is important, therefore, to understand the nature of both the bonded interface and the fibers.

Fiber Properties

Wood pulp fibers are composed primarily of crystalline and noncrystalline cellulose. Cellulose chains are organized into microfibrils, which are inclined at some angle (fibril angle) to the fiber's longitudinal axis and embedded in a matrix of hemicelluloses and lignin. This cell wall architecture has been characterized as that of a helically wound laminated composite tube structure. Fiber mechanical properties are influenced primarily by the fibril angle and thickness of the S2 layer of the secondary wall. Beginning with Mark[6] in 1967, researchers have applied the theory for orthotropic elastic materials to the relationship between S2 fibril angle and fiber modulus. In later work, Mark and Gillis[7] concluded that the modulus was highly dependent on fibril angle at smaller angles (< 10°) and on the matrix material at larger angles (> 25°). By using a least-squares regression technique for fitting orthotropic elastic plate theory equations to experimental data, Page, et al.[8] were able to calculate the elastic constants for the fiber wall. A high degree of anisotropy was found; the modulus in the microfibril direction was an order of magnitude larger than the transverse and shear moduli. Their results indicated that the axial modulus of their undamaged fibers decreased from 7700 dynes/μm^2 to 1700 dynes/μm^2 as fibril angle increased from 0 to 50°.

Two fairly distinct morphological types of fibers are represented in the above range of fibril angles. Earlywood fibers have many more natural defects (pits and ray crossings) and larger fibril angles (30 to 60°) than latewood fibers (0 to 30°).[9] There are other differences, such as McMillen's[10] observation that loblolly pine latewood tracheids were longer (4.04 mm vs. 3.81 mm)

and narrower (33.4 μm vs. 46.0 μm), and had much thicker cell walls (9.78 μm vs. 4.58 μm) than earlywood tracheids. The variations among commercial wood fibers are much greater than indicated by this limited example. The interdependence of the above variables is, however, a general condition that hampers investigations of the impact that these morphological and mechanical parameters have on paper properties.

Fiber wall thickness, fibril angle, fiber strength and length are the morphology factors found to correlate most consistently with paper strength properties.[11-13] Fiber wall thickness[12,13] has shown negative and, fibril angle,[12] fiber length,[12] and fiber strength,[13] positive correlations with paper strength. Most explanations for these observed relationships center on changes in sheet structure and extent of bonding.

Nature of Interfiber Bonding

The present view of the molecular forces in fiber-fiber bonding was initiated with Huggins'[14] prediction that hydrogen bonding was the main interchain force in cellulosic polymers. According to Van den Akker,[15] the hydrogen-bonding concept has been best supported by the deuterium oxide/water exchange experiment of Corte and Schaschek.[16] Their research indicated that only 1.4% of all OH groups in their paper was involved in interfiber bonding. Nissan[17] has proposed a hydrogen-bonded solid theory, in which the intra- and interfiber hydrogen bonds are mainly responsible for the physical properties of paper. Observations by Robertson[18] on the interaction of various liquids with paper indicated that hydrogen bonding was not the exclusive bond type, since even non-polar hydrocarbons reduced paper strength. He estimated that Van der Waals' forces might account for 25% of the interfiber bonding.

Our concepts of fiber-fiber bond formation have been strongly influenced by Campbell's[19] view of the pressure generated by the receding water meniscus during paper consolidation and drying. This pressure is believed to aid fiber-fiber bond formation by promoting intimacy of contact between contiguous fibers. Van den Akker[15] has discussed the various structural factors that may influence the nature and strength of the bond formed. His conclusion that lateral fiber shrinkage may lead to residual stresses in the bond region was supported by the demonstration of Page and Tydeman[20] that fibers may develop wall micro-compression zones as a result of the lateral shrinkage of a fiber bonded to it. Van den Akker[15] suggested that bonds formed between fibers with intact cell wall layers might be different from those fibers with fibrillated surfaces. The extent of actual molecular contact in any bond area is unknown, but studies using the electron microscope indicate that separations between bonded fibers are less than 20 Å.[21]

A wide variety of techniques have been employed for determining the extent of bonding between fibers in paper. Electrical conductivities,[22] light scattering,[23,24] gas absorption,[24] and direct microscopic examination with plane polarized light,[25] or electrons[26] have all been used. The first methods provide average bond areas for the entire sample while the microscopic examinations yield distributions of bonds, plus total contact area for the scanning electron microscopy method. The gas adsorption technique should allow the most complete measurement of the unbonded surface area, except that the use of BET gas adsorption equations may not be appropriate for cellulosic surfaces.[27]

Using the direct microscopic examination technique with vertical plane polarized light, Page, et al.[28] studied the effects of beating and drying tension on the size and frequency of bonds in handsheets made from bleached spruce

sulfite pulp. The most pertinent among their many observations were: (1) beating increased average bond size (643 to 956 μm^2) and frequency of bonding (12.3 to 16.9/mm), and (2) multipoint bonding was reduced by beating. The average projected interbond distance, which was not large even for the unbeaten state (34.0 μm), decreased to 13.2 μm with beating. In fact, very little totally free fiber span existed along a fiber. These measurements showed quite clearly that bonds constituted a large portion of the entire paper network.

Bond Behavior Under Load

Very little is known about fiber-fiber bond behavior under load. Van den Akker[15] speculated that most bond failures would result from shear forces, primarily from axial tension loading, and also from in-the-plane torsional loading. He predicted that stress intensifications would exist along the bond perimeter. Only Page, et al.[29] have made direct observations of fiber-fiber bond behavior under load. In an extension of the previously cited work,[28] they concluded that: (1) few bonds failed completely (7 to 17%), (2) those bonds that did fail completely were smaller (510 vs. 930 μm^2), (3) stressing in the direction of unrestrained drying broke 3 times as much bond area as stretching in the direction of restrained drying, (4) 70% of the bonds in the unrestrained direction and only 33% of the bonds in the restrained direction showed some failure, and (5) the energy (no value given) required to break a unit bond area was several orders of magnitude less than a typical Nordman's bonding strength value.[30]

Bond Strength Measurements

Nordman, et al.[30] developed their technique from the observation that the light-scattering properties of paper changed as paper was strained beyond the initial linear portion of the load/elongation curve. Fiber-fiber bond breakage was believed to cause the change in scattering coefficient and, therefore, any

energy consumed in this portion of the curve might correlate with the bonding strength of paper. The energy consumed per unit change in the scattering coefficient (ergs/cm^2) was called the bonding strength value for a given pulp.[30] At first thought to depend only on a pulp type, the bonding strength was shown by Karna to depend on both beating and wet pressing.[31] The high bonding strength values (1.4 to 7.9 x 10^5 ergs/cm^2) for this technique produced considerable discussion and criticism.[32] When gas adsorption techniques were substituted for the optical method, bonding strength values dropped nearly two orders of magnitude (0.8 to 2.2 x 10^4 ergs/cm^2).[33] Even with this alteration, Nordman's technique has found acceptance only as a relative measure mainly because the bonding strength values exceed, by several orders of magnitude, the surface free energy of cellulose (44 ergs/cm^2).

From a fracture mechanics viewpoint, this discrepancy is to be expected because the energy required to break the interfiber bonds typically must be supplied through an energy-consuming structure. A measure of bond strength thus becomes dependent on both the bonds across the interface and the material through which the energy must be transmitted.[34]

Smith and Graminski proposed another energy method based on the energy to break individual bonds in a two-dimensional network.[35] From plots of cumulative work vs. number of bonds broken, they concluded that beating softwood pulps considerably increased the energy required to break fiber-fiber bonds (from 0.85 and 0.88 erg to 7.3 and 6.8 ergs). If one assumes Page's average bond area (930 μm^2) for beaten spruce pulp,[28] a rather high bonding strength value of 7.9 x 10^5 ergs/cm^2 is obtained for their northern softwood. This high value may be attributable to the observed large torsional deformations of the network fibers.[35]

Several maximum load approaches to bond strength measurements have been employed. The z-direction tensile strength test has been used as an indicator of changes in total bond strength. Wink and Van Eperen[36] found this method depended on basis weight, but they showed, at constant basis weight, that strength increased with increasing wet pressure and decreasing scattering coefficient. Bond strength values cannot be calculated because the bond area broken is unknown. In addition, high z-direction stressing is not characteristic of most paper in-use stresses.

Page[37] developed a semiempirical equation which allows a bond shear strength value to be calculated from fiber strength and dimensions, paper strength, and relative bonded area information. This equation was based on a force balance analysis in which the number of fibers breaking in the fracture zone is controlled by the stress levels developed in the fibers, the fiber stress level being dependent on the fiber length, bond area, and bond shear strength of those bonds. Page's tensile strength equation

$$1/T_b = (9/8Z) + (12\,\overline{A}_x \rho_f\, \underline{g})/[\overline{\tau}\,\overline{P}\,\overline{L}_f\,(RBA)], \qquad (1)$$

where T_b = tensile breaking length, km

Z = zero-span tensile breaking length, km

$\overline{A}_x$ = average fiber cross-sectional area, cm^2

ρ_f = fiber material density, g/cm^3

$\underline{g}$ = gravitational acceleration, cm/sec^2

$\overline{\tau}$ = bond shear strength, $dynes/cm^2$

$\overline{P}$ = average fiber perimeter, cm

$\overline{L}_f$ = average fiber length, cm

RBA = relative bonded area

embraces the concept of a constant bond shear strength (i.e., independent of the bond structure and fiber stress/strain properties). Jones[38] used Page's equation[37] to calculate the bond shear strength for three unbleached kraft pulps. These calculated bond shear strength values (0.71 to 0.93 dyne/μm^2) are comparable to the results obtained from fiber-fiber bond model studies. The difficulties of studying fiber-fiber bonds in paper have prompted researchers to investigate model structures.

FIBER-FIBER BONDS - MODEL STRUCTURE STUDIES

Bond Strength

McIntosh and Leopold,[39] in 1961, reported the results of the first individual fiber-fiber bond strength tests. Nine similar studies of the strength of fiber-fiber bond model structures have now been published. All of the models are 90° crossing angle configurations in which one fiber is axially loaded until its bond to the crossing fiber, shive, or cellophane strip fails. Bond areas have varied from 320 to over 100,000 μm^2 and failure loads from less than 0.1 to over 21 g. Average bond shear strengths, the maximum load per unit bond area (either geometric projection or optical contact), varied from 0.03 to 0.81 dyne/μm^2 with the highest single value reported by Thorpe, et al.[40] as 1.33 dynes/μm^2 for a thermomechanical fiber to shive bond formed at 210°C. Many structures fail before testing and those that survive typically show large coefficients of variation (20 to over 100%). Most of this variation has been attributed to: (1) a natural large variation in fiber intrinsic bonding capabilities (both between and along fibers), (2) variation in the preparation and testing procedures, and (3) an inability to measure the areas of true bonding between fibers.

McIntosh and Leopold[39] bonded loblolly pine tracheids (pulped by a per-acetic acid holocellulose procedure) to a cellophane film, wood pulp shives and fibers. They reported an increase in average bond shear strength for shives vs. cellophane, and fibers vs. shives. Regardless of substrate, latewood fibers produced bond shear strengths 2 to 3 times that of earlywood fibers.

The normal consolidation forces of handsheet making were used by Mayhood, et al.[41] to form bonds between pairs of ribbonlike (probably earlywood) fibers of three northern softwood pulps. Similar bond shear strengths were obtained for all three pulps with the exception of the highly beaten bleached pulp, which was slightly higher. Their uncontrolled humidity conditions make the results difficult to interpret.

In 1963, McIntosh[42] again noted the bond shear strength difference between earlywood (0.21 dyne/μm^2) and latewood fibers (0.62 dyne/μm^2), this time for various pulp yields from a kraft delignification process. The bond shear strength of the latewood fibers decreased more rapidly with decreasing yield than did the earlywood fibers. Decreasing hemicellulose content may have been responsible for the decline in bonding strength.[42] Schniewind, et al.,[43] finding the same higher bond shear strength for white fir latewood fibers, reported intermediate strengths for combinations of earlywood fibers bonded to latewood fibers (all were prepared by a nitric acid holocellulose procedure). Two factors, an increase in apparent bonding pressure (25 to 250 psi) and storage of the pulp, appeared to reduce bond shear strengths.[43] One notes that the average bond areas for the stored pulp fiber tests were larger, indicating either alteration in measurement techniques or inclusion of more earlywood fibers (either one could contribute to the decreased bond shear strength). From the knowledge that latewood fiber cross sections are roughly 50% larger than

those of earlywood fibers,[10] and with the maximum load data of Schniewind, et al.,[43] it is apparent that even though latewood fiber bonds are stronger per unit bond area, the axial tensile stress in earlywood fiber free spans was 2 to 3 times higher than latewood fibers. This may provide some clue to the as yet unexplained difference in earlywood and latewood bond strength.

Russell, et al.[44] presented evidence that the addition of commercial wet strength resins substantially increased the strength of their wet fiber-fiber bonds. In response to questions concerning the previous use of their technique,[41] Russell, et al.[44] indicated that very little peeling stress (compared to the supposed shear stress) occurred, in that the bonds did not rotate out of an 8 μm depth of focus field.

In a series of four articles, Mohlin presents a slightly modified technique for determining interfiber bond shear strength,[45] Hartler and Mohlin examine pulping effects,[46] and Mohlin reports studies of beating and drying effects[47] and chemical modification[48] on fiber bond shear strength. Her technique modifications mainly consist of: (1) substituting a 0.5-mm wide strip of never-dried unoriented cellulose film for the crossing cellophane (commercial) strip, shive, or fiber, (2) obtaining load/elongation curves instead of just maximum loads, and (3) using cumulative loads resulting from partial bond failures rather than the highest single load for calculating bond shear strengths. She reported, contrary to previous findings,[39,42,43] no difference between the bond shear strengths of earlywood and latewood fibers of a kraft pulp (three different yields) and bisulfite pulp.[45] No significant correlation ($r = -0.14$) was found between bond length and bond shear strength for 89 earlywood and latewood fiber-fiber bonds. As a result, bond strengths were reported as an average of all tests within a pulp. To evaluate the suitability of the cellulose substrate, a

comparison was made between the bond shear strength of: (1) rayon fibers on cellulose strip (0.34 dyne/μm^2), (2) sulfite fiber to cellulose strip (0.412 dyne/μm^2), and (3) sulfite fiber to sulfite fiber (0.598 dyne/μm^2).[45] Typical coefficients of variation were 30-40% for wood fiber and 20-25% for rayon fiber tests. In spite of the obvious bonding difference of the substrates and even though the cellulose strip shrank 20% laterally (resulting in numerous micro-compressions in earlywood fiber walls), it was concluded that the ease of handling, the apparent consistency of cellulose film bonding capabilities, and the rigid glue connection obtained for testing were worth the compromise.[45]

Hartler and Mohlin[46] found that the maximum bond shear strength occurred at lignin contents of 7% for unbleached kraft, 10-12% for unbleached sulfite, and 9-12% for these pulps bleached. They suggested that kraft lignins on the fiber surface are detrimental to bond shear strength, while the sulfonic acid groups of sulfite lignins are beneficial. The lower bond shear strengths of the lower yields were attributed to decreasing hemicellulose content.[46]

Beating and drying were observed by Mohlin[47] to decrease the bond shear strength of kraft fibers. Kraft earlywood fiber bond shear strengths showed larger reductions from drying than did latewood fibers. Beating increased the bond shear strength of 54.3% yield sulfite fibers, but decreased bond shear strength for the 57.6% yield fibers.[47]

Hydroxyethylation of rayon fibers increased bond shear strength with little effect on fiber strength.[48] Mohlin[48] observed that bond shear strength increased from 0.342 dyne/μm^2 for no C6 substitution (MS = 0.0) to 0.544 dyne/μm^2 for MS = 0.054. Oxidation of the fiber surface produced an increase in bond shear strength for the low level treatments, but extended oxidation reduced bond shear strength and caused rapid decline in fiber strength.[48]

All of the preceding model structure studies have been concerned solely with bond shear strength. Thorpe, et al.,[40] while being mainly interested in fiber-fiber bond deformations and stiffnesses, acquired data on the bond shear strength of loblolly pine chlorite, holocellulose and 160°C thermomechanical Scotch pine fibers bonded to shives. They reported an average bond shear strength of: (1) 0.400 dyne/μm^2 for holocellulose fibers bonded at room temperature, (2) 0.284 dyne/μm^2 for thermomechanical fibers bonded at 110°C, and (3) 0.812 dyne/μm^2 for thermomechanical fibers bonded at 210°C. They noted that from the theory of elasticity the stress distributions in the bond area should not be uniform with respect to bond length, and therefore changes in bond length should have little influence on failure load.[40]

Several other researchers have used model structures to investigate the bonding strength of cellulose films. Goring[49] employed 90° crossing-angle lap joints (2.0 mm wide x 0.254 mm thick) made from deacetylated cellulose acetate film to study the effects of corona discharge on the bond shear strength of a cellulosic material. A substantially increased bond shear strength resulted from the corona discharge treatment (0.74 vs. 0.11 dyne/μm^2 for untreated).

In an investigation of the mechanism of wet-strength development in paper, Bates[50] wet bonded strips of cellophane dialysis tubing wall (unplasticized cellulose film, 1 inch wide x 0.004 inch thick) with a commercial polyamine epichlorohydrin (PAE) wet-strength resin. An increase in the wet bond strength of the lap shear joint to 0.40 dyne/μm^2 was obtained for curing at 105°C for 24 hours. He observed that the bond areas needed to be controlled very close to 0.5 mm^2 because an increase in bond area decreased bond shear strength.[50]

Janes[51] used a butt joint model to study the adhesion of the cellulose-starch-cellulose system. He concluded that the amylose and amylopectin layer between two layers of cellophane film increased the bond strength (1.18 to 3.04 dynes/μm^2) by a bridging mechanism between the rough film surfaces. Cellophane film surface abrasion and increased bonding pressure (up to about 2000 psi) increased the bond strength for those bonded with water only.[51]

Bond Deformation

Thorpe, et al.[40] have published the only study of fiber-fiber bond model deformations under load. By attaching Xerox toner particles to the surface of fiber-shive bonded structures, they were able to measure spring force constants of the bond overlap region. They found the thermomechanical fibers, bonded at 210°C, had a bond spring force constant of 6.9 kg/mm compared to 3.6 kg/mm for both holocellulose and thermomechanical fibers bonded at 110°C.[40] Average strains in the free fiber spans ranged from 0.60 to 1.49%, while strains in the bonded overlap region extended from 0.36 to 0.56%.

From scanning electron micrographs of the failure zones, they concluded the holocellulose fiber-shive bond failures tended to be largely interfacial, while the thermomechanical bonds failed at various distances from the interface. Those thermomechanical fibers bonded at 110°C showed failures mainly in the middle lamella or S1 regions, but the 210°C bonds failed primarily through shearing across the entire cell-wall thickness. A thermal flow of lignin and hemicelluloses to form a continuum between the fiber and shive was suggested by the cohesiveness of the 210°C bonds.[40]

In an attempt to understand the experimentally observed variations in bond stiffnesses and the bond shear strengths, Thorpe, et al.[40] presented the first

theoretical analysis of the stresses and displacements throughout the bond area. A linear elastic planar model with perfect bonding across the fiber-shive interface was assumed. No evaluation of this suggested model was presented.[40]

An inherent assumption in the bond shear strength measurements of all the fiber-fiber bond model studies was an independence of that measurement for bond area (bond length). Only if the model has an appreciable viscous or plastic character will that be a valid assumption. Although concern over this inherent assumption has been expressed[15,40,52] for at least 20 years, the theoretical model of Thorpe, et al.[40] was the first model in which a linear elastic material was assumed.

In studies of the behavior of adhesive joints (which are, in many features, analogous to the bond models) both viscous and linear elastic adhesives have been assumed. Brief reviews of these experimental studies and theoretical analyses follow.

BEHAVIOR AND ANALYSIS OF ADHESIVE JOINTS

Adhesive Joints and Adhesive Tests

An adhesive joint is formed from two separate phases. The adherends are bonded together through autohesion (self-bonding) or heterohesion, the interposing of a third phase, the adhesive. The number of adhesive joint configurations is virtually unlimited, but two basic types are: (1) the lap joints, where the adherends are usually striplike in shape and usually share overlap (bonded area) parallel to the major axis of the adherends, and (2) butt joints, where the adherends share a common bond area that is usually perpendicular to the major axis of the adherends. Lap joint adhesive layers are typically loaded in a shear mode, while the butt joint adhesive is loaded primarily

in tension. Several of the many forms of adhesive joints are illustrated in Fig. 2.

A basic tenet of adhesive testing has been that a test configuration, to be valid, should have a geometry similar to that during application.[53] Anderson, et al.,[54] in their recent book on adhesive bond analysis and testing, have classified adhesive tests into tensile, shear, peel, and fracture mechanics type tests. The first three test groups produce strength information for some standard adhesive joint and do not directly provide failure criteria upon which the adhesive in-use performance can be predicted. They point out that, in principle (with appropriate modifications), virtually any test configuration can yield fracture mechanics parameters which can be used to predict adhesive joint performance. Further information on adhesion is contained in Patrick's book on adhesion and adhesives.[55]

Bikerman[56] has long advocated the view that adhesive joints are composite structures whose mechanical properties (deformation and failure) can be described by applying the principles of analytical mechanics. Sharpe[57] suggested that the use of energy criteria with the detailed mechanics of the adhesive joint is probably far more productive in understanding joint response than uncritical use of an average failure stress.

The remaining two parts of this adhesive joint review focus primarily on analytical and fracture mechanics of single lap joints.

Analytical Mechanics Approach to Joint Behavior

Schonhorn, et al.[58] have studied the effects of symmetrical bonding defects on the bond shear strength of ASTM D1002-72 standard single lap shear test.

(a) Single Lap Joint

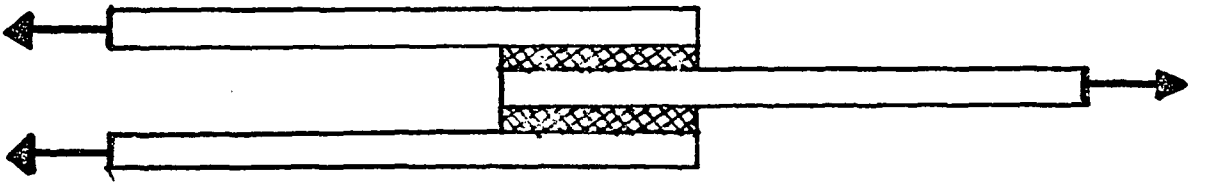

(b) Double Lap Joint

(c) Scarf Joint

(d) Butt Joint

Figure 2. Common forms of adhesive joints.

Aluminum adherends (25.4 mm wide x 1.62 mm thick x 127.0 mm long) were bonded with a ductile polyethylene adhesive over a 25.4 mm length rather than the recommended 12.7 mm. Through systematic elimination of various portions of the bond they found that the bond shear strength was independent of bond area, while the critical tensile stress decreased linearly with bond area. Failure was determined to occur by a general yielding in shear throughout the adhesive. From Goland and Reissner's theory[59] of stress in lap joints with low modulus adhesives, they calculated the peeling (normal to the bond plane) and shear (in the bond plane) stresses. Through application of von Mises' yield or failure criterion and limit analysis to the calculated stresses, they concluded that in ductile adhesives edge effects (stress concentrations at the edges) are not important.[58]

A companion study of a brittle (epoxy) adhesive, reported by Wang, et al.,[60] showed that bond shear strength was dependent on bond area. Since the strength of the adhesive joint remained constant, bond shear strength varied as the inverse of the total length of the bonded overlap. Adhesive joint strength was found to be linearly dependent on bonded width as long as symmetry with respect to loading was preserved. Goland and Reissner's theory[59] for relatively inflexible lap joints was employed to calculate the stress distributions. They noted two main differences from the ductile adhesive case: (1) tearing and shear stresses concentrated in a much smaller region near the bond edges, and (2) in the brittle adhesive the maximum peeling stress was much higher than the maximum shearing stress.[60] The strength of brittle adhesives is, therefore, believed to be controlled primarily by the narrow bonded area near the bond edges.[60]

A study of the creep behavior of structural adhesive joints by Allen and Shanahan[61] produced evidence that elastic stress concentrations in lap shear joints were ameliorated as creep progressed. An increasing bond shear strength with decreasing bond length and a slightly increased joint strength per unit width with increased joint width can be seen in the three adhesives investigated by Lewis, et al.[62]

The theoretical analysis of the single lap joint by Goland and Reissner[59] is frequently cited as the first analysis which remains largely acceptable today. Their theoretical approach was to assume geometrical and property symmetry in the lap joint and then treat it as if it were a cylindrically bent plate with a discontinuous thickness variation. The unjoined adherend ends were assumed to be simply supported and acted upon by tensile forces. Through strain energy minimization considerations they were able to select two ranges of conditions (i.e., a thin layer of a stiff adhesive or a very flexible adhesive) for which their treatment gave reasonable approximations of the stress distributions. Peeling and shear stresses in the stiff adhesive were found to be concentrated in a very small region near the joint ends, while these stresses were more widely distributed and less intense at the joint ends for the flexible adhesive.[59]

Goodier and Hsu[63] investigated the case of an elastic rod continuously bonded to an elastic plate. For a no out-of-plane bending assumption, they found intense shear stresses along the bond edge. Muki and Sternberg[64] examined a more generalized problem of overlapping sheets with a common bond. Differences in Poisson ratios between the two sheets led to the development of bond interior forces and increased bond edge forces.[64] An analytical mechanics approach to the problem of anisotropic adherends bonded by an isotropic adhesive

was formulated by Wah.[65] For composite type dissimilar adherends his calculations showed more intense stresses in the portion of the adhesive layer associated with the joint end of the lower modulus adherend.

Analyses of lap joints are commonly made with the assumption that the joint end is a flawless right angle. In practical constructions this is usually not the case. Westmann[66] conducted a theoretical investigation of the effects of adherend end taper angle on the nature of the stress field at the end of the overlap. He concluded that for included angles of less than 77° (tapered ends) the stress singularity (tendency for stress to become infinite) can be removed, thus increasing the strength of the adhesive joint.

Most of the preceding studies have used various analytical approaches to determine stress distributions in lap joints. This approach typically generates complex equations, and is limited, in practice, to simple problems. With the advent of large high speed digital computers, numerical techniques such as finite elements (discussed in the final portion of this review) and finite differences are being developed to allow solution of a host of increasingly complex problems in mechanics.

In 1971, Wooley and Carver[67] presented perhaps the first stress analysis of a single lap joint using a finite element technique. Maximum stress concentrations in the adhesive layer were calculated for a variety of adherend modulus/adhesive modulus and glue line thickness/adherend thickness ratios. Their calculations indicated that increased lap length would result in substantial reductions in stress concentrations. A limited, favorable comparison[67] was found with the analytical theory of Goland and Reissner.[59] As adhesive modulus was decreased, stress concentrations at a given bond thickness decreased. A

decrease in adhesive thickness increased stress concentration for modulus ratios greater than 1 (i.e., adherend > adhesive). A deficiency in their model results from stresses being calculated at changing distances from the joint end. This produced excessive reductions in stress concentrations as the lap length-to-thickness ratio increased. Excessive lap joint rotation would result from their choice of triangular end sections with single point loading.[67]

Adams and Peppiatt,[68] using a finite difference method, calculated transverse stresses resulting from Poisson ratio strains in adherends of a lap joint. They concluded that: (1) shear stress was more intense at the corners of the joint end, (2) corner sheet stresses remained constant for adherend width-to-thickness ratios (W/T) greater than 16, and (3) shear stresses were more intense when the two adherends were different (i.e., steel and aluminum). Pirvics[69] applied his finite difference program for two-dimensional stress analysis of general shapes to the lap joint configuration and obtained results qualitatively similar to the analytical solutions of Goland and Reissner.[59] Adams and Peppiatt[70] found similar agreement for their finite element model. They also investigated the stress distribution within an assumed triangular adhesive spew at the joint ends; showing that the principal stresses were very intense in the 45° spew apex region and that their calculations were consistent with fracture patterns for this geometry.

All of the preceding investigations have assumed some connection exists between stresses calculated and ultimate strength. Except for the instance of ductile failure, however, this connection may only be qualitative, allowing a ranking but no specific strength predictions. Following is a review of studies in which energy criteria for fracture have been incorporated.

Fracture Mechanics Approach to Joint Strength

Williams[71] discussed the essential similarity of cohesive specific fracture energy, γ_c, and the adhesive specific fracture energy, γ_a, from the continuum mechanics viewpoint. He demonstrated that Griffith's energy concept of fracture applies equally well to bulk phase (cohesive) fracture and interfacial (adhesive) fracture. Good[72] used the fracture mechanics approach to examine the relationship among the variables associated with the fracture of an adhering system. The most probable location for fracture was developed for various relative combinations of Young's moduli, fracture toughness, and strengths of the interface bonding. Among his conclusions were: (1) cracks are most likely to propagate in a weak interface region, (2) the probability of the propagating crack leaving the interface region is dependent on the relative bond strengths among the interface and the other contiguous materials, and (3) strong interface bonding tends to force cracks into the other phases.

A combination of energy criteria and analytical mechanics was used by DeVries, et al.[73] to analyze the fracture of the lap shear joint. Goland and Reissner's equations[59] were employed to obtain separate strain energies at failure for the bending and shearing modes of their experimental lap joints. These calculations showed that adhesive specific fracture energy (γ_a) increased with increasing lap length (a fact they attributed to the changes in the relative portions of shearing and tensile strains). They also noted that the observed decrease in bond shear strength with increasing lap length could only be predicted if one used a fracture mechanics type approach to failure.[73]

Fracture toughness, G_c, was calculated directly from experimental data on lap joint strength and compliance by Jemian and Ventrice.[74] Their data had considerable scatter, but they were able to eliminate many of the weaker bonds

because of obvious poor bond formation. A five-term expanded polynomial was then fitted to the experimental compliance (C) versus crack length (a) data. They were then able to calculate a reasonably constant fracture toughness (G_c = 2.07 x 10^5 to 2.49 x 10^5 ergs/cm^2) for their experimental epoxy/aluminum adhesive joints from the following equation:

$$G_c = (P_c^2/4W)(\partial C/\partial a)_{P_c}, \qquad (2)$$

where P_c = critical load (the load at failure)

W = lap joint width[74]

The partial derivative of compliance with respect to crack length was evaluated at specific experimental data points along the fitted curve.[75] Equation (2) has not been stated[74] to give fracture toughness on the basis of new surface area generated, nor on crack area as is the usual custom in fracture mechanics.[75] It, therefore, produces a fracture toughness which is lower by a factor of 2.

Chang and Muki[76] have reduced the general case of two bonded isotropic elastic sheets to a lap shear joint. Continuous load transfer across the infinitesimally thin bond is assumed. Goland and Reissner's equations[59] were used for calculating a bond rotation which was then substituted into a pair of Fredholm integral equations of the second kind to obtain the bond line stresses and eventually the stress intensity factors. Failure load decreased slightly for decreasing lap length, and decreased approximately proportional to the square root of the adherend thickness.[76] The failure of the single lap joint has been called a mixed mode fracture problem because fracture may result from a combination of shearing and peeling stresses.[73]

Trantina[77] studied the general problem of mixed mode fracture in adhesive joints by using finite element models to calculate peeling (Mode I) and shearing (Mode II) stress intensity factors (K_I, K_{II}). The single-edge-notch specimen with the adhesive layer oriented at various angles to the applied load was also investigated experimentally. He found good agreement between the finite element model results and analytical solutions. He concluded that the summation of strain energies ($G_I + G_{II} = G_c$) is not an appropriate failure criterion for the adhesive system because G_I and G_{II} are not independent.[77]

The double lap joint (Fig. 2b) was believed to be free of any significant peeling (normal to the adhesive) stress. Keer and Chantaramungkorn[78] have shown, however, that appreciable tearing stress will exist, especially when lap strength is less than 2 times the thickness of the adherend. Walsh, et al.[79] have shown, with the aid of stress intensity factors, from a calibrated finite element technique that (for linear elastic double lap joints) joint strength will not be linearly related to the lap length-to-adherend thickness ratio (L/T), but will approach a maximum strength value asymptotically. The stress intensity factors of Walsh, et al.[79] were obtained by comparing the stresses (on a fixed boundary around the crack tip) calculated by the finite element method to those predicted by analytical fracture mechanics equations for a unit stress intensity factor.

Anderson, et al.[54] discuss analytical and numerical approaches to the determination of the fracture energy of adhesive systems. All of these approaches are based on the continuum theory of fracture mechanics. Several of these are reviewed in the model development portion of the theoretical program of this thesis.

FRACTURE MECHANICS AND FAILURE

Brittle and Ductile Fracture

Failure in the body of a solid is characterized as either a rupture or a fracture. At one extreme, rupture is failure by deformation that reduces a body section to zero area; at the other extreme, fracture (brittle) is failure in which no permanent deformation has occurred.[80] Between these two extremes is ductile fracture (significant permanent deformation without total reduction of the body section). The distinction between brittle and ductile materials is not sharp, but brittle solids typically have high bond energies (covalent, metallic, or ionic bonds) and resultant high moduli [$E = 10^{20}$ dynes/$(\mu m)^2$]. Theoretically, brittle materials should have tensile strengths of 0.05 to 0.1E, but observed moduli are considerably lower [10^{17}-10^{18} dynes/$(\mu m)^2$]. This apparent discrepancy was attributed by Griffith,[4] in 1920, to larger than atomic scale flaws (cracks) which produced intense local stresses. From this concept the study of fracture mechanics began.[81]

Fracture Mechanics - Strain Energy Concept

Using Inglis's[82] stress field equation, Griffith[4] calculated the energy consumed as a crack propagates in brittle isotropic materials. His calculations showed that this energy, the strain energy release rate (G), was equivalent to the energy required to generate new surfaces. Griffith[4] proposed that sharp cracks would propagate in brittle solids if the energy released was at least sufficient to provide the energy required to generate the new surfaces.

Griffith's concept may be illustrated as follows. Consider an infinite plate with unit thickness, containing a central transverse crack (length = 2a) and fixed ends. This plate, shown in Fig. 3a, has a uniform stress (σ) and a

load elongation curve as shown in Fig. 3b. Prior to crack elongation the plate energy is represented by the area OAB, but following symmetric crack extension (Δa) under constant strain, the stress will decrease to give the smaller area OCB. The strain energy release rate is, therefore, the difference between the stored elastic energy of these two configurations. The strain energy release rate equation may be stated as

$$G = -1/B\ (\partial U_t/\partial a)_v, \tag{3}$$

where B = plate thickness

U_t = total elastic energy

v = plate boundary displacement

This concept also applies to the constant load condition, as in Eq. (2), where $(CP^2)/(2W)$ is equivalent to U_t/B for linear elastic materials. When G is obtained under conditions of unstable crack propagation (initiation of crack resulting in catastrophic failure), a material fracture toughness parameter, G_c, is obtained.[83]

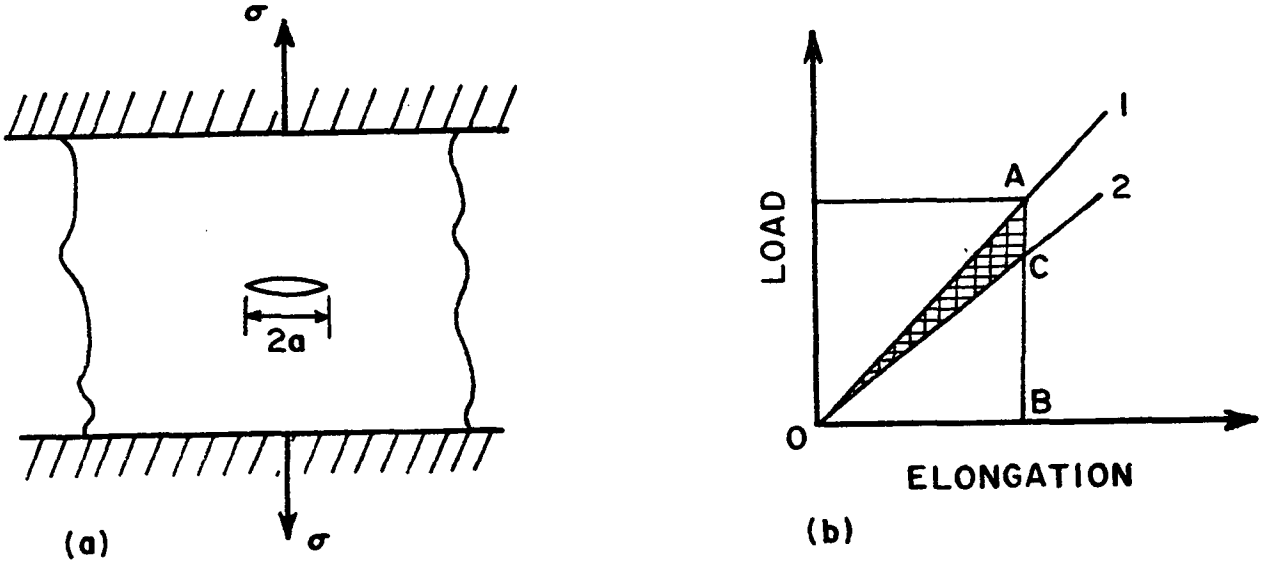

Figure 3. Griffith criterion for fixed grips with, (a) uniform thickness plate with central crack and fixed ends, and (b) load/elongation curves showing stored elastic energy for crack length = 2a (curve 1) and 2a+Δa (curve 2).

Fracture Mechanics - Stress Intensity Factors

Griffith[4] avoided a stress singularity at the sharp crack tip by using the energy approach, but many of the developments in fracture mechanics have resulted from investigating the stress fields in the immediate crack tip vicinity.

Consider an infinite planar linear elastic medium subjected to a uniform stress at infinity, so that the stress field is everywhere the same. Introduction of a sharp crack can be shown to change the distribution of stress in the vicinity of the crack tip. This stress field alteration results from the introduction of stress free boundaries. Stress free boundaries associated with cracks, notches, and other sharp discontinuities contribute to locally much higher stress levels, leading to structural failures at reduced nominal stresses.

Stress distributions around the crack tip are controlled by the shape and orientation of the crack, but the intensity of the stress field is controlled by more remote boundaries and the mode of loading.[84]

Consider the crack, shown in Fig. 4, in an isotropic elastic body under a general stress. Three basic types of stress can exist near a crack tip; each is associated with a particular mode of deformation.

In Fig. 5 these are illustrated as opening, Mode I, crack surfaces moving directly apart; edge-sliding, Mode II, crack surfaces sliding over each other perpendicular to the cracks leading edge; and tearing, Mode III, crack surfaces sliding over each other parallel to the leading edge.

Irwin[5] determined the stress and displacements for each mode by analyzing Modes I and II as plane-extensional problems subdivided as symmetric and skew-

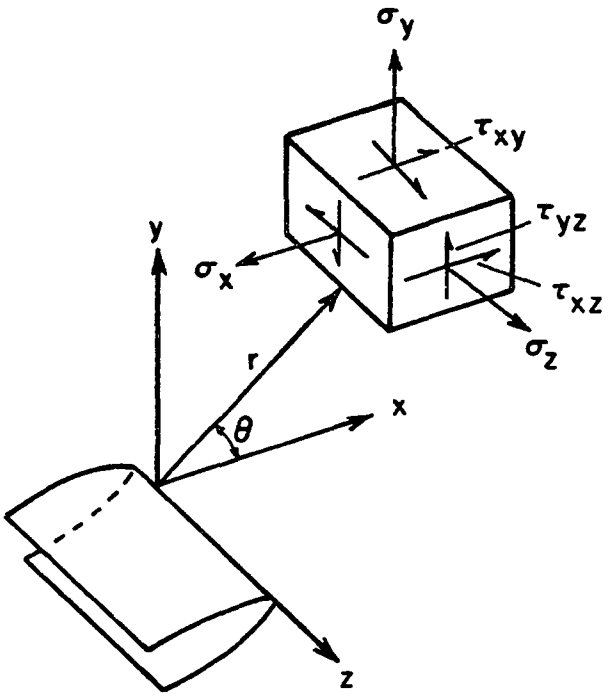

Figure 4. Coordinates measured for crack leading edge and stress components in stress field.

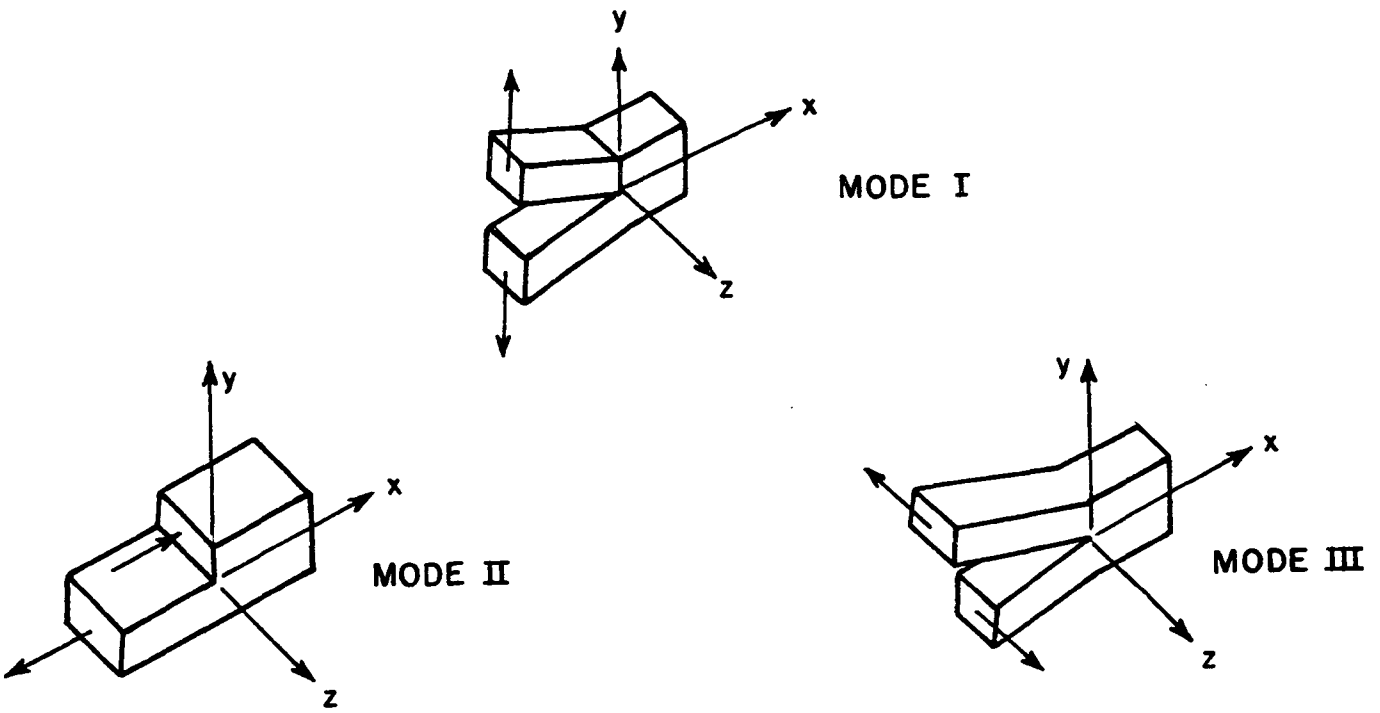

Figure 5. Modes of crack surface displacements.

symmetric, respectively. Mode III was considered as a pure shear problem. For the case of plane strain, using the method of Westergaard,[85] the stress fields in the immediate vicinity of the crack tip were found to be:[84]

$$\text{Mode I} - \begin{aligned} \sigma_x &= [K_I/(2\pi r)^{1/2}]\cos(\theta/2)[1 - \sin(\theta/2)\sin(3\theta/2)] \\ \sigma_y &= [K_I/(2\pi r)^{1/2}]\cos(\theta/2)[1 + \sin(\theta/2)\sin(3\theta/2)] \\ \tau_{xy} &= [K_I/(2\pi r)^{1/2}]\sin(\theta/2)\cos(\theta/2)\cos(3\theta/2) \\ \sigma_z &= \nu(\sigma_x + \sigma_y) \end{aligned} \qquad (4)$$

where $\tau_{xz} = \tau_{yz} = 0$

ν = Poisson's ratio

$$\text{Mode II} - \begin{aligned} \sigma_x &= -[K_{II}/(2\pi r)^{1/2}]\sin(\theta/2)[2 + \cos(\theta/2)\cos(3\theta/2)] \\ \sigma_y &= [K_{II}/(2\pi r)^{1/2}]\sin(\theta/2)\cos(\theta/2)\cos(3\theta/2) \\ \tau_{xy} &= [K_{II}/(2\pi r)^{1/2}]\cos(\theta/2)[1 - \sin(\theta/2)\sin(3\theta/2)] \\ \sigma_z &= \nu(\sigma_x + \sigma_y) \end{aligned} \qquad (5)$$

where $\tau_{xz} = \tau_{yz} = 0$

$$\text{Mode III} - \begin{aligned} \tau_{xz} &= -[K_{III}/(2\pi r)^{1/2}]\sin(\theta/2) \\ \tau_{yz} &= [K_{III}/(2\pi r)^{1/2}]\cos(\theta/2) \\ \sigma_x &= \sigma_y = \sigma_z = \tau_{xy} = 0 \end{aligned} \qquad (6)$$

Superposition of the stress fields for these three modes gives the most general description of the crack tip stress field. The higher order terms in r are neglected, and therefore the above equations are exact only in the limit as $r \to 0$. These show a singularity of stress as the crack tip is approached (i.e., stress tending to become infinite).

Since it is presumed that fracture will occur when the local stress level is greater than the local material strength, cracks should always propagate (this obviously does not occur). The tendency for real materials to change

structure to accommodate the intense stress at the crack tip (i.e., become plastic) effectively limits stress levels. If, however, the area of plasticity is small, parameters such as K_I, K_{II}, and K_{III}, called stress intensity factors, describe the mode and magnitude of force transmission through the crack tip region.

From dimensional considerations, the stress intensity factors relate to the crack length, a, and the appropriate stresses in the following manner:[84]

$$\begin{aligned} K_I &= \sigma(\pi a)^{1/2} \\ K_{II} &= \tau(\pi a)^{1/2} \\ K_{III} &= \tau(\pi a)^{1/2} \end{aligned} \tag{7}$$

Experimental investigations of the relationship between the critical stress at failure for a given mode (i.e., σ_c, τ_c) and crack length allow determination of critical stress intensity factors (K_{I_c}, K_{II_c}, K_{III_c}), which are material constants indicating the fracture resistance level of a particular material.

Irwin[5] has demonstrated the equivalence of the Griffith strain energy release rate and the stress intensity factor approaches by showing that, for an isotropic elastic plane strain problem,

$$G = 1 - \nu^2/E \; [(K_I^2 + K_{II}^2) + K_{III}^2/1 - (\nu)] \tag{8}$$

Theoretically, under linear elastic fracture mechanics (LEFM) conditions, G is most applicable to the combined mode fracture problem. According to Eq. (8), a mixed mode fracture could be initiated when the individual stress intensity factors (K_I, K_{II}, K_{III}) result in a calculated G value exceeding the material constant value G_c (i.e., $G > G_c$).

Experimental investigations of combined mode (I and II) fracture have not supported the assumed constancy of G_c with changes in crack orientation relative to direction of stress application.[86] This lack of agreement with fracture mechanics theory appears to be associated with an increased energy consumption as the contribution of Mode II increases.[86] Shih[87] found evidence that, for elastic-plastic materials with strain-hardening, any deviation from Mode I fracture will result in a higher fracture toughness. Rice[88] has pointed out that stress intensity factors are only a convenient measure of the load applied to the crack tip region; they do not contain any information on the response of the material to this load.

Hein and Erdogan[89] have analyzed the stress fields and singularities produced at a crack in a bimaterial interface. They have shown that stress singularities exist for many crack opening angles and configurations. The strength of the singularity [the magnitude of the exponent of r in Eq. (4)-(6)] depends on the crack opening angles and configurations and the elastic property differences between the two materials bonded at that interface.[89]

Sih, et al.[90] have shown that, for cracked anisotropic bodies with self-equilibrating loads (i.e., no resultant force on the crack surface), the stress intensity factors are identical with those completed for cracked isotropic bodies. Because of mathematical difficulties involved in treating cracks at any angle, strain energy release rate can only be calculated for cracks propagating along one of the planes of symmetry of an orthotropic elastic body.[90]

The analytical approach to fracture mechanics problems carries the same limitations as mentioned previously (p. 24); the introduction of the finite element method has expanded the application of fracture mechanics theory to fracture problems of increasing complexity.

AN INTRODUCTION TO THE FINITE ELEMENT METHOD

Zienkiewicz[91] credits Courant with the first stress analysis employing the technique now known as the finite element method. Twelve years later, in 1955, Argyris and Kelsey[92] used the term "finite elements" to describe the discrete units, with multiple point connections, which they used to simulate a continuum. The finite element method, initially formulated on an intuitive basis, became mathematically respectable in the early 1960's when it was realized that the method involved an application of the 'direct' procedures of the calculus of variations, as applied to the principle of total potential energy minimization.[91] The finite element method differs from the usual Rayleigh-Ritz technique in that its trial functions are piecewise continuous polynomials. These polynomials are zero over most of the continuum, entering the calculations only in the immediate vicinity of the connecting points (nodes) between elements. The use of finite elements allows a continuum with irregular boundaries to be easily modeled. The finite element method tends to produce a system of simultaneous equations which are banded matrices that may be solved readily by direct or iterative methods.

Finite Element Models

After the continuum is represented as an assemblage of finite elements, displacement fields, or stress fields, or both are assumed within each element. From the application of variational principles simultaneous algebraic (or matrix) equations result. These equations may be expressed in terms of generalized displacements, or stresses, or both as unknowns to be evaluated. These three possible formulations have been called, "the displacement method" (by far the most commonly used), "the force method," and "the mixed method."

Pian and Tong[93] have further classified the various finite element models on the basis of the energy principles and field assumptions involved. The

displacement method, which is derived from the principle of minimum potential energy and an assumed continuous displacement field (in general) over the entire body, is classified as a compatible model. Two subdivisions of the force method are given. Both are derived from the principle of minimum complementary energy. The equilibrium model is based on an assumed equilibrium stress field, while the hybrid model additionally assumes displacement functions that are compatible along the interelement boundaries. The mixed method is derived from Reissner's variational principle based on an assumed continuous displacement field over the entire body and assumed stress fields for the elements. Since the widely used direct displacement method was employed in this thesis, a review of finite element formulation and element displacement functions for this method is presented in Appendix I.

APPROACH TO THE PROBLEM

A review of the fiber-fiber bond literature showed that large variabilities and some contradictions existed in the published bond shear strength data. In the adhesive joint literature reviewed, there were many examples of the influence of structural and material parameters on bond shear strength. The analogy between these two structures leads one to conclude that fiber-fiber bond structure, as defined in this thesis, should be considered when one studies bond strength. An analytical investigation of these parameters, however, confronts the complex wood fiber structure and the interrelated effects of fiber dimensions, cell-wall construction, and stress/strain properties. These complications were avoided by devising an experimental program to study the independent effects of fiber dimensions and stress/strain properties.

Model fibers were prepared from commercial cellophane film. These self-bonding orthotropic elastic cellulose fibers had dimensions within an order of magnitude of wood fibers (100 to 500 vs. 20 to 80 μm widths). Wide (12.7 mm) cellophane strips were also studied. Only the single lap joint configuration (the zero crossing angle of the general fiber-fiber bond model structure, $\Phi = 0°$ in Fig. 1b) was investigated. The relationship of bond strength to bond length, fiber width, fiber thickness, axial Young's modulus, conformability, and interfacial cracks was examined in symmetric and asymmetric cellophane fiber lap joints.

These experimental structures were tensile loaded to failure in the IPC Fiber Load/Elongation Recorder. A group of wide (macro) lap joints were strained to failure by an Instron testing machine. From these data, compliance (C), strain to failure (ε_t), nominal axial stress (σ_{nom_c}) and apparent bond shear stress at failure ($\overline{\tau}$) were calculated.

Each experimental structure was represented in finite elements, and stress distributions and displacements were calculated with a general structural analysis computer program for static and dynamic linear systems, SAP IV.[94] A two-dimensional linear elastic model was assumed for most calculations. The two-dimensional model was developed with the aid of calculations with a three-dimensional model.

The fracture toughness of a series of cellophane lap joint experimental structures was calculated according to linear elastic fracture mechanics theory. This experimentally derived fracture toughness was used to predict the bond shear strength of the other experimental lap joint configurations. The linear elastic model predictions of the structural and material parameter effects on bond shear strength were also calculated.

EXPERIMENTAL PROGRAM

BACKGROUND

Two types of lap joints were employed in this experimental investigation. Lap joints, which were formed from 12.7-mm wide cellophane film strips, were termed macrolap joints. The preparation and testing of macrolap joints are discussed separately from the microlap joints which, although prepared from the same cellophane films, were composed of much smaller strips. These smaller cellophane strips (0.1 to 0.5 mm in width and 3.5 mm in length) will be referred to as fibers. In the results and discussion portion of the Experimental Program, the presentation is organized in terms of the variables examined. As a result, the discussions sometimes include a combination of these two types of lap joints.

MATERIALS

Cellophane

Three cellophane films (listed in Table 1) were formed into lap joints. All films were prepared commercially from cellulose xanthate by E. I. du Pont de Nemours & Company. Films were stored at 73°F and 50% relative humidity (TAPPI Standard T 402) until used. All preparation and testing was performed under these same conditions unless otherwise specified.

Table 1. Cellophane film properties.

Film Designation	Thickness	Film Type
134 PUD-O	38.1 μm (1.5 mil.)	Unplasticized
193 PUD-O	25.4 μm (1.0 mil.)	Unplasticized
215 PD	25.4 μm (1.0 mil.)	21% Glycerol, surface sized

Solvents

Deionized triple distilled water was used throughout the experiments. Using the procedure of Bauer and Lewin,[95] deionized water was distilled in a Corning AG1 glass still, distilled again from a solution of 0.02% potassium permanganate and 0.05% sodium hydroxide, finally distilled in an Ace glass still, and collected and stored in rigid polyethylene containers until used. Conductivity of the water was less than 1.5×10^{-6} mho/cm.

All other solvents employed were reagent grade.

EXPERIMENTAL PROCEDURES

Macrolap Joint Preparation

Cellophane films were cut into 12.7 x 25.4-mm strips on a guillotine-type cutter. The desired axis of orientation [e.g., machine direction (MD), cross-machine direction (CD), etc.] was maintained parallel to the long axis of the cellophane strip.

Except for some preliminary experiments, all film strips were cleaned according to the following procedure [similar to Jane's technique[51]]. Each strip was sequentially washed for 10 minutes in carbon tetrachloride, CCl_4 (2 times), 95% ethyl alcohol, C_2H_5OH (3 times), and triple distilled water (5 times). Before transfer to the next bath, the strips were rinsed with the same fresh solvent from a wash bottle. The strips were maintained in the water for a minimum of 2 hours before assembly into lap joints.

Wet cellophane strips were assembled in the single lap joint configuration on 3 layers of water-saturated cellulose ester type membrane filter (Millipore No. GSWP 00010 or VSWP 29300). Three additional layers of wet membrane filters

were placed over the macrolap joints before being sandwiched between 20 layers of filter paper. An entire assembly was positioned between steel platens (surface ground and covered with 150 mesh stainless steel screens). Each platen had central and lateral drilled holes which, when connected to a vacuum line, facilitated moisture equilibration of the entire lap joint assemblies.

A compressive load was maintained at the desired level for a minimum of 8 hours by a Baldwin-Southwark Universal Testing Machine. Bonding pressure over the range of 100 to 1500 psi was studied in preliminary work (see Appendix II). An average bonding pressure of 100 psi was chosen because it produced bonding equivalent to the higher pressures with minimal distortion of the lap joints. Following the pressing, drying, and separation from the membrane filters, the lap joints were allowed a minimum of 24 hours for equilibration before measurement and testing.

Macrolap Joint Measurement

The lap joint width (W) was measured with a machinist's rule graduated to 0.5 mm. A Bausch and Lomb stereomicroscope with a graduated eyepiece was used to measure the extent of the overlap. Lap length ($\overline{L}$) was taken as the average of two measurements (one along each side of the overlap). Film thickness ($\overline{T}$) and strip width ($\overline{W}$) were also averages of two measurements, one on the free span of each of the adherends. A Schopper dial micrometer graduated to 0.0001 inch was used to perform the thickness measurements (TAPPI Standard T 411-76).

Macrolap Joint Testing

Following completion of these measurements, each lap joint was strained to failure at 12.7 mm/minute in an Instron Universal Testing Machine. Total test span (S_t) was 34.9 mm between line-type clamps. From the load/elongation

tracings thus obtained, the slope of the initial portion of the curve (P_o/δ_o) and the maximum load (P_c) and overall elongation at failure (δ_c) were recorded. The compliance (C), overall strain to failure (ε_t), bond shear strength ($\overline{\tau}$) and nominal axial stress at failure (σ_{nom_c}) were calculated from this data according to the following definitions:

Bond shear strength,

$$\overline{\tau} = P_c/A_b \tag{9}$$

Nominal axial stress at failure,

$$\sigma_{nom_c} = P_c/\overline{A}_x \tag{10}$$

Total strain at failure,

$$\varepsilon_t = \delta_t/S_t \tag{11}$$

Compliance,

$$C = \delta_o/P_o \tag{12}$$

Bond area,

$$A_b = W \times \overline{L} \tag{13}$$

Cross-sectional area (average),

$$\overline{A}_x = \overline{T} \times \overline{W} \tag{14}$$

Apparent linear elastic modulus,

$$E_a = (P_o \times S_t)/(\delta_o \times \overline{A}_x) \tag{15}$$

where δ_o and P_o are the elongation and associated load for the initial linear portion of the load/elongation curve.

During testing the lap joints were observed with plane polarized light to allow monitoring of the bond breakage. Postfailure examination utilizing both plane polarized light and electron microscopy was employed to determine the locus of failure and the extent of permanent deformation in the adherends. The

examinations were performed with the stereomicroscope mentioned previously, outfitted with polarizing disks installed at the tungsten filament light source and both oculars. Electron microscopic examinations were performed with a JSM-U3 Scanning Electron Microscope (SEM).

Cellophane Fiber Preparation

A guillotine-type cutter was used to cut 12.7 mm x 50.8 mm pieces from a sheet of the desired film. The long axis of each piece was maintained parallel to the desired axis of orientation of the subsequent fibers. A fiber cutter (shown in Fig. 6) constructed with a gang arrangement of stainless steel razor blades (A) was attached to the upper plate (B) of a spring tester. A series of cellophane fibers were prepared by lowering the tester's upper plate and pressing the cutter against the film (C), which was secured to a polymethyl methacrylate block (D) resting on the tester bottom plate. A second cutting with a single blade at right angle to the first cutting produced adherend pairs, which remained attached at one end to the piece of film. This permitted the entire piece of film containing approximately fifty adherends to be cleaned as one unit. The cleaning process was the same as that used for the macrolap joints.

Matching adherend pairs were cut from the cleaned film pieces using a stainless steel razor blade. This procedure and all subsequent lap joint preparations were performed under the stereomicroscope with magnifications ranging from 10 to 112.5X. Stainless steel forceps were used to transfer the adherend pairs to individual water-filled receptacles in the fiber bonding tray prior to forming a lap joint from each pair.

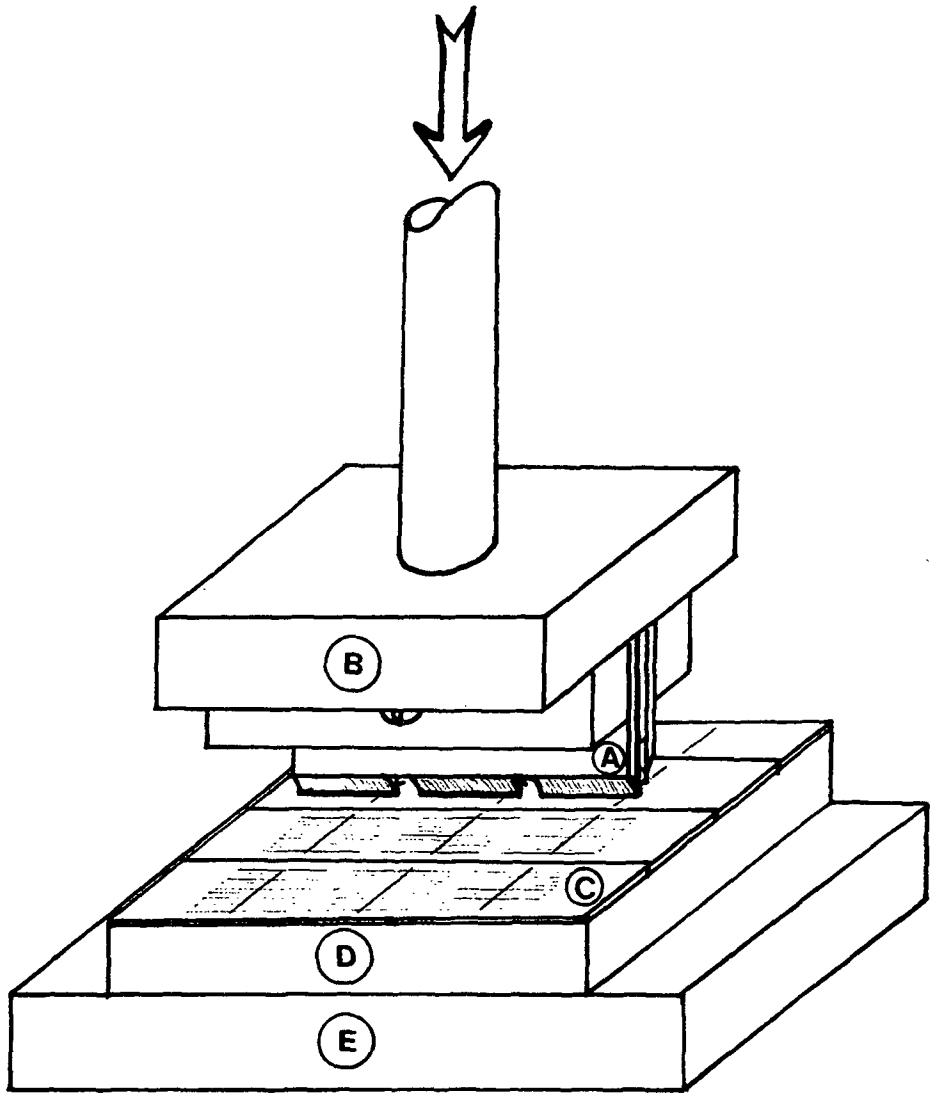

Figure 6. Cutter apparatus for preparation of cellophane fibers, which consists of (A) parallel razor blades separated by shim stock, (B) upper plate of spring tester, (C) cellophane film strips, (D) PMMA cutting block, and (E) the bottom spring tester plate.

Microlap Joint Preparation

The apparatus (shown in Fig. 7) for forming the microlap joint consisted of:

1. a fiber bonding tray (A), containing triple distilled water, mounted on the stereomicroscope base (B)
2. a pair of Bausch and Lomb micromanipulators (C) attached to the same base and projecting over the bonding tray edge

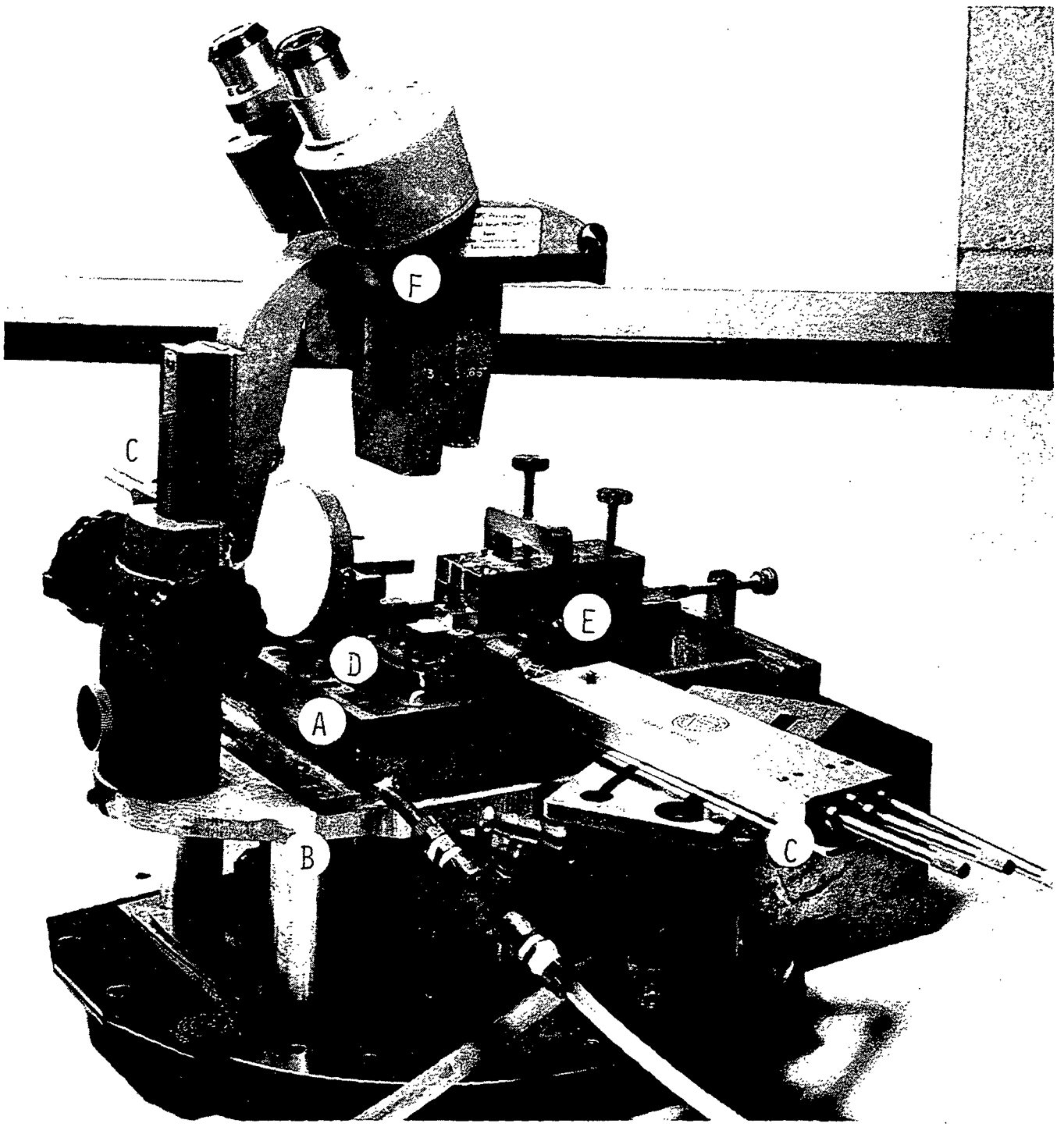

Figure 7. Microlap joint forming apparatus, consisting of (A) fiber bonding tray, (B) microscope base, (C) micromanipulators, (D) fiber clamps, (E) fiber bonder, and (F) a stereomicroscope.

3. two fiber clamps (D) attached to the projecting micromanipulator arms and set below the bonding tray water line
4. a fiber bonded (E) with a stationary anvil and a movable anvil between which the lap joint could be pressed while submerged in the tray water
5. A Bausch and Lomb stereomicroscope (F) mounted on the post of the microscope base.

The fiber bonding tray, fiber clamps, and fiber bonder were constructed of brass sheet stock. The fiber bonding tray was contructed with a submerged water inlet from a gravity feed and an overflow outlet, allowing the continual removal of surface contamination.

Figure 8 shows the arrangement of the various pieces of equipment in the immediate bonding operations area. Individual cellophane fibers (A) are inserted into the fiber clamps (B) with the resulting lap joint being formed from a matched pair. The fibers are aligned, overlapped, and positioned over the Teflon covered bottom anvil (C). The upper anvil (D) is lowered slowly onto the lap joint (covered by a Teflon strip) and a load is applied by a spring plunger (E) precalibrated to produce 6.89×10^6 dynes/cm^2 (= 100 psi) pressure over the entire anvil contact area. This pressure condition, when combined with a very soft Teflon tape (Chemfluor thread tape, 0.0035-inch thick), produced lap joints with each fiber conforming to the other's free end in the overlap region (approximately a 45° notch). To prepare the single lap joint configuration, approximately a 90° notch, a stiffer Teflon tape (Chemfluor skived tape, 0.0035-inch thick) and a pressure of 0.345×10^6 dynes/cm^2 (= 5 psi) were employed. While the bonding load is maintained, water is drained from the tray, the fiber ends are released from the clamps, and the bonder is removed from the

tray to allow the lap joint to equilibrate under load at 50% RH and 73°F for a minimum of 8 hours.

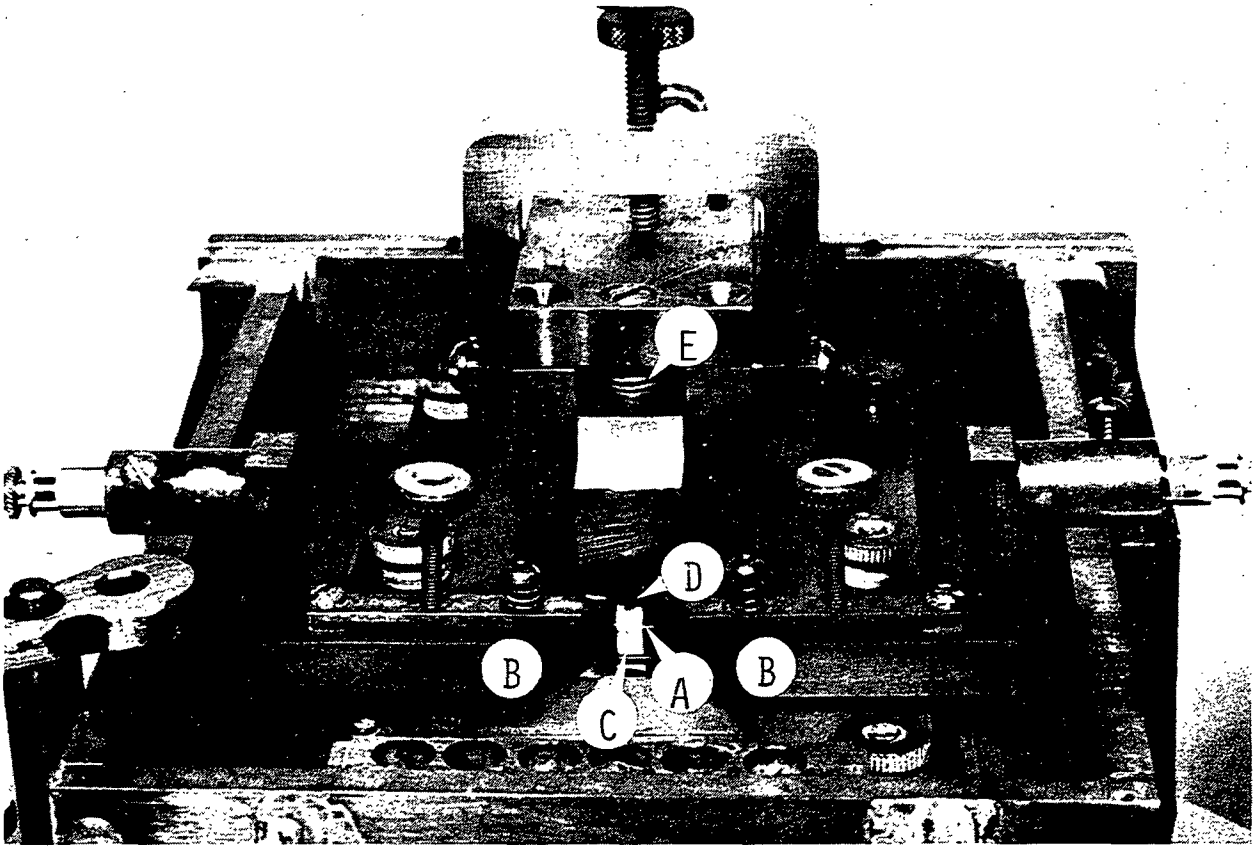

Figure 8. Microlap joint preparation area where (A) the fibers are held by (B) the clamps and placed on (C) the bottom anvil to be pressed by (D) the upper anvil and (E) the spring plunger.

Before use, strips of both Teflon tapes are cleaned by the same procedure as the cellophane fibers. These anvil coverings are replaced after each lap joint prepared.

Following drying, the bonding load and the upper anvil are removed to allow the self-bonded lap joint to be mounted on stainless steel dowel pins (0.794-mm diameter) for measurement and testing. While the bonder and lap joint are viewed through the microscope, the pin clamps (A), shown in Fig. 9, are

maneuvered so that the lap joint (B) and pin (C) long axis coincide. A microdrop of cellulose paste is applied to the tip of the lap joint adherend to attach it to the pin's flat surface and temporarily hold it in place before final gluing. As soon as the paste hardens (approximately 5 minutes), the lap joint is gently removed from the Teflon. To complete the mounting, a 0.6-mm diameter epoxy resin (Epon 907, Miller Stephenson Chemical Co.) bead (D), which surrounds and attaches the fiber to the pin, is carefully applied with a dissecting needle so that the resin is flush with the pin end. A spring clip type pin holder (E) is used for transferring the lap joint assembly to measuring and testing apparatuses.

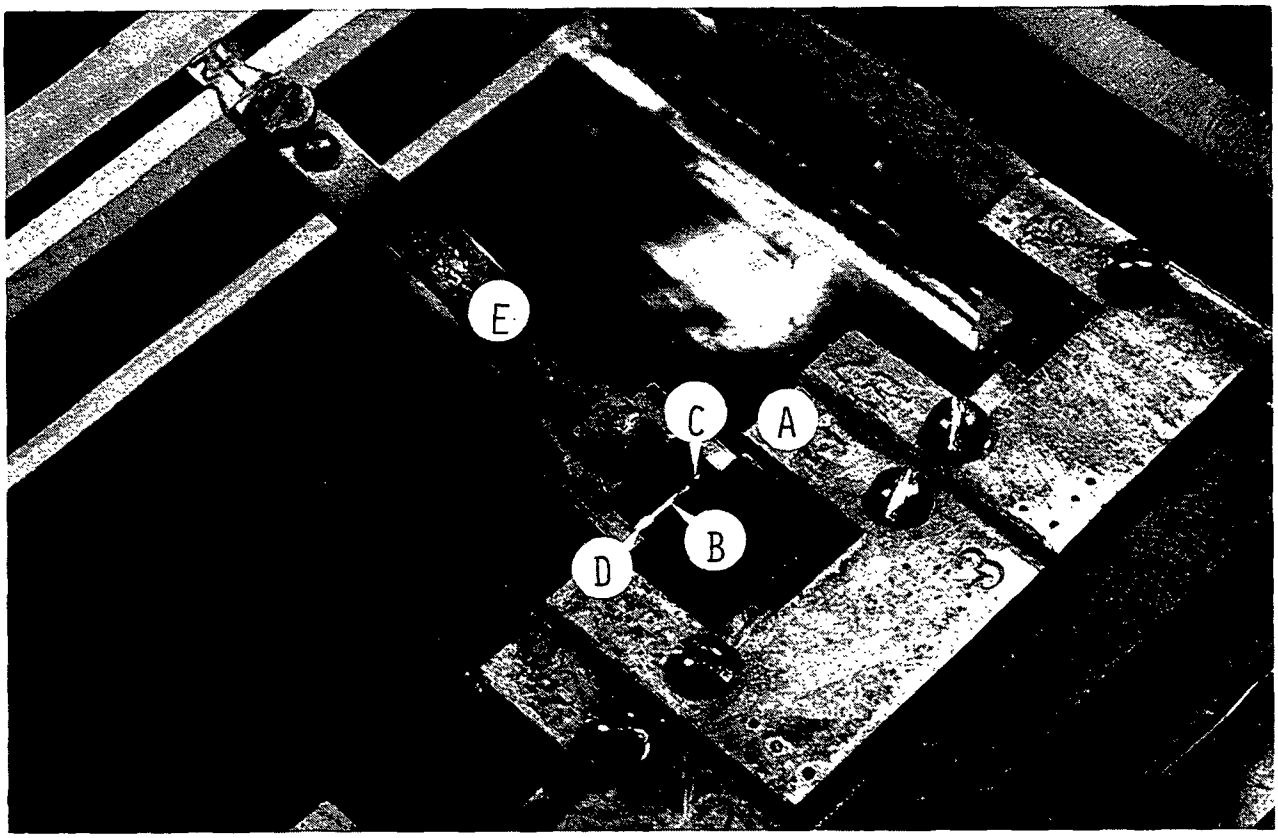

Figure 9. A mounted lap joint and mounting apparatus consisting of: (A) pin clamps, (B) lap joint, (C) dowel pins, (D) epoxy resin bead, and (E) pin holder.

All mounted lap joints were examined through cross polarizers in a Zeiss Standard Polarizing Microscope using reflected vertical (epi)-illumination. In several specimens, the presence of interfacial cracks was clearly evident (as in Fig. 10) from the interference fringes extending away from the darker areas of optical contact. Those lap joints showing partial debonding were also retained for measurement and testing.

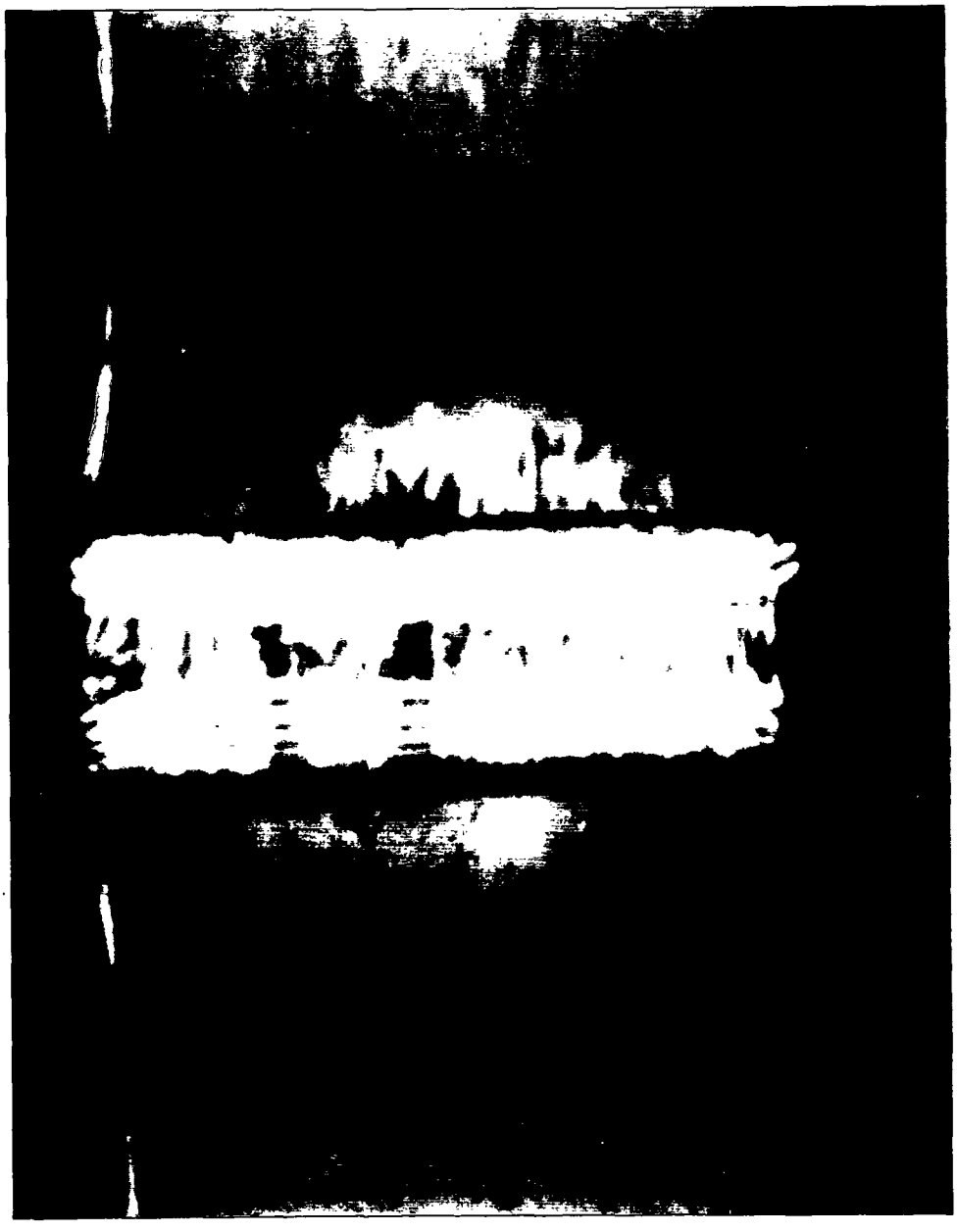

Figure 10. Cellophane microlap joint (L-112) showing interfacial cracks and optical bonded area. Photographed at 300X magnification with plane polarized vertical illumination.

Microlap Joint Measurement

The total span (S_t) between pins, the free spans (S_1, S_2) from the pin to the beginning of the overlap area, and the large overlap lengths ($L > 0.5$ mm) were measured with the graduated eyepiece of the stereomicroscope. A Cooke image-splitting eyepiece (A), mounted (as shown in Fig. 11) on a monocular microscope tube (B) with 10X and 20X objectives, was used to measure small overlap lengths, fiber widths (W_1, W_2), fiber thicknesses (T_1, T_2), and lap joint width (W_ℓ) and thickness (T_ℓ). To allow alignment of the fiber for width and thickness measurement, the lap joints were attached to a hemispherical microscope stage (C). A vacuum was generated to hold the hemisphere against a Teflon O-ring seat, permitting adjustments through a 150° arc. All eyepieces were calibrated against a stage micrometer with smallest graduation of 0.01 mm.

Immediately prior to mechanical testing, the lap joint bond area was examined. Those with interfacial cracks were photographed with the Zeiss microscope using a Leica 35-mm camera, Kodak EX-135-20 film and crossed polarizers with plane polarized epi-illumination. The developed images were projected onto paper with a photographic enlarger and the bond area was carefully traced. Total magnification was 420 times. A planimeter was used to determine the bond areas. Bond areas of the uncracked joints were calculated from the product of lap length and lap width (i.e., a rectangular shape was assumed). When the lap joint measurements were completed and the epoxy resin had cured at least 24 hours at 73°F, the mechanical testing was begun.

Microlap Joint Testing

The objective of the lap joint testing was to measure the maximum axial load and elongation a given specimen would sustain before totally debonding. The IPC

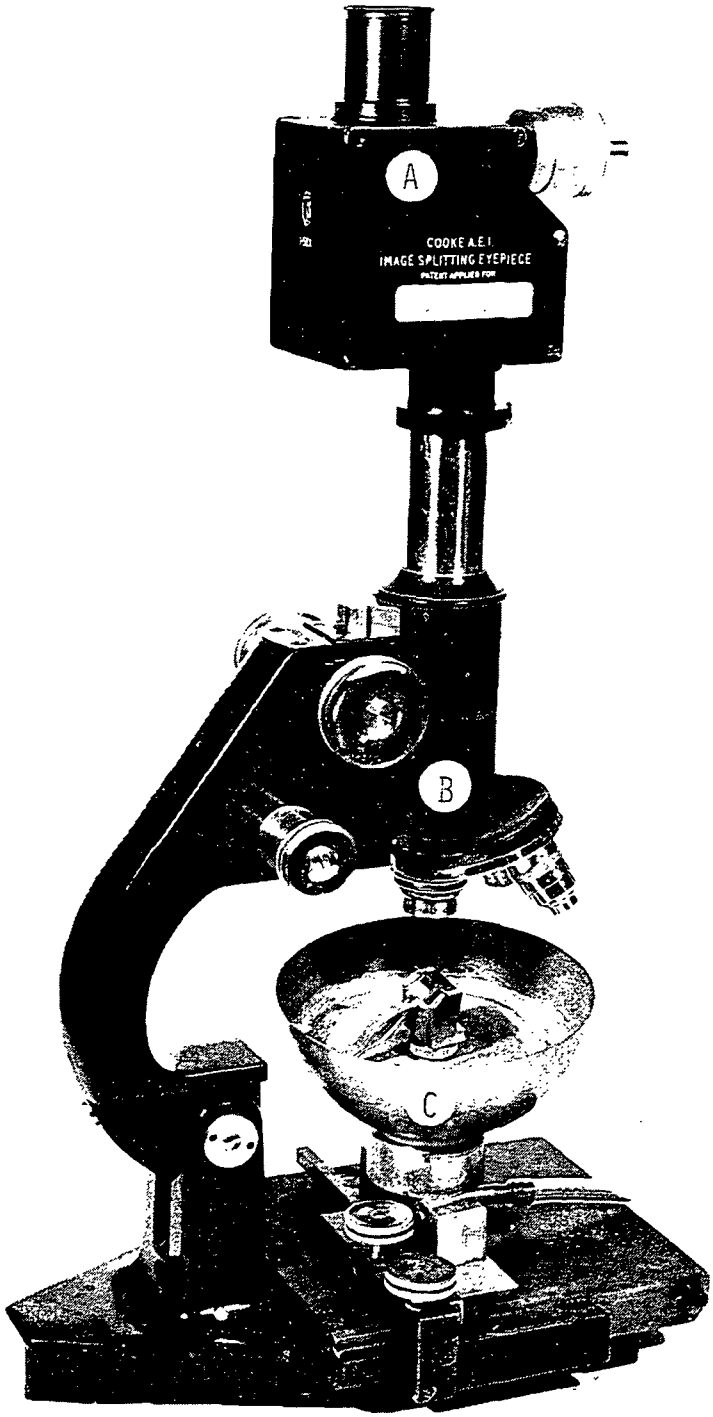

Figure 11. Monocular microscope equipped with (A) Cooke image splitting eyepiece, (B) 10X and 20X objectives, and (C) hemispherical microscope stage.

Fiber Load/Elongation Recorder (FLER) used for this testing is shown in Fig. 12. FLER functions much as a chain-o-matic balance[96] where the lap joint is attached to a balanced beam (A) at a point away from the beam pivot and close to the beam end where the load is applied. A constant rate motor simultaneously lowers a calibrated link chain (B) (producing a constant rate of change in loading force) and rotates a recording drum (C). Lap joint elongation is sensed by a calibrated linear variable permeance transducer (D) whose signal is applied to the drum recorder, thereby producing a trace of the load/elongation (P/δ) curve. This machine tends to maintain a constant load during unstable fracture and an increasing load with stable fracture.

Before they were loaded, the lap joints were observed at 112.5X magnification through the stereomicroscope mounted on FLER. A sketch was made of the lap joint before and after failure. Any deviation from ideal lap joint construction was noted. Microscopic observation continued during loading and any significant events were recorded. These included the failure characteristics (i.e., fracture stability and location), the deviation from elastic behavior (including visible local yielding), and any evidence of asymmetric loading. The relation of the mounted lap joint (A) to the beam (B) and transducer (C) is shown in Fig. 13. Axial tensile loading rates ranged from 0.70 to 2.06 g/sec, depending on lap length and specimen width, and produced time to failure values of 10.6 to 47 seconds.

Measurement of Cellophane Elastic Constants

The linear elastic theoretical model to be developed later required a complete set of elastic constants for cellophane film. Since commercially prepared cellophane may reasonably be considered orthotropic in nature, nine elastic constants are necessary. A combination of uniaxial and biaxial static

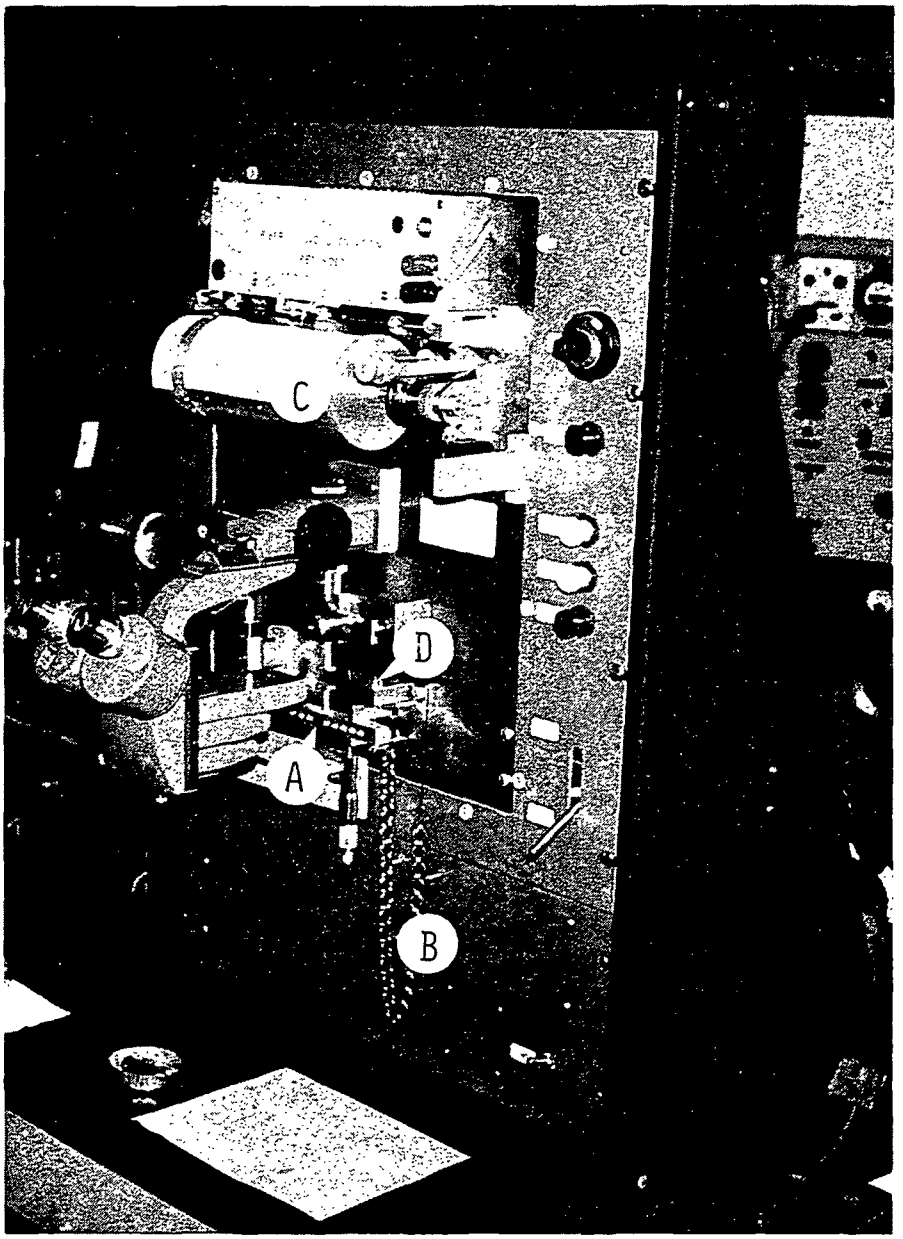

Figure 12. IPC Fiber Load/Elongation Recorder equipped with (A) a balanced beam, (B) a calibrated link chain, (C) drum recorder, and (D) displacement sensing transducer.

mechanical tests plus acoustic wave techniques were employed to experimentally determine five of these constants. The remaining elastic constants (the two out-of-plane Poisson ratios, ν_{zy}, ν_{zx}, and two shear moduli, μ_{zy}, μ_{zx}) were estimated from theoretical models of cellophane structure available in the

literature.[97] The detailed measurement procedures and results are presented in Appendix III. A brief summary of the cellophane elastic constants are given in the following Experimental Results and Discussion.

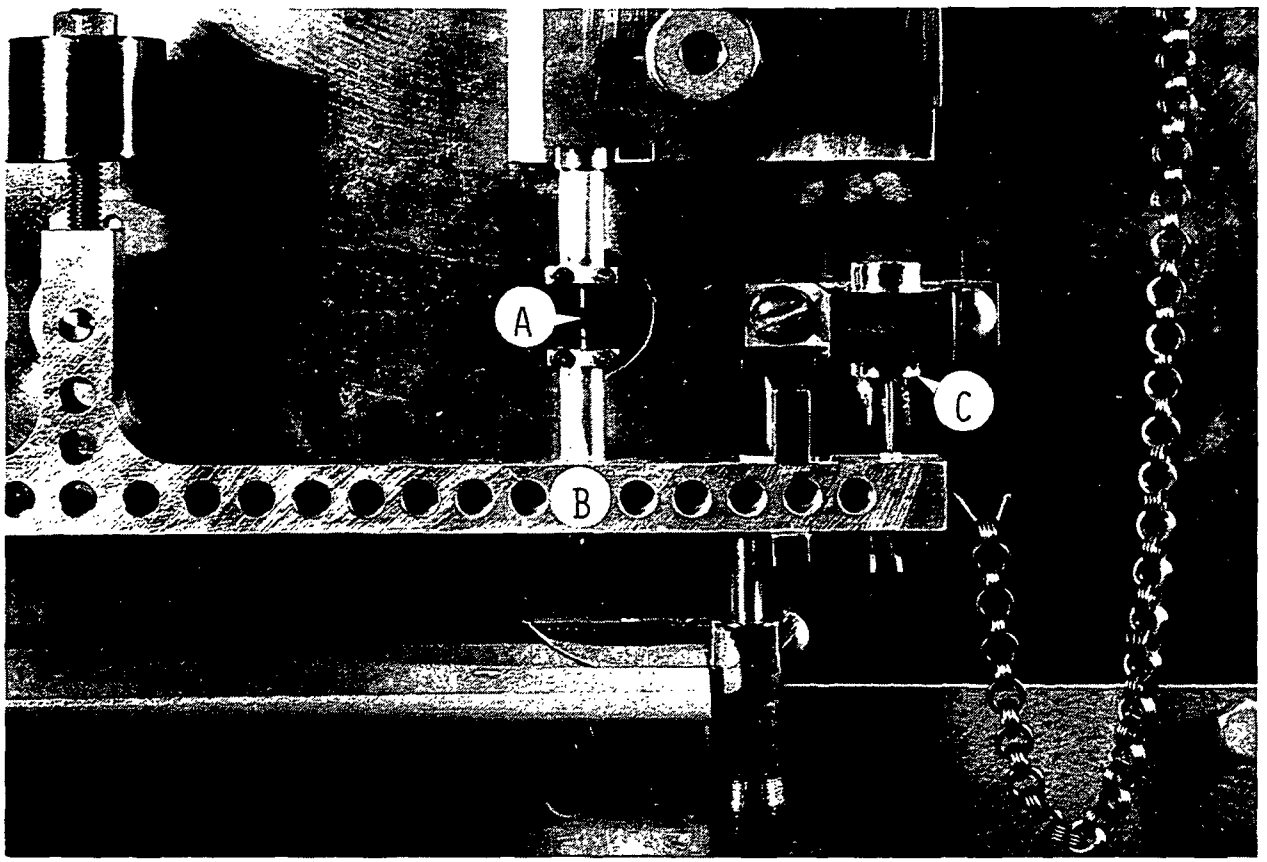

Figure 13. The relationship of (A) the lap joint mounted in FLER to (B) the balanced beam and (C) the variable permeance transducer.

EXPERIMENTAL RESULTS AND DISCUSSION

Cellophane Film Mechanical Properties

Cellophane film, prepared by the commercial xanthate process, is a lamellar viscoelastic material composed of amorphous and crystalline cellulose II polymers. Jayme and Balser[98] characterized commercial cellophane film as a symmetrical structure consisting of three distinct layers: (1) a thin surface cuticle of highly-oriented fibrils, (2) a homogeneous cellulose core, and

sandwiched between the two, (3) a vacuole layer resulting from entrapped gas bubbles. According to supplier literature, the cellophane film used in these experiments had a density of 1.43 g/cm^3. Cellophane has a preferred molecular orientation in the machine direction as a result of its manufacturing process. This produces anisotropic swelling and shrinking,[99] and mechanical properties that are characterized as orthotropic.[97] A typical response to tensile load in the film plane is shown in Fig. 14. An initial linear portion (up to $\varepsilon_t \sim 0.5\%$) is followed by a zone of yielding and finally an extended reasonably linear portion with positive slope maintained almost to failure (at 10-20% strain). An extensive program of elastic constant and other relevant mechanical property measurements was undertaken. A brief summary of the results of these determinations, which are presented in greater detail in Appendix III, is given in Table 2. The properties of the two unplasticized films, 134 PUD-0 and 193 PUD-0, are almost identical. In this experiment, they are treated as two different thicknesses of the same film. The cellophane MD modulus is similar to the average axial initial modulus [1089 to 1809 dynes/μm^2] reported for wood fibers from commercial pulps.[100]

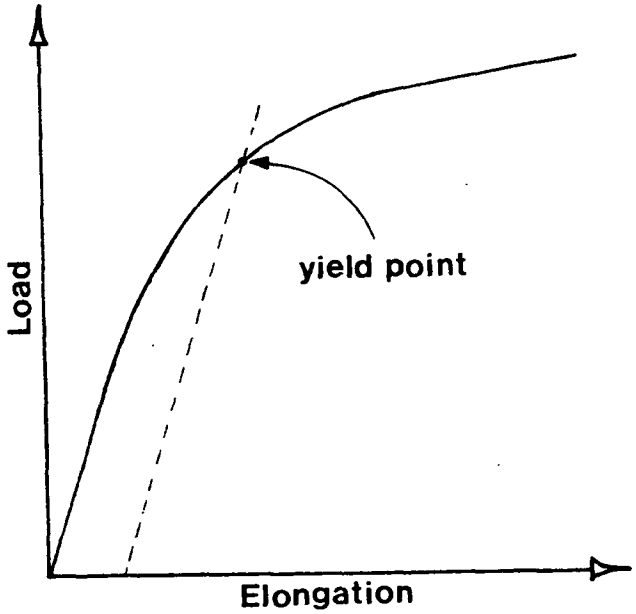

Figure 14. Typical load/elongation curve for 193 PUD-0 MD cellophane fibers.

These engineering constants have been obtained through a combination of uniaxial, biaxial,[102] and acoustic[103] means, plus some estimations based on cellophane structure theory.[97] Elastic moduli were measured on both 12.7-mm wide strips and 0.3 to 0.5-mm wide fibers. Those engineering constants given in the above table are based on the wide strips. The elastic moduli of the cellophane fibers were lower than the 12.7-mm wide strips, but the coefficients of variation for both ranged from 5 to 10%. Part of this variation may be material variation, particularly in the fibers, and another portion seems to be associated with variation in drying restraint.

Table 2. Cellophane film mechanical properties.

Film Designation	Engineering Elastic Constants									Yield Stress[a,b]	
	E_x[a]	E_y[a]	E_z[a]	ν_{yx}	ν_{zy}	ν_{zx}	μ_{xy}[a]	μ_{yz}[a]	μ_{xz}[a]	MD	CD
134 PUD-O	9.49	6.96	2.33	0.48	0.58	0.66	2.59	1.35	1.49	0.0752	0.0545
193 PUD-O	9.69	6.74	2.29	0.47	0.58	0.64	2.79	1.32	1.49	0.0737	0.0538
215 PD	10.51	7.93	--	0.37	0.46	0.51	--	--	--	0.0716	0.0531

[a][x 10^2 dynes/$(\mu m)^2$], x = MD, y = CD, z = z-direction.
[b]Determined by 0.2% offset method.[101]

Description of Cellophane Lap Joints

As a result of the extremely conformable nature of wet cellophane, a mechanical interlock developed between the two layers of porous Teflon tape and the lap joint being formed between them. A difficult separation was thus created and about 50% of the first sets of microlap joints (Experiments D1 and 2) were prematurely broken.

This problem was eliminated by substituting a harder nonporous Teflon tape and reducing the bonding load. This alteration in preparatory technique

decreased the extent to which adherends conform to each other. Two adherends (postfailure) from each of these two preparation techniques are shown in Fig. 15, a and b (higher load, softer Teflon) and Fig. 16, a and b (lower load, harder Teflon) to illustrate the difference. Those adherends bonded at higher loads have an equal and high degree of conformity about the end of the adherend to which they were bonded. These will be referred to as conforming lap joints. Forming the bonds at lower loads reduces the degree of conformity and appears to make it dependent on bond area (compare Fig. 16a to 16b). Lap joints prepared at the lower load will be termed single lap joints. Note the undisrupted postfracture interfacial surfaces of Fig. 15 and 16. The nature of failure in these lap joints will be discussed later.

A total of 144 macrolap joints was prepared from the three cellophane films (134 PUD-0, 193 PUD-0, and 215 PD). Three configurations (MD/MD, CD/CD, and MD/CD) with 16 lap joints each were constructed for each film. Each configuration had four replications of four nominal lap lengths (0.5, 1.0, 1.5, and 2.0 mm). One macrolap joint was accidentally broken and 19 were rejected because of misalignments, asymmetric bonding, and other defects to leave a net of 124 specimens.

Table 3 contains a total of 58 microlap joints that were tested in three separate experiments. Six of these were rejected because of defects. The most common defect was misalignment, usually in the form of a lateral offset in the bond plane. For a lap joint to be acceptable, the width of the bond area had to be equal to or greater than the fiber average width (i.e., $W_\ell > W$). Precise control of the bond lengths and alignments could not be achieved because the overlaps were very small, the drying occurred (under pressure) with anisotropic shrinkage, and the wet cellophane was quite flexible. Therefore, the selection

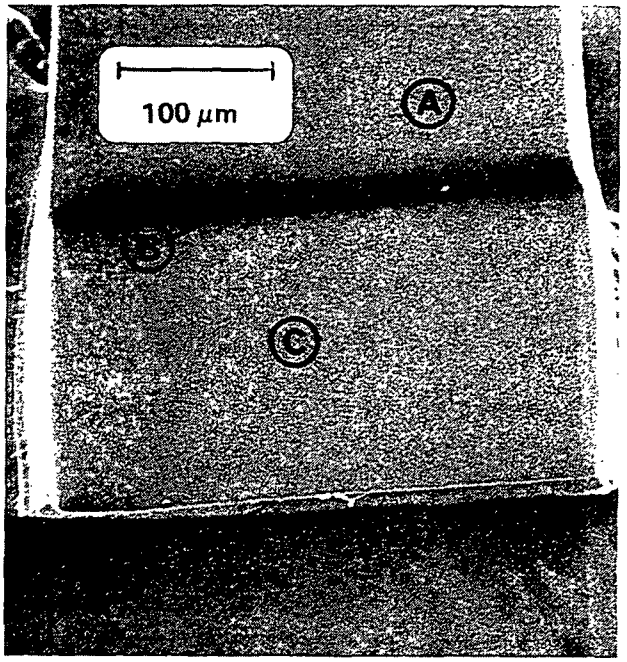

Figure 15a. K-998, top view of a conforming microlap joint adherend, with (A) free span, (B) conforming zone, (C) postfracture interfacial surface, and (D) adherend end shown.*

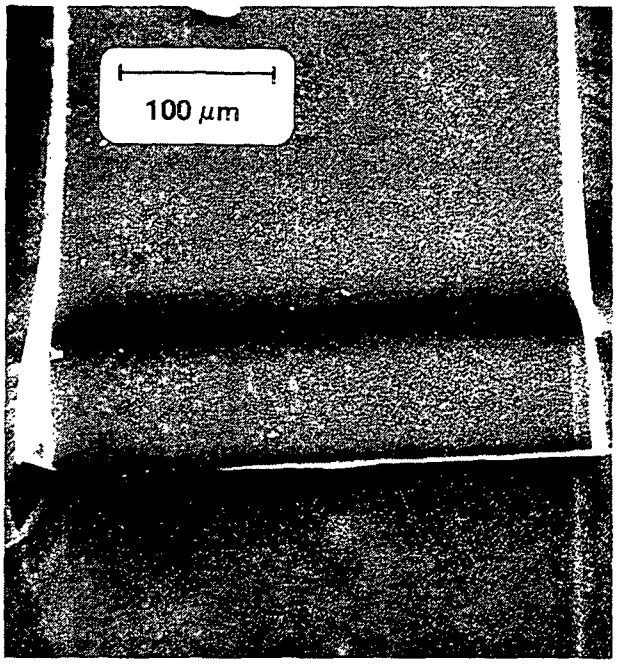

Figure 15b. K-999, top view of a conforming microlap joint adherend (postfracture).*

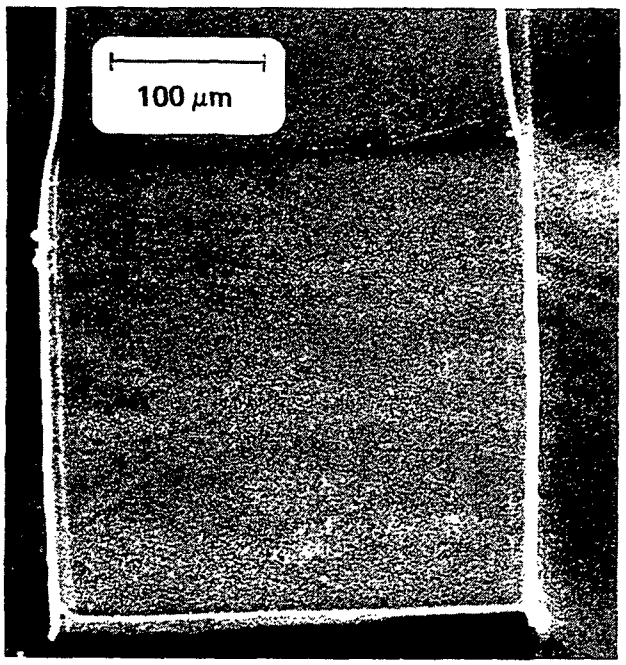

Figure 16a. L-105, top view of a single microlap joint adherend (postfracture).*

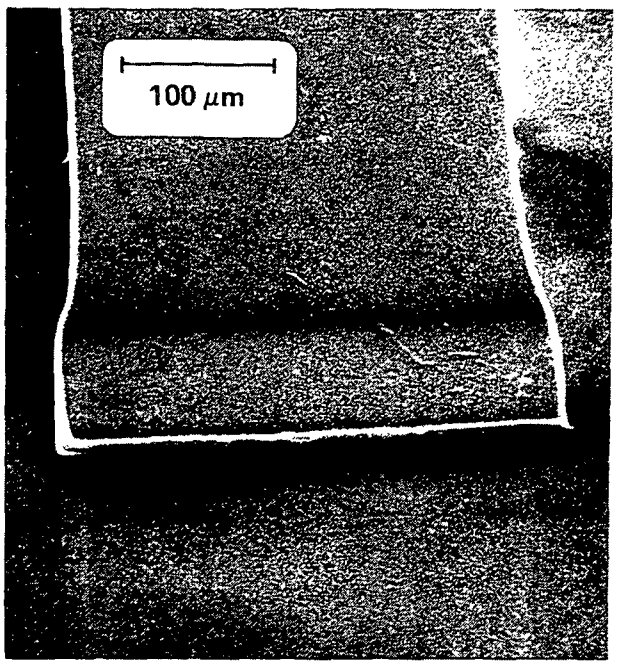

Figure 16b. L-112, top view of a single microlap joint adherend (postfracture).*

*Photographed in scanning electron microscope with stage tilted at a 45° angle, as a result, top to bottom dimensions are reduced.

criteria were employed and all lap joint experiments were performed for a range of overlap lengths. All experimental results are presented as a function of the actual bond lengths.

Table 3. Cellophane microlap joint experiments.

Experimental Group	Designation	Configuration	Tested	Variable of Interest
D-1	193 PUD-0	MD/MD	7	Interfacial cracks
-2	193 PUD-0	MD/MD	15	Conformity
J-1	134 PUD-0	MD/MD	6	Thickness
-2	193 PUD-0	MD/MD	4	Width
-3	193 PUD-0	MD/CD	6	Asymmetry
-4	193, 134 PUD-0	193/134 MD/MD	6	Asymmetry
-5	193 PUD-0	CD/CD	4	Modulus
K-1	193 PUD-0	MD/MD	10	Bond length

Response of Cellophane Lap Joints to Axial Loading

Lap joint load/elongation curves were, in general, very similar to that of cellophane film (Fig. 14). A curve typical of those lap joints failing at stresses below the yield stress of the cellophane is shown in Fig. 17. An edge view (two-dimensional) of a microlap joint in the preload configuration is presented in Fig. 18. This perspective shows that the tensile forces applied to the fibers must be transmitted to the interfacial plane by adherends whose axes do not pass through that plane. Moments will be generated, the overlap region will rotate, and the fiber-free spans will bend. This deformation can be seen in Fig. 19 for a preliminary microlap joint (215 PD) experiencing stable fracture and general structural yielding. It is clear that peeling (perpendicular to the interface) and shearing (parallel to the interface) stresses are present. This is indicative of a mixed mode fracture process. Many lap joints in which general structural yielding occurred were strained to 10 to 20% before the bond or fiber failed.

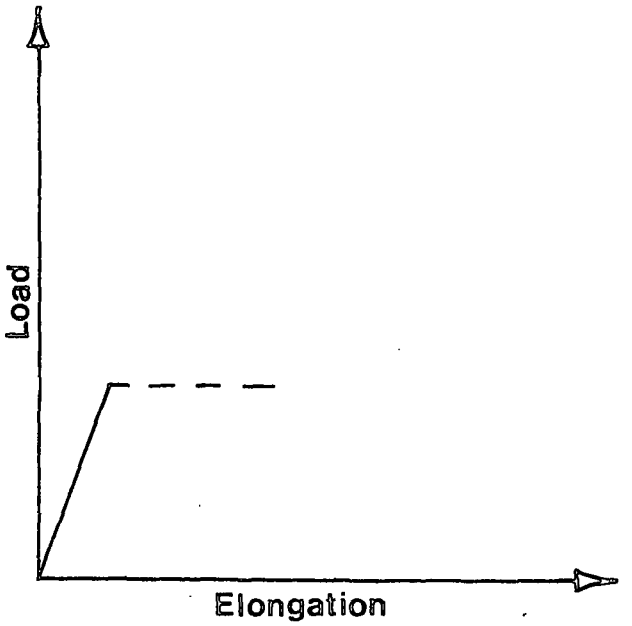

Figure 17. Typical load/elongation curve for a 193 PUD-0 microlap joint.

Figure 18. An edge view of a cellophane microlap joint photographed with plane polarized vertical illumination at 300X magnification.

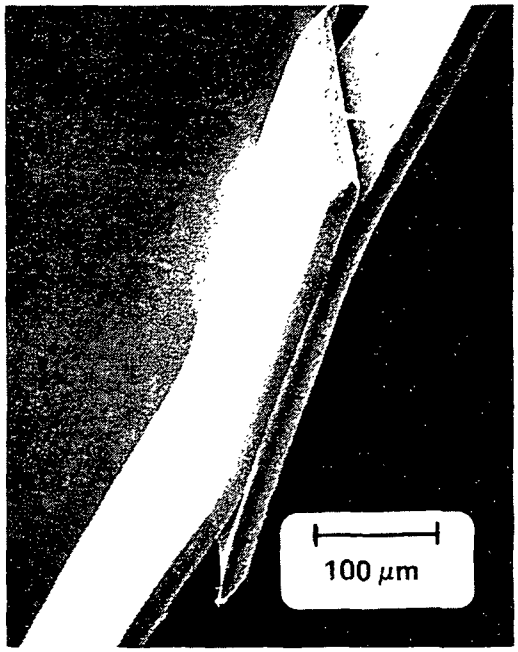

Figure 19. Scanning electron micrograph of a microlap joint (215 PD) showing stable fracture and general structural yielding following load removal.

Cellophane Lap Joint Compliance, Strength, and Failure

Bond Shear Strength

The bond shear strength ($\bar{\tau}$) of all macro- and microlap joints constructed of 193 PUD-0 cellophane adherends having the machine direction parallel to their long axis (MD/MD) is presented in Fig. 20. Bond shear strength clearly depends on bond length (bond area at constant bond width). At short overlaps (L < 300 μm) bond shear strength increases rapidly as bond length decreases, but at large overlaps (L > 1000 μm) the change is much less drastic. Between these two extremes is a region in which bond shear strength appears to depend on the lap joint type (i.e., micro or macro).

The bond strength value (1.45 dynes/μm^2) at the shortest overlap shown (68 μm) is higher than the highest value reported for wood fibers.[40] In this thesis research, the highest value recorded was 2.7 dynes/μm^2 for a similar lap joint which, however, had interfacial cracks and a very short bond length of 25.8 μm

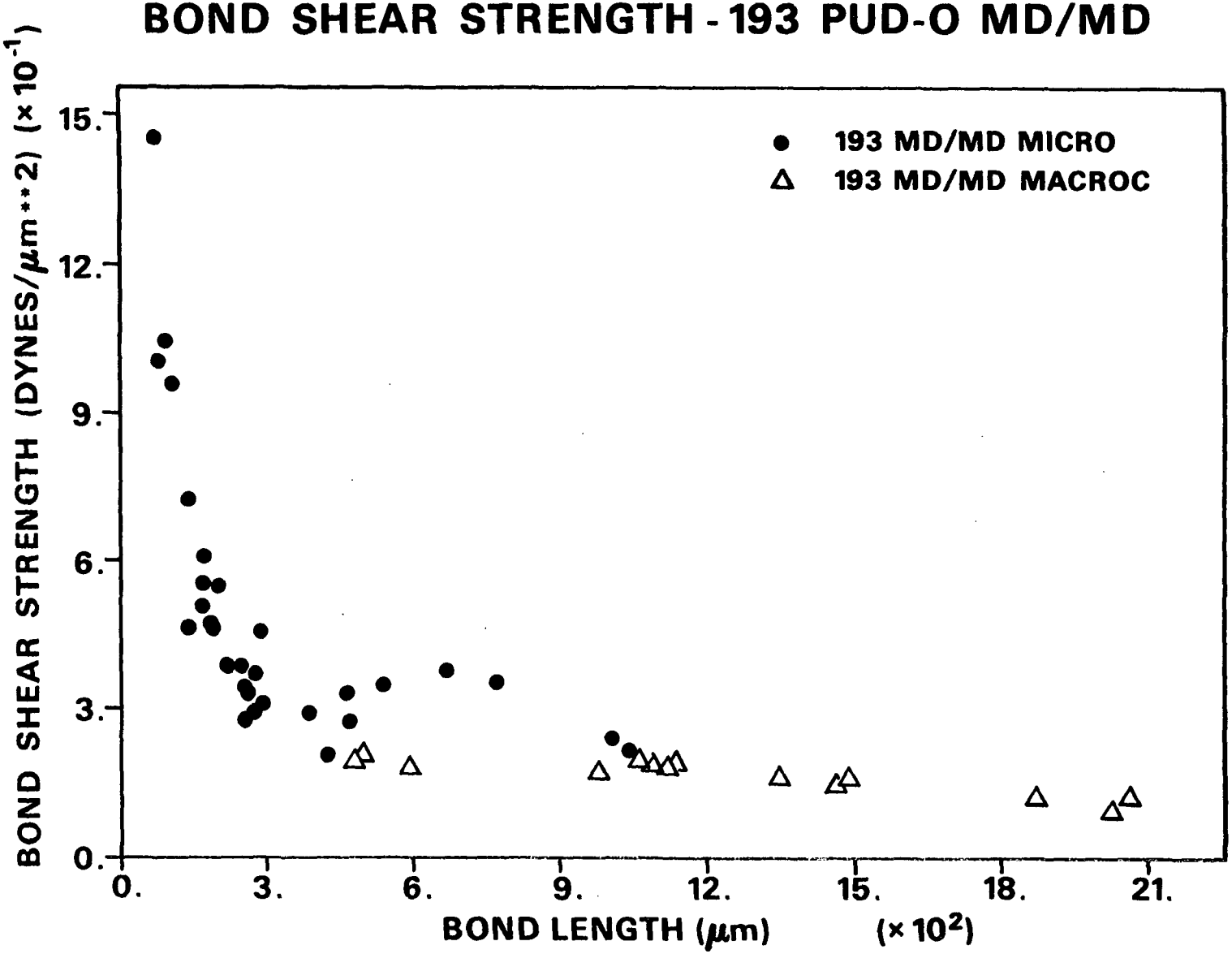

Figure 20. Relationship of bond shear strength to bond length for all 193 PUD-O cellophane lap joints (macro and micro).

*The pure numbers on the axis are to be multiplied by the axis scaling factors (x 10^2, x 10^{-1}) to obtain the value of the variable (e.g., bond length = 21 x 10^2 = 2100 μm).

(see Fig. 10). There is considerable agreement between the bond strength values of this thesis and those found in the literature. At the longest overlap of 2000 μm, the average bond shear strength value of 0.116 dyne/μm^2 is comparable to Goring's[49] results of 0.108 dyne/μm^2 for untreated deacetylated cellulose acetate 90° crossing joints at the same overlap length. These results are also similar (at the same bond lengths) to the average bond shear strength reported by Thorpe, et al.[40] for loblolly pine holocellulose fiber-shive bonds [0.400 dyne/μm^2] with an average bond length of 204 μm. The microlap joint bond shear strengths at 500 μm are roughly equivalent to Mohlin's[45] value [0.34 dyne/μm^2] for rayon fibers bonded to a 500-μm wide cellophane strip. Having made these favorable comparisons, one should qualify them because there are many differences in structure between those used to generate the literature values and the lap joints of this thesis. A more in-depth examination of the behavior of these cellophane lap joints follows.

The strong influence of bond length on bond shear strength in the short overlap region is behavior typical of brittle material fracture.[60] It is, therefore, quite likely that linear elastic fracture mechanics (LEFM) theory[4] can be invoked to predict the bond shear strength of short bond length cellophane lap joint structures. This view is supported further by the relationship between bond length and nominal axial stress at failure (σ_{nom_c}, axial load per unit fiber average cross-sectional area).

Nominal Axial Stress at Failure

When σ_{nom_c} (a measure of lap joint strength) is plotted as a function of bond length, the three regions evident in Fig. 20 become quite distinct. In the short bond length region of Fig. 21, a trend of slightly increasing σ_{nom_c} with increasing bond length can be seen. As the intermediate region is entered,

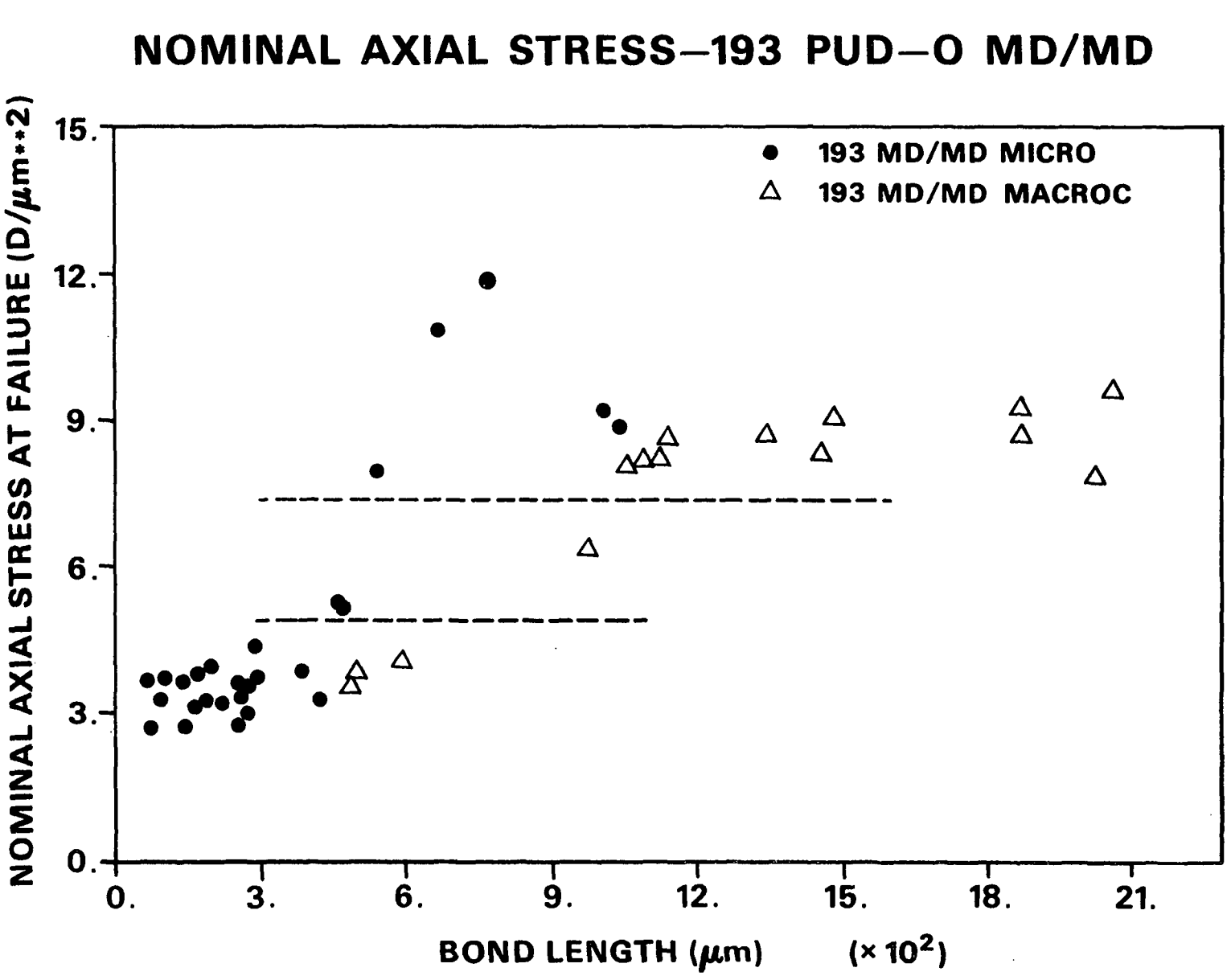

Figure 21. Relationship of nominal axial stress at failure to bond length for all 193 PUD-O cellophane lap joints (macro and micro).

σ_{nom_c} increases sharply to a reasonably constant value for L > 1000 μm. Superimposed on Fig. 21 are two constant stress lines representing the yield stress (σ_{ys}) for 193 PUD-O and $(2/3)\sigma_{ys}$. The intermediate region can now be viewed as representing a transitional zone where the fracture process changes from one of brittle fracture for bond lengths less than 600 μm to one of failure under conditions of general structural yielding and viscous flow. According to Broek,[83] under conditions where $\sigma_{nom_c} \leq (2/3)\sigma_{ys}$, linear elastic fracture mechanics parameters can be used to describe the resistance of a brittle material to fracture. That region below $(2/3)\sigma_{ys}$ will be referred to as the LEFM region. The slight dependence of σ_{nom_c} on bond length is also consistent with the LEFM concepts of stress concentrations in a narrow zone at each end of the overlap.[60]

Amplification and extension of the trends observed in Fig. 21 can be seen in Fig. 22 for the 215 PD macrolap joints. This graph presents the results for the MD/MD, CD/CD, and MD/CD configurations. The asymmetric configuration (MD/CD) has reduced strength and a LEFM region extending to much longer bond lengths (L ≤ 900 vs. L ≤ 300 μm) than either symmetric constructions. The pronounced curvature noted in the overlap region of the unstressed asymmetric lap joints is evidence of residual stress. This may contribute to the reduced strength of this configuration. Lap joint strength in the viscous region approaches the tensile strength of the weakest adherend (i.e., CD less than MD). Here, the transition zone encompasses the yield stresses of the weakest adherend and connects the LEFM region to the viscous region. Similar behavior for 193 PUD-O and 134 PUD-O macrolap joints can be seen in Appendix IV.

The bond length at which LEFM behavior ends and the transition zone begins depends on the strength of the structure. If a structure is inherently weaker, as in the asymmetric construction case, LEFM behavior will be maintained to

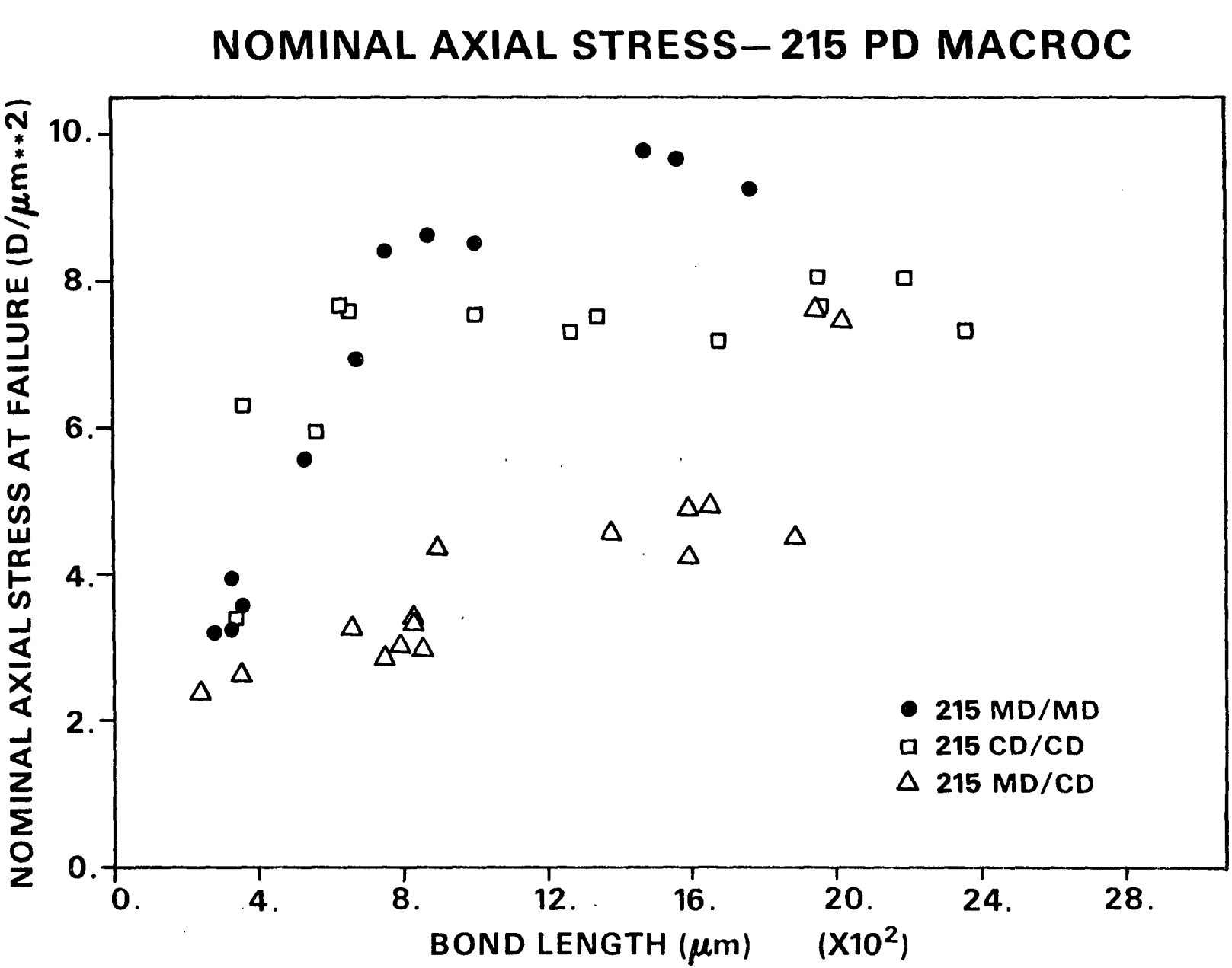

Figure 22. Relationship of nominal axial stress at failure to bond length for 215 PD cellophane macrolap joints with three configurations (MD/MD, CD/CD, MD/CD).

longer overlaps because the $(2/3)\sigma_{ys}$ limit will not be reached at the shorter overlaps. In the case of the micro- and macrodata in Fig. 21, the data and explanation are not clear. Macro- and microlap joints differ primarily in test span (34.9 vs. 3.6 mm) and width (12,700 vs. 300 μm). Test span should not be an important factor because both are long compared to the bond length and adherend thickness. The effect of width is neither clearly evident from the literature,[62,69] nor from the experimental results of this thesis. In general, the transition from the LEFM behavior represents a loss in a structure's ability to intensify stress sufficiently to produce fracture. This change usually results from an inability of the material to confine the yield zone to a small region immediately surrounding the crack (notch) tip.[83] Since this cellophane film has a thickness of only 30 μm, it is quite likely that this did occur. Differences in failure characteristics of macro- and microlap joints have been observed.

Nature of Lap Joint Failure

Earlier it was noted that the locus of fracture for the shorter bond lengths of both conforming and single microlap joints was along the interfacial plane (see Fig. 15 and 16). No perceptible difference existed between the unbonded adherend surface and the fracture plane surface. This same condition was observed for the shorter bond lengths of the macrolap joints. Based on the analysis of Good,[73] one concludes that the interfacial bonding is weak compared to the cohesive bonds of the bulk cellophane. Similar failure characteristics were observed in this thesis (see Appendix VI) and by Thorpe, et al.[40] for loblolly pine holocellulose fiber-fiber bonds.

For those lap joints failing in the viscous region, a distinct difference in the micro- and macrostructure behavior has been noted. Even in the viscous

region the microlap joint fracture surfaces, shown in Fig. 23, b and c, are not substantially altered from the unbonded surface of Fig. 23a. In Fig. 23b, a small yield zone of 3.2 m at the fiber edge decreases quickly toward the center of the fiber. Some localized surface disruption (tearing) occurs in the yield zone of Fig. 23b and along the end of the previously bonded fiber shown in Fig. 23c. These small changes in the fracture surfaces of the microlap joints sharply contrast with large yield zone observed in the macrolap joints shown in Fig. 24-26. The macrolap joint in Fig. 24 has a large yield zone of up to 510 m and presents a yield zone shape analogous to a large plane stress area at the edge gradually decreasing to a plane strain area in the interior.[83] This macrolap joint also illustrates the asymmetric cracking that may accompany material and dimensional asymmetries (e.g., cellophane 215 PD bonded to 134 PUD-0). If strain levels exceed 2%, corrugations, such as those shown in Fig. 25 and 26, develop in the overlap as a result of the forces of lateral contraction. Large yield zones can be seen along these stabilized crack fronts. Striated interfacial surface disruptions were observed to form similar patterns. The initial fracture, which became stabilized, was often accompanied by audible clicks. As bond length decreased, it was observed that the number of nodes across the overlap increased up to a maximum of four. The number of nodes were observed to increase for thinner films. This behavior appears to result from Poisson effects.

No attempt will be made to evaluate the extremely complex stress fields that must accompany these out-of-plane distortions. One may conclude, however, that the corrugations represent a mechanism for energy minimization and contribute to the difference between micro- and macrolap joint transition and viscous zone behavior.

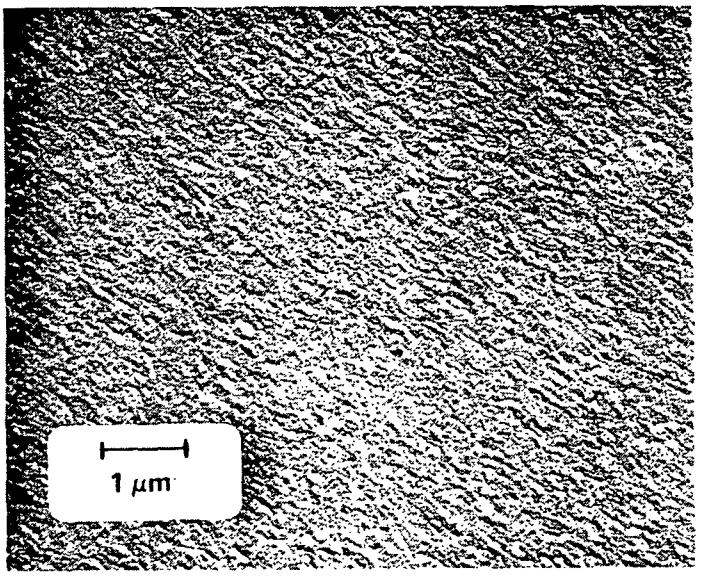

Figure 23a. Transmission electron micrograph of the unbonded surface of a 193 PUD-0 cellophane microlap joint adherend.

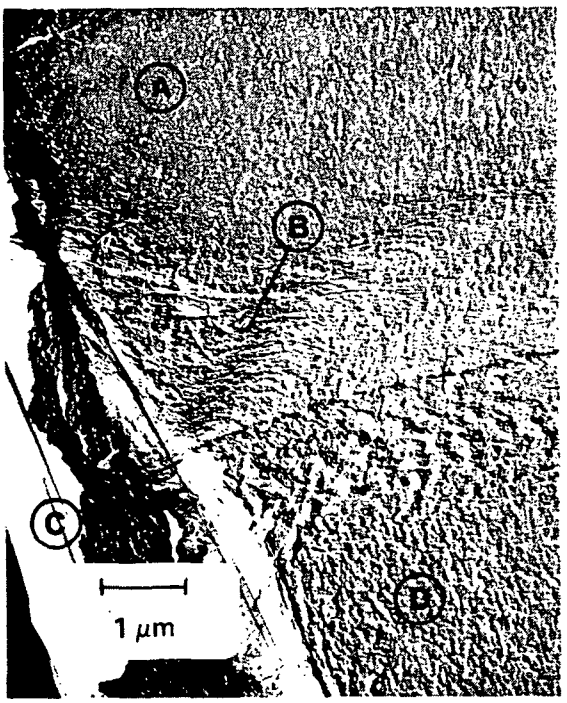

Figure 23b. Transmission electron micrograph of (B) the yield zone adjacent to (C) the corner of the overlap of microlap joint K-996, with (A) postfracture interface surface, and (D) free span.

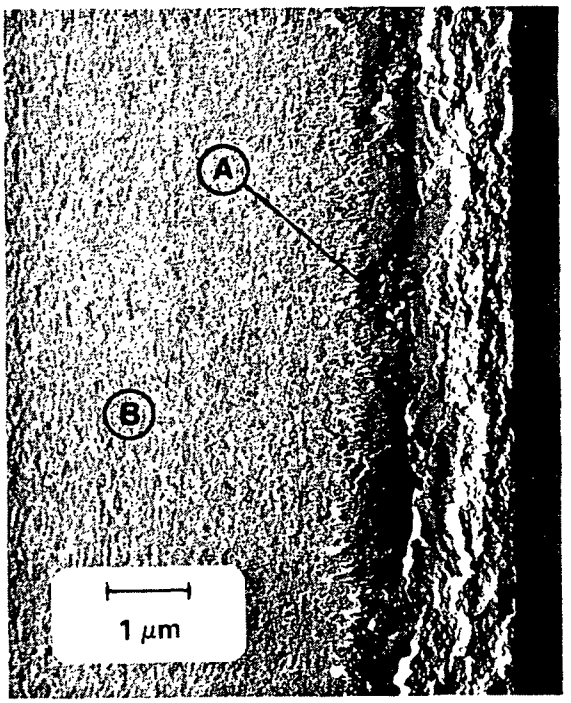

Figure 23c. Transmission electron micrograph of (A) the end of the overlapping adherend of microlap joint K-996, and (B) the postfracture interface surface.

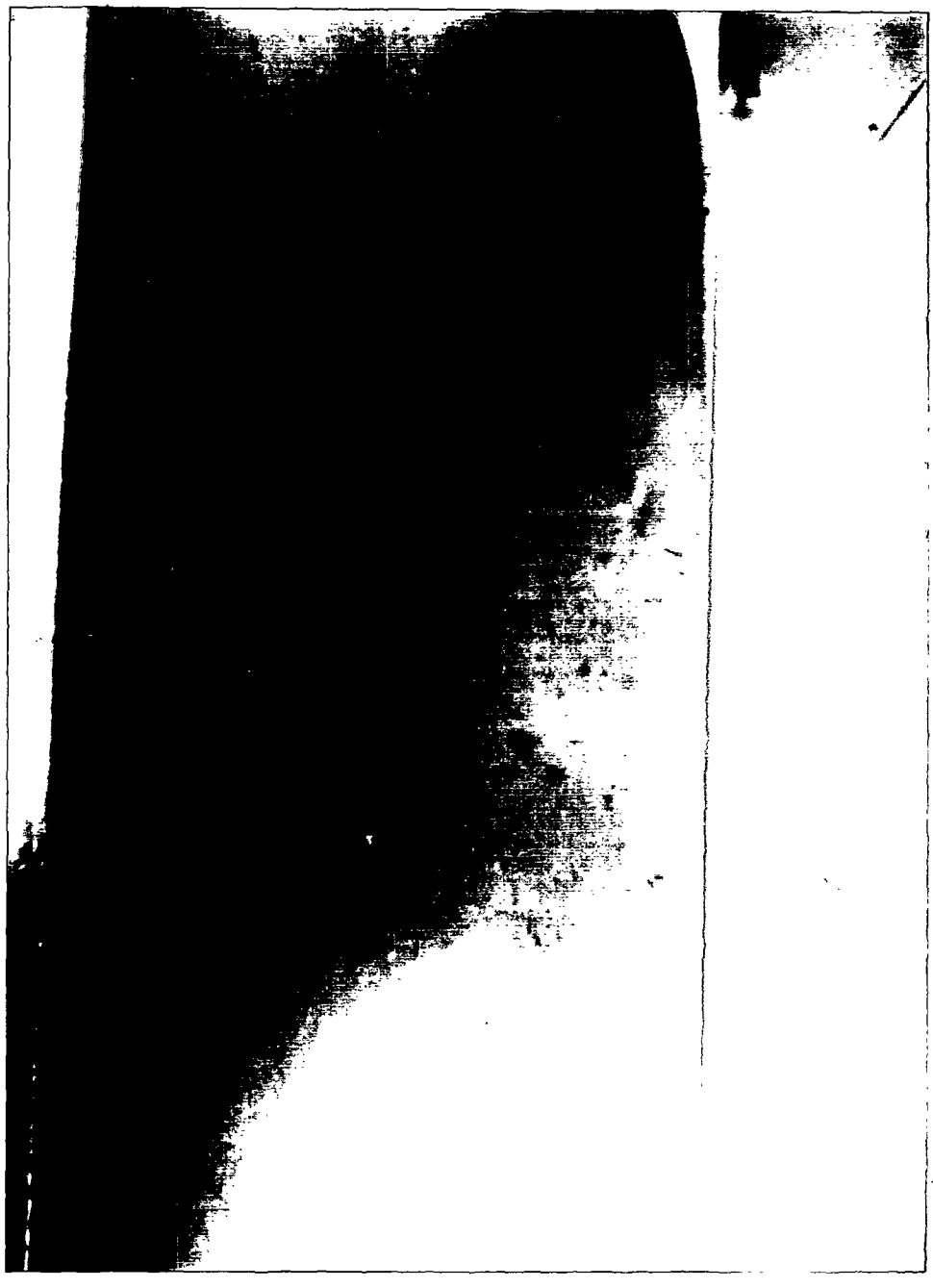

Figure 24. Top view of C-124-3, an asymmetric macrolap joint showing stable fracture and plane stress/plane strain type yield zone along end of the overlap.* Tensile loading was perpendicular to the edge of the overlap (i.e., across the page). Lap joint was photographed with plane polarized illumination at 16X magnification.

*Dark area is bonded portion of overlap. Lighter triangular areas of the overlap are debonded.

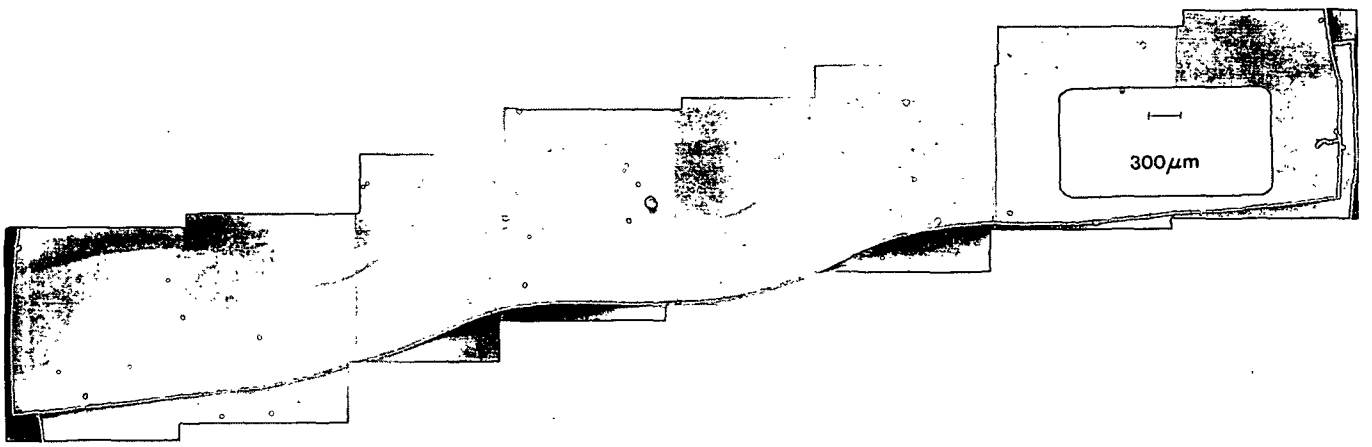

Figure 25. Top view of C-224-1, a scanning electron micrograph composite showing the three-dimensional corrugations that occur during stable fracture of some macrolap joints.*

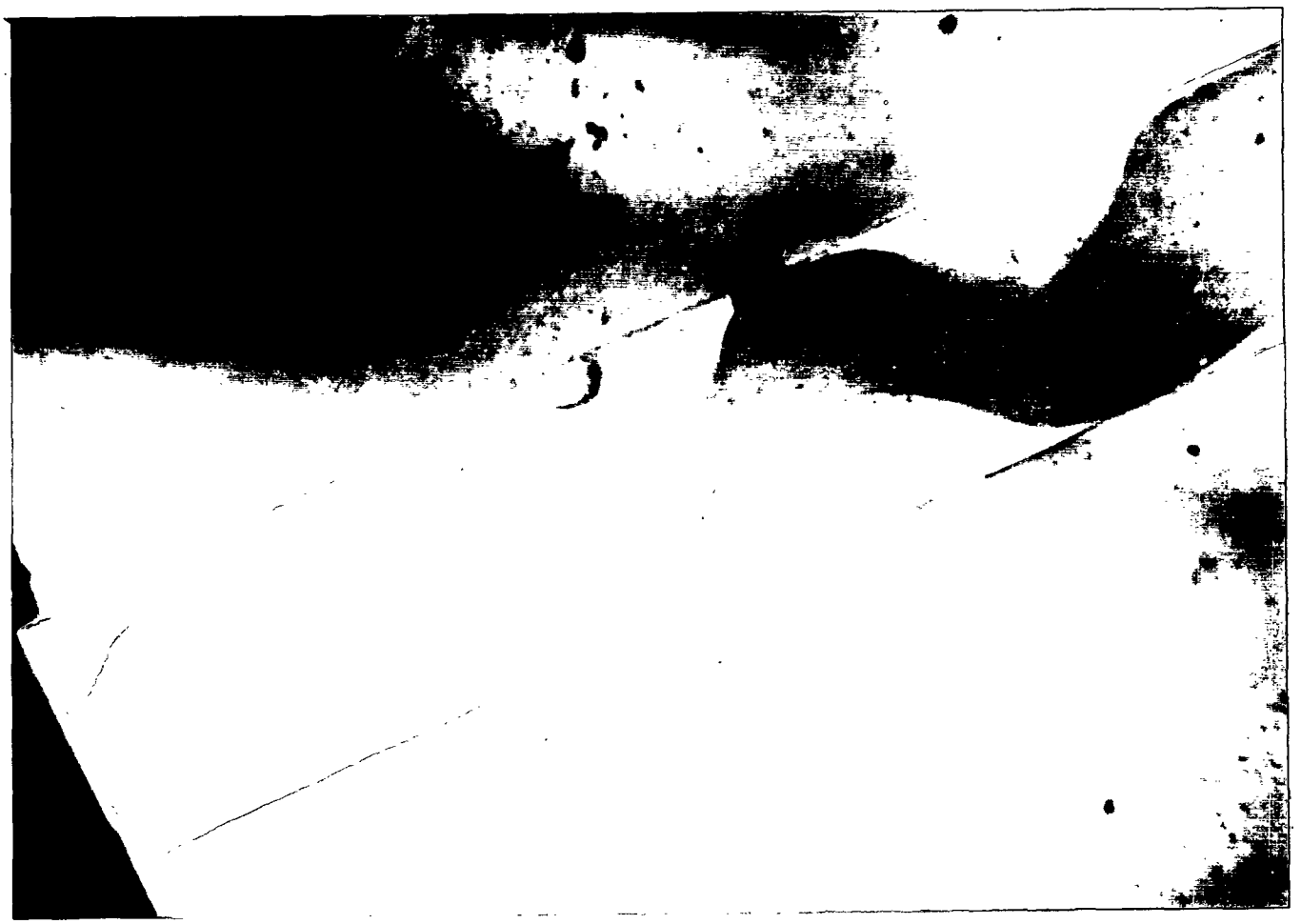

Figure 26. Top view of C-322-2, a corrugated stable fracture pattern for a 215 PD CD/CD macrolap joint. The darker oscillatory zone is the bond area as seen with plane polarized light at 16X magnification.*

*Tensile loading was perpendicular to the overlap edge (i.e., roughly top to bottom of page).

Compliance

Compliance (C) is the displacement of a body per unit applied load. For linear elastic bodies it is a constant for a given material, geometry, and direction of load application. To incorporate the same basic information (i.e., ease of deformation), the inverse of the apparent modulus, $1/E_a$ (obtained from the initial slope of the lap joint load/elongation curve), is substituted. Use of this modulus allows minor adjustments for differences in span and thickness, and a major adjustment for width. A plot of the inverse modulus of all symmetric lap joints prepared from 193 PUD-O cellophane is shown in Fig. 27. A general trend of decreasing inverse modulus with increasing bond length (L) is seen. This would be expected because total test span (S_t) is constant and as the overlap increases the amount of material increases, thereby reducing the average stress and total strain for a given load. Some of the differences between the macro- and microresults occur because the microtest span is much shorter, resulting in a greater reduction in inverse modulus from an increase in the overlap. This effect can be demonstrated through a simple equation based on the assumption that the overlap region carries a uniform stress which is half the uniform free fiber stress,

$$1/E_a = (2S_t - L)/(2S_tE), \qquad (16)$$

where E = cellophane adherend axial elastic modulus. This equation will be called the minimum inverse modulus model. It also represents a minimum stored elastic energy assumption.

From a comparison between these superimposed lines and the appropriate experimental results, it can be seen that the experimental lap joints have a higher inverse modulus than that predicted by Eq. (16). In virtually every case

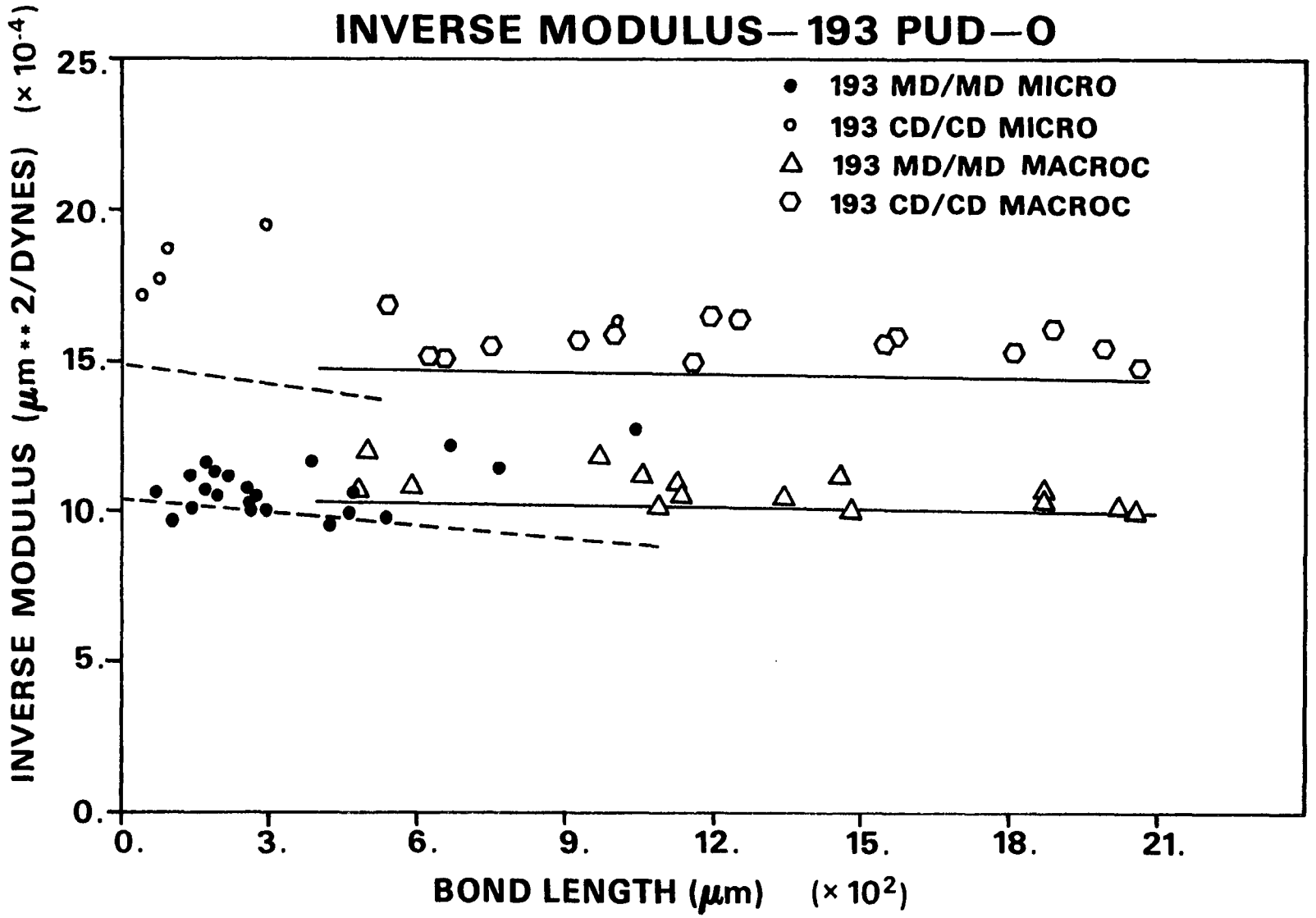

Figure 27. Relationship of inverse apparent modulus to bond length for the MD/MD and CD/CD configurations of the macro- and microlap joints. The minimum inverse modulus model is represented by the solid lines for macrolap joints and dashed lines for the microlap joints.

the lap joints have inverse moduli equal to, or greater than, the minimum case. The generally increased inverse modulus implies that the experimental structures have a stress distribution less uniform than that assumed for Eq. (16).

The inverse modulus data for the macrolap joints have a coefficient of variation similar to that obtained from the measurement of cellophane film elastic moduli, suggesting that material variability may be a substantial contributor to the inverse modulus variations observed for lap joints. No explanation has been found for the apparent systematic trend to more compliant microlap joints at the longer bond lengths. This trend does not seem to be directly associated with bond length. Both the high inverse modulus MD/MD and CD/CD lap joints are structures that ultimately show general yielding before failure.

Influence of Specific Structural and Material Parameters

The preceding experimental results and discussion have been focused on the behavior of all the lap joints, in general. All the mechanical parameters were presented as a function of bond length. From a continuum and fracture mechanics point of view the ratio of bond length to adherend thickness ($L/\overline{T}$) is more desirable because it provides a dimensionless parameter which describes the two-dimensional geometry of a lap joint. This facilitates the selection of lap joint geometries analogous to that of bonded wood fiber structures, where $L/\overline{T}$'s may range from 2 up to 20. This $L/\overline{T}$ range also encompasses the LEFM behavior region of most of the cellophane lap joints. It is this portion of the experimental results that will be discussed further, but from the perspective of individual parameter influences on lap joint strength. The separation between LEFM and transitional behavior was based on strain at failure, where a strain no greater than 0.5% was the criterion for inclusion in the following discussion of

linear elastic type behavior. This selection criterion assured that all lap joints included in the discussion failed at nominal axial stresses less than $(2/3)\sigma_{ys}$.

Bond Length

Bond length (bond area at constant width) is obviously a variable of interest. Essentially, it is the bond dimension in the direction of load application. From the previous discussions, it is clear that bond shear strength is highly dependent on L for the LEFM region (see Fig. 20). A linear regression analysis, employing a least-squares technique, confirmed that $\overline{\tau}$ and $L/\overline{T}$ are inversely correlated. The bond shear strength data from the LEFM region of Fig. 20 is plotted in Fig. 28 as a function of the inverse, $\overline{T}/L$. Superimposed on these data is the curve obtained for the regression analysis of these same data. An excellent fit of the curve to the experimental data is seen. Since all fibers were from 193 PUD-O film, $\overline{T}$ varies little, making $\overline{\tau}$ linearly dependent on 1/L. This is in accordance with the results obtained by Wang, et al.[60] for brittle fracture, where the stresses are concentrated in narrow zones at the bond ends. The reasonably constant value for the σ_{nom_c} results of Fig. 21 are also in agreement with this conclusion. If similar elastic behavior is present in bonded wood fiber structures, bond shear strength would be expected to vary as the bond area dimension in the direction of load application varied.

Fiber Width

Another aspect of bond area is the width, the bond dimension perpendicular to the direction of load application. Fiber widths in paper differ as a result of morphological factors and the degree of collapse resulting from process influences (e.g., pulping, beating, and wet pressing). From the literature, contradictory information was found about the influence of adherend width on lap

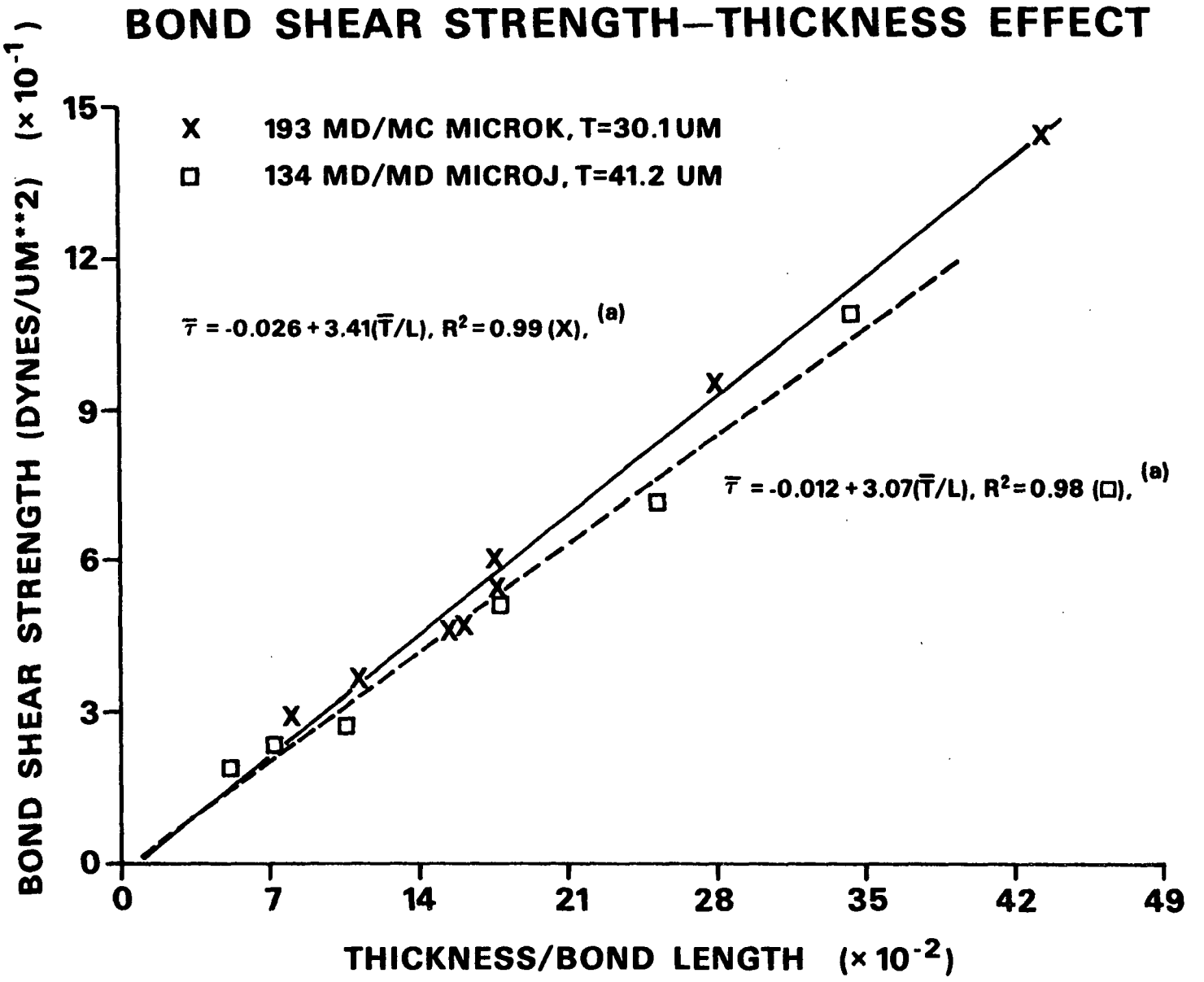

Figure 28. Effect of fiber thickness to bond length ratio on the bond shear strength of 193 PUD-O MD/MD microlap joints (ε_t < 0.5%).

[a] 99% confidence level based on F-test.

joint strength.[62,68] The results obtained from this experimental program are inconclusive. In Fig. 29 and 30 a slight decrease to no discernable effect on σ_{nom_c} is observed for increased bond width. Neither the limited macrolap joint data nor the regression analysis shown in Fig. 29 are sufficient to establish a definite influence for bond width. The difference shown in Fig. 31, however, is clearly evident and the regression analysis provides an equation in which most of the 76% explained variation is attributable to the variation in $1/\overline{W}$.

Why this inverse relationship between σ_{nom_c} and $\overline{W}$ is not shown in other plots is not known. Perhaps it is associated with the observed lesser tendency of the 134 PUD-0 macrolap joints to form corrugated overlap regions. This stability in the plane may result in more intense stresses from lateral contraction and thereby produce the lower strength for the wider lap joints of Fig. 31. Adams and Peppiat's[68] calculations for the effects of lateral contraction predict reduced lap joint strength as width increases up to an adherend width-to-thickness ratio ($\overline{W}/\overline{T}$) of 16. Macrolap joints are much wider, and the microlap joints narrower than $\overline{W}/\overline{T} = 16$.

Fiber Thickness

The same factors, natural and process, that determine fiber width, produce the differences in fiber thickness. An order of magnitude difference in fiber thickness could exist between an uncollapsed thick-walled latewood tracheid and a collapsed thin-walled earlywood tracheid. The macrolap joint results of Fig. 32 provide evidence that an increase in cellophane fiber thickness of less than a factor of two can substantially reduce the nominal axial stress at failure. From multiple linear regression analysis, it was found that over 50% of the variation in σ_{nom_c} is assignable to the variation in adherend thickness. A reasonably good fit of the three regression curves (one for each film average

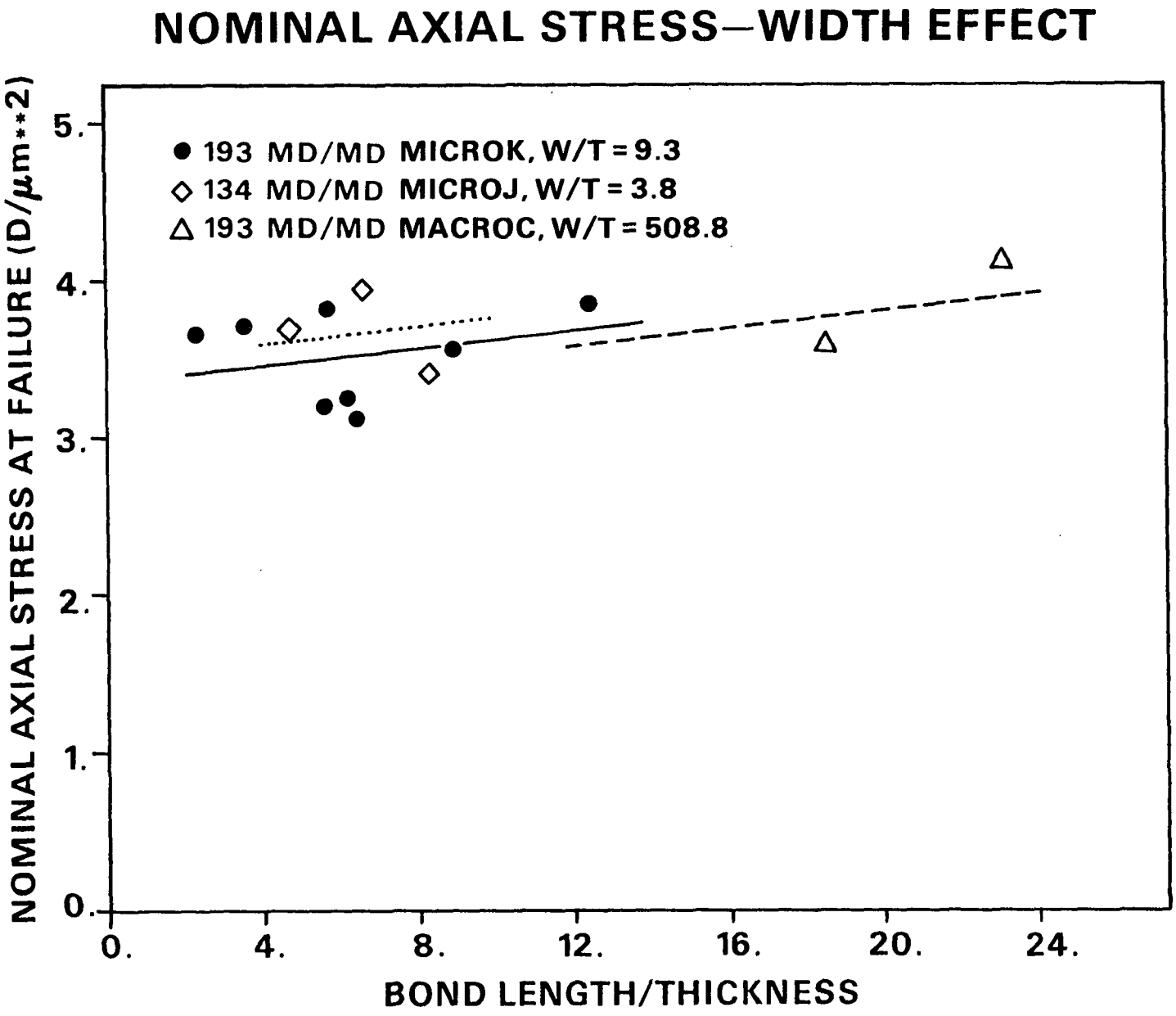

Figure 29. Effect of fiber width on the nominal axial stress at failure of 193 PUD-O MD/MD micro- and macrolap joints (ε_t < 0.5%).

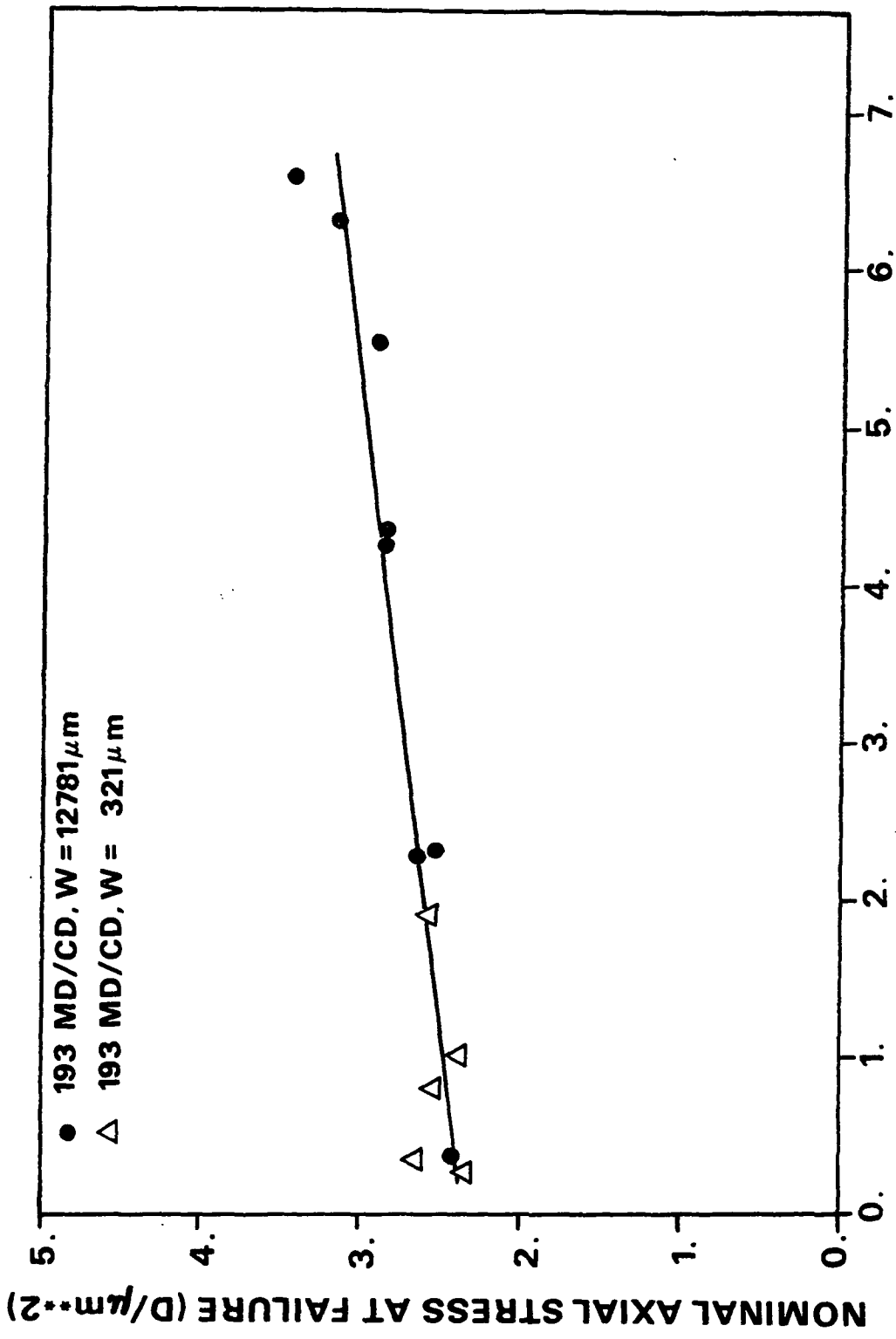

Figure 30. Effect of fiber width on the nominal apial stress at failure of 193 PUD-O MD/CD micro- and macrolap joints (ε_t < 0.5%).

---

a99% confidence level based on F-test.

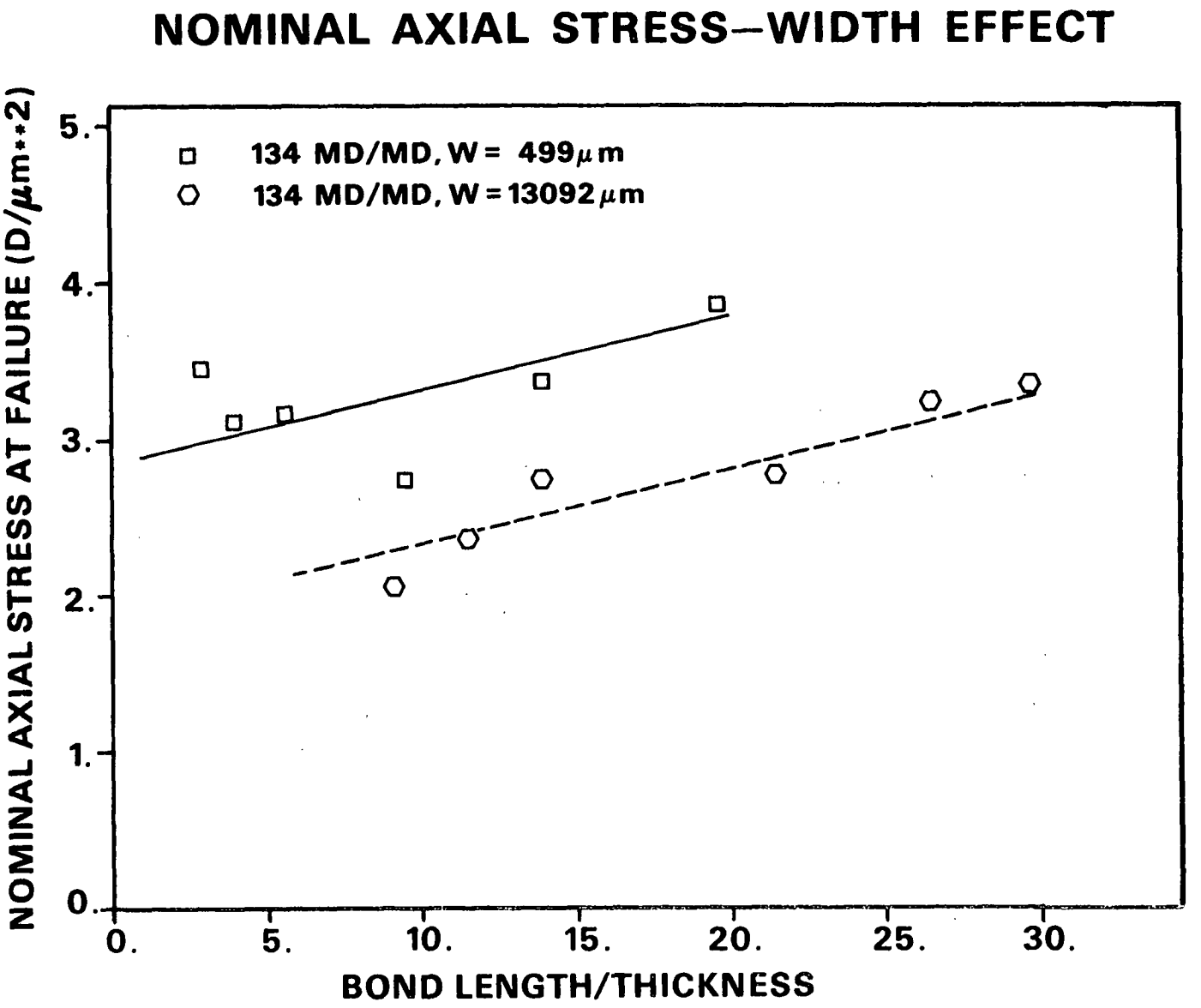

Figure 31. Effect of fiber width on the nominal axial stress at failure for 134 PUD-O MD/MD micro- and macrolap joints (ε_t < 0.5%).

[a]99% confidence level based on F-test.

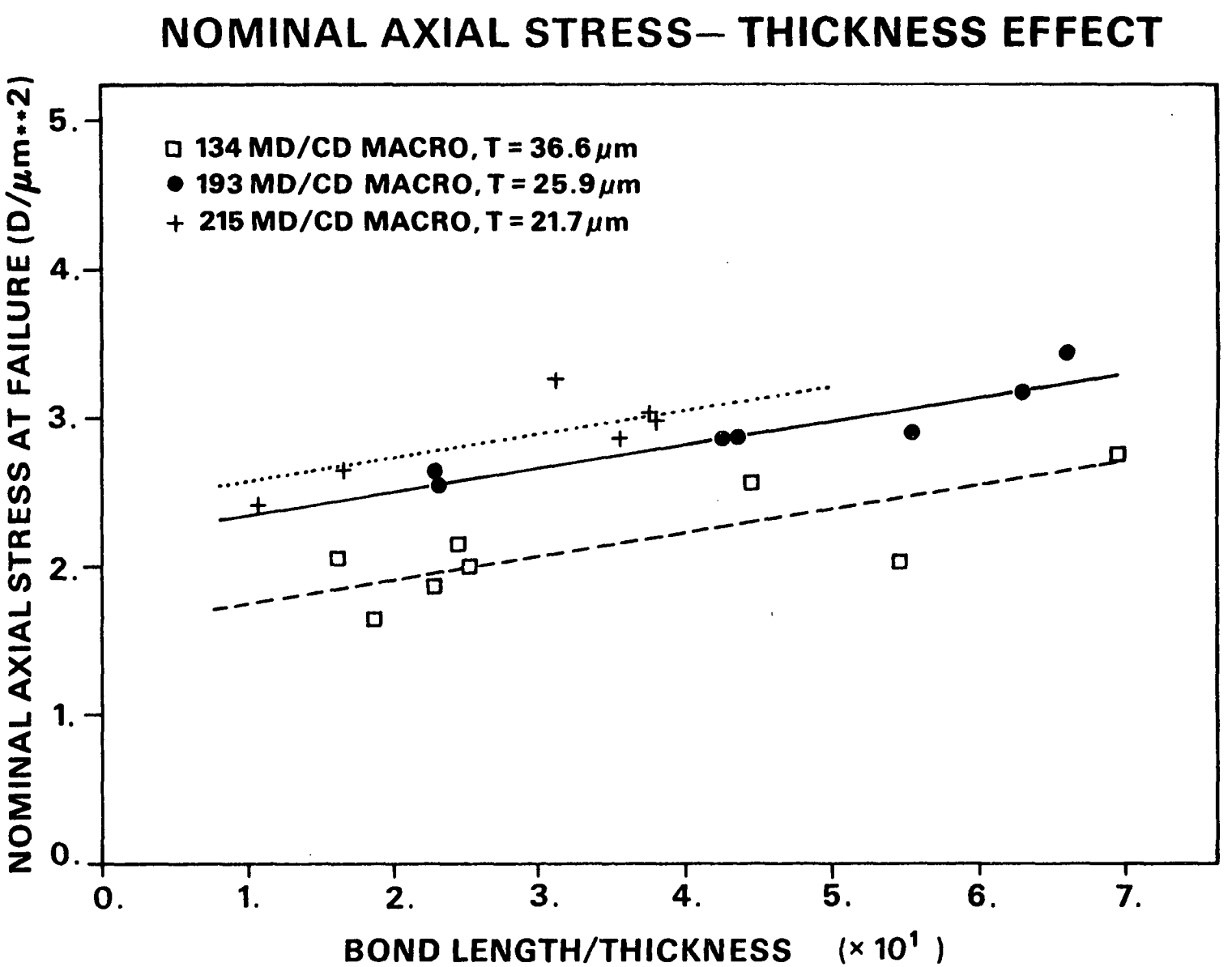

Figure 32. Effect of fiber thickness on the nominal axial stress at failure for cellophane macrolap joints with the MD/CD configuration (ε_t < 0.5%).

[a]99% confidence level based on F-test.

thickness) to the data can be seen in Fig. 32. A similar effect of reduced σ_{nom_c} for increased fiber thickness occurred in the microlap joint experiments (see Appendix V). The negative influence of fiber thickness on bond shear strength of the same microlap joints can be seen in Fig. 33. From the slopes of the regression lines, the decrease in bond shear strength for the thicker ($\overline{W}$ = 41.2 μm) 134 PUD-O fibers is evident.

In Fig. 32 and 33 the joint strength variables are plotted against the dimensionless structural geometry parameters, $L/\overline{T}$ and $\overline{T}/L$ (i.e., normalized bond length and its inverse). The value of using these dimensionless parameters is illustrated by noting that regression analyses employing L and 1/L show that $\overline{\tau}$ increased with fiber thickness while σ_{nom_c} declined. This apparent contradiction can be resolved by examining the basis for the effects of fiber thickness.

An increase in thickness moves the axis of loading further from the interfacial plane, thereby generating larger moments about that plane. An increasing tendency for the overlap region to rotate and a higher inverse modulus result. At the same nominal axial stress level more elastic energy will be stored in the system and, therefore, fracture can be expected to occur at a lower axial stress level. Thus, the effects seen in the case of σ_{nom_c}. From literature evidence,[76] the reduction in σ_{nom_c} should be approximately proportional to $T^{-0.5}$. Since fiber cross-sectional area is increasing as $\overline{T}$, the total load at failure (P_c) increases as $T^{+0.5}$. Bond shear strength, at the assumed constant bond length, depends only on P_c and, therefore, is increasing as $T^{0.5}$.

If, however, constancy of the dimensionless parameter, $L/\overline{T}$, is assumed, bond length increases as $\overline{T}$ and bond shear strength changes as $T^{-0.5}$. To illustrate this predicted effect, the $\overline{\tau}$ and $\overline{T}$ data from Fig. 33 are examined.

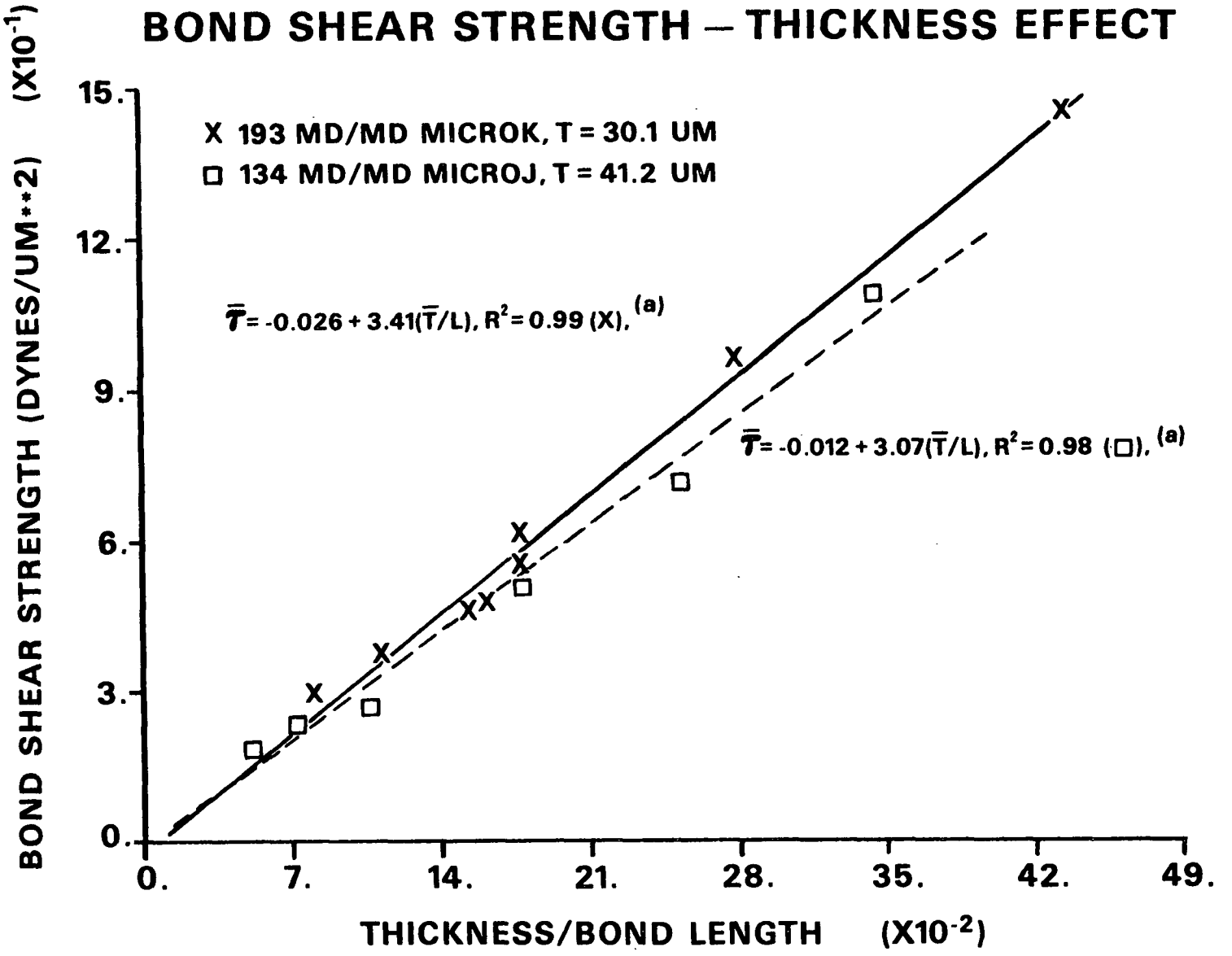

Figure 33. Effect of fiber thickness on the bond shear strength of MD/MD cellophane microlap joints ($\varepsilon_t \leq 0.5\%$).

[a]99% confidence level based on F-test.

From the increase in fiber thickness of 134 PUD-0 over 193 PUD-0, the bond shear strength ratio should be 0.85. The ratio of the slopes of the regression line is 0.90; a quite reasonable agreement. In the case of constant width lap joints, the dimensionless variable is preferred because it automatically adjusts for the amount of material in the fiber cross section. If one assumes sufficient fiber strength, these results suggest that the same mass of material distributed in fewer, but thicker, fibers would reduce the total load supportable by that mass. This suggested result coincides with the known strength difference between papers composed of latewood fibers and those papers made from earlywood fibers.

Fiber Modulus

In wood fibers, greater thickness is usually associated with smaller fibril angles and consequently higher axial moduli (E). Page, et al.[8] have shown that these moduli may differ by a factor greater than four. Fiber modulus definitely is a variable of interest. It is incorporated in the fracture mechanics displacement field equations and it is fundamental to the ability of a structure to store elastic strain energy. The higher the elastic modulus, the higher the stress required to store the same strain energy. If the energy required for fracture is a constant, a higher stress will be required to fracture a higher modulus material. The expected relationship from fracture mechanics,[83] is that σ_{nom_c} will increase as $E^{0.5}$. A change for the 193 PUD-0 fibers from the machine direction modulus (E_{MD}) parallel to the cross-direction modulus (E_{CD}) to the fiber axis would be expected to reduce nominal axial stress at failure to 83.4% of the MD/MD value. For the microlap joint results shown in Fig. 34, σ_{nom_c} for the CD/CD configuration decreased to 88.6% of the MD/MD value. This compares favorably with the predicted change.

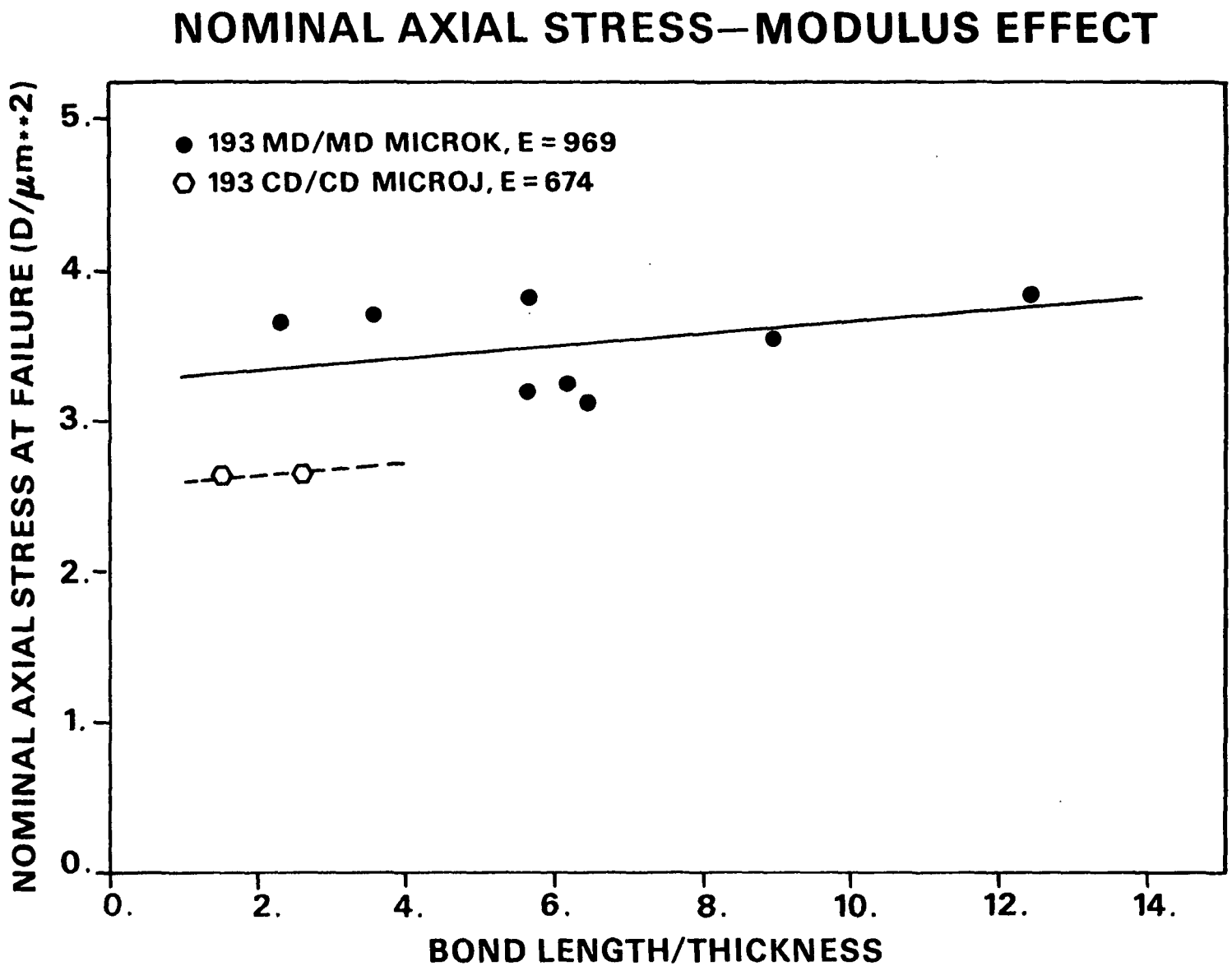

Figure 34. Effect of fiber axial modulus on the nominal axial stress at failure of 193 PUD-O microlap joints ($\varepsilon_t \leq 0.5\%$).

[a]99% confidence level based on F-test.

The limited range of the CD/CD configuration data results from its lower yield stress in the CD direction of cellophane (5.38 vs. 7.37 dynes/μm^2). Linear elastic behavior is confined to shorter bond lengths ($L/\overline{T} < 3$), because σ_{nom_c} only decreases as $E^{0.5}$ while σ_{ys} decreases by approximately E. At larger $L/\overline{T}$'s, the 193 PUD-O CD/CD microlap joints pass through the transition region and exhibit extensive yielding (both in the free fiber span and the overlap region). Evidence of free span yielding can be seen in Fig. 35, where enlarged subsurface vacuoles have developed slitlike openings in the surface. Above the bright line, which is the line delineating the beginning of the overlap, fracture plane disruptions and blistered elongated vacuoles (subsurface) are visible. Closer examination of a similar fracture surface region of the second adherend, shown in Fig. 36, reveals surface striations perpendicular to the loading axis. They are parallel to the machine direction and have a fairly regular spacing of 1.5 to 2.0 μm.

If the implications of the modulus effects observed are extended to the bond shear strength difference between earlywood and latewood fibers, a ready explanation can be obtained. Latewood fibers have a much higher axial modulus than earlywood fibers and, therefore, would tend to have higher bond strengths. Unfortunately this single parameter explanation ignores the influence of fiber thickness, bond length, and bond asymmetries.

Bond asymmetries could result from fibers of different thickness or modulus forming a fiber lap joint. In the general fiber-fiber bond case, crossing angle produces additional asymmetries. Asymmetry is obviously a common feature of fiber-fiber bonds.

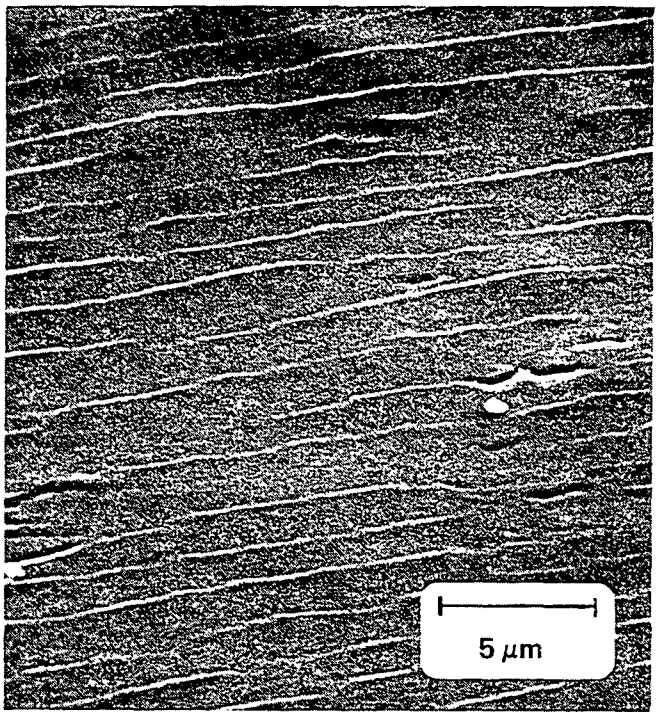

Figure 35. Scanning electron micrograph of the fracture surface of a 193 PUD-0 CD/CD cellophane microlap joint, L-096.*

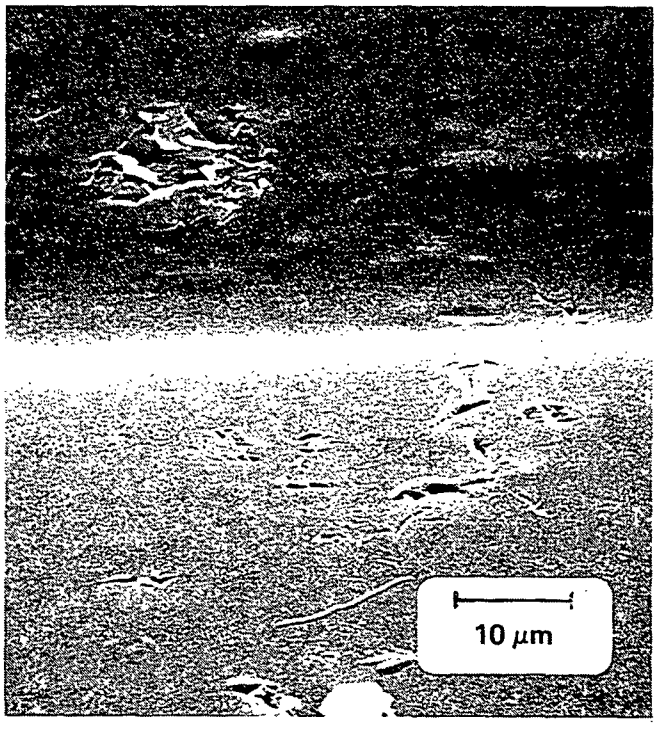

Figure 36. Scanning electron micrograph of the postfracture adherend surface of a 193 PUD-0 CD/CD cellophane microlap joint, L-096.*

[a]Photographed with stage tilted at 45° angle, as a result, top to bottom dimensions are reduced. Tensile loading was from top to bottom of photograph.

Material Asymmetry - Modulus

Material asymmetry effects have already been shown to be a significant factor in the strength of 215 PD MD/CD macrolap joints (see Fig. 22). They were observed to produce a substantial reduction in σ_{nom_c} and extend the bond length range within the elastic region. The results for a similar modulus asymmetry in 193 PUD-O MD/CD microlap joints are presented in Fig. 37. Data from Fig. 34 are included for comparison purposes. Nominal axial stress at failure is reduced 29% from the MD/MD configuration. When a dummy variable was used, multiple linear regression analysis produced the two equations of Fig. 37. About 80% of the variation in σ_{nom_c} can be assigned to the asymmetric configuration. Only a slightly greater decrease than that produced by the lower modulus CD/CD symmetric construction is seen. The similar modulus asymmetry effect on bond shear strength is illustrated by the difference between the regression line slopes of Fig. 38. Both regression equations show excellent fit to the data.

For a given applied axial stress, the CD fiber will deform more than the MD fiber. This will produce an intense strain gradient across the bonded bimaterial interface. Shear stresses will be more intense in the crack tip region,[104] particularly at the crack tip associated with the end of the high modulus (MD) fiber. Poisson ratio differences also help intensify stresses by promoting lateral contraction differences between the two adherends. Fracture initiation will preferentially occur at the crack tip with the most intense stress field.

This modulus asymmetry condition is recognized easily in the 90° crossing bond models using commercial cellophane, wood fibers, and various combinations thereof. The same is true for virtually every bond in paper. Another asymmetry results from different thickness fibers forming a bonded structure.

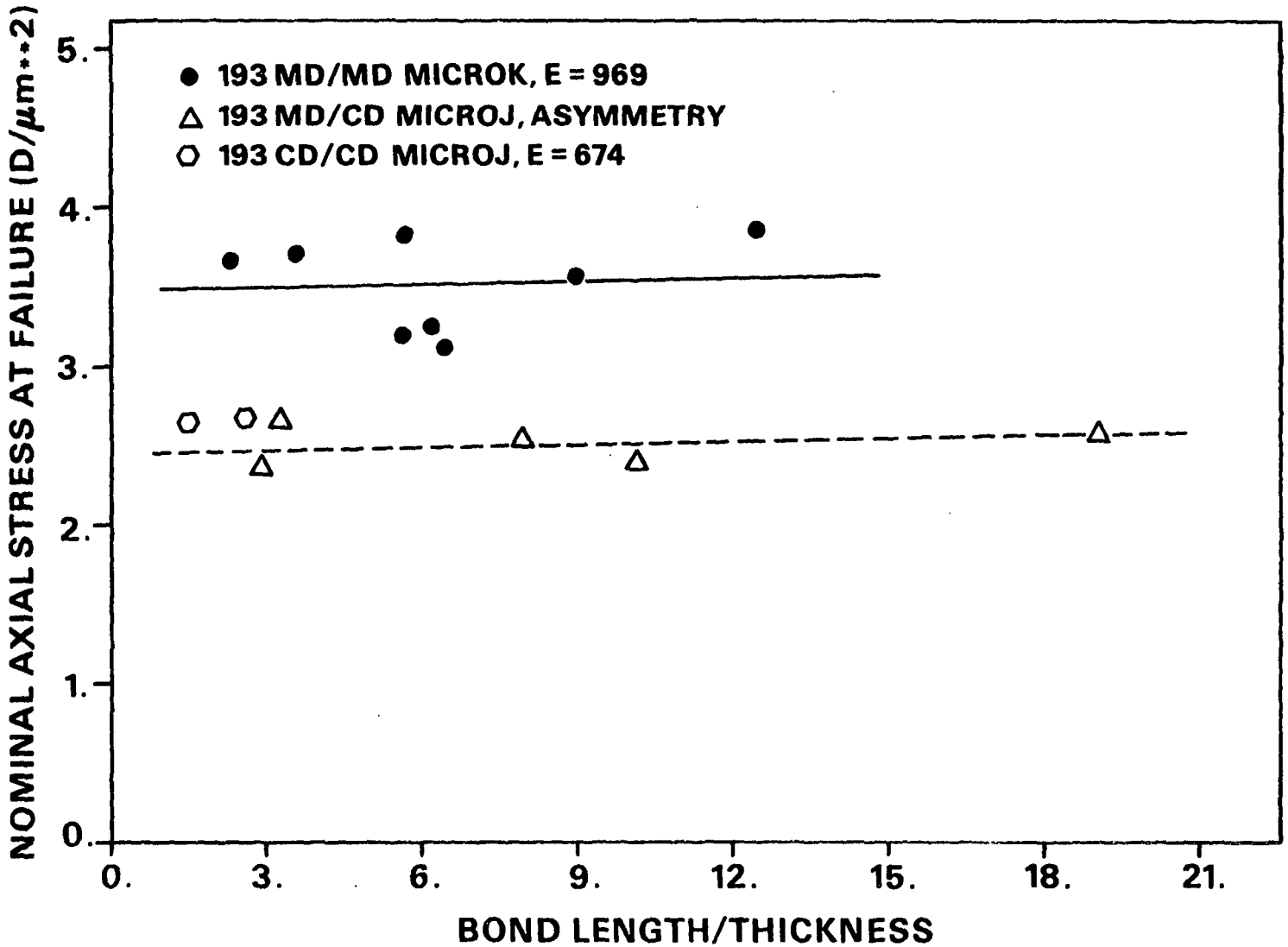

Figure 37. Effect of modulus asymmetry on the nominal axial stress at failure of 193 PUD-O microlap joints ($\varepsilon_t \leq 0.5\%$).

[a]99% confidence level based on F-test.

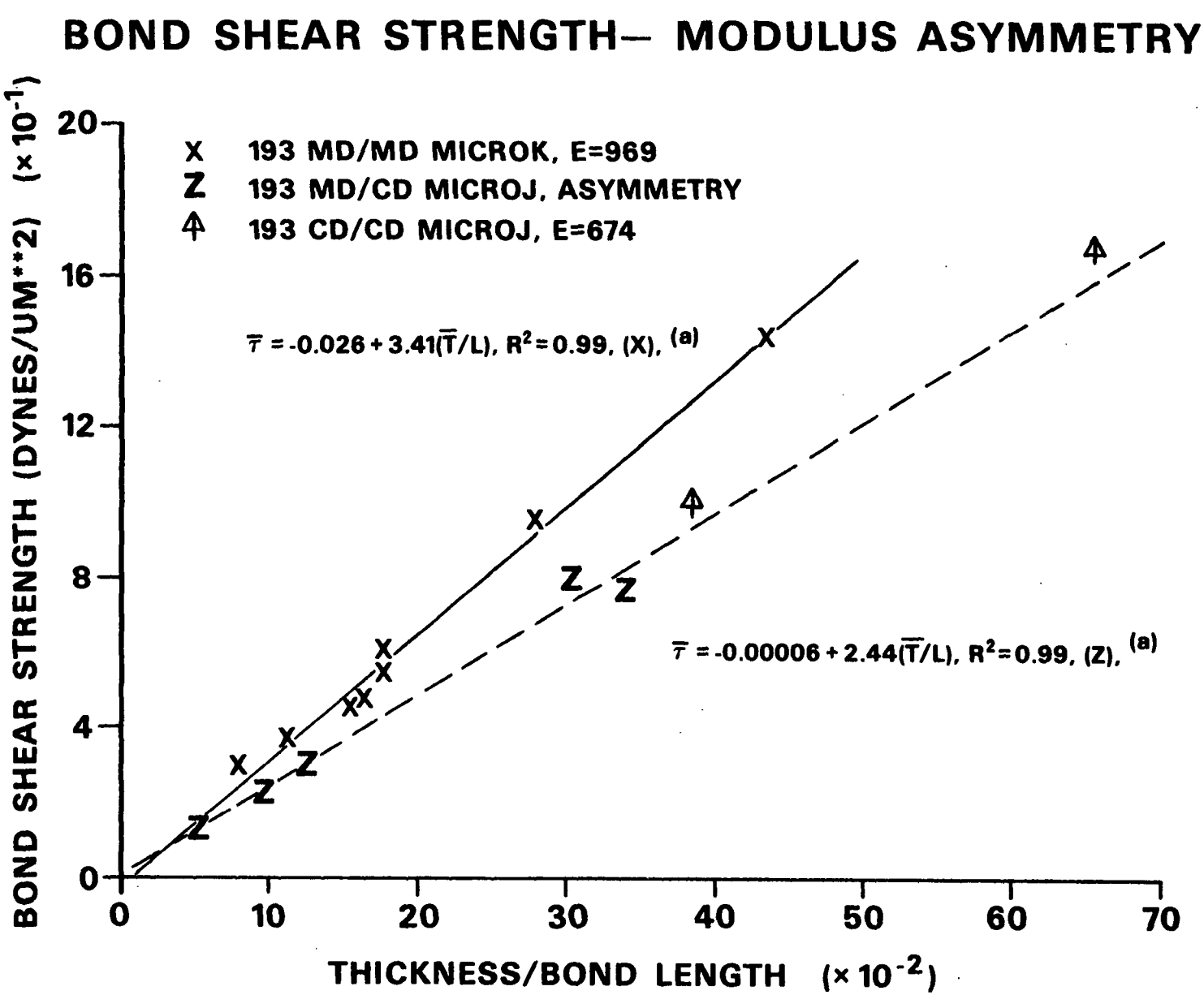

Figure 38. Effect of modulus asymmetry on the bond shear strength of 193 PUD-O microlap joints ($\varepsilon_t \leq 0.5\%$).

[a] 99% confidence level based on F-test.

Dimensional Asymmetry - Thickness

Most paper is formed from pulps with broad fiber-thickness distributions resulting from morphological and process factors. At least minor thickness differences should be present in every bond. The data presented in Fig. 39 leave little doubt about the detrimental effects of this type of asymmetry on bond shear strength. A 33% reduction in $\bar{\tau}$ from the 193 PUD-O MD/MD condition is found for the 193/134 combination. Since there is no significant difference between the mechanical properties of these two films (see Table 2), most of the substantial bond strength decrease must be attributed to the asymmetry. The 134 PUD-O fiber will experience an axial stress which is only 73% of stress in the 193 PUD-O fiber. As a result of this difference in axial stress between the two adherends, a sharp strain gradient will exist across the bond resulting in more intense stresses, particularly around the crack tip at the end of the thicker fiber (134 PUD-O). Fracture will be more likely to initiate at that crack tip, as was seen for the asymmetric structure in Fig. 24. The more intense stress fields result in failure at lower axial stress and bond shear strength for this thickness asymmetry.

The implications are the same for both asymmetries. They will reduce bond strength through the production of more intense stress fields than the symmetric case. Because these asymmetries are inherent in the paper structure, all bonds may experience significant strength reduction.

Conformability

Two other factors, conformability and interfacial cracks, were investigated. The extent that one fiber conformed to the end of the fiber to which it was bonded was called conformability. Conformability effects are of interest in

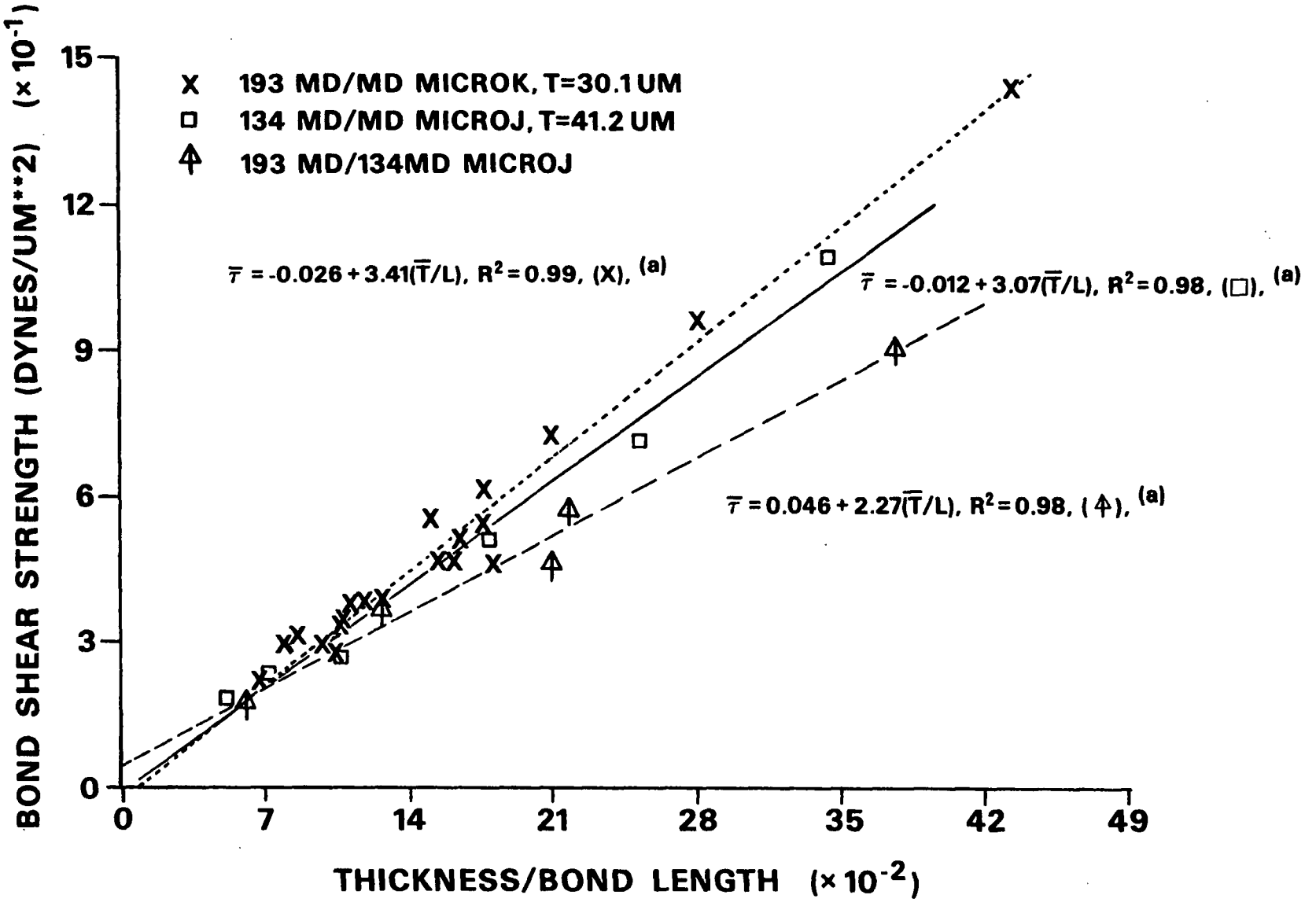

Figure 39. Effect of thickness asymmetry on the bond shear strength of cellophane microlap joints ($\varepsilon_t \leq 0.5\%$).

[a] 99% confidence level based on F-test.

relation to the influence of beating and wet pressing on bond strength and compliance.

As discussed earlier in the presentation of these experimental results, two microlap joint preparation techniques were used (p. 58). The conforming lap joints exhibited a higher and more uniform degree of conformity than did the single lap joints (compare Fig. 15 and 16). Statistical analyses of the bond shear strength of microlap experiments K and D-2 suggest that the separate regression curves shown in Fig. 40 describe the results better than a single curve or parallel curves. Some small difference may exist between these experiments, but since $\overline{T}/L$ tends to 0.0 as L increases (at constant $\overline{T}$) $\overline{\tau}$ should tend to 0.0 and therefore the intercept (b_o = 0.106) should be much closer to 0.0 to provide the necessary confidence in the conforming lap joint data. The nominal axial stress data for the conforming lap joints (Fig. 41) show a sharper decline with decreasing $L/\overline{T}$ than would be expected based on the behavior of the other lap joints, including the conforming lap joints with interfacial cracks. This may be a result of (1) data variability, or (2) an increased amount of greater energy consuming shear type failure as a result of reduced moments about the bond plane.[73,87]

Interfacial Cracks

Like asymmetries, interfacial cracks in the fiber-fiber bonds of paper show a decrease in joint strength of 14.2%. The uncracked conforming lap joint data (Experiment D-2) are between these two extremes (see Fig. 41). Scanning electron microscopic examination of the fracture surfaces of the interfacially cracked structures did not reveal any evidence of other than interfacial failure. No permanent deformation could be found to be associated with the stable cracks that existed in these microlap joints (Fig. 10 and 16b).

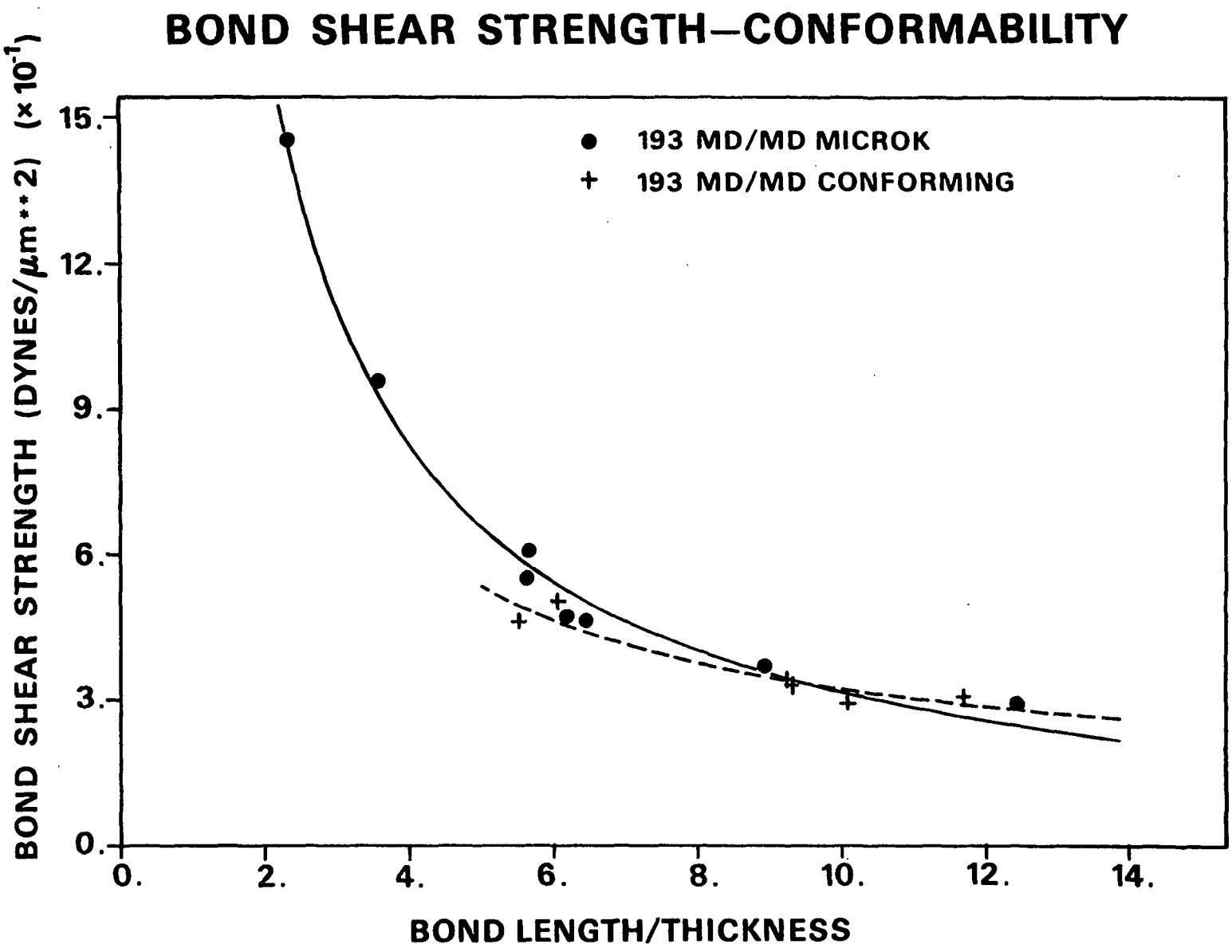

Figure 40. Effect of fiber conformity on the bond shear strength of 193 PUD-0 MD/MD microlap joints (ε_t < 0.5%).

[a]99% confidence level based on F-test.

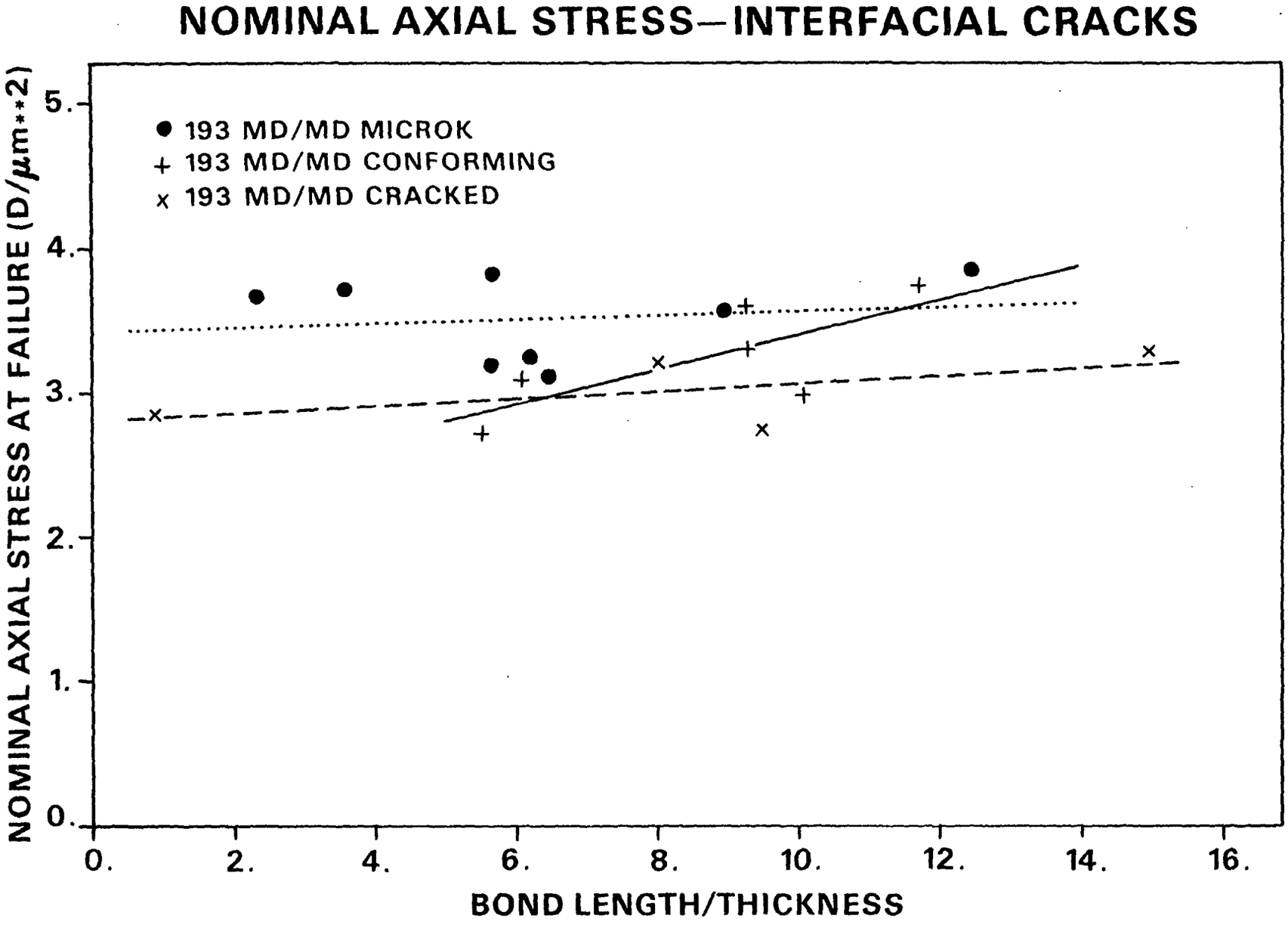

Figure 41. Effect of interfacial cracks on the nominal axial stress at failure for 193 PUD-O MD/MD microlap joints ($\varepsilon_t \leq 0.5\%$).

In addition to changes in the notch are the changes in the spatial arrangement of the adherend center lines relative to the bonded interface. As the adherend center lines move toward the bond center line, the moments are reduced and tendency for the overlap region to rotate decreases. As a result, the compliance of the lap joint decreases as conformity increases. In Fig. 42 is the same minimum inverse modulus line [based on Eq. (16)] shown in Fig. 23. The conforming microlap joints fit this line very well. So do the shorter bond lengths of Experiment K, the least conforming microlap joints. In fact, the trend of the MICROK results is for a decreasing compliance with decreasing bond length, a result expected from the previous observation that conformity increased with decreasing bond length (a consequence of the preparatory method) as observed in Fig. 16, a and b. The conforming lap joints with interfacial cracks (CRACKED) generally have a higher inverse modulus than the uncracked, MICROK. The concept of increased fiber thickness increasing moments about the bond, leading to increased inverse moduli (energy storage), is supported by the obviously higher inverse moduli of the thicker 134 PUD-O microlap joints.

The increased in-plane moduli of paper resulting from increased beating and wet pressing may be arrived at simultaneously by the dual routes of increased bond conformity and decreasing fiber thickness through fiber collapse. Increased bond area and number of bonds may be incidental beyond certain minimums required for structural integrity, because bond conformity and fiber thickness has such strong influence on the apparent modulus of the bond structure.

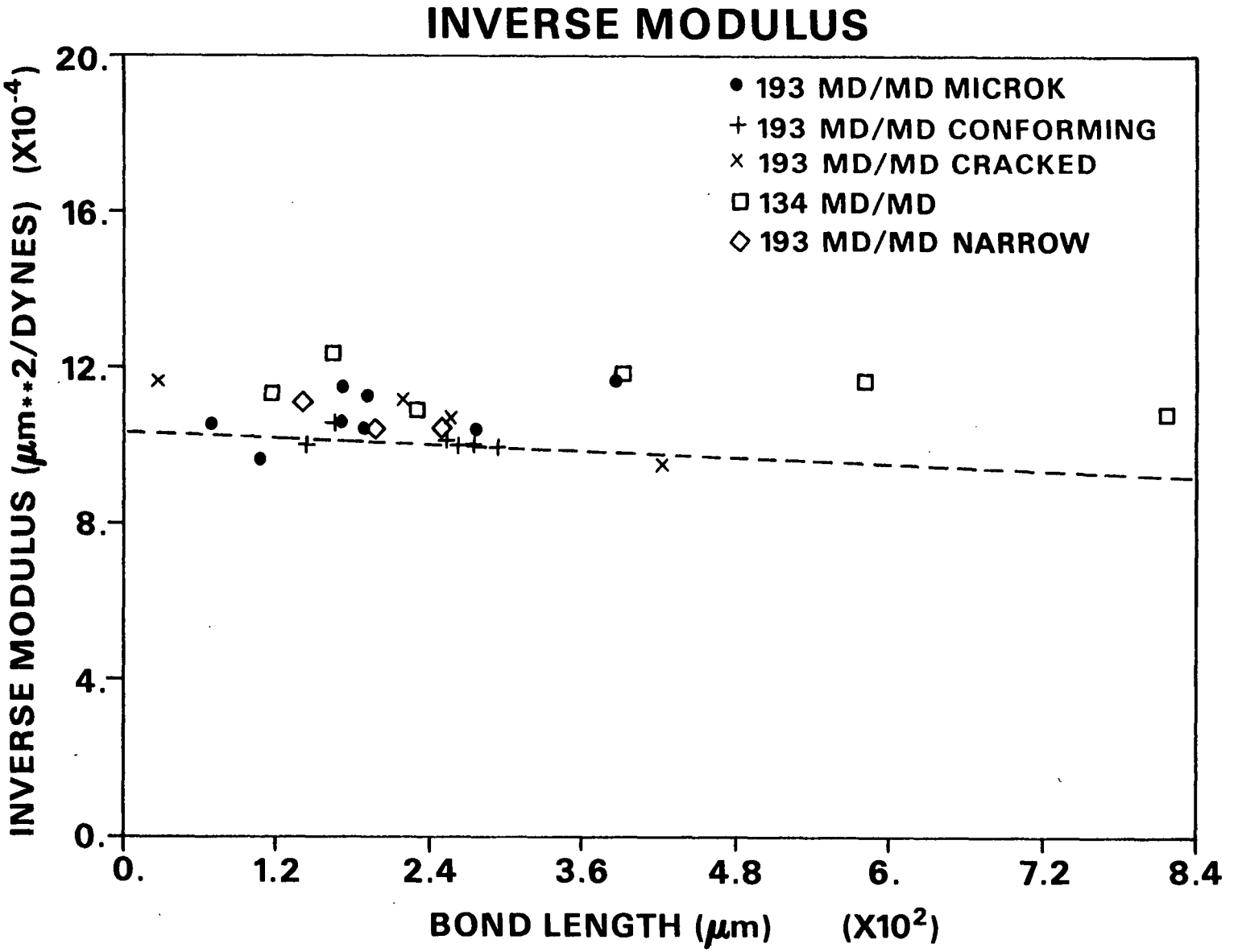

Figure 42. Relationship of inverse modulus to bond length for 134 and 193 PUD-O MD/MD microlap joints ($\varepsilon_t \leq 0.5\%$). Dashed line represents the minimum inverse apparent modulus model.

ANALYSIS OF THE EXPERIMENTAL RESULTS

If one could isolate the preceding variables for wood fibers, a similar experimental analysis could be accomplished. Unfortunately, such experiments are not readily performed. Knowledge of the expected relationship between these variables and bond strength, however, can be used to direct experimental measurements and the selection of independent variables and their form for inclusion in regression equations. From the experimental results we expect bond length, thickness, width, modulus, total crack length (a_t), and asymmetries to be important variables in determining lap joint strength.

Although bond shear strength has been used as a measure of the strength of the adhesive and the lap shear joint, its usefulness depends on the extent of linear elastic behavior. For bond shear strength to be useful in a predictive manner, a consistent bond region configuration and size must be maintained in testing and use. In linear elastic structures, where the failure loads (per unit fiber width) are reasonably constant, bond shear strength is dominated by bond length, precluding the reasonable examination of other influences on lap joint strength. Since the critical load (P_c) is normalized by the adherend cross-sectional area ($\overline{A_x}$), σ_{nom_c} describes the strength per unit of material, indicating the relative strength efficiency of that adhesive joint structure. Therefore, nominal axial stress at failure, σ_{nom_c}, is a better measure of lap joint strength in linear elastic systems.

Regression Analysis of Microlap Joint Data

Multiple linear regression analysis was performed on the overall experimental microlap joint data from the elastic behavior region. As can be seen in Table 4, about 64% of the variation in σ_{nom_c} could be correlated with $L/\overline{T}$, $\overline{W/T}$, a_t and E_a. As expected, $L/\overline{T}$ ($r = 0.21$) and E_a ($r = 0.67$) showed positive and

a_t (r = -0.24) negative correlations with the nominal axial stress at failure. A surprisingly strong negative correlation (r = -0.45) was found for $\overline{W/T}$. A coincidental link, to asymmetries, resulting from the asymmetric 193/134 configuration having higher $\overline{W/T}$ and considerably lower σ_{nom_c} values, may account for that outcome.

Table 4. Regression analysis results: nominal axial stress.

	—— Coefficient of Independent Variables ——							
Data Group	Intercept	L/T	W/T	E_a	a_t	R^2	F	$\frac{DF1}{DF2}$
All microlap[a] joints	1.821	0.0158	-0.0663	0.00223	-0.00481	0.64	14.99	4/34
All symmetric[a] microlap joints	2.559	0.0285	-0.0629	0.00133	-0.00501	0.55	7.26	4/24
All symmetric[a] single microlap joints	1.832	0.0230	-0.0397	0.00201	--	0.64	8.78	3/15

[a] $\varepsilon_t \leq 0.5\%$.

Subgroups of the microlap joints were also subjected to regression analysis. The results of the analyses are presented in Table 4. The same variables found important in the previous analysis remained prominent in the regression equations for the symmetric microlap joints. For the combined conforming and single lap structures, these variables accounted for 55% of the variation in σ_{nom_c}. Without cracked joints, the single lap joint group correlated with $L/\overline{T}$ (r = 0.36), $\overline{W/T}$ (r = -0.42), and E_a (r = 0.74) to the extent that 64% of σ_{nom_c} variation was attributable to the variation of these structural parameters. While it is agreeable to see the influence of these structural parameters confirmed, one must admit no great enthusiasm for explained variations of 64% or

less. The linear elastic lap joint behavior combined with fracture mechanics theory allows a more fundamental bond strength parameter, fracture toughness (G_c), to be estimated from the cracked lap joint data.

Fracture Toughness

An approach similar to Jemian and Ventrice's[74] is used. Equation (2) can be modified to accept the partial derivative of $1/E_a$ with respect to a_t, as follows:

$$C = S_t/(E_a\bar{A}_x) \quad , \tag{18}$$

which when substituted into Eq. (2) gives

$$G_c = [(P_c^2 S_t)/(2W_\ell \bar{A}_x)]\ \partial(1/E_a)/\partial a_t \tag{19}$$

S_t and $\bar{A}_x$ are constant for any given lap joint. If one assumes that $1/E_a$ is a linear function of a_t, the partial derivative can be approximated by the regression coefficient of a_t in a multiple linear regression analysis of $1/E_a$ against $(L + a_t)$ and other important structure parameters. L is the residual bond length in cracked structures; thus $(L + a_t)$ is needed for representing the original bond length and the structure's precracked compliance. The derivative is then approximated by the difference in the inverse modulus at crack length = 0 and a_t. Previous examination of the experimental compliance data showed a different relationship between $1/E_a$ and L for the single and the conforming lap joints (see Fig. 42). As a result, the conforming lap joints (Experiment D, 1 and 2) were regressed separately from the single lap joints (Experiment K). Table 5 contains a list of the results of these regression analyses. The regression coefficient of a_t was substituted into Eq. (19), along with the other required parameters, and G_c was calculated for each of the cracked microlap

joints. These parameters and calculated results are presented in Table 6. This fracture toughness, G_c, is an estimate of the fracture resistance of the bonded interface, not the bulk cellophane.

Table 5. Regression analysis results: inverse modulus.

Data Group	Intercept	—— Coefficient of Independent Variables —— $L_t + a_t$	W/T	W_ℓ	a_t[b]	R^2	F	$\frac{DF1}{DF2}$
Experiment[a] D1 and D2	0.144×10^{-2}	-0.437×10^{-6}	-0.105×10^{-4}	-0.590×10^{-6}	0.115×10^{-5}	0.62	1.64	4/4
Experiment K[a]	0.194×10^{-3}	0.304×10^{-6}	0.192×10^{-3}	-0.320×10^{-5}	0.171×10^{-5}	0.80	3.90	4/4

[a] $\varepsilon_t < 0.5\%$.
[b] Units = μm/dyne.

Table 6. Cellophane fracture toughness: interface bond.

FLER Curve No.	$\alpha(1/E_a)/\alpha a_t$ (μm/dyne)	P_c (dynes)	W_ℓ (μm)	S_t (μm)	A_x (μm²)	a_t (μm)	G_c [ergs/(cm²)]
K-989	0.115×10^{-5}	23,353	332	3512	8512	109.0	3900
K-992	0.115×10^{-5}	29,767	342	3555	9054	69.0	5860
L-001	0.115×10^{-5}	25,719	320	3598	8030	21.0	5326
L-112	0.171×10^{-5}	23,353	299	3570	8202	81.7	6777
						Mean =	5466
						Standard Deviation =	1204
						Coefficient of Variation =	22%

The mean, 5466 ergs/cm², is more than two orders of magnitude greater than the surface energy of a cellulose substrate, but comparable to the lower Nordman bonding strength values of paper, when the gas adsorption technique is employed. The fracture toughness of cellulose acetate, as listed by Seth and Page,[106] is

three orders larger, and their G_c values for commercial papers are up to four orders of magnitude larger than the 5466 ergs/cm^2 obtained here.

A coefficient of variation of 22% and the limited amount of data on which G_c is based, invite caution. Its worth can only be assessed through an examination of its ability to allow prediction of the strengths of a variety of cellophane lap joint configurations. The following Theoretical Program provides a test of this predictive capability in a linear elastic fracture mechanics model of the experimental cellophane lap joint structures.

THEORETICAL PROGRAM

BACKGROUND

From the preceding experimental results and discussion, it is clear that those cellophane lap joints which fail at total strains less than 0.5% do so in a manner consistent (in a qualitative sense) with linear elastic fracture mechanics theory. In this Theoretical Program, the development and evaluation of a linear elastic model of these experimental fiber-fiber bonds is presented. To meet the objective of this portion of the thesis, a direct displacement finite element method of stress analysis is combined with linear elastic fracture mechanics theory to yield a model capable of predicting the displacements, stress distributions, and strength of the experimental fiber-fiber bonds.

A brief review of the literature on the use of standard code finite elements in fracture mechanics is presented. The development of the model, and a discussion of the computer programs which implement it, follow the literature review. Presentation and discussion of the model predictions conclude this section.

FINITE ELEMENT METHODS IN FRACTURE MECHANICS

Utilization of Standard Code Elements

One of the first publications in which the finite element method was used to solve standard fracture mechanics problems was that of Chan, et al.[107] in 1970. Kobayashi, et al.,[108] Anderson et al.,[109] and others presented similar applications shortly thereafter. In 1971, Gallagher[110] surveyed and evaluated the numerous early attempts to use the finite element method in fracture mechanics. He separated these efforts into four classifications: (a) direct, (b) energy-based, (c) superposition, and (d) singular function methods. The direct,

energy-based, and superposition methods involve no change in the standard finite element codes. The singular function method requires the inclusion of the crack tip singularity in a special element which is usually restricted to the immediate crack tip zone.

In the direct method, two approaches were used. Fracture problems were solved with highly refined element meshes in the crack tip zone. In the one case, Chan, et al.,[107] the analytical fracture mechanics stress field equations were used to calculate the Mode I stress intensity factor, K_I, which was calculated along a radius from the crack tip by substituting the calculated element stresses, the corresponding radial distance from the crack tip (r), and other parameters into Eq. (4). These estimated stress intensity factors were then plotted against r. Typical plots showed lower K_I values for the elements close to the crack tip, but as r increased K_I increased to a maximum and then declined linearly. The approximately linear portion was extrapolated to r = 0 to obtain K_I. A similar, but better, approach for the direct displacement type formulation used the linear elastic displacement field equations and the calculated model displacements to obtain the K_I vs. r plot.[107-109]

Equation (4) and its displacement field counterpart are only valid as $r \to 0$. By using the expanded form of Eq. (4), Oglesby and Lomacky[111] found that the questionable extrapolation technique could be avoided because a reasonably constant maximum K_I value was obtained. They also found that these results were within 1% of the values obtained analytically. A set of expanded displacement field equations are formed for pairs of adjacent nodes.

$$u_r = (K_I/4\mu)(r/2\pi)^{1/2} f_1(\nu,\theta) - (K_{II}/4\mu)(r/2\pi)^{1/2} f_2(\nu,\theta) + 2\alpha_1(r/4\mu) f_3(\nu,\theta)$$
$$U_\theta = (K_I/4\mu)(r/2\pi)^{1/2} f_4(\nu,\theta) - (K_{II}/4\mu)(r/2\pi)^{1/2} f_5(\nu,\theta) - 2_1(r/\mu) f_6(\theta) + \alpha_2(r/\mu) f_7(\nu), \quad (20)$$

where u_r = radial displacement

u_θ = angular displacement

μ = shear modulus

These equations are then solved simultaneously to yield the stress intensity factors, K_I, K_{II}, and the expanded term coefficients, α_1 and α_2.

Two of the three energy approaches that Gallagher[110] identified have found general acceptance. The first is a total energy method, in which the total stored elastic energy (U_0) is calculated at crack length a_0 and again (U_1) for an incremental increase (Δa) in crack length. Using Griffith's concept [Eq. (3)] at constant load conditions, a fracture toughness (G_c) is calculated through estimation of the derivative $\partial U_t/\partial a$ by $(U_1 - U_0)/\Delta a)$. Anderson, et al.[109] found that this approach provided very good fracture toughness estimates [or stress intensity factors by Eq. (8) for pure mode problems] for fewer degrees of freedom than did the direct methods. This approach requires double sets of finite element calculations.

An energy technique which requires only one set of finite element calculations is the line-integral method (J-Integral) of Rice.[112] This path independent integral, taken over the boundary (Γ) of a region containing the crack, is equal to a constant J. Rice[112] has shown that under conditions of linear elastic behavior, J is equal to the strain energy release rate (G). The J-Integral approach also appears to be a useful fracture criterion for situations involving either small or large scale plasticity prior to fracture.[113] Chan, et al.,[107] Anderson, et al.,[109] and Kobayashi, et al.[108] found this approach to provide more accurate stress intensity factor estimates than the direct methods at equal degrees of freedom. The energy methods do not permit

calculation of separate stress intensity factors from mixed mode fracture problems.

The superposition technique mentioned by Gallagher[110] involved fitting the finite element displacement calculations, by external load adjustment, to the analytical solution displacements in the crack tip region. This approach has extreme data manipulation difficulties.

The fourth approach mentioned by Gallagher[110] was the use of special crack tip elements which incorporate the known singularity in the element formulation. These singular elements are discussed in Appendix I, along with the general review of the various types of finite element displacement functions.

DEVELOPMENT OF MODEL

The material to be modeled is viscoelastic, but behaves approximately as an orthotropic linear elastic medium at strains less than 0.5%. Axial extension, out-of-plane bending, and overlap region rotation occur as a result of moment generation by asymmetric and complex loading/restraint conditions. As a consequence of the conformable nature of wet cellophane, the geometry of the included angle of the notch tip may range from perhaps 45° to a maximum 90°. The model must be able to represent interfacial cracks. Finally, the model must be able to predict the fracture of structures with these various features through a consistent set of fracture criteria. A discussion of how each of these model requirements are satisfied follows.

Selection of Analysis Technique

Two very basic approaches to the development of the model are the analytical and the numerical routes. While it may be possible to model this problem by

analytical approaches similar to DeVries, et al.[73] or Chang and Muki,[76] that path considerably restricts extension of the model to the more general fiber-fiber bond structure (see Fig. 1) and to the more complex material properties of the wood fiber wall. Numerical techniques, in general, and the finite element method, in particular, are much less restrictive. Of the numerical approaches, the finite element method appears to be the technique of choice, because both complex geometries and material properties are accessible thereby.

Having made the decision to use a finite element technique, one must also decide how that capability will be realized. Two alternatives are usually available. A totally new limited purpose finite element computer program may be developed, or a general purpose program with the appropriate capabilities may be obtained from a private or public agency. Gallagher[114] has surveyed the general purpose finite element programs and concluded that properly formulated and documented general purpose computer programs will, in most cases, be a better choice than the development of a highly specialized in-house finite element computer program. Of course, this conclusion is contingent upon the general purpose program's ability to solve the type of problem in question. The modular organization of most general purpose programs, however, does allow the formation of small special purpose programs plus the addition of other specialized elements and capabilities. Most general purpose finite element computer programs are not formulated for proper modeling of stress singularities. After a review of the literature on structural analysis finite element programs,[114] the capabilities of the various programs, and user experience with them,[115] it was decided that SAP IV, a structural analysis program for static and dynamic response of linear system, would meet all of the essential model requirements, with the exception of the stress singularity.[94] A complete discussion of the features of SAP IV is deferred until the model development part is concluded.

Material Description

Commercial cellophane film was chosen as the experimental material partly because it was orthotropic and approximately linear elastic and orthotropic[97] at strain less than 0.5%. The wood fiber wall has been given a similar characterization.[8] SAP IV has elements with that material formulation.[94] Nine elastic constants are required to describe the stiffness of an orthotropic elastic material. These constants were obtained experimentally through a combination of uniaxial and biaxial static measurements, acoustic measurements, and estimations from theoretical models of cellophane structure. Appendix III presents the details of the calculation of these nine constants.

Bending and Extension

The physical arrangement of an experimental lap joint in the test configuration is shown schematically in Fig. 43. As can be seen from this schematic and the experimental results (see Fig. 19), axial extension and moment generation about the bond will occur for axial tension loading of the experimental structures, resulting in overlap region rotation and adherend bending. Qualitatively similar behavior should occur in paper. In paper, nonuniform stress distributions, stress decay length,[116] may make span length more important in terms of overall axial extension than in the experimental structures. With the experimental end conditions, the adherend free span is similar to a cantilever beam. Several SAP IV elements are possibilities for this feature of the model. In most instances, a two-dimensional representation (as in previous investigations) will adequately approximate the lap joint behavior. The two-dimensional approach is used in the model developed here, with some specific comparisons to a three-dimensional model to help in the choice of a plane stress or plane strain assumption. Contrary to expectations the plane stress assumption was found to be a closer approximation of the three-dimensional case (i.e.,

approximately 30% plane strain and 70% plane stress) and, therefore, the plane stress assumption is used throughout. A discussion of these results is included with the general model response discussions. An evaluation of SAP IV's ability to handle these deformations is given along with the discussion on implementation of the model.

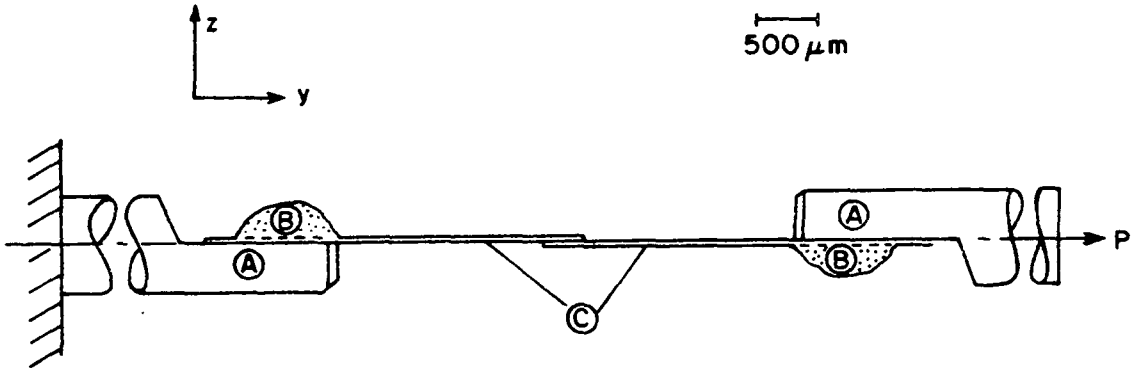

Figure 43. Schematic representation of the experimental microlap joint configuration (single type), with (A) stainless steel dowel pins, (B) epoxy resin, and (C) cellophane fibers.

Complex Loading

The schematic of the experimental test configuration reveals a complex end condition, where the cellophane fiber is attached by an epoxy resin bead to a semicylindrical portion of a 1/32-inch diameter stainless steel dowel pin. Attempts to simplify the representation, primarily by assuming a rigid connection, did perform satisfactorily for symmetrical structures. Unfortunately, most structures are not symmetrical. The moments generated in this structure and the importance of end restraint conditions to the stress decay length,[116] prompted a more realistic approach. This was accomplished by closely representing the complete end geometry and materials (dowel pin, epoxy resin, and cellophane fiber) in three-dimensional linear elastic finite elements as shown in Fig. 44. The external nodes of the last set of elements at the ends of dowel

pins are restricted to displacements parallel to the longitudinal axis. The results of the calculations with this model were then used to develop the two-dimensional representation shown in Fig. 45. It was found that the rigidity of the epoxy resin had little to do with the lap joint behavior, if it was assumed that the layer of epoxy resin between the fiber and the dowel pin had insignificant thickness and the cellophane was continuously bonded to the dowel pin. The two-dimensional plane stress representation (Fig. 45) was found to behave substantially the same as the three-dimensional model (allowing for the plane stress assumptions). This two-dimensional representation of the glue connection was used throughout, unless otherwise stated.

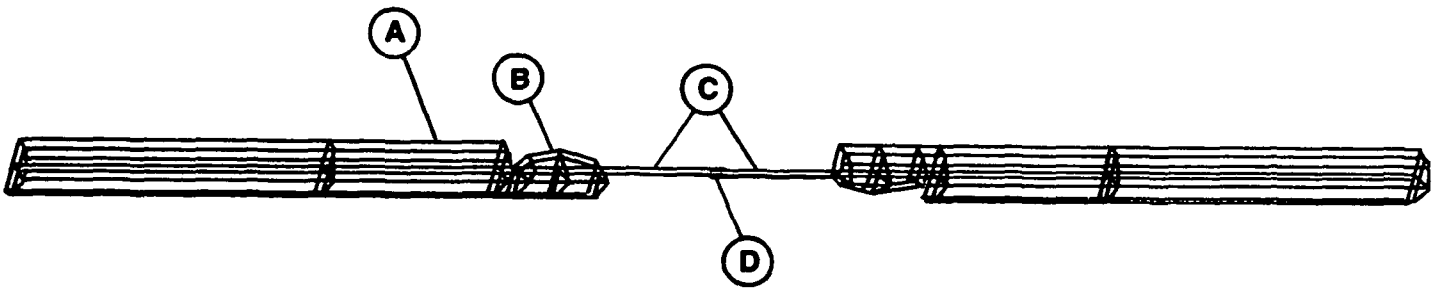

Figure 44. Three-dimensional finite element representation of the experimental cellophane microlap joint configuration with (A) the dowel pin, (B) the epoxy resin bead, (C) the cellophane fibers, and (D) the overlap region.

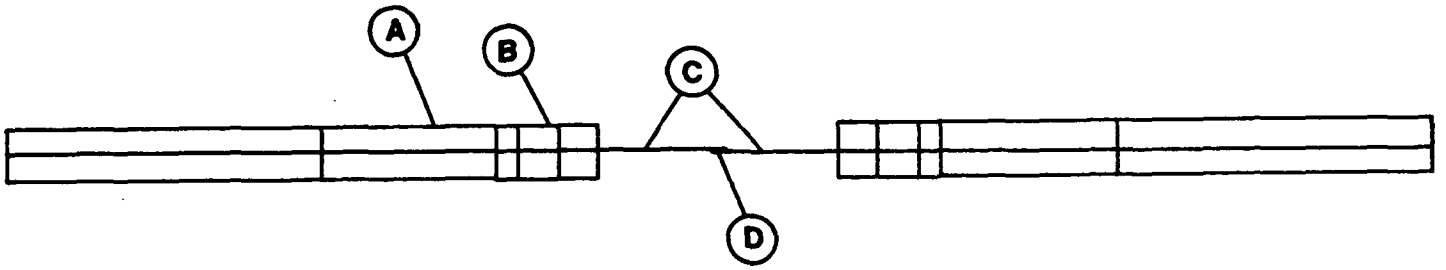

Figure 45. Two-dimensional finite element representation of the experimental cellophane microlap joint configuration with (A) the dowel pin, (B) the epoxy resin bead, (C) the cellophane fibers, and (D) the overlap region.

Notch/Crack Tip Representation

Although the gross features of the notch tip are as stated previously (i.e., possible extremes of 90 and 45°, plus a 0° sharp crack), the geometry of the immediate notch/crack tip is not known. To allow some flexibility, both a 90° angle single lap joint (Fig. 46) and a conforming lap joint (Fig. 47) were represented in models. The models were also provided with an ability to represent 0° angle sharp cracks (Fig. 48) with arbitrary length in either of these two types of lap joints.

Superimposed on these finite element grids are normalized shear and peeling stress contours. Single lap joints (Fig. 46) have substantially different shear stress distributions than does the conforming lap joint (Fig. 49). The introduction of an interfacial crack can be seen, in Fig. 48, to considerably alter the shear stress distribution around the conforming lap joint crack tip. All of the shear stress and peeling stress contours provide clear evidence that stress is intensified in the crack tip region, although differently for each type. From the experimental data (see Fig. 42), it was tentatively concluded that conformability and interfacial cracks will have an observable influence on lap joint compliance. This conclusion was further supported by the behavior of these various model types. The effects were clear enough to allow the selection of the conforming lap joint as the best representation of the experimental lap joint structures. This evidence will be presented in the general model behavior section.

Interface Treatment

There has been much debate about the nature and extent of bonding between the wood fibers of a fiber-fiber bond. In this model, it is assumed that the

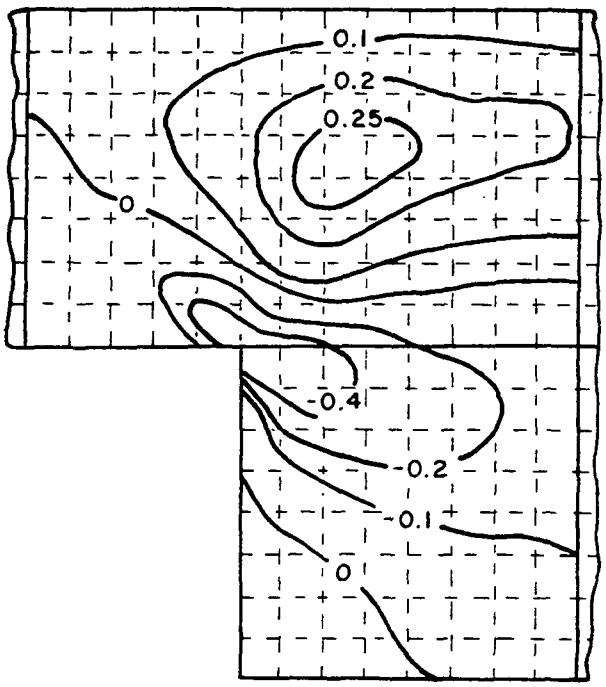

Figure 46. Normalized shear stress (τ/σ_{nom}) contour map for single lap joint.

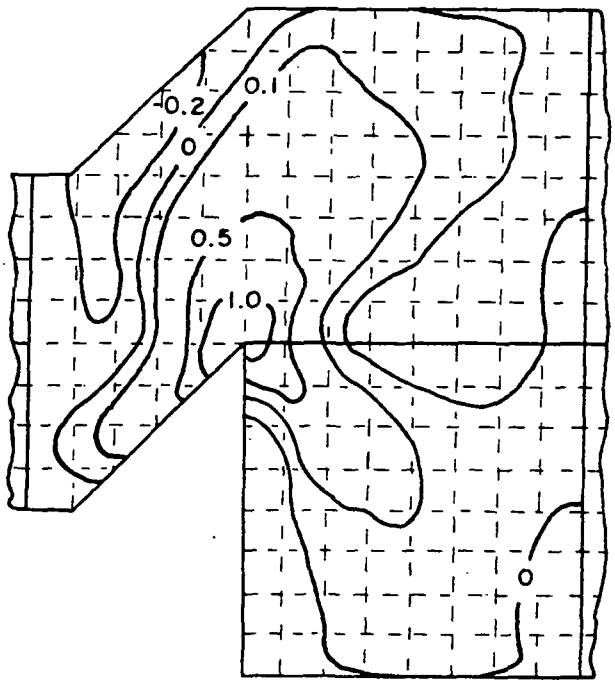

Figure 47. Normalized peeling stress (σ_z/σ_{nom}) contour map for conforming lap joint.

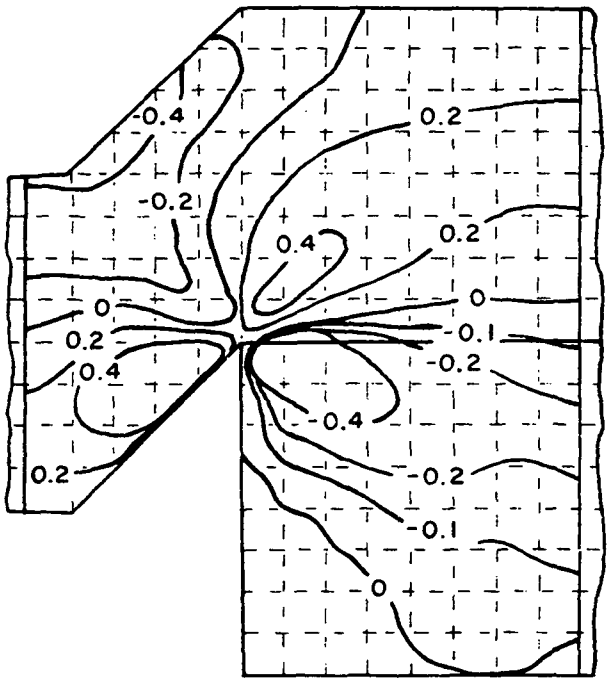

Figure 48. Normalized shear stress (τ/σ_{nom}) contour map for conforming lap joint.

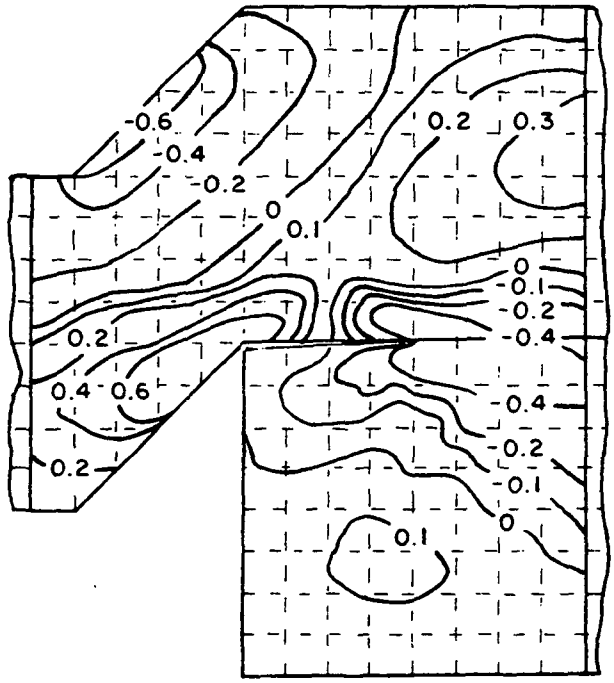

Figure 49. Normalized shear stress (τ/σ_{nom}) contour map for cracked conforming lap joint.

bonding across the interface is continuous and infinitesimally thin, when compared to test structure dimensions. As a result of this assumption, the interface is not given a separate representation and, therefore, contributes nothing to the overall deformation of lap joint model. A similar assumption has been employed by Chang and Muki[76] and Thorpe, et al.[40] The interface, however, is not ignored. From the experimental evidence it is known that the failure propagates along this interface and the fracture toughness of these structures appears to be considerably below that of the bulk cellophane.[72,106] The fracture toughness calculated from the experimental data, and that which this model can be used to calculate, indirectly represent a quantitative characterization of the interface of this system.

Fracture Parameters

Nature of Fracture Problem

While extension of this model to the more complex wood fibers has been an ever-present consideration, when one examines the nature of the cellophane lap joint fracture there is sufficient complexity without considering the wood fiber. To illustrate this point, a list of the factors involved in this fracture problem is as follows:

1. Mixed mode fracture; at least Modes I and II present.
2. Complex crack tip geometry; four possible configurations, two of which do not have an $r^{-0.5}$ singularity. A possible stress intensity factor dependence on material orientation.
3. Anisotropic material properties; literature incomplete for this type of material.
4. Bimaterial interface; stress field theory related to this case not fully developed.

5. Almost microscopic structures; other boundaries close enough to the crack tip to have interacting stress singularities.
6. Potential material nonlinearities; possible in cellophane and in wood fibers, particularly in a local sense (i.e., surface hemicellulose).

Selection of Fracture Criteria

Given the findings of Wu,[86] Trantina,[77] and others, the mixed mode fracture almost precludes the direct use of stress intensity factors, except, perhaps, in a relative sense. Complex crack tip geometry, anisotropic material, and bi-material interfaces also prevent the use of stress intensity factors. The energy approach, fracture based on the strain energy release rate (G), is the method of choice.

Several compensatory type approaches were given by Gallagher[114] for use with standard code finite element programs, such as SAP IV. A more involved technique with computational savings is that of Park.[117] The stored elastic energy difference for an incremental crack length increase, used by Anderson, et al.,[109] and the J-Integral technique of Rice[112] are the other two. The accuracy of these energy approaches is excellent with rather coarsely refined element grids[109,117] as compared to the extrapolation technique of Chan, et al.[107] With no particular reason to choose the more complex system, the simplest, more direct approach (the energy difference technique), was selected for inclusion in this model.

Implementation of Predictive Model

The predictive model can be approached from two directions. If the fracture toughness (G_c) of the material is known, the particular model calculation can be performed with a unit nominal axial stress ($\hat{\sigma}$) to yield a unit fracture toughness

($\hat{G}$). A predicted nominal axial stress at failure ($\sigma^*_{nom_c}$) may then be obtained. This predictive model is derived for the case of Mode I fracture, as follows.

From linear elastic fracture mechanics theory the relationship between the stress intensity factor and applied stress at a given crack length is given by Eq. (7) which in terms of the unit stress is

$$K_I = \hat{\sigma}(\pi a)^{1/2} \tag{21}$$

When this is substituted in Irwin's[5] relationship between K_I and the strain energy release rate, Eq. (8), the following is obtained:

$$\hat{G} = [(\pi a(1 - \nu^2))/E]\hat{\sigma}^2, \; K_{II} = K_{III} = 0 \tag{22}$$

which for a particular material, fixed crack length, and known fracture toughness is,

$$G_c = [(\pi a(1 - \nu^2))/E]\sigma^2_{nom_c} \tag{23}$$

Combining Eq. (22) and (23) gives the predictive model

$$\sigma^*_{nom_c} = \hat{\sigma}(G_c/\hat{G})^{1/2} \tag{24}$$

If the nominal axial stress at failure (σ_{nom_c}) for an experimental structure is known, an estimated fracture toughness (G_c^*) may be calculated as an alternative.

The value of the unit strain energy release rate is obtained from a finite difference approximation to the partial derivative of the stored elastic energy with respect to crack length at constant unit load (stress), i.e.,

$$G = (\partial U/\partial a_t)\Big|_{\hat{\sigma}} = [U_1 - U_0)/(a_{t_1} - a_{t_0})]\Big|_{\hat{\sigma}} \tag{25}$$

Two SAP IV displacement calculations are performed. The first with $a_t = a_{t_0}$ and the second, $a_t = a_{t_1}$ (where $a_{t_1} - a_{t_0} = \Delta a_t$), to give the stored elastic energies U_0 and U_1. The finite element grids for those two calculations are given in Fig. 50. An examination of the relationship of U to Δa_t produced the results shown in Fig. 51. The slope is essentially linear and therefore a constant G would be obtained from this model calculation. In this particular calculation, $\hat{\sigma} = \sigma_{nom_c}$, and therefore $G = G_c^* = 3594$ ergs/cm^2. All other model calculations were performed at $\Delta a_t = 20$ μm. Stress intensity factors are calculated by the use of expanded displacement field equations (20) as qualitative indicators of relative intensity of the stress fields about the two crack tips. This feature is outlined in the discussion of the computer program, FRACTR.

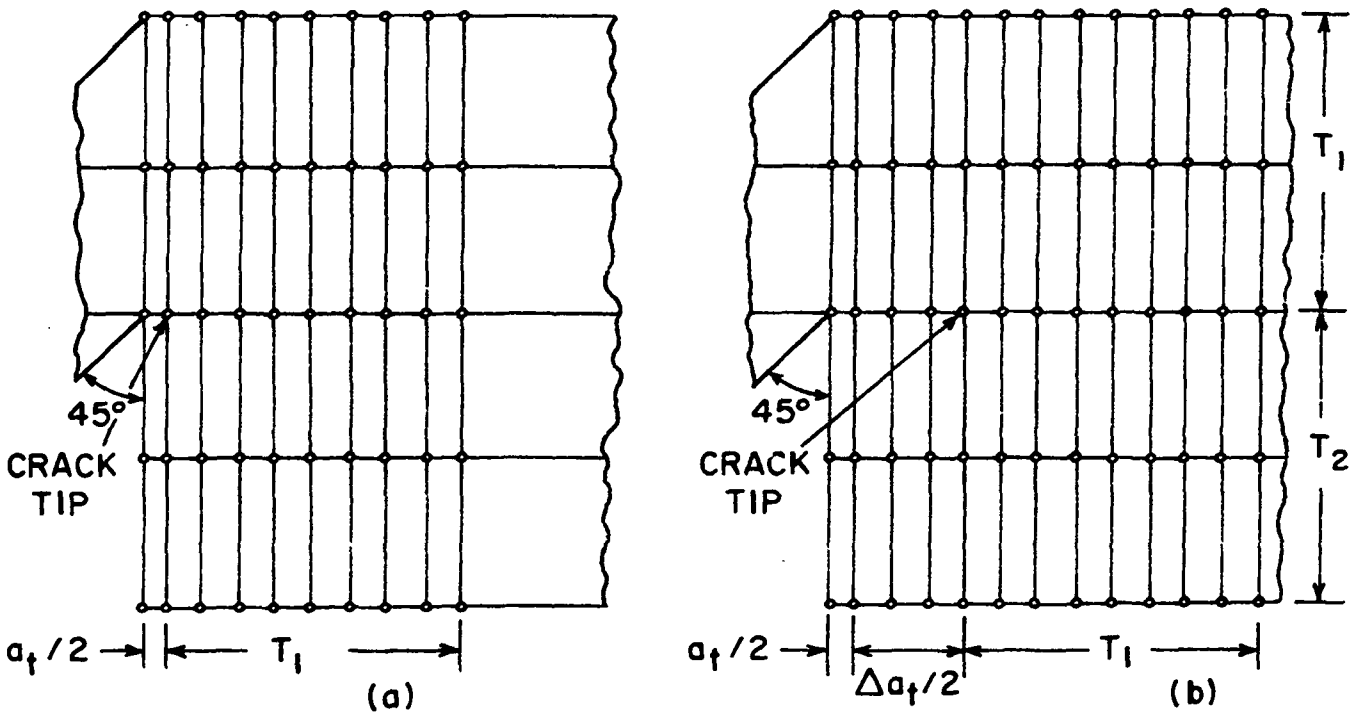

Figure 50. Finite element grids in the crack tip region of a conforming microlap joint at (a) original crack length $a_t/2$ and (b) increased crack length $(a_t + \Delta a_t)/2$.

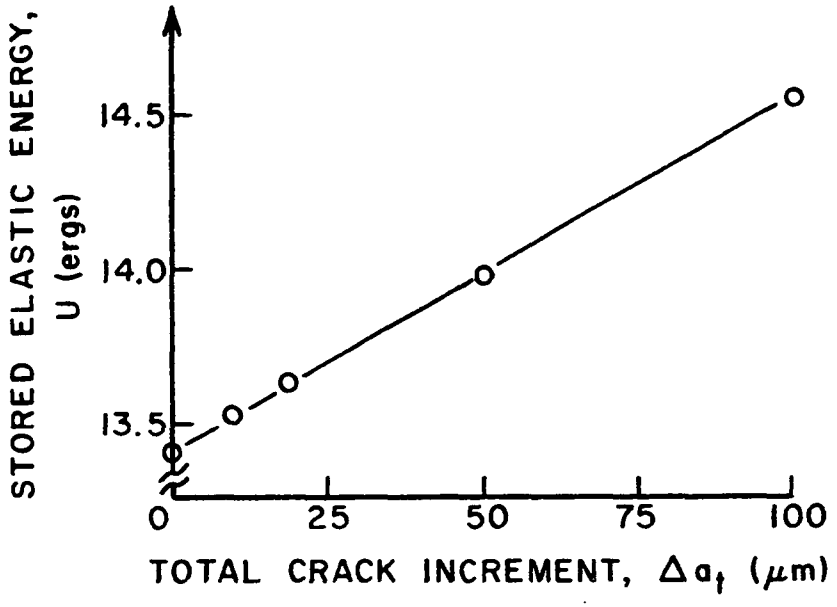

Figure 51. Relationship of stored elastic energy (U) to total incremental crack length (Δa_t) for cellophane microlap joint K-989.

COMPUTER PROGRAMS FOR IMPLEMENTING THE MODEL

Background

The fiber-fiber bond linear elastic model is represented primarily by three computer programs (SAP IV, PRESAP, and FRACTR). To facilitate the preparation of the input to SAP IV, a preprocessor, PRESAP was developed. Its many faceted capabilities are presented after the discussion of SAP IV. The program for the calculation of the fracture parameters, FRACTR, is discussed last.

SAP IV - Structural Analysis Program

The finite element method capabilities for this thesis were supplied by the structural analysis computer program for static and dynamic response of linear systems, SAP IV.[94] This program, developed at the University of California - Berkeley by Bathe, et al.,[94] has been widely used and the results of its analyses have been found to be satisfactory.[115] Its modular construction allows

selection of the elements most appropriate for a particular analysis. The element library includes: two-dimensional plane stress and plane strain, and axis symmetric solid elements; three-dimensional truss, beam and solid elements; plate and shell elements; pipe elements; and a variable 8 to 21 node thick shell and three-dimensional solid element.

Assembly and Solution of Equilibrium Equations

SAP IV employs the direct displacement method to generate a set of linear equations of the form

$$[M]\{\ddot{u}\} + [C]\{\dot{u}\} + [K]\{u\} - \{R\} = 0, \tag{26}$$

where $[M]$ = mass matrix

$[C]$ = damping matrix

$[K]$ = stiffness matrix of the element assemblage

$\{u\}$ = nodal displacements

$\{\dot{u}\}$ = velocities

$\{\ddot{u}\}$ = accelerations

$\{R\}$ = general loads

The structure stiffness matrix, $[K]$, is assembled by:

1. reading nodal input data and assigning equation numbers for each active degree of freedom at each nodal point (up to six per node)
2. calculating the element stiffness matrices along with the connection array and placing them in order on slow-speed storage
3. forming the structure stiffness matrix by adding the element matrices and then storing it in block form on slow-speed storage.

The number of equations per block is calculated on the basis of the allotted high-speed core. The stiffness matrix is assembled two blocks at a time by direct addition. The structure stiffness matrix is symmetric, positive definite, and banded (i.e., all nonzero elements are positioned near the diagonal), which allows block storage of just the nonzero equations. The load vector {R} is assembled at the same time as [K].

Since only static calculations were performed ($\ddot{u} = 0$, $\dot{u} = 0$), the set of equilibrium equations (26) reduced to $[K]\{u\} = \{R\}$. These equilibrium equations are solved with the large capacity linear equation solver SESOL.[118] The solution algorithm uses a Gauss elimination technique to perform a minimum of operations (only nonzeros). [K] is decomposed into an upper and lower triangular matrix, i.e.,

$$[K] = [L]^T [G], \tag{27}$$

where $[G]$ = upper triangular

$[L]^T$ = lower triangular

normalized so that $\ell_{ii} = 1$. Because [K] is symmetric, $g_{ij} = d_{ii}\, \ell_{ij}$, Eq. (27) is written

$$[K] = [L]^T [D][L] \tag{28}$$

Since the $[L]^T [D][L]$ decomposition of [K] is used, the equilibrium equation may be written as

$$[L]^T \{s\} = R \tag{29}$$

and

$$\{s\} = [D][L]\{u\}, \tag{30}$$

where the solution for {s} in Eq. (29) is obtained by a reduction of the load vectors. The displacement vectors {u} are then calculated by a back-substitution. Element stresses are calculated through the element stress-displacement matrices, Eq. (38) and (39) in Appendix I. A discussion of the element formulations that contribute to [K] follows.

Element Formulations

Only the elements used in this thesis will be reviewed. These were the two-dimensional plane stress and plane strain elements and the variable 8 to 21 node thick shell and three-dimensional solid element. They all are isoparametric elements with added incompatible bending modes. The material models include an orthotropic elastic capability. The two-dimensional element formulation will be used as an example and only the added features of the three-dimensional element will be mentioned. For the general isoparametric quadrilateral element, as shown in Fig. 52, the local and global coordinate systems are related by,[119]

$$x = \sum_{i=1}^{4} N_i X_i; \qquad y = \sum_{i=1}^{4} N_i Y_i, \tag{31}$$

where the interpolation (shape) functions are given by

$$\begin{aligned} N_1 &= 1/4(1 - \xi)(1 - \eta) \qquad N_3 = 1/4(1 + \xi)(1 + \eta) \\ N_2 &= 1/4(1 + \xi)(1 - \eta) \qquad N_4 = 1/4(1 - \xi)(1 + \eta) \end{aligned} \tag{32}$$

The same interpolation functions are used in the displacement approximation

$$\begin{aligned} u(\xi,\eta) &= \sum_{i=1}^{4} N_i u_i; \\ v(\xi,\eta) &= \sum_{i=1}^{4} N_i v_i, \end{aligned} \tag{33}$$

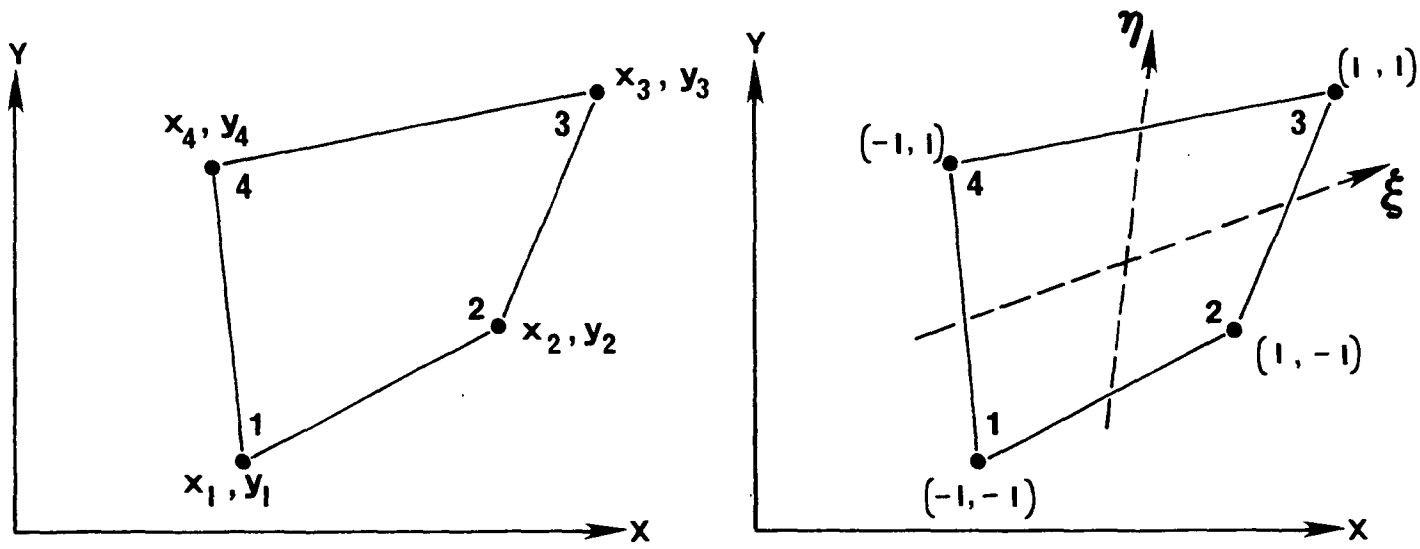

Figure 52. Coordinates for (a) global system and (b) local system of the two-dimensional isoparametric element.

When the incompatible modes are added for better representation of element bending, the displacement approximation becomes

$$u = \sum_{i=1}^{4} N_i u_i + N_5\alpha_1 + N_6\alpha_2$$

$$v = \sum_{i=1}^{4} N_i v_i + N_5\alpha_3 + N_6\alpha_4 \qquad (34)$$

The function N_5 and N_6 must be zero at the four nodes. Since the displacement amplitudes α_i are additional degrees of freedom, the resulting stiffness matrix will be 12 x 12. Through minimization of the element strain energy with respect to α_i, four additional equations can be generated and a reduced 8 x 8 stiffness matrix developed. The functions N_5 and N_6, chosen to mimic the usual element

errors in bending deformation (i.e., inability to represent bending displacements along the y-axis), have the form $N_5 = (1 - \xi^2)$ and $N_6 = (1 - \eta^2)$. For rectangular elements only the y displacement is modified, while both displacement components are modified for the general quadrilateral.

In the formation of the individual element matrices, a two-point Gaussian quadrature technique is used for numerical integration of the two-dimensional elements. The three-dimensional element has a variable number of integration points, with a 2 x 2 minimum.

Cook[120] has pointed out that the two-dimensional element with incompatible modes added is only valid in the regular rectangular form. Bathe, et al.[94] indirectly acknowledged this by indicating that the incompatible modes should be included only in rectangular elements. The triangular element with the same basic isoparametric formulation is a constant strain type and does not have the incompatible modes option. They recommend minimal usage of this triangular element.[94]

The three-dimensional element has the same formulation as the two-dimensional rectangular element (extended to the third dimension). From 8 to 21 nodes may be used. If the element is straight-sided, a more efficient subparametric formulation may be employed (i.e., only 8 nodes are needed to describe the element geometry).

Input Requirements and Output Utilization

SAP IV input requirements fall into four natural groups: (1) node coordinate and boundary conditions (i.e., degrees of freedom), (2) material parameter specifications (i.e., engineering elastic constants, temperature coefficients, density), (3) element type, arrangements, groupings, and associated

nodal point numbers, and (4) load specifications (i.e., uniform pressures, concentrated nodal loads with magnitude and direction). SAP IV has nodal and element generation capacities for repetitive features, but, in general, a preprocessor program is needed to generate the input for other than simple structures to avoid an excessive amount of preparatory effort with greater possibility for input errors in the generated structure.

One displacement for each degree of freedom and from six to 42 stresses per element per load case are calculated by SAP IV. A postprocessor program is very useful for rendering the output comprehensible.

Element Response

As pointed out by Dunder and Ridlon,[121] even though many finite element program user's manuals provide some documentation and information about the form of the inputs, ultimately the use of a program for a given model is the responsibility of the individual user. It, therefore, is the user's responsibility to establish the satisfactory performance of that program for his particular model. In finite element programs that usually means to establish the monotonic convergence of the model solution for regular refinement with successively greater degrees of freedom. Comparison of the finite element program calculations with analytical solutions of simple problems is also necessary. Following satisfactory solution of the sample problems provided with SAP IV, a systematic study of the response of the three elements of interest was initiated. In accordance with the principal deformations expected in the model, the response of these elements to bending, extension, and a stress singularity was examined.

Bending - The bending characteristics of cantilever beams composed of these elements show, in Table 7, an asymptotic approach to a maximum deflection as the total degrees of freedom (total elements) increase. A close approach by the plane stress and three-dimensional elements to the maximum deflection predicted from simple beam theory[122] is seen. These elements have excellent bending characteristics when the incompatible modes are included. A very brief examination of the plane stress element behavior with the incompatible modes suppressed showed that, even at the highest refinement level in Table 7, the beam deflected only 60% of the predicted value. Incompatible modes therefore greatly improve the basic isoparametric element bending behavior and thereby provide an important capability to the model studied in this thesis.

Table 7. Grid refinement effect on 2/D and 3/D cantilever beam models.[a]

	Maximum Deflection, δ_z, (μm)				
	Number of Elements Along Beam Length				
Model Type	2	4	8	16	32
Plane strain, NELSZ = 1	290.8	305.3	309.0	310.0	310.1
Plane strain, NELSZ = 2	267.4	292.9	302.5	306.6	308.5
Plane stress, NELSZ = 1	342.5	359.7	363.9	365.0	365.3
Plane stress, NELSZ = 2	332.5	354.3	361.2	363.6	365.6
Three-dimensional	342.2	353.1	358.1	359.9	--
Simple beam theory	--	--	--	--	365.8

[a]All models with total end restraint (one end), S_t = 3600 μm, T = 26 μm, W = 300 μm, P = 10.0 dynes, E = 969.1 dynes/(μm)^2.

Axial Extension - An investigation of the axial extension characteristics of the same beams mentioned previously showed that the load/deformation curve was linear for all reasonable loads. Under an axial tension load, the increased refinement of these beams resulted in a convergence of the apparent modulus

toward the modulus of the beam material. These results, presented in Table 8, also illustrate the stiffer nature of the model when plane strain is assumed.

Table 8. SAP IV element response to axial extension.[a]

Number of Elements in			Apparent Modulus, E_a [dynes/(μm)^2] Element Type		
Width	Length	Thickness	Plain Strain	Plane Stress	3/D
0	4	1	1183.5	982.7	--
0	8	2	1161.6	975.9	--
0	16	4	1150.7	972.5	--
0	32	8	1145.4	970.8	--
2	8	1	--	--	981.2
2	16	1	--	--	974.0

[a] S_t = 3600 μm, T = 26 μm, W = 300 μm, E = 969.1 dynes/(μm)^2. Total end restraint on one end and uniform axial tension load on the other.

The interaction of test span, end restraint/load distribution, and refinement were studied to see how sensitive these elements were to the first two factors. Under conditions of perimeter restraint on one end and axial tension loading on the perimeter of the other, the apparent modulus was found to decrease with both increased refinement and decreasing span. This results from the nonuniform stress distributions at the fiber ends. With a more refined grid the stress gradients are better modeled, and at shorter spans this stress decay region (low apparent modulus region) constitutes a greater portion of the total fiber length. Both would result in a lower apparent modulus. From these data, it is concluded that the response of these three elements to axial extension is quite acceptable.

Singularity - Since the 90° notch which exists at the end of the overlap region of a single lap joint is known to have a stress singularity, an investigation of the stress distributions in the notch tip region was performed. The single lap joint configuration was used as the model for evaluation of the element response to a stress singularity. The changes in the shear stress of the three elements surrounding the notch tip as the element grid was alternately refined along the two coordinate directions is presented in Fig. 53.

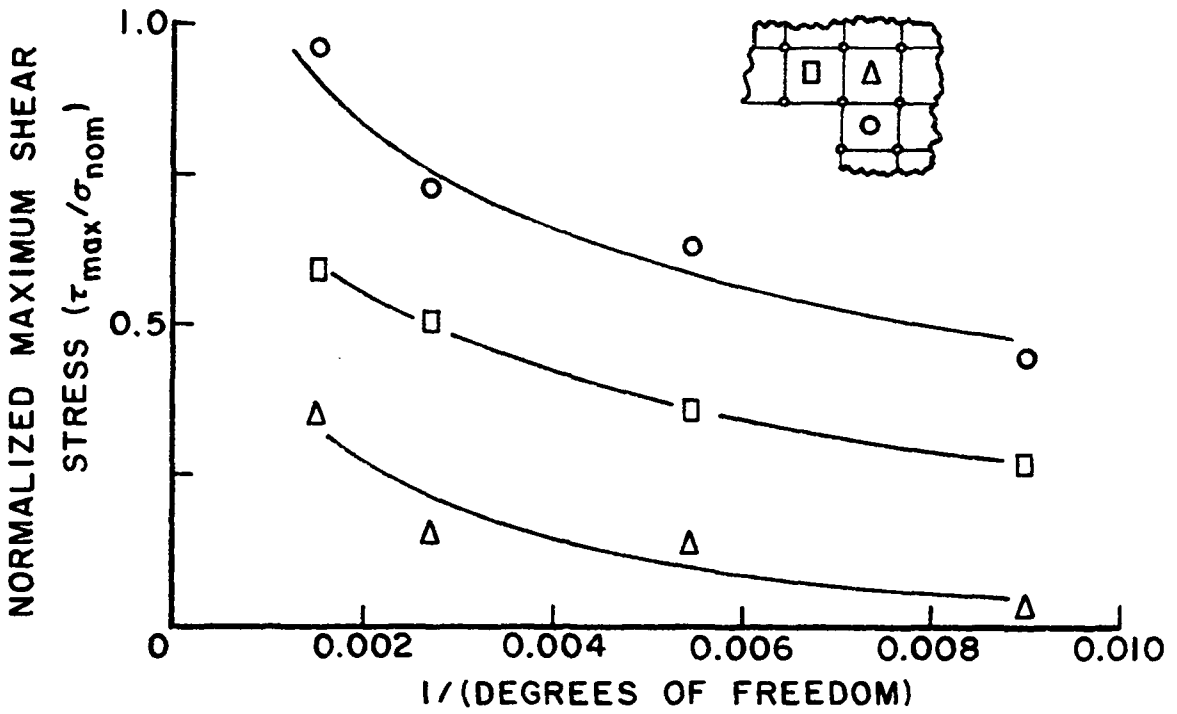

Figure 53. Grid refinement effects on the shear stress of notch tip plane strain elements of a single lap joint model.

The expected increase in shear stress level with refinement is evident. The change in the stress distribution along the interface with grid refinement was also examined. As shown in Fig. 54, the grid refinement was found to increase the maximum calculated stress and to provide a better representation of the stress singularity about the notch tip. Although these elements do not have

a stress singularity modeling capability, it appears that they can adequately approximate the intense stress field when a fine grid is employed.

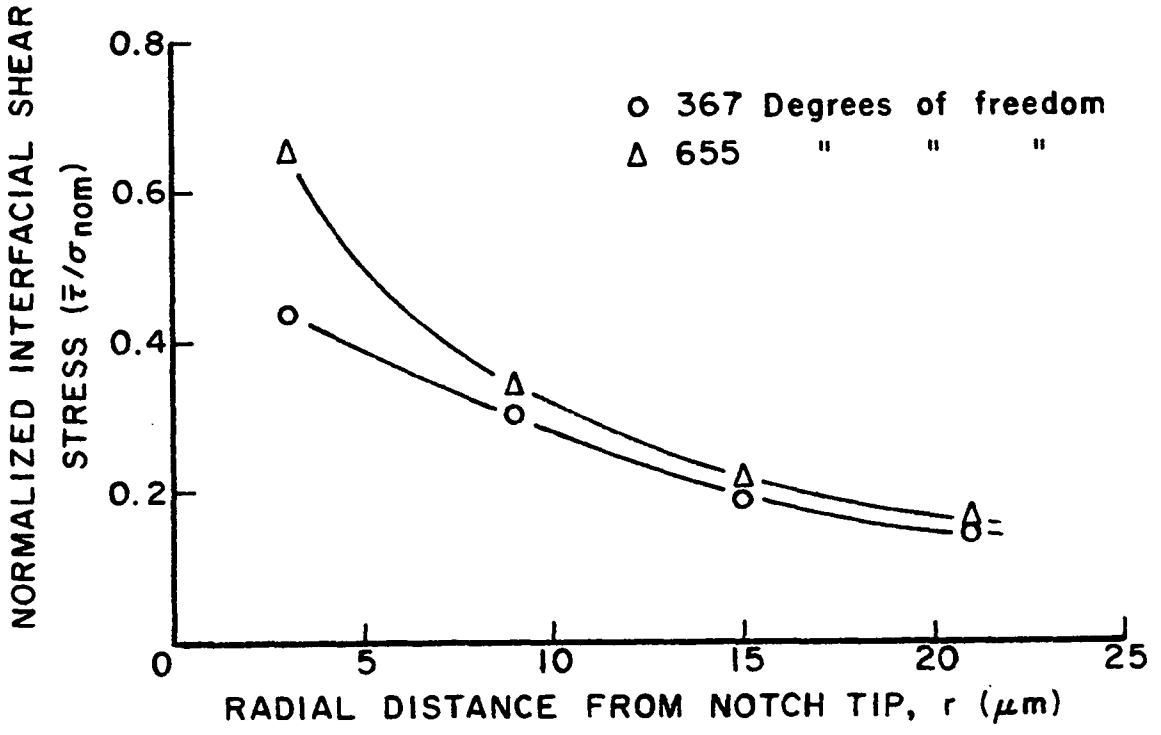

Figure 54. Grid refinement effects on the average interfacial shear stress of a single lap joint model.

Analysis of Literature Problem - The SAP IV two-dimensional plane stress element was examined further by developing the same finite element grid and single lap joint model studied by Wooley and Carver.[67] Stress concentrations were calculated for the same conditions that they listed in a comparison between their results and an analytical calculation based on Goland and Reissner's model.[59] A comparison between the SAP IV calculations and their results can be made in Table 9. Calculations performed with SAP IV compare favorably with Wooley and Carver's[67] calculations. The shear stress concentration results closely agree, particularly for the rigid adherend/flexible adhesive cases

($E/E_a > 10.0$). The same is true for the peeling stress concentration calculations, except for the tendency of these results to diverge as the stiffness of the adhesive is increased. This trend is not particularly disturbing. The divergence is associated with the difference in the bending capabilities of SAP IV (which has been established as being excellent, see p. 134) and that of Wooley and Carver's finite element formulation.[67] Their plane stress quadrilateral elements were composed of four constant strain triangles rather than the isoparametric elements with added incompatible bending modes used in SAP IV. Triangular element stresses were used to calculate Wooley and Carver's quadrilateral element stresses. Their constant strain triangles would behave much as the SAP IV elements with the incompatible modes suppressed, which has shown to be undesirable for accurate modeling of bending behavior (see p. 134).

Table 9. Comparison of SAP IV calculations with Wooley and Carver's results.[67]

Joint Parameters			Shear Stress Concentration, (τ/σ_{nom})			Peeling Stress Concentration, (σ_c/σ_{nom})		
E/E_A	L/T	T_A/T	SAP IV	Wooley & Carver	Goland & Reissner	SAP IV	Wooley & Carver	Goland & Reissner
1.0	5	0.06	1.73	1.85	—	3.06	2.28	—
10.0	5	0.06	0.94	0.92	—	1.76	1.43	1.44
50.0	5	0.06	0.50	0.49	—	0.84	0.65	0.64
100.0	5	0.06	0.38	0.37	—	0.60	0.59	0.63

All of the investigations of SAP IV have shown that the overall program performs quite well. Those specific response capabilities deemed important to the model (i.e., bending, axial extension, and singularity) were found to closely approximate theoretical results with a minimum of grid refinements (degrees of freedom). Only the approximation to stress singularities was less than desirable (see p. 136); a result expected because none of the SAP IV

elements were formulated with a singularity type displacement function. This limitation is not particularly significant in light of the strain energy release rate approach used in this model.

Organization of Model Computer Programs

With the finite element performance determined to be satisfactory, all the various computer programs necessary for this model were integrated. This organization, given schematically in Fig. 55, consists of: (1) PRESAP, a preprocessor (structure generator); (2) SAP IV, a general finite element structural analysis program; (3) FRACTR, a fracture parameter calculator; (4) STPLOT, a program for three-dimensional plotting of the crack tip stress surface, and (5) SAPLOT, a program for plotting the generated and deformed two- and three-dimensional structures.

PRESAP - Structure Generating Program

Capabilities

PRESAP is a preprocessor for generating the SAP IV input data. PRESAP can be readily modified to include new structural forms. Based on the concept of separate generation of each structural unit (i.e., free spans, overlap region, cracks, connectors, load distributions/restraint structure type) in plane stress, plane strain, or three-dimensional solid elements, PRESAP can produce a variety of structures as input for SAP IV. The three separate element types, three general models (single fiber, single lap joint, or conforming lap joint) and ten distinct combinations of perimeter or total restraint; cantilever beam, uniform axial, or perimeter axial loading; plus glue connectors (3/D) or simulators (2/D) may be selected.

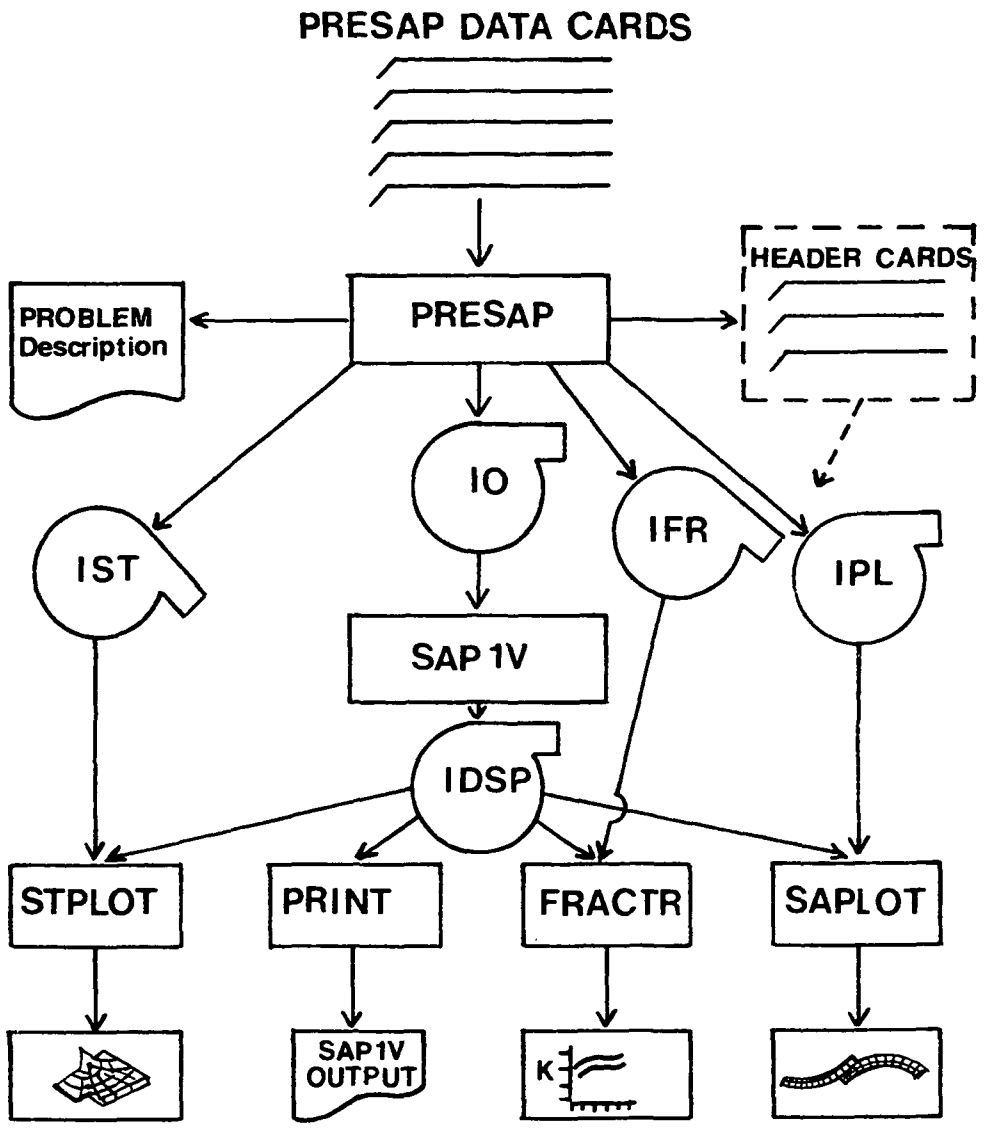

Figure 55. Flow chart for the computer solution procedure.

In addition, the degree of grid refinement along (1) the three principal axes (NELSX, NELSY, NELSZ), (2) the free span adjacent to the crack tip, and (3) the area ahead of the crack tip may be specified. Machine or cross-machine material axis orientation may be selected, and from library storage any desired set of elastic constants may be included. Nodal point generation is such that the simultaneous equation bandwidths are minimized. Another feature allows the generation of the precise crack lengths desired.

Files

To allow efficient utilization of the SAP IV calculations, PRESAP can generate three files (IST, IFR, IPL, see Fig. 55). File IST contains the crack tip area finite element numbers and the respective element centroid coordinates, which when used by STPLOT in conjunction with the SAP IV calculated element stresses, produce a plot of the stress surface (vertical coordinate) on a two-dimensional geometric representation of the crack tip region. In file IFR are sets of vectors, which contain nodal point numbers and radial distances from the crack tip for each point lying on one of seven possible radii around the tip. When combined as input to FRACTR with the SAP IV displacement calculations, stress intensity factors (K_I, K_{II}), strain energy release rate (G), and stored elastic energy can be calculated. Various specified portions of any given structure can be saved in the file IPL. When transmitted to SAPLOT, a plot of the structure as a finite element grid is obtained. The structural configuration (element distortions) under load can be plotted through reading the SAP IV output tape.

FRACTR - Fracture Parameter Computation

Fracture parameters are calculated by two techniques, both of which were previously mentioned in the literature review and model development sections. Both techniques utilize the nodal displacements calculated by SAP IV. In the first case, these calculated displacements are directly incorporated into analytical linear elastic fracture mechanics equations describing the displacement field around the crack tip. Using the expanded equation forms, Eq. (20), a set of four simultaneous equations (two each for two adjacent nodes) are assembled from finite element displacement calculations (u_t, u_θ), the shear modulus (μ), and the radial distance (r) from the crack tip. Solution of these equations by

a Gaussian elimination technique, yields the stress intensity factors (K_I, K_{II}) and the coefficients of the nonsingular terms (α_1, α_2) at various angles and radial distances around the crack tips. K_I and K_{II} are combined, using Eq. (8), to generate the strain energy release rate (G). For the orthotropic elastic case, these calculations are limited to just those angles which coincide with a principal elastic axis of the cellophane.[90]

A second technique, based directly on energy considerations, utilizes the derivative of the stored elastic energy (U) with respect to the change in total crack length (a_t) to calculate G. Two sets of finite element displacement calculations are employed. FRACTR calculates U_0 and U_1 by

$$U = 1/2 \sum_{i=1}^{n} P_i u_i, \tag{35}$$

where u_i is the displacement calculated by SAP IV for the node to which load P_i was applied. The summation is made over all n concentrated loads. G is calculated from the finite difference approximation, Eq. (25). If a known fracture toughness has been given, the program calculates the predicted strength ratio, $(G_c/G)^{0.5} = \sigma^*_{nom_c}/\hat{\sigma}$. Both techniques required no SAP IV modifications.

THEORETICAL MODEL RESULTS AND DISCUSSION

Introduction

The presentation of the theoretical model results and discussion follows lines similar to that of the Experimental Program. General model behavior is reviewed and evaluated, and then some representations are eliminated from future discussions. The predicted effects of experimental parameters are examined in light of the experimental data. Finally, a direct comparison between individual

experimental bond structure results and the model predictions for each experimental structure is presented.

General Model Behavior

The property most scrutinized in this discussion is the model compliance. Differences among the various representations of the microlap joints are quite distinct when compared on this basis. Unless otherwise indicated, model predictions in this general behavior section have been obtained with the elastic constants of 193 PUD-0 cellophane film at dimensions and loads that are in the range of the experiment parameters.

Grid Refinement Effects

The effects of finite element grid refinement in lap joint models were quite similar to those obtained with the beams (discussed along with the SAP IV program). Refinements along the free spans (NELSY) had a minimal effect on the conforming lap joint model, particularly for the two-dimensional assumptions. For the single lap joint models, grid refinement had a more pronounced effect, as can be seen in Table 10. Neither thickness nor width refinements produced much change in compliance. A free span refinement (NELSY) of six to eight elements and a thickness refinement (NELSZ) of two to four appear to be sufficient. A more refined grid, however, is necessary in the crack tip region to accommodate the stress singularity better.

Three-Dimensional Versus Two-Dimensional Models

The three-dimensional model has been treated as a guide to the acceptability of the two-dimensional representation. On this basis, a comparison between it and plane stress and plane strain was made for $L/\overline{T} = 10$ and both the single and conforming lap joints. From the results shown in Table 11, it is

evident that the plane stress assumption (0.153) is a closer approximation to the three-dimensional results (0.145) than is the plane strain assumption (0.129). This approximation would be expected to predict displacement greater than that of the three-dimensional model.

Table 10. Finite element grid refinement and model compliance.

Grid Refinement			Compliance (μm/dyne, per unit width)	
Width	Thickness	Length	Conforming	Single
		Plane Stress Model ($L/\overline{T}$ = 5)		
0	4	4	0.154	0.237
0	4	8	0.154	0.241
0	4	16	0.155	0.242
		Three-Dimensional Model ($L/\overline{T}$ = 10)		
2	1	2	0.144	0.194
2	1	4	0.145	0.211
2	1	8	0.145	0.216
4	1	6	0.145	--
2	2	6	0.146	--
2	4	6	0.146	--

Table 11. Compliance of two- and three-dimensional models.

Model Type	Compliance (μm/dyne, per unit width)	
	Conforming Lap Joint	Single Lap Joint
Plane stress	0.153	0.225
Three-dimensional	0.145	0.216
Plane strain	0.129	0.191

Evaluation of Notch/Crack Tip Representation

It is quite evident from the data presented in Tables 10 and 11 that the single lap joint representation is much more compliant than the conforming lap joint model (0.225 vs. 0.153). When these results are compared to the microlap

joint experimental results, which range from 0.120 to 0.147 for 193 PUD-0 MD/MD (see Appendix V), it is quite clear that the conforming lap joint model (plane stress) more closely approximates the experimental results. Another difference can be seen in the predicted rotation of the overlap region and the out-of-plane (plane of the bonded interface) deformations. Typical predictions for the overlap region rotation are 12° for the single lap joint vs. 2° for the conforming lap joint models. Experimental observations did not indicate any significant overlap region rotation and out-of-plane bending. Finally, interfacial cracks were found to increase the inverse modulus of conforming microlap joints (see Fig. 42). The conforming lap joint model exhibits this behavior, as shown in Fig. 56, where the inverse modulus linearly increases as crack length increases from the initial condition of a_t = 100 μm, L = 600 μm to a_t = 640 μm, L = 60 μm. In contrast to the conforming lap joint, the inverse modulus of the single lap joint model (at the same residual bond length) is not influenced by interfacial cracks.

All of these factors provide strong evidence for concluding that the plane stress assumption of the conforming lap joint model best represents the behavior of the experimental microlap joint structure. This model therefore is adopted and used, unless otherwise designated, for all the following model calculations.

Predicted Influence of Specific Structural and Material Parameters

This section of the Theoretical Program focuses on the predicted effects of specific structural and material parameters on the behavior of cellophane microlap joints. In most cases these are treated as qualitative predictions. Where possible, quantitative comparisons are made with other theoretical approaches and the results from the cellophane microlap joint experiments.

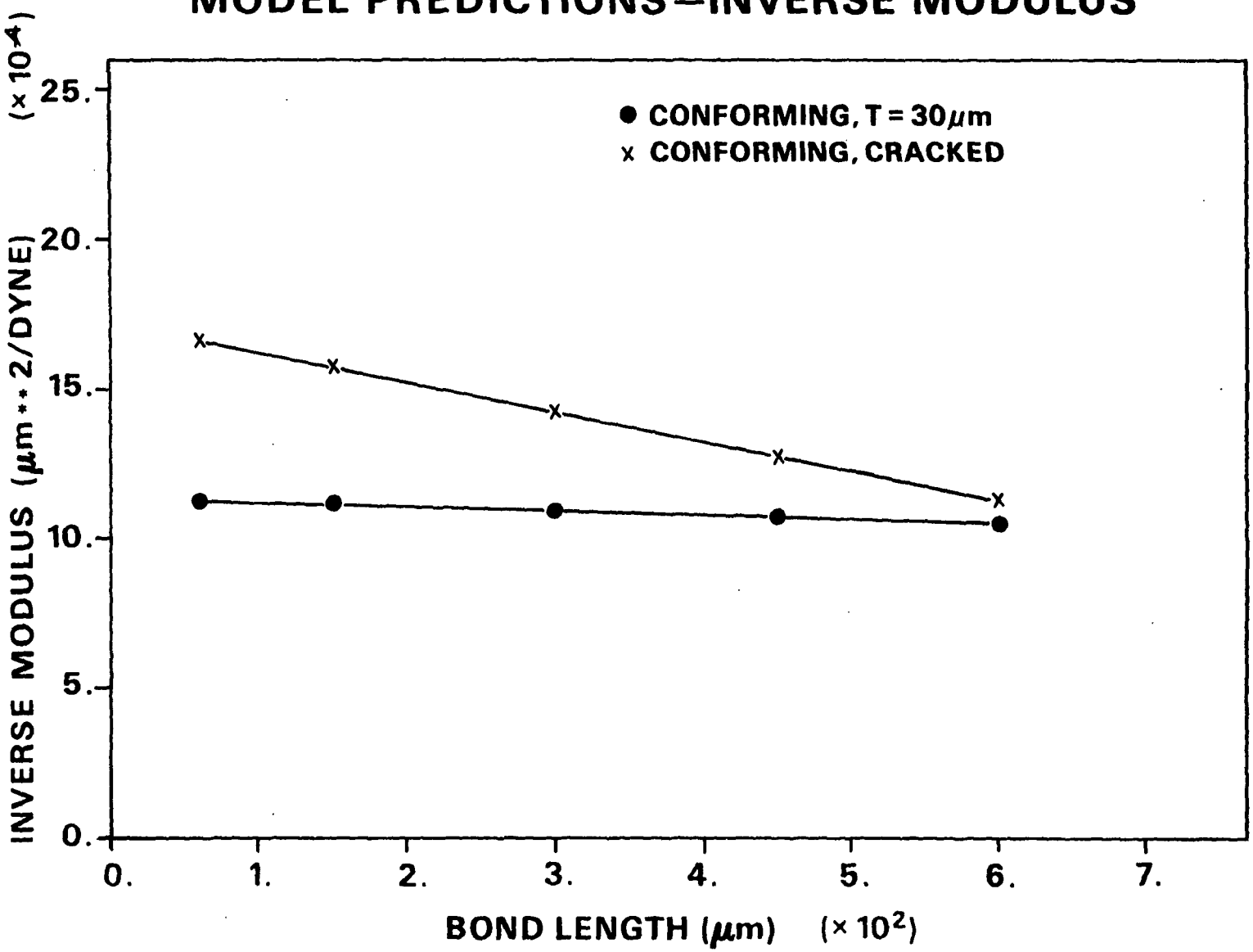

Figure 56. Predicted effect of interfacial cracks[a] on microlap joint inverse modulus.

[a]Original overlap length was 700 μm, the crack length is: a_t = 700 μm - bond length.

Bond Length

A short recapitulation of the predicted results for the plane stress single lap joint model and the plane strain conforming lap joint model is presented along with the adopted plane stress conforming lap joint model results to show the expected influence of bond length. The predicted influence of bond length on inverse modulus, plotted in Fig. 57, is as previously discussed for these three models. All three become less compliant as the bond length increases, but the conforming lap joint models change less drastically than does the single lap joint model. The higher inverse modulus of the single lap joint results from the greater moment being generated and the increased free span as bond length decreases.

The strong influence of bond length on bond shear strength ($\bar{\tau}$) seen in the experimental results (see p. 77) is predicted by all of these models. All of the models predict that bond shear strength, shown in Fig. 58a, will have the same dependence on the inverse of the bond length that was observed for experimental results of Fig. 58b. These predictions are all calculated on the basis of an assumed constant fracture toughness which throughout these results and discussions is G_c = 5466 ergs/cm^2, the value derived from the cracked lap joint data given in Table 6.

As was the case in the experimental results, this strong dependence on bond length results from a fairly constant nominal axial stress at failure (σ_{nom_c}). In Fig. 59, the predicted σ_{nom_c} is little influenced by bond length. Only the single lap joint model exhibits any significant dependence.

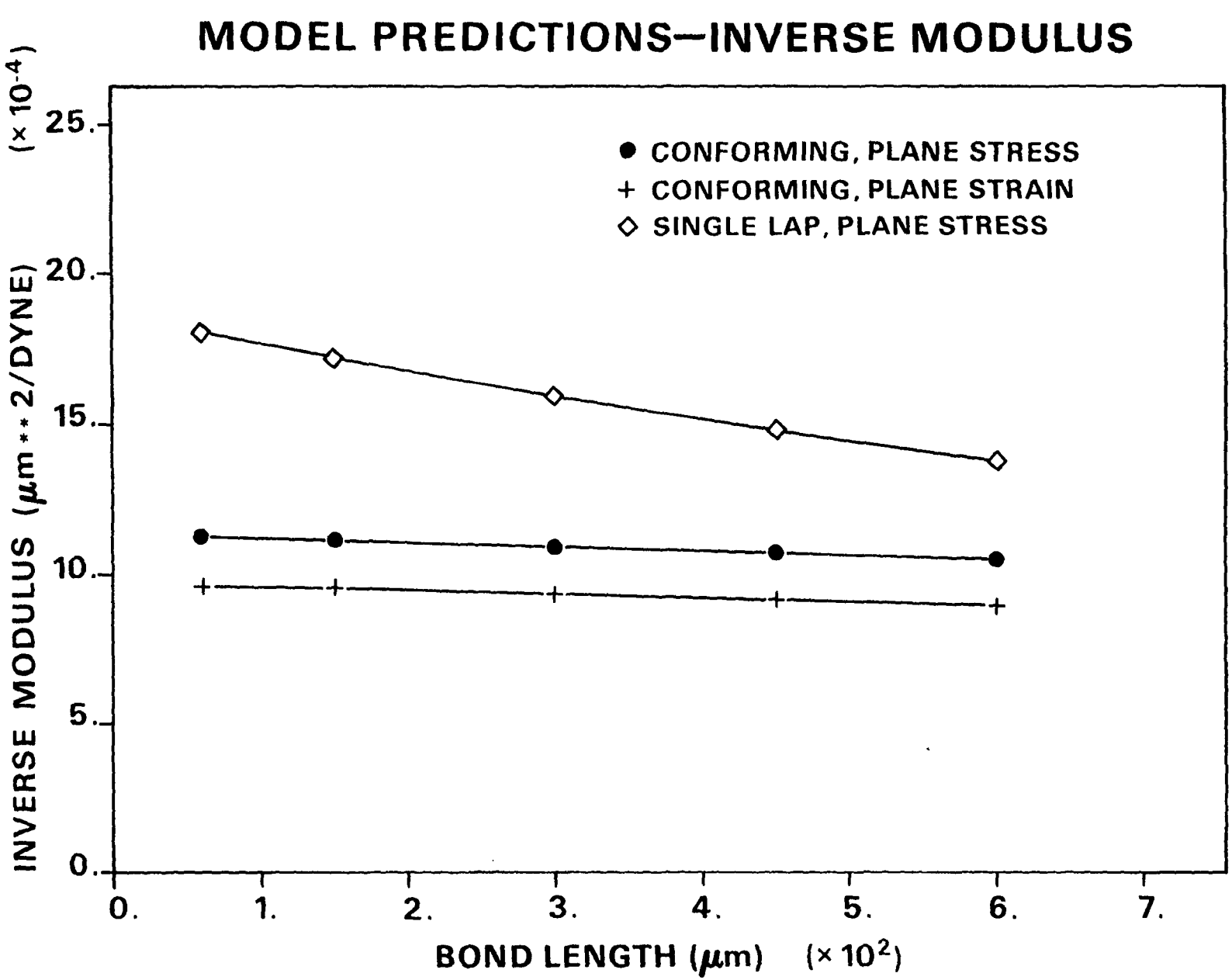

Figure 57. Predicted effect of bond length on inverse modulus.

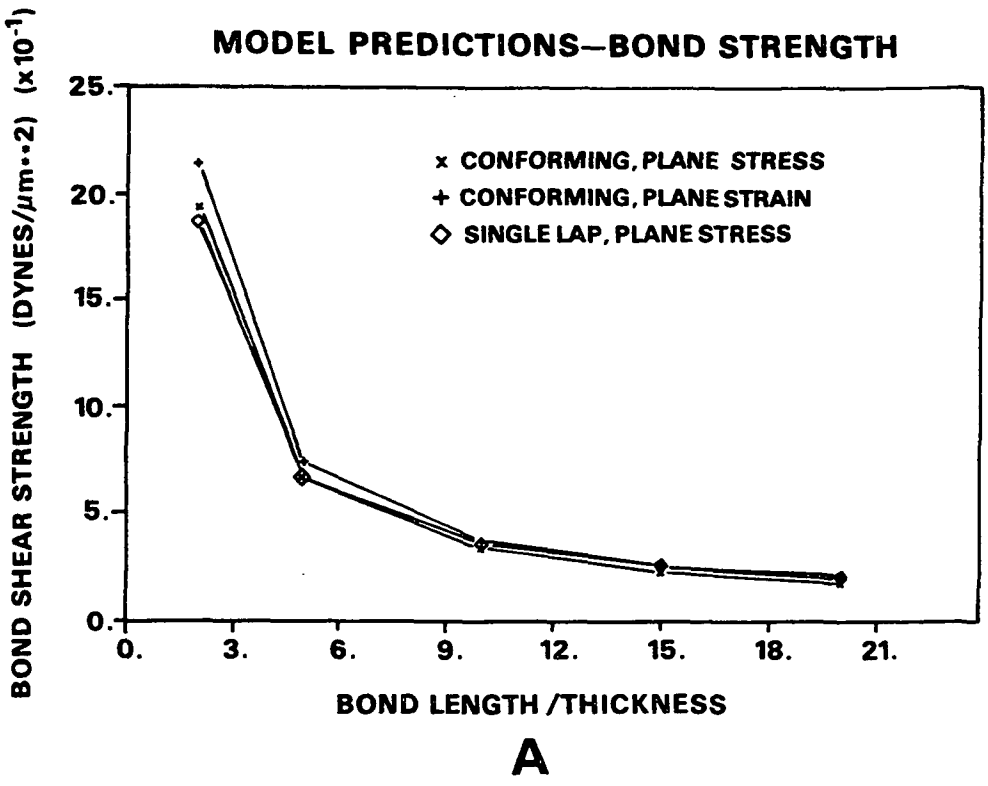

A

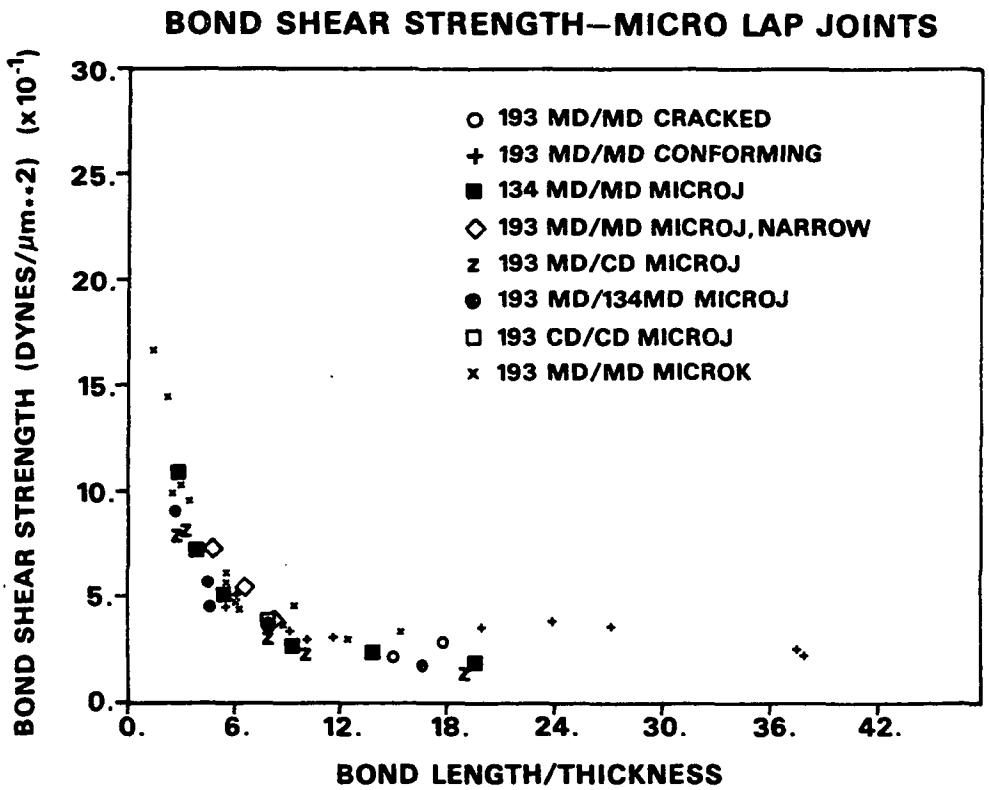

B

Figure 58. Effect of bond length on bond shear strength for microlap joint, (a) model predictions and (b) experimental results.

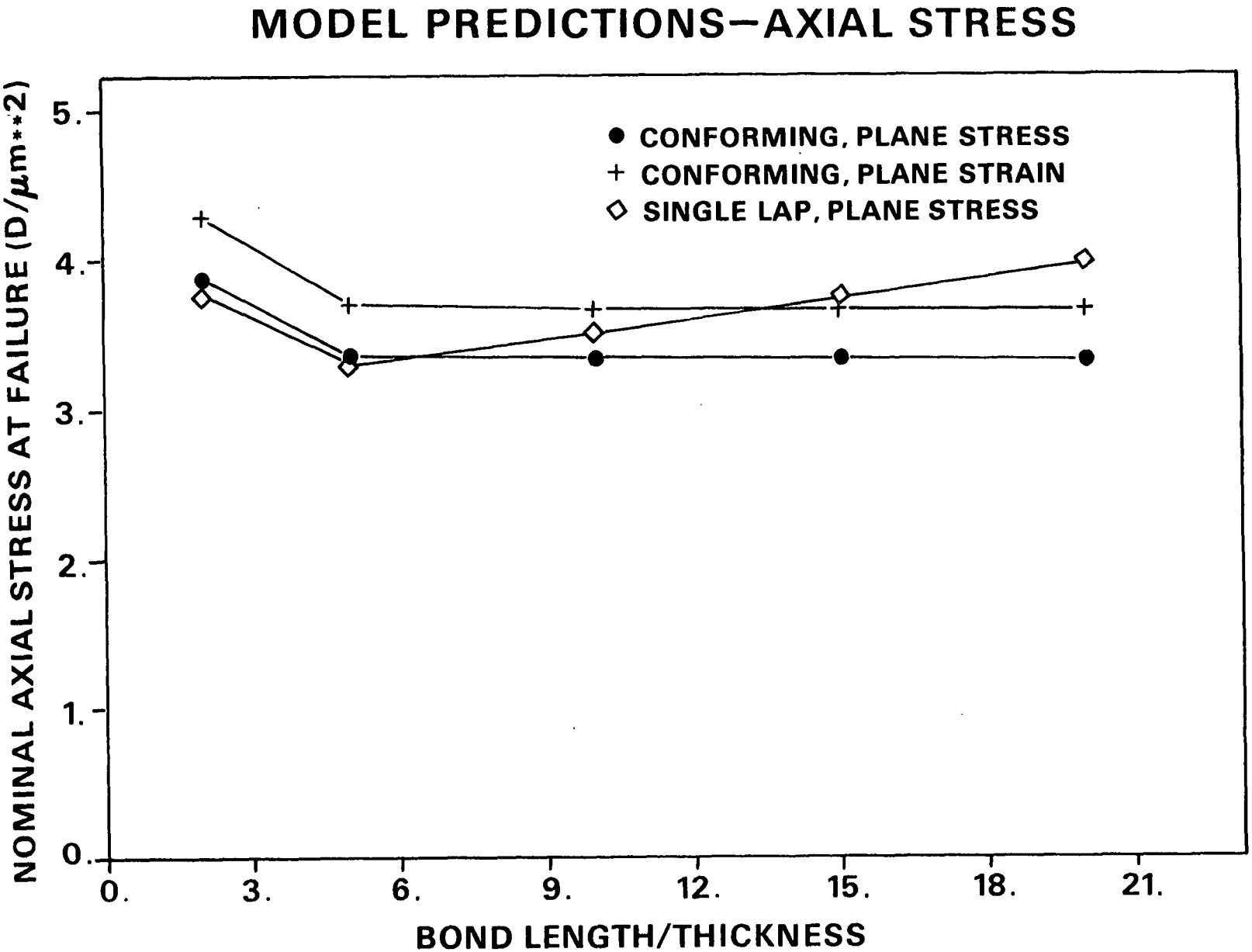

Figure 59. Predicted effect of bond length on nominal axial stress at failure.

The predicted σ_{nom_c} for the shortest bond length shows a sharp increase when compared to the other bond lengths. This model behavior is seen throughout the results and seems to be essentially independent of the other variable in question. This aberration may be associated with changes in the finite element grid refinement at $L/\overline{T} \leq 2.0$. Anderson, et al.[54] suggest maintaining as constant a finite element grid refinement in the crack tip region as possible to avoid erratic calculations. The model predictions for $L/\overline{T} \leq 2.0$ should be viewed with caution.

Interfacial Cracks

Compliance is the conforming lap joint mechanical property most seriously affected by interfacial cracks, and has been previously noted and seen in Fig. 56. The model also predicts a reduction in nominal axial stress at failure when an interfacial crack is present (Fig. 60). This strength reduction of about 4.5% is expected on the basis of the stronger singularity for 0° sharp cracks when compared to the 45° angle notch of the conforming model.[105] This trend also coincides with the experimental results on p. 95.

Fiber Thickness

The predicted effects of fiber thickness on the inverse modulus are shown in Fig. 61a. Thicker fibers are predicted to have a higher inverse modulus at the same bond length, a result expected on the basis of the experimental data in Fig. 61b.

This result agrees with the concept of larger moment generation around the overlap region leading to structures with increased inverse moduli for thicker fibers. The rate of change in $1/E_a$ with bond length change appears to be independent of thickness, a result in agreement with Eq. (16), the uniform stress

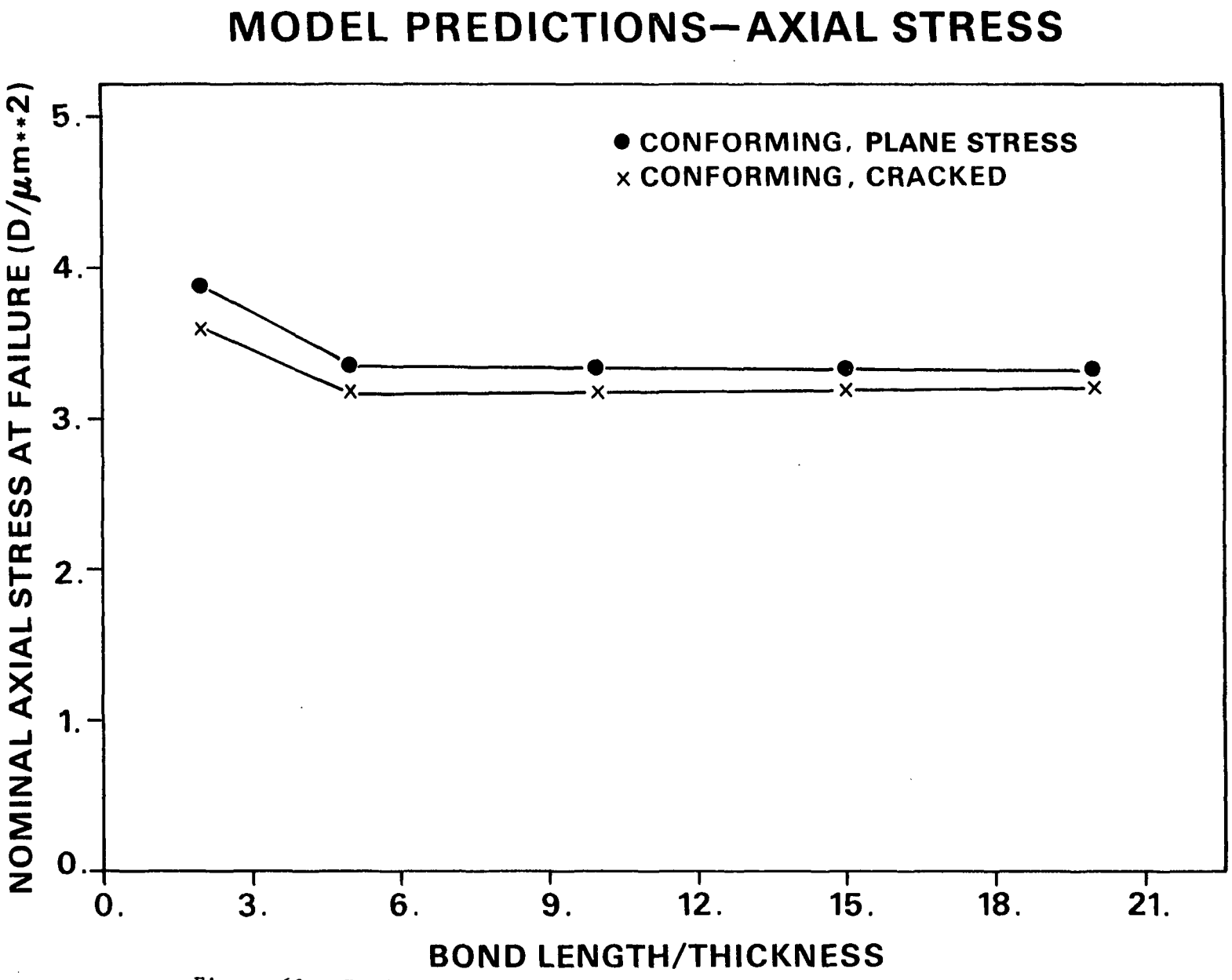

Figure 60. Predicted effects of interfacial cracks on the nominal axial stress at failure for microlap joints.

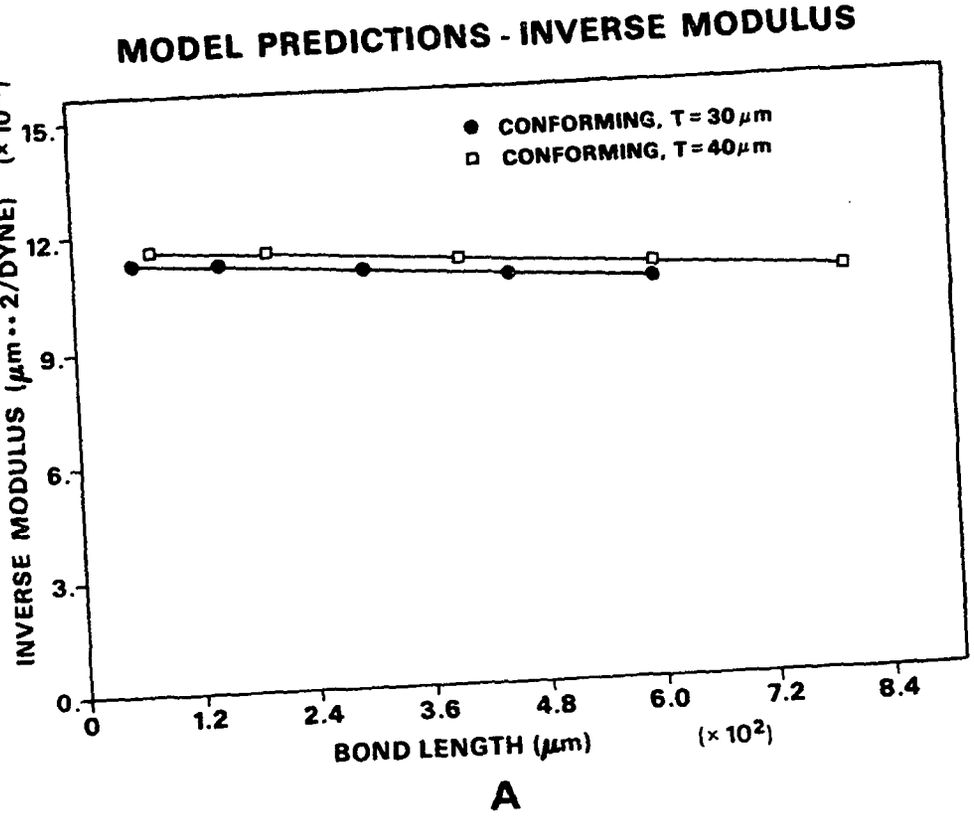

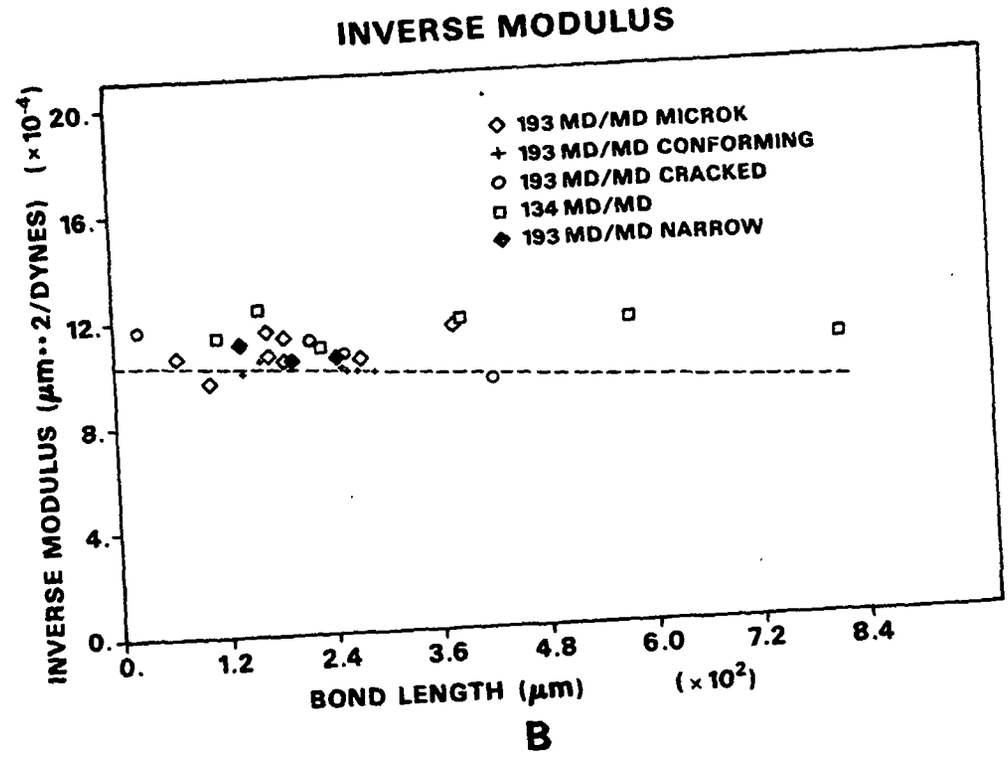

Figure 61. Effects of fiber thickness on the inverse modulus for microlap joint, (a) model predictions and (b) experimental data.

concept (dashed line in Fig. 61b). The slopes predicted by Eq. (16) and the theoretical model also agree (-0.14×10^{-6} μ m/dyne for both).

In Fig. 62a, the ratio of the nominal axial stress at failure of the thicker fiber (T = 40 μm) to that of the thinner fiber (T = 30 μm) is about 0.864. If the theoretical model were behaving in accordance with the findings of Chang and Muki,[76] the ratio should be 0.866. Chang and Muki[76] incorporated Goland and Reissner's equations[59] and linear elastic fracture mechanics theory (stress intensity factors) into their analytical model of a cracked lap joint with an infinitesimally thin adhesive layer. Excellent agreement is observed with their analytical model prediction of a $T^{-0.5}$ dependency. The experimental results of Fig. 62b exhibit a similar dependency.

Fiber Modulus

An influence of similar magnitude can be seen in Fig. 63a for a decreased fiber modulus. From continuum fracture mechanics theory, an expected nominal axial stress at failure dependence on $E^{0.5}$ would predict a decrease of 16.6% in σ_{nom_c} when CD modulus fibers are substituted for MD fibers. The model predicts an 18.2% decrease from the MD modulus value. The model appears to be performing according to the linear elastic fracture mechanics theory upon which it is based, especially when it is considered that other elastic constant changes are considered in the model, but not in the simple fracture mechanics relationship. Reasonable agreement with trend of the experimental data of Fig. 63b is noted.

Fiber Modulus Asymmetry

One of the limitations of a strictly energy approach to a fracture model is encountered when one considers asymmetric structures. When an asymmetry is present in a lap joint, the crack tip stress fields are also not symmetrical. Due

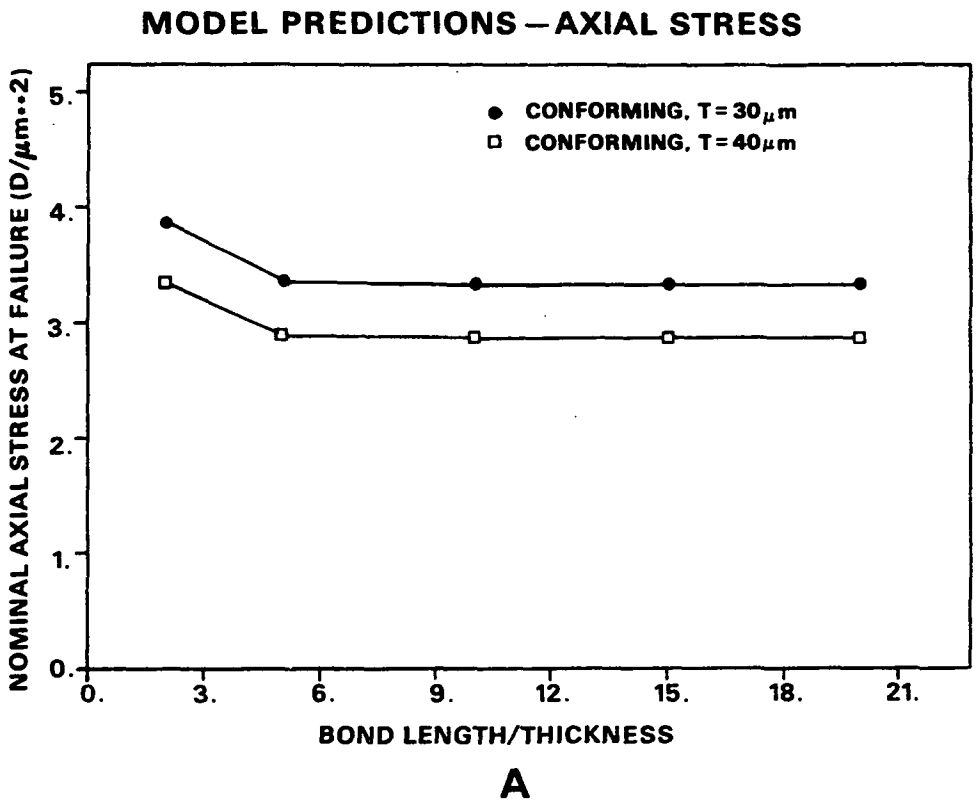

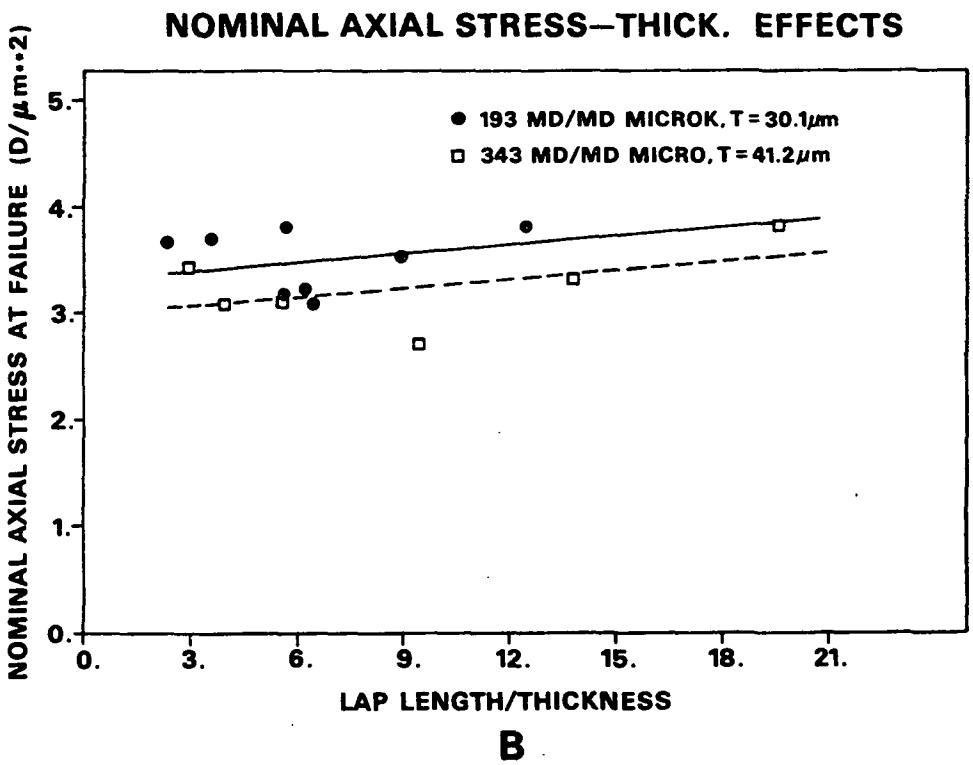

Figure 62. Effect of fiber thickness on nominal axial stress at failure for microlap joint, (a) model predictions and (b) experimental results.

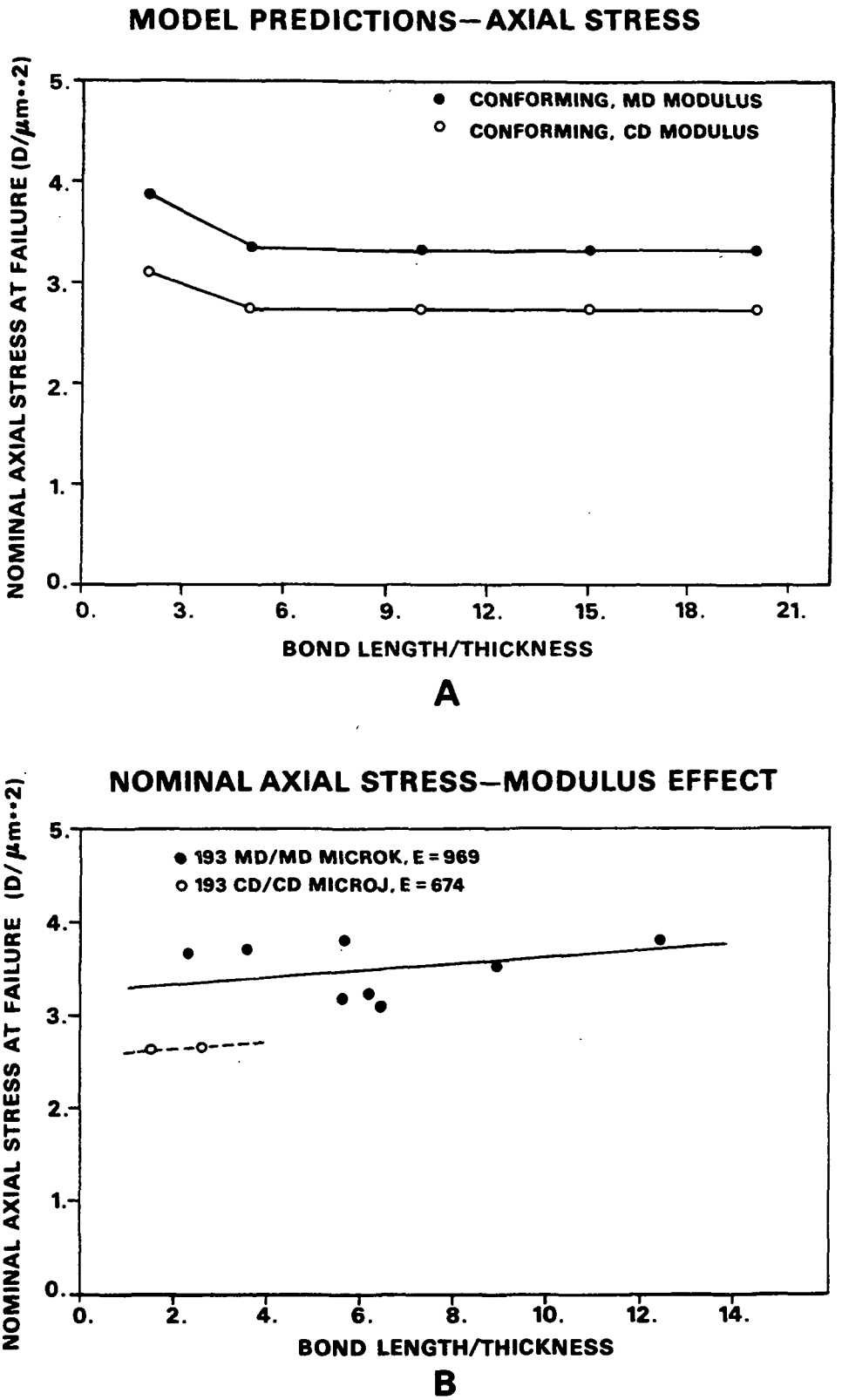

Figure 63. Effect of fiber modulus on nominal axial stress at failure for microlap joint, (a) model predictions and (b) experimental results.

to this asymmetry one crack tip stress field may be more intense than another. In a stored elastic energy difference approach, information about which crack tip stress field is initial cannot be obtained directly from the G calculation. Either prior knowledge of the influence of the asymmetry, or additional calculations will be required. By calculating the predicted strength for incremental cracking beginning at only one crack tip (one calculation for each crack tip), one can obtain the lowest predicted strength. In the asymmetric structure calculations shown in Fig. 64a and 65a and later in the comparison section, cracks were assumed, from prior knowledge of which stress field should be the more intense, to propagate from one end. To assure that a given single crack assumption was correct, the stress intensity factors calculated by FRACTR were examined to determine if the crack tip selected had the larger stress intensity factors.

The predicted effects of modulus asymmetry are presented in Fig. 64a. The model calculations show that the asymmetric construction is weaker than that with solely MD or CD modulus fibers. There is qualitative agreement with the experimental data in Fig. 64b; however, the experimental results show a decrease to 70.6%, while the model predicts a decrease to only 80.8% of the MD modulus configuration. Residual stress may account for this discrepancy. Some evidence of residual stress was noted in the MD/CD macrolap joints. Residual stress may occur in the MD/CD configuration from anisotropic swelling and shrinkage (i.e., CD shrinks more than MD). If residual stress was a factor in the MD/CD arrangement, it should not be a factor in the thickness asymmetry case because the anisotropy is aligned in the 193 MD/134 MD case, but not in the MD/CD case.

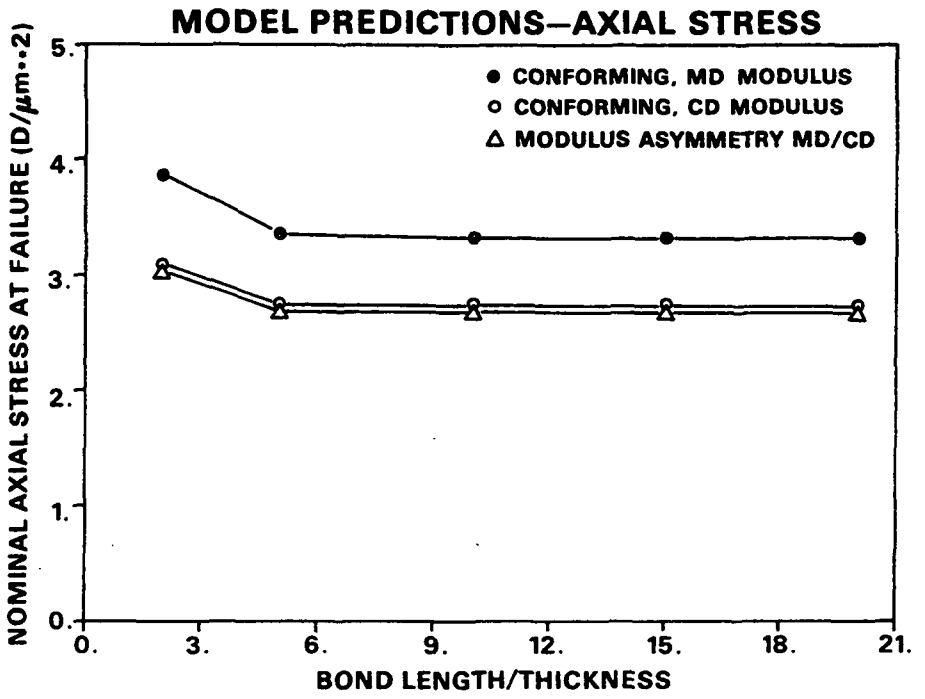

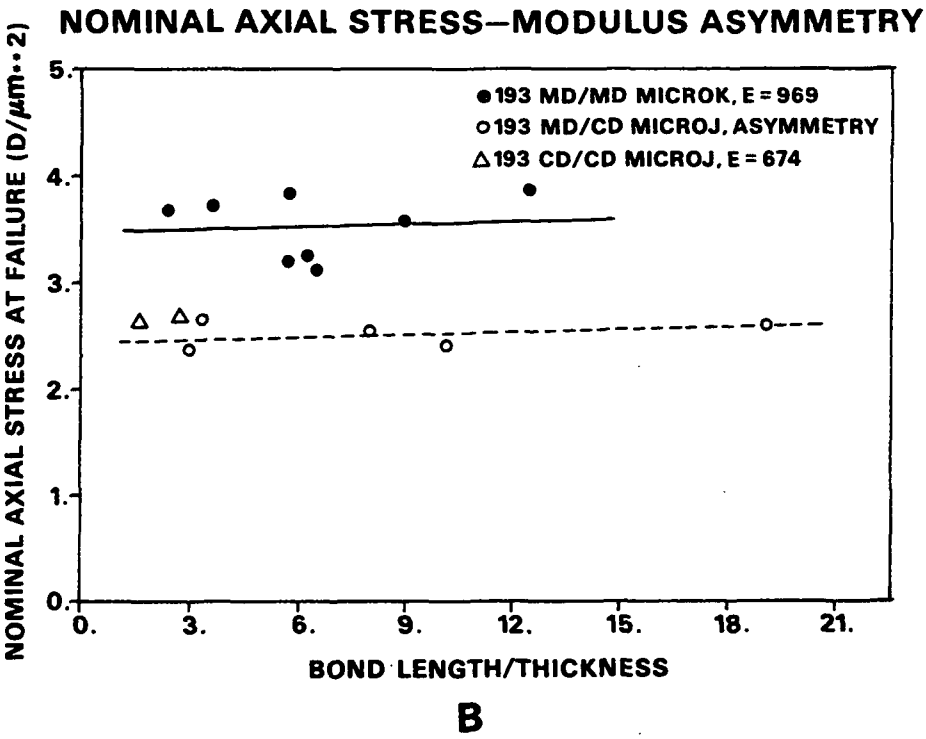

Figure 64. Effect of fiber modulus asymmetry on the nominal axial stress at failure for microlap joint, (a) model predictions and (b) experimental results.

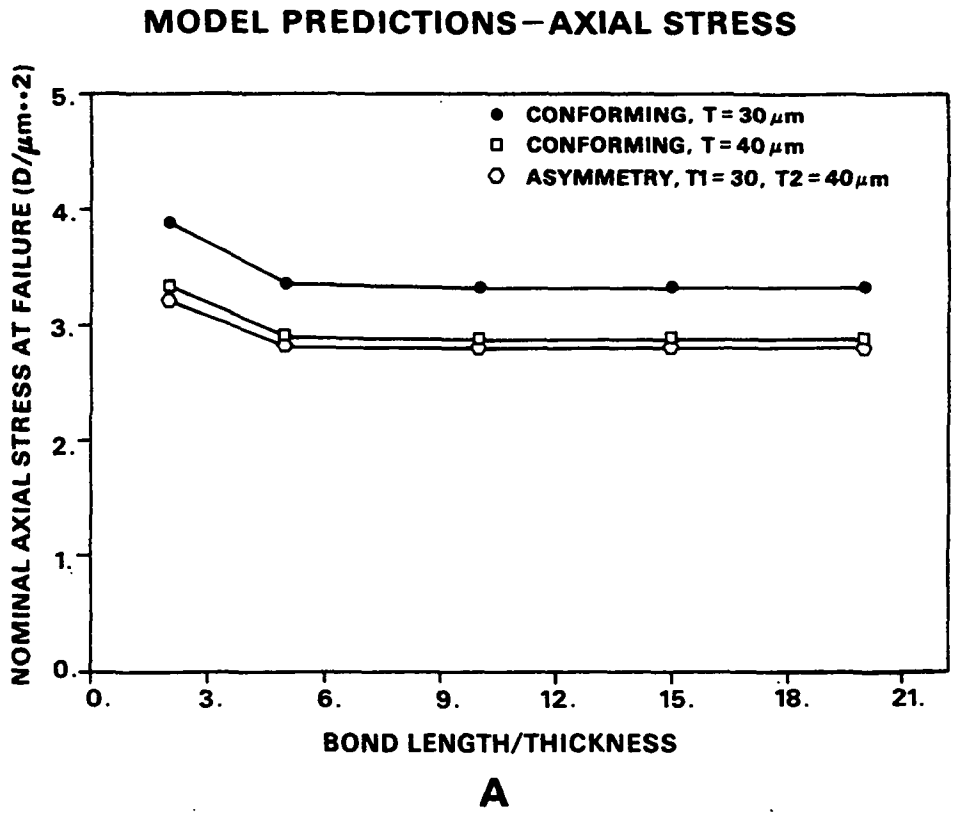

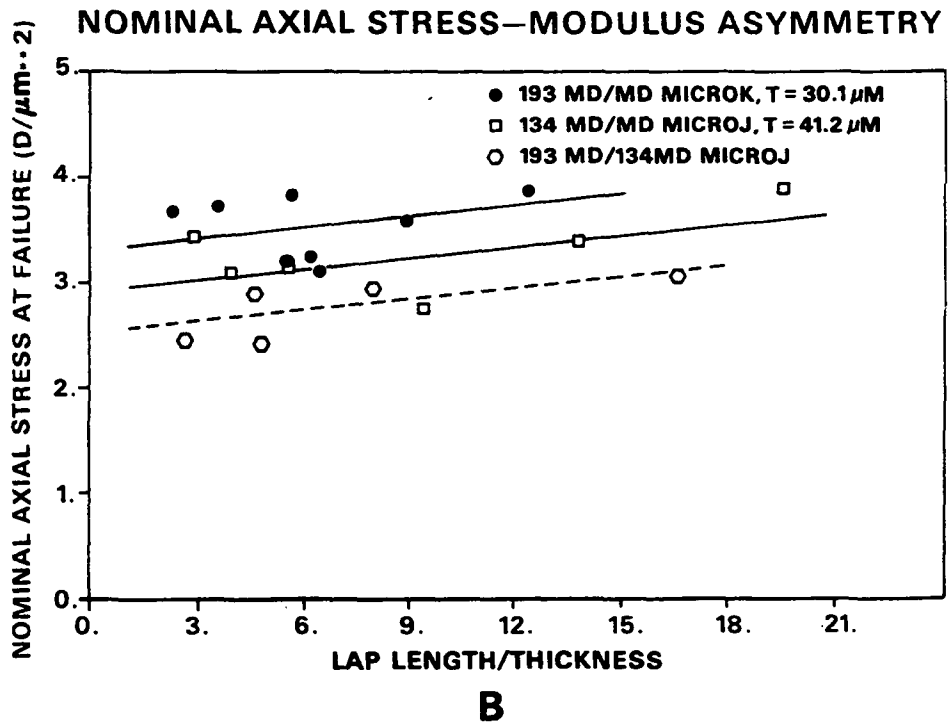

Figure 65. Effect of fiber thickness asymmetry on the nominal axial stress at failure for microlap joint, (a) model predictions and (b) experimental results.

Fiber Thickness Asymmetry

The minor additional decrease in σ_{nom_c} for the asymmetric condition, shown in Fig. 65a, is similar to that of Fig. 64a. When the model predictions (Fig. 65a) are compared to the experimental results (Fig. 65b), it is clear that the experimental asymmetry effect was greater than predicted (i.e., a decrease of 66.6% vs. the 84.1% predicted). There are apparently other factors influencing the experimental results that are not properly accounted for in these model calculations. The more direct case-by-case comparison, to be presented later, may be informative on this question.

Test Span

One of the difficulties encountered in any attempt to test fiber-fiber bonds in a manner closely analogous to that existing in paper is the test span. For most papers, the free spans between the bonded fiber crossings are quite short [e.g., 13.2 to 34.0 μm[28]]. In fact, totally free spans are, in many cases, not common. At such short spans in a highly anisotropic material, such as a wood fiber, there is a very distinct possibility that the fiber cross section is not uniformly stressed. This may occur because the load transfer is not uniform and the free fiber spans are not sufficiently long to allow the stress to become uniform across the fiber section.[116] The net effect of this is a considerably reduced apparent in-plane modulus. It is therefore of interest to put this model to use in examining a condition, which is not readily treated experimentally, to obtain some insight on the effects of these short test spans.

A cellophane microlap joint with a reasonable L/T = 10 (L = 300 μm) configuration was modeled at total test spans ranging from 3600 down to 450 μm (equal free spans of 75 μm). The results are shown in Fig. 66 for the prediction of σ_{nom_c}, and Fig. 67 for the prediction of $1/E_a$. At very short free

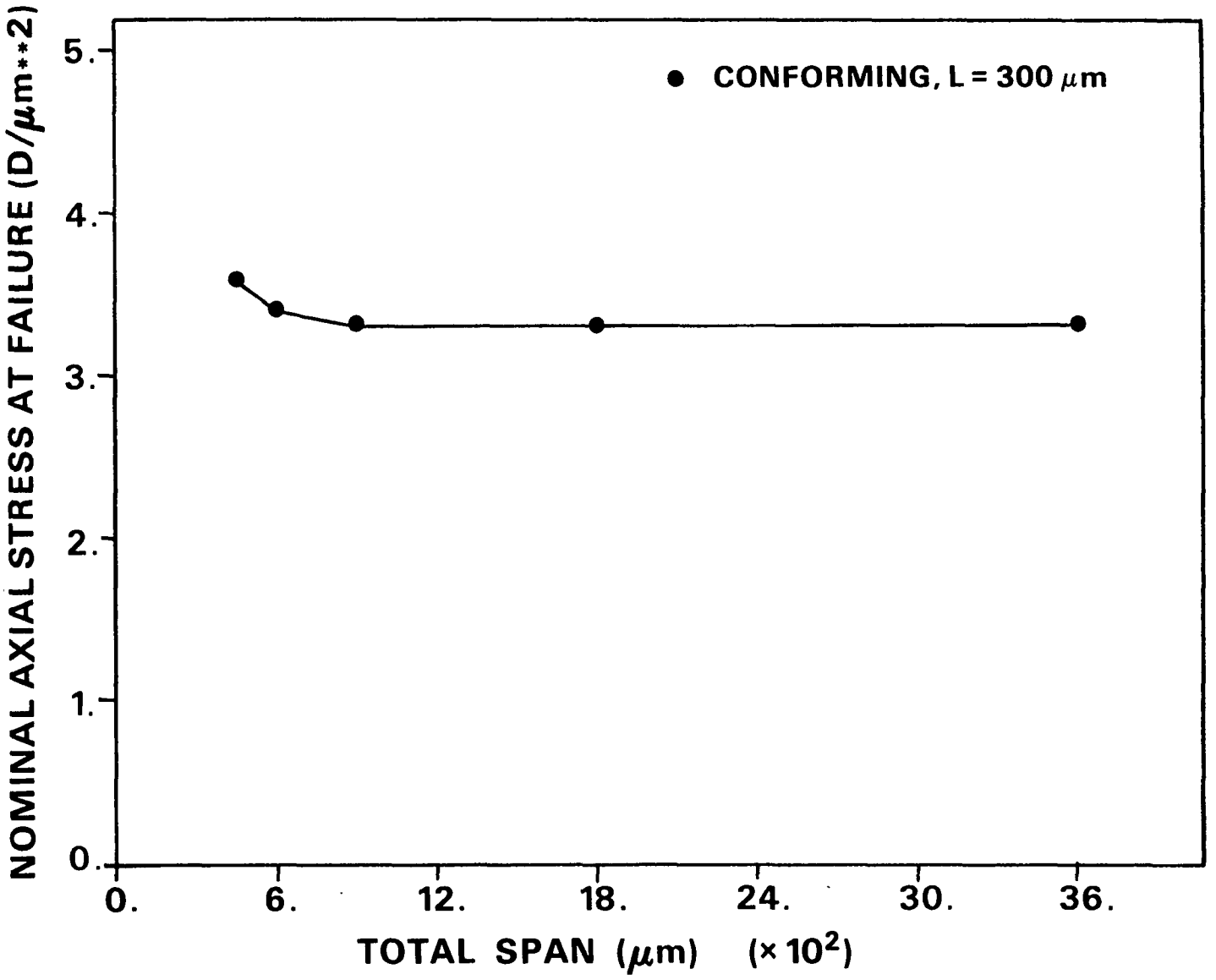

Figure 66. Predicted effect of total test span on nominal axial stress at failure for microlap joints.

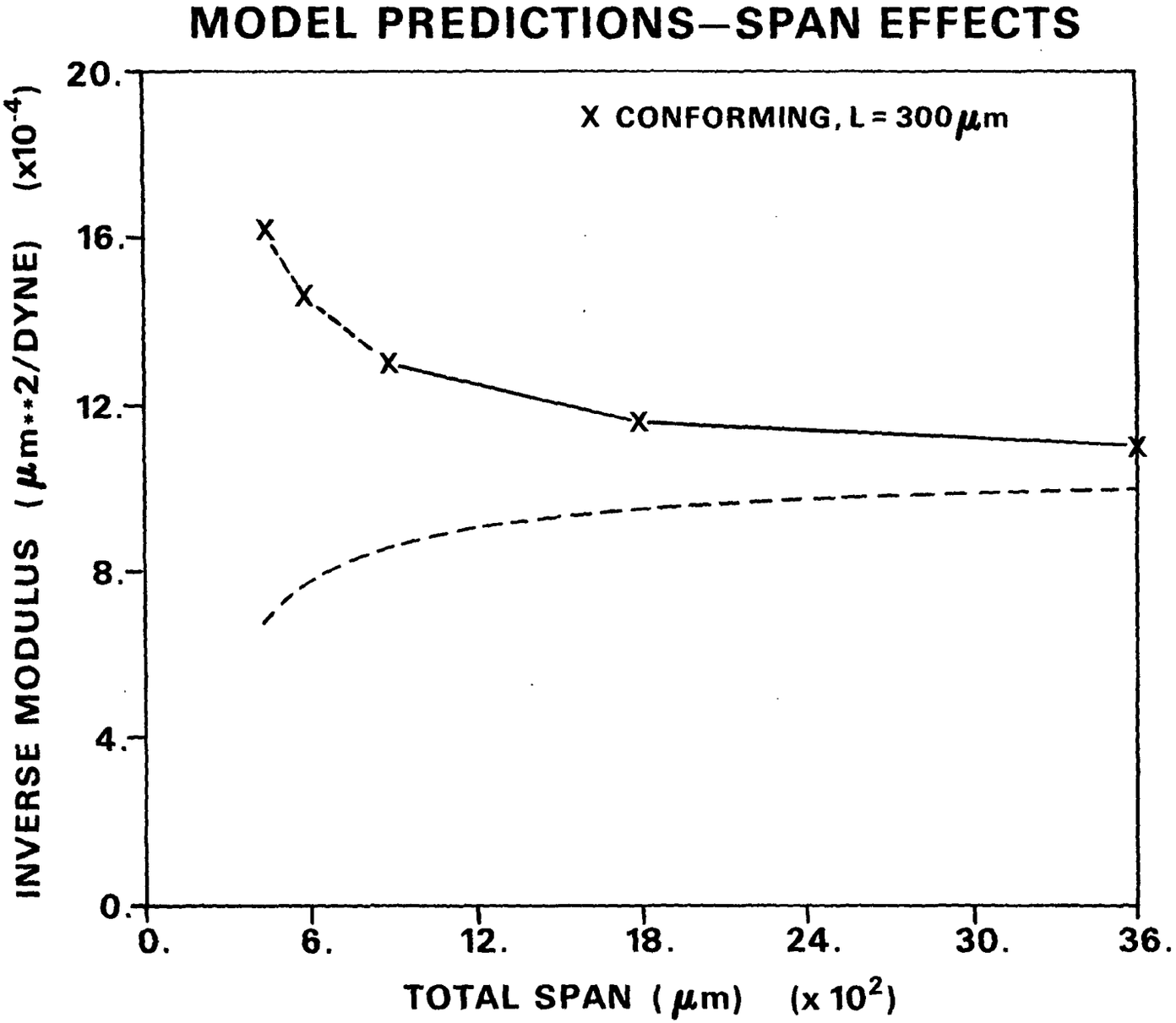

Figure 67. Predicted effect of total test span on inverse modulus for microlap joints. The dashed line represents the predictions of Eq. (16).

spans, σ_{nom_c} is predicted to increase about 10%. This probably results from less bond rotation and perhaps some alteration of the crack tip stress fields.

The changes in $1/E_a$, shown in Fig. 67, are more pronounced. The short test span lap joint has a roughly 1/3 higher inverse modulus than the structures typical of the Experimental Program. In reality, as the superimposed uniform stress assumption curve from Eq. (16) shows, the change is much greater. These predictions indicate that a very nonuniform stress distribution may occur in the cellophane lap joints at short test spans. This effect, if present in paper, may alter the assumed influence of fiber axial modulus on the in-plane modulus of paper.

Comparison of Theoretical Model and Experimental Results

To facilitate a more complete assessment of the ability of the theoretical model to predict the behavior of cellophane microlap joints, direct comparisons follow. All microlap joints that failed $\varepsilon_t < 0.5\%$ are included in each graph to allow a unified picture of the model capabilities to emerge. The model calculations were performed with all the experimental parameters for an individual microlap joint. There were three exceptions: (1) the elastic constants of the particular film in question were assumed constant for all fibers prepared from that film, (2) the fiber width was assumed to be constant along the span, and (3) the fracture toughness was assumed to be the same for all films (i.e., G_c = 5466 ergs/cm^2). Failure was assumed to occur simultaneously from both crack tips, except in those known asymmetric structures.

Bond Shear Strength

In the graph, shown in Fig. 68, a direct comparison between the theoretical model predictions and the experimental results for the bond shear strength ($\bar{\tau}$)

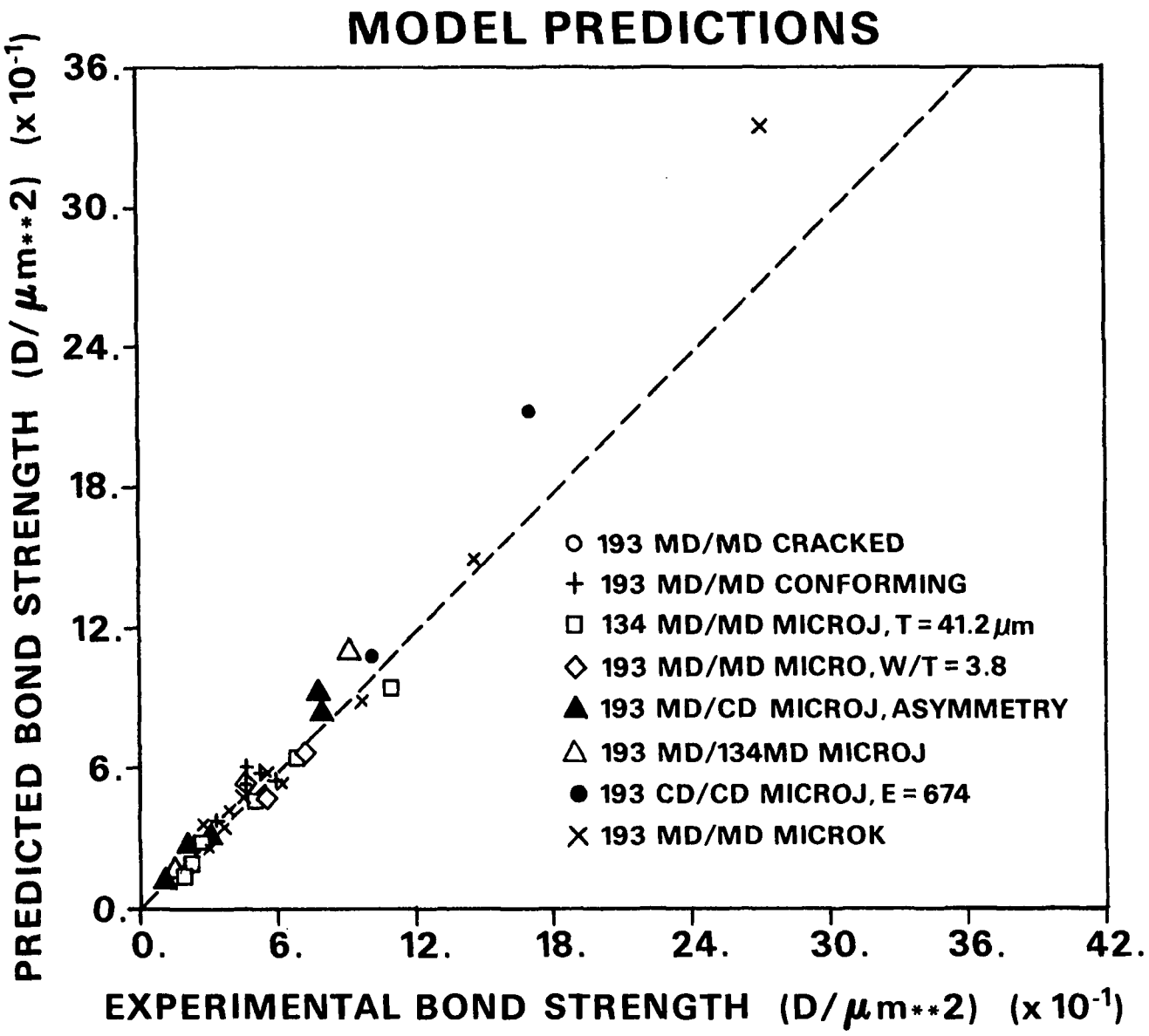

Figure 68. Comparison of theoretical model predictions to experiment results for the bond shear strength of microlap joints.

of cellophane microlap joints is presented. The dashed line represents a one-to-one correspondence between the two results. The theoretical model predictions are clearly in close agreement with the experimental bond shear strength data (maximum deviation ± 30%). Only the model predictions for some unusually low strength and 134 PUD-0 lap joints deviate appreciably. As might be expected, these high bond shear strength data points correspond to the shortest bond lengths (i.e., $L/\overline{T} \leq 2.0$). The tendency of the theoretical model to predict higher failure loads for these short bond length structures was pointed out and discussed previously.

The ability of the model to treat all of the experimental data is excellent. There are different bond lengths, moduli, thicknesses, widths, asymmetries, cracks, and degrees of conformity in the notch tip region among these data points. Most individual groups are scattered about the line, but the 134 PUD-0 MD/MD lap joint results appear to be consistently greater than the model predicts. In the model calculations, the same fracture toughness was assumed for all films. Although the 134 PUD-0 mechanical properties were virtually identical to that of 193 PUD-0, it is possible that the fracture toughness of 134 PUD-0 was greater than 193 PUD-0. An estimate of the average fracture toughness of 134 PUD-0 film from the model calculations is $G_c^* = 7360$ ergs/cm^2 compared to the $G_c = 5466$ ergs/cm^2 estimate from the experimental results for 193 PUD-0.

Nominal Axial Stress at Failure

This underprediction of the strength of the 134 PUD-0 MD/MD microlap joints is also seen in Fig. 69. Here a comparison between the model predictions and the experimental results is on the basis of the nominal axial stress at failure, σ_{nom_c}. The theoretical model predictions for the strength of a particular experimental data group do not vary as much as the experimental data. Thus, the

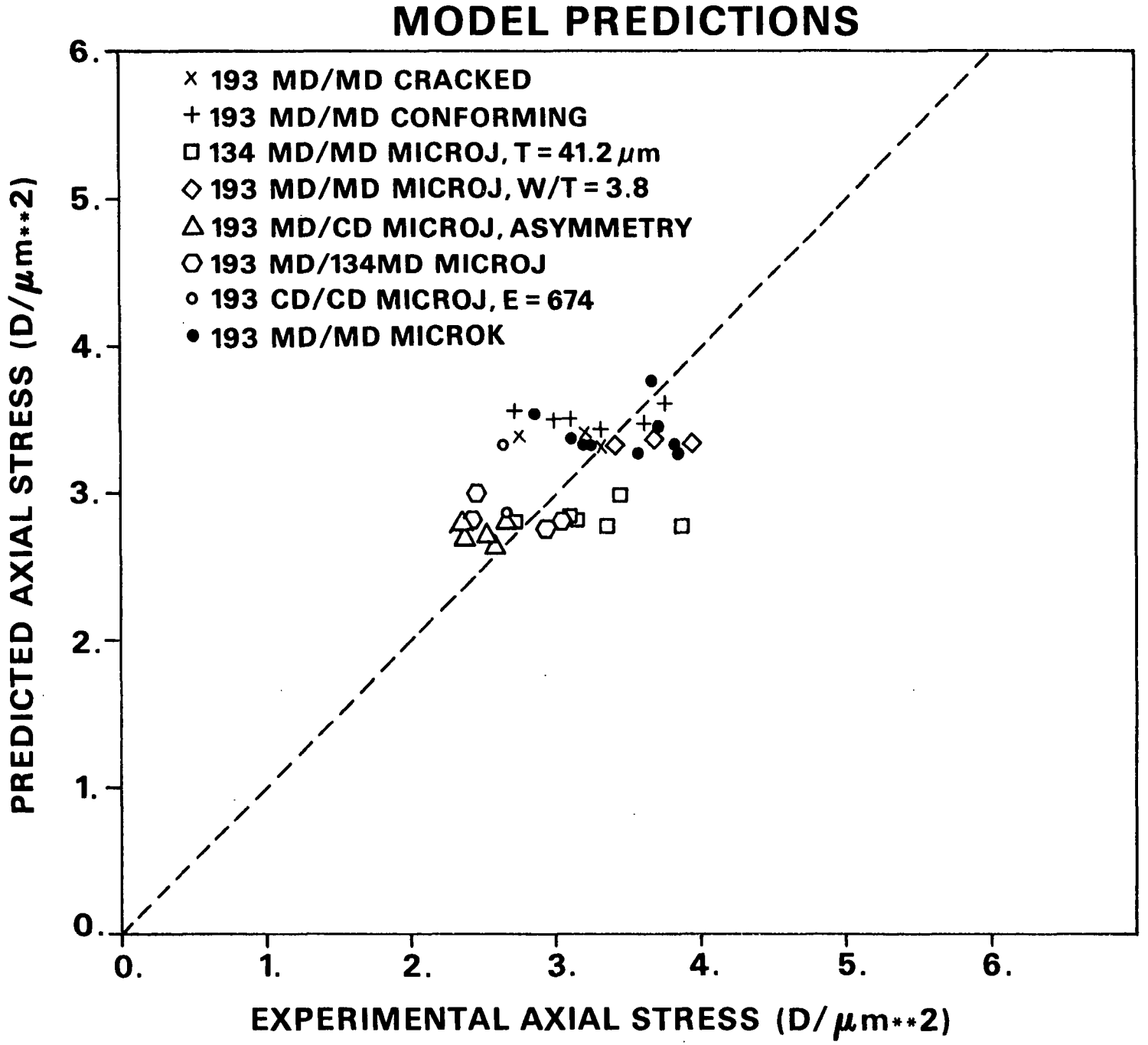

Figure 69. Comparison of the theoretical model predictions to the experimental results for nominal axial stress at failure of microlap joints.

data points tend to be stratified by groups. Most of the data groups are not uniformly distributed about the line. This is particularly true for the 134 PUD-O MD/MD structure (for the same possible reason given previously), the narrow 193 PUD-O MD/MD structures, and the 193 PUD-O MD/CD microlap joints. The narrow structure, if there is a width effect, would not be adequately treated by a two-dimensional assumption.

Janes,[51] noting a decrease in the bond strength of a butt joint composed of 193 PUD-O cellophane in the MD/CD configuration, suggested that the preferred orientation of the cellulose molecules in the MD direction might reduce the opportunities for molecular bonding as a result of 90° orientation angle difference (MD to CD). While a portion of his observed strength difference may be attributable to modulus asymmetry effects (as seen in this thesis), it is possible that there is a slight decrease in the bonding across the interface. There is also the likely, but unknown, contribution of residual stress generated by the asymmetric shrinkage of cellophane.

Critical Displacement

It is difficult to assess how well the theoretical model displacement predictions compare to the experimental results, except in total axial deformation sense. Such a comparison is presented in Fig. 70 for the critical displacement (total axial deformation at failure). In general, the agreement between the theoretical model predictions and the experimental results is good. It is clear, however, that the model is consistently less deformed at failure. The model predicts an overall average critical displacement of 13.1 μm compared to the experimental average of 14.4 μm, a difference of approximately 10%. With a plane stress assumption, the model was expected to be more compliant than the experimental structure. The plane stress assumption may have been more than

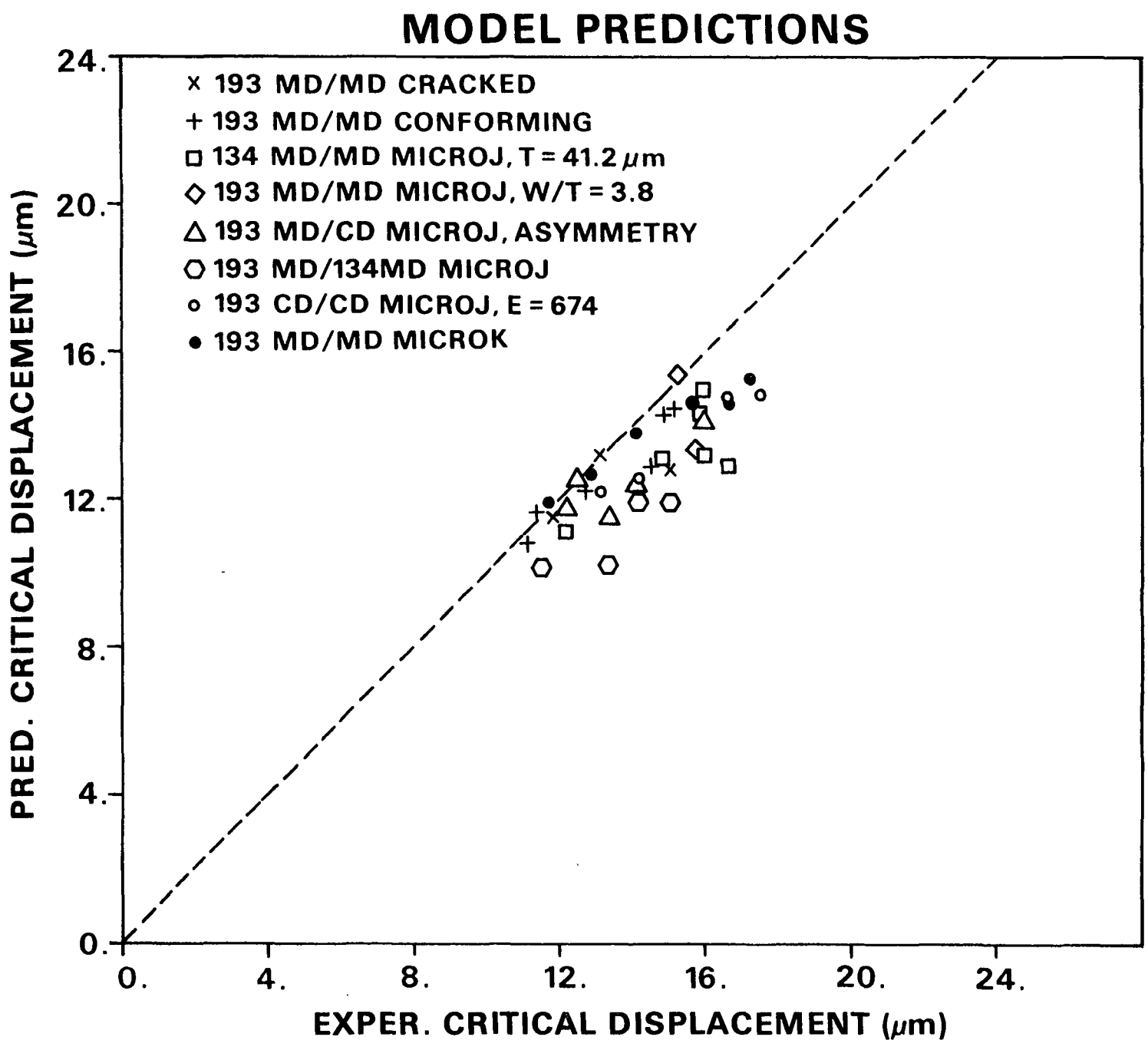

Figure 70. Comparison of the theoretical model predictions to the experimental results for the critical displacement of microlap joints.

adequately countered by the 45° notch assumption in the conforming model used in the calculations. From the compliance data, there was some evidence that the experimental structures were more compliant than would be expected if all the structures had a 45° notch configuration. The most likely explanation comes from the basic viscoelastic nature of cellophane (see Fig. 14). Many of the experimental load/elongation curves had some slight amount of nonlinearity, which could easily account for this difference of 1.3 μm. In a few cases, there was also some evidence of stable cracking, which would make the experiment structure deform more at the same load and contribute to this difference.

Strength Ratio

When the strength ratio, the ratio of the nominal axial stress at failure for the experimental results to that predicted by the theoretical model ($\sigma_{nom_c}/\sigma^*_{nom_c}$), is plotted against $L/\overline{T}$, as in Fig. 71, the influence of the viscoelastic material is also evident. There is a very slight trend of an increasing strength ratio as $L/\overline{T}$ increases, particularly for 134 PUD-O. With a viscoelastic material, such as cellophane, this trend is not surprising, because this tendency has been observed by DeVries, et al.[73] in viscoelastic adhesive joint systems. They found that the contribution of Mode II type fracture (shear) became larger as $L/\overline{T}$ increased (this was also observed in the model calculations in this thesis). Shih[87] has shown that, for nonideal brittle materials, Mode II fracture consumes more energy resulting in stronger lap joints at larger $L/\overline{T}$ values.

The plot in Fig. 71 shows that the theoretical model has a consistently good ability to predict the strength of the experimental structures.

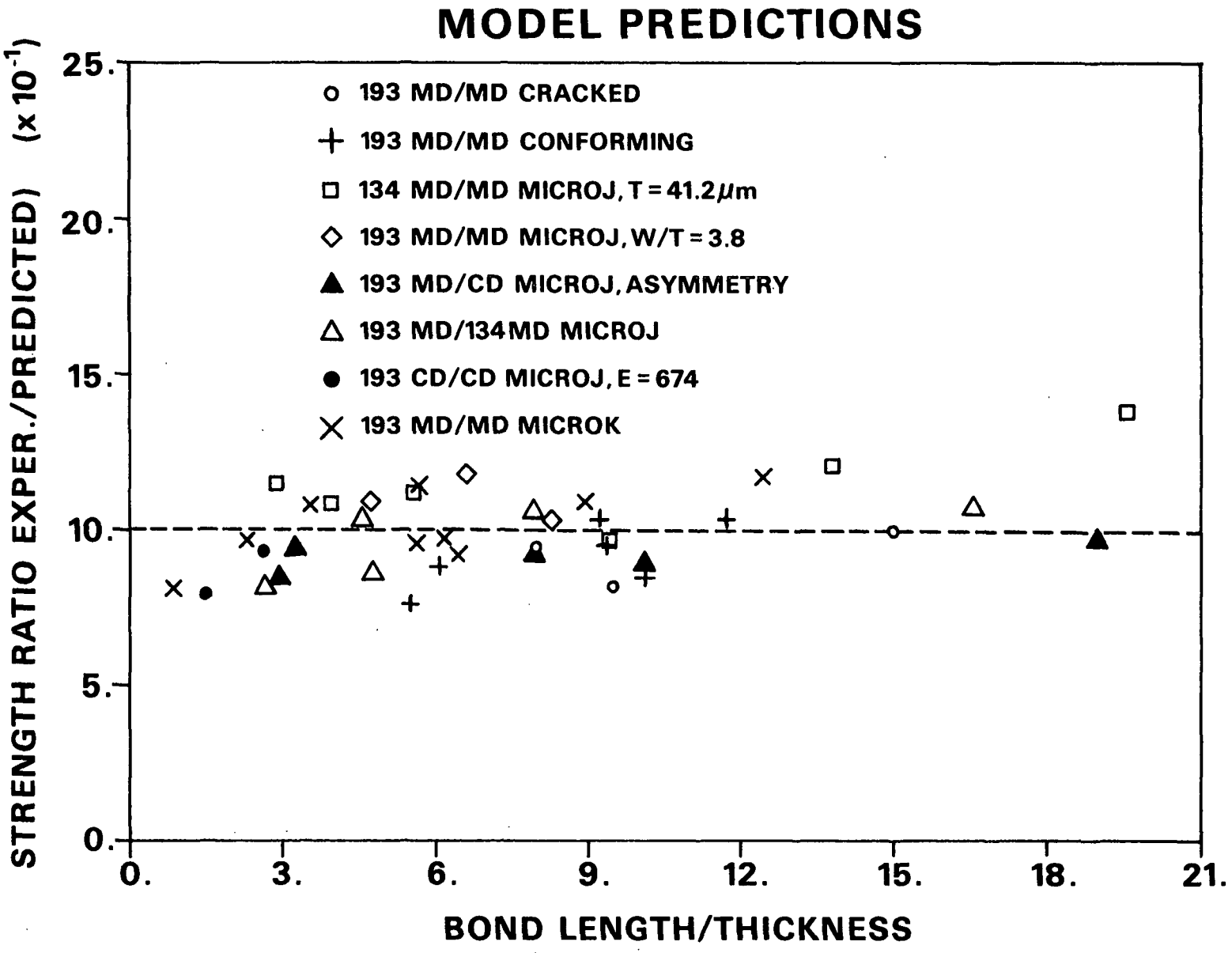

Figure 71. Relationship of the strength ratio ($\sigma_{nom_c}/\sigma^*_{nom}$) to the bond length to thickness ratio ($L/\bar{T}$) for the microlap joints.

The strength ratio mean value is 1.024, with a standard deviation of 0.135 and therefore a coefficient of variation of 13.2%. As a result of the two principal assumptions in the model calculations, there are built-in variations for which the model cannot account. The coefficient of variation of the experimentally derived fracture toughness presented in Table 6 (p. 103) was 22% and the elastic moduli listed in Appendix III was 5 to 10%. Fracture toughness was assumed constant for all lap joints and the elastic moduli were considered to be constant for a given film from which the fibers were obtained. When the model predictions are considered along with these two assumptions and the variation they may introduce, one can readily see that the model is capable of predicting the strength of the experimental fiber-fiber bond structures.

CONCLUSIONS

From the combined evidence of the Experimental and Theoretical Programs, it is concluded that the strength of the fiber-fiber bond is dependent on a variety of structural and material parameters. It should be possible to extrapolate our conclusions to the behavior of the bonds in paper to the extent that a cellophane fiber lap joint is analogous to the bonded wood fiber structure. The more nearly linear elastic the response of the bonded wood fiber, the more applicable the conclusions derived from the theoretical model should be.

Bond length is the dominant parameter in determining the bond shear strength (i.e., failure load per unit bond area). Bond shear strength is inversely proportional to bond length (the bond area dimension in the direction of loading). This conclusion is at variance with the current view, widely held in the paper industry, that bond shear strength is a constant for a given pulp. Unless the bond between wood fibers is highly viscous in nature, this dependency on bond length should exist.

A better measure of the strength of fiber-fiber bonds is the nominal axial stress at failure (i.e., the failure load per fiber cross-sectional area). From the experimental and theoretical results, it is concluded that the nominal axial stress at failure (σ_{nom_c}) changes very little with bond length changes. It, however, is considerably more sensitive to other structural and material parameters, such as fiber thickness, fiber modulus, conformity, interfacial cracks, and structural and material asymmetries.

Fiber thickness (T) is found to have an approximately $1/\sqrt{T}$ relationship with σ_{nom_c}. Thicker fibers therefore can be expected to reduce the load carrying capacity of a bonded fiber network such as paper.

The effects of fiber width (W) on σ_{nom_c} are unclear. Some slight reduction in bond strength is indicated.

Fiber modulus (E) effects on σ_{nom_c} are very evident. The theoretical and experimental results show that nominal axial stress at failure is proportional to the square root of the fiber modulus (i.e., $\sigma_{nom_c} \propto \sqrt{E}$). Therefore, when fiber modulus, which is very morphology dependent, increases, it would tend to increase the strength of bonded structures.

Two types of asymmetries have been studied. Both asymmetry conditions, fiber modulus and fiber thickness differences, are found to cause a decrease in the strength of the lap joint structures. Asymmetric constructions are the natural state for bonded wood fiber structures.

Other structural parameters, fiber conformity and interfacial cracks, are found to have only a very minor impact on σ_{nom_c}. Fiber conformity, however, is found to have a pronounced influence on the compliance of the lap joint structure. As a fiber increasingly conforms to the other fiber of the pair bond, the lap joint structure becomes much less compliant. This result may mean that the increased modulus in paper, resulting from beating and wet pressing, occurs specifically because fibers conform better to each other, in addition to the effects of increased bond area and number of bonds. Interfacial cracks were found to considerably increase the compliance of the conforming type bonds. The partial bond breakages observed by Page, et al.[29] may, therefore, result in a reduced resistance to deformation in the paper, a conclusion compatible with the reduced slope of that portion of the load/elongation curve of paper where partial bond breakages are known to occur frequently.

The fracture toughness of the 193 PUD-O cellophane fiber lap joints is estimated directly from experimental results and indirectly confirmed by the theoretical results to be $G_c \sim 5466$ ergs/cm^2.

The theoretical model incorporating orthotropic linear elastic material and continuum fracture mechanics assumptions is found to be capable of predicting the bond shear strength of the experimental cellophane microlap joints within ± 30%. The effects of all the major structural and material variables are accounted for by this model. Experimental critical displacements (maximum axial displacements) are found to be consistently larger (+ 10%) than those predicted by the model. This is attributed to the viscoelastic nature of the experimental material. There was some evidence that as bond length increases, the fracture toughness of the cellophane lap joint increases. This is explained on the basis of an increase in Mode II (shear) contribution to fracture as bond length increases. Energy consumption is expected to be greater for Mode II fracture in any real material (i.e., not purely elastic).

An underlying objective of this thesis has been to develop a model that could be refined and extended to wood fiber lap joints and eventually to the general fiber-fiber bond case. In Appendix VI some preliminary experimental results for wood fiber lap joints are presented. Multiple linear regression analysis of these data provide evidence that structural parameters found to correlate with the strength of cellophane lap joints (L/T, T/W, T) also correlate with the strength of the wood fiber lap joints. The fracture behavior of wood fiber lap joints exhibited substantial linear elastic character. These results lead one to believe that the same techniques developed in this thesis can be applied to general fiber-fiber bond structures.

SUGGESTIONS FOR FUTURE WORK

Cellophane fiber lap joints have been shown, in this thesis, to fracture in a manner consistent with linear elastic fracture mechanics theory. The most obvious suggestion for future work is to extend the investigation to lap joints constructed of wood fibers. The preliminary experimental results, presented in Appendix VI, provide evidence that lap joints of loblolly pine holocellulose tracheids fail with substantial linear elastic character. An extension of the present two-dimensional linear elastic fracture mechanics model to the wood fiber lap joint structure would appear to be useful only as a first approximation, since the microfibril orientation, and other variables, could not be represented adequately. It may be possible to empirically establish the role of microfibril angle in the strength of lap joints by studying the relationship between it and the two-dimensional model strength predictions.

Expansion of the linear elastic fracture mechanics model to three-dimensions should allow a systematic study of the effects of microfibril angle and crossing angle on fiber-fiber bond strength. The additional computation time and expense of including the third dimension warrants development of more efficient algorithms for fracture toughness calculation. Computation time should be reduced by a factor of two by using Parks'[117] technique to obtain fracture toughness from the derivative of the stiffness matrix. The inherent asymmetries of the fiber-fiber bond structure present a major obstacle to model predictions of bond strength because the direction of crack propagation must be assumed. Some systematic approach to making this assumption would need to be developed.

The three-dimensional model may be more valuable if it is used in a qualitative sense to expand our understanding of the nature of the deformations and

stress distributions which are likely to occur in fiber-fiber bonds under load in paper. Analysis of the stress distributions in a unit cell of paper should be attainable by combining direct digitalization of paper structure data from image analysis of paper surfaces and cross sections with a representation of that structure in an optimized finite element grid.

LIST OF SYMBOLS AND NOMENCLATURE

A_b = bond area, $(W \times \overline{L})$

$\overline{A_x}$ = average cross-sectional area, $(\overline{T} \times \overline{W})$

a = crack length

a_t = total crack length

$[B]$ = strain-displacement matrix

C = compliance

C_{ij} = elastic stiffness coefficients

CD = cross-machine direction

coefficient of variation = (standard deviation)/(arithmetic mean), $(S.D.)/\overline{X}$

$[D]$ = elasticity matrix

d = virtual displacement

E = axial elastic modulus, general

E_a = apparent modulus

E_x = elastic modulus in MD direction

E_y = elastic modulus in CD direction

E_z = elastic modulus in z-direction

F = nodal force on element

f = force, general

$f(x,y)$ = function of variables x, y

G = strain energy release rate

G_c = fracture toughness

G^* = predicted fracture toughness

$\hat{G}$ = unit strain energy release rate

g = distributed external loadings

$i,j,k,\ldots$ = general indices

J = J-Integral

$[K]$ = stiffness matrix

K_I = stress intensity factor, Mode I

K_{II} = stress intensity factor, Mode II

K_{III} = stress intensity factor, Mode III

$[k]$ = element stiffness matrix

L = bond length

$\overline{L}$ = average bond length, $(L_1 + L_2)/2$

MD = machine direction

$[\ ]^T$ = transpose of matrix

$[\ ]^e$ = matrix associated with a specific element

N_i = shape function

P, P_i = loads

P_c = critical load

P_o = load at δ_o

p = distributed load on element

Q = specific singular assumption

R^2 = square of correlation coefficient

$[R]$ = boundary nodal force matrix

r = radial distance from crack tip

S_1, S_2 = free span length

S_t = total free span length

$\{s\}$ = dummy matrix, for solution of equilibrium equations

T = thickness, general

T_A = thickness of adhesive layer

T_b = tensile breaking length

$\overline{T}$ = average fiber thickness, $(T_1 + T_2)/2$

T	=	thickness of overlap region
T_1, T_2	=	free span fiber thickness
U	=	strain energy
u, v	=	displacement along x-axis and y-axis
u_i	=	displacement in the i-direction
u_r, u_θ	=	displacements along and perpendicular to radius, r
$\dot{u}$	=	velocity, time derivative of displacement, u
$\ddot{u}$	=	acceleration, time derivative of velocity; u
V	=	potential energy from external loads
$V_{so_{ij}}$	=	acoustic wave velocity in planar material
V_{xx}, V_{yy}, V_{zz}	=	acoustic wave velocity in infinite material
W	=	width, general
$\overline{W}$	=	average width, $(W_1 + W_2)/2$
W	=	width of overlap region
W_1, W_2	=	free span fiber width
w	=	displacement along z-axis
x, y	=	global coordinate system
$\overline{X}$	=	arithmetic mean
α_i	=	polynominal coefficient, general
Γ	=	line contour enclosing crack tip
γ_a	=	adhesive specific fracture energy
γ_c	=	cohesive specific fracture energy
γ_{xy}	=	shear strain
δ	=	displacement, general
δ_o	=	displacement resulting from load P_o
δ_t	=	total axial displacement

ACKNOWLEDGMENTS

My sincere appreciation is extended to my Thesis Advisory Committee: Dr. Richard W. Nelson, Chairman, for a kind disposition and insightful, but gentle, criticism which caused one more manuscript to take shape with a minimum of student anguish; Dr. John W. Swanson, for many worthwhile suggestions and encouragement to apply to the Institute; and Dr. William S. Peterson, for stimulating discussions about the finite element method, in particular, and my thesis, in general. To my former thesis chairman, Dr. J. P. Brezinski, goes my admiration for having perceived the analogy, and my thanks for allowing me to exploit it.

I am grateful to John J. Bachhuber, John O. Church, and John C. Teed for a willingness to listen, encouragement to try, and help to complete my computations. I am indebted to Keith W. Hardacker for listening, suggesting, and helping with my equipment design and experimental testing, and Marvin C. Filz, Jr. and Paul F. Van Rossum for their patience with this and other student ideas and for skillful creation of my equipment. To Fred Sweeney and his helpful group, many thanks for all the image reproductions. I am thankful for the expert manuscript typing and kind heart of Linda Kroiss. To all the other faculty and staff to whom I am indebted, I offer my appreciation and apology for not making this list unduly long.

My gratitude goes to my fellow students for allowing this mature person to be a student. Thanks go to Ron Mann for acoustic measurements, and special thanks go to F.-J. Chen for broadening my education.

For making this unique educational experience possible, I sincerely thank The Institute of Paper Chemistry and its member companies.

My wife, Christina, and our children, Alan II and Angela, have shown tremendous stamina, self-sacrifice, and support through all the years of my education. I can never appropriately thank them.

LITERATURE CITED

1. Van den Akker, J. A. Some theoretical considerations on the mechanical properties of fibrous structures. Vol. I. p. 205-41. In Formation and Structure of Paper (F. Bolam ed.). Trans. of Symp. held at Oxford, Sept. 1961. Tech. Sect. Brit. Paper and Board Makers' Assocn., London, 1962.

2. Perkins, R. W., Wood Fiber 5(1):26-33(1973).

3. Dodson, C. T. J. A survey of paper mechanics in fundamental terms. Vol. I. p. 202-26. In Fundamental Properties of Paper Related to Its Uses (F. Bolam ed.). Trans. of Symp. held at Cambridge, 1973. Tech. Sect. Brit. Paper and Board Makers' Assocn., London, 1974.

4. Griffith, A. A., Philosophical transactions, Royal Soc. (London), Series A, 221:163-98(1920).

5. Irwin, G. R., J. Appl. Mech. 24:361-4(1957).

6. Mark, R. E. Cell wall mechanics of tracheids. New Haven, Yale University Press, 1967.

7. Mark, R. E.; Gillis, P. P., Tappi 56(4):164-5(1973).

8. Page, D. H.; El-Hosseiny, F.; Winkler, K.; Lancaster, A. P. S., Tappi 60(4):114-7(1977).

9. Panshin, A. J.; de Zeeuw, C. Textbook of Wood Technology. 3rd ed. Vol. I, New York, McGraw-Hill, 1970.

10. McMillen, C. W., Wood Sci. Technol. 2:166-76(1968).

11. Dinwoodie, J. M., Tappi 48(8):440-7(1965).

12. Horn, R. A. Morphology of wood pulp fiber from softwoods and influence on paper strength. Madison, WI, USDA Forest Serv. FPL 242, 1974.

13. Tamolang, F. N.; Wangaard, F. F., Tappi 44(3):201-16(1961).

14. Huggins, M. L., J. Org. Chem. 1:407-56(1936).

15. Van den Akker, J. A., Tappi 42(12):940-7(1959).

16. Corte, H.; Schaschek, H., Papier 9:519-30(1955).

17. Nissan, A. H., Tappi 42(12):928-33(1959).

18. Robertson, A. A., Tappi 53(7):1331-9(1970).

19. Campbell, W. B., Forest Serv. Bull. 84, Dept. of Interior, Canada, 1933.

20. Page D. H.; Tydeman, P. A. Theory of the shrinkage, structure, and properties of paper. Vol. II. p. 397-413. In Formation and Structure of Paper (F. Bolam ed.). Trans. of Symp. held at Oxford, Sept. 1961. Tech. Sect. Brit. Paper and Board Makers' Assocn., London, 1962.

21. Asunmaa, S.; Steenberg, B., Svensk Papperstid. 61(186):686-95(1958).

22. Smith, W. E. Investigation of a method for measuring interfiber bonding in pulp handsheets based on sheet and fiber d.c. electrical conductivities. Doctor's Dissertation. Raleigh, N.C., North Carolina State University, 1969.

23. Luner, P.; Karna, A. E. U.; Donofrio, C. P., Tappi 44(6):409-14(1961).

24. Swanson, J. W.; Steber, A. J., Tappi 42(12):986-94(1959).

25. Page, D. H., Paper Technol. 1(4):407-11(1960).

26. Button, A. F., unpublished work, 1975.

27. Barber, H. A. The determination of the energy site distribution of the surface of cellulose fibers by gas adsorption methods. Doctor's Dissertation. Appleton, WI, The Institute of Paper Chemistry, 1969.

28. Page, D. H.; Tydeman, P. A.; Hunt, M. A study of fibre-to-fibre bonding by direct observation. Vol. I. p. 171-93. In Formation and Structure of Paper (F. Bolam ed.). Trans. of Symp. held at Oxford. Tech. Sect. Brit. Paper and Board Makers' Assocn., London, 1962.

29. Page, D. H.; Tydeman, P. A.; Hunt, M. The behavior of fibre-to-fibre bonds in sheets under dynamic conditions. Vol. I. p. 249-63. In Formation and Structure of Paper (F. Bolam ed.). Trans. of Symp. held at Oxford. Tech. Sect. Brit. Paper and Board Makers' Assocn., London, 1962.

30. Nordman, L.; Gustafsson, C.; Olofsson, G., Paperi Puu 34(3):47-52 (1952); 36(8):315-20(1954).

31. Karna, A., Paperi Puu 43(8):465-72(1961).

32. Van den Akker, J. A., Tappi 52(12):2386-9(1969).

33. Stone, J. E., Pulp Paper Mag. Can. 64(12):T528-32(1963).

34. Erdogen, F. Crack-Propagation Theories. Vol. II. p. 500. In Fracture: An Advanced Treatise (H. Liebowitz ed.). New York, Academic Press, 1968.

35. Smith, J. C.; Graminski, E. L. Characterizing the interfiber bond strengths of paper pulps in terms of a breaking energy. In Preprints, Ann. TAPPI Mtg., Atlanta, GA, 1977.

36. Wink, W. A.; Van Eperen, R. H., Tappi 50(8):393-400(1967).

37. Page, D. H., Tappi 52(4):674-81(1969).

38. Jones, A. R., Tappi 55(10):1522-7(1972).

39. McIntosh, D. C.; Leopold, B. Bonding strength of individual fibres. Vol. I. p. 265-70. In Formation and Structure of Paper (F. Bolam ed.). Trans. of Symp. held at Oxford, Sept. 1961. Tech. Sect. Brit. Paper and Board Makers' Assocn., London, 1962.

40. Thorpe, J. L.; Mark, R. E.; Eusufzai, A. R. K.; Perkins, R. W., Tappi 59(5):96-100(1976).

41. Mayhood, C. H., Jr.; Kallmes, O. J.; Cauley, M. M., Tappi 45(1):69-73 (1962).

42. McIntosh, D. C., Tappi 46(5):273-7(1963).

43. Schniewind, A. P.; Nemeth, L. J.; Brink, D. L., Tappi 47(4):244-8(1964).

44. Russell, J.; Kallmes, O. J.; Mayhood, C. H., Tappi 47(1):22-5(1964).

45. Mohlin, U.-B., Svensk Papperstid. 77(4):131-7(1974).

46. Hartler, N.; Mohlin, U.-B., Svensk Papperstid. 78(8):295-9(1975).

47. Mohlin, U.-B., Svensk Papperstid. 78(9):338-41(1975).

48. Mohlin, U.-B., Svensk Papperstid. 78(10):373-5(1975).

49. Goring, D. A. I., Pulp Paper Mag. Can. 68(8):T372-6(1967).

50. Bates, N. A., Tappi 52(6):1162-8(1969).

51. Janes, R. L. A study of adhesion in the cellulose-starch-cellulose system. Doctor's Dissertation, Appleton, WI, The Institute of Paper Chemistry, 1968.

52. Page, D. H. Discussion. Vol. I. p. 272-3. In Formation and Structure of Paper (F. Bolam ed.). Trans. of Symp. held at Oxford, Sept., 1961. Tech. Sect. Brit. Paper and Board Makers' Assocn., London, 1962.

53. Gallent, P. E.; Swaffer, C. S. The assessment of structural bonds by destructive methods. p. 51-75. In Aspects of Adhesion 5 (D. J. Alner ed.). London, University of London Press, 1969.

54. Anderson, G. P.; Bennett, S. J.; DeVries, K. L. Analysis and testing of adhesive bonds. New York, Academic Press, 1977.

55. Patrick, R. L. Treatise on adhesion and adhesives. New York, M. Dekker, 1967.

56. Bikerman, J. J. The science of adhesive joints. 2nd ed. New York, Academic Press, 1968.

57. Sharpe, L. H., J. Adhesion 4(1):51-64(1972).

58. Schonhorn, H.; Ryan, F. W.; Wang, T. T., J. Appl. Polymer Sci. 15:1069-78(1971).

59. Goland, M.; Reissner, E., J. Appl. Mech. 11:A17-27(1944).

60. Wang, T. T.; Ryan, F. W.; Schonhorn, H., J. Appl. Polymer Sci. 16:1901-9(1972).

61. Allen, K. W.; Shanahan, M. E. R., J. Adhesion 8(1):43-56(1976).

62. Lewis, A. F.; Kinmonth, R. A.; Kreahling, R. P., J. Adhesion 3(3):249-57(1972).

63. Goodier, J. N.; Hsu, C. S., J. Appl. Mech. 21(6):147-50(1954).

64. Muki, R.; Sternberg, E., Internl. J. Solids Structures 4:75-94(1968).

65. Wah, T., J. Eng. Materials Tech. 95 (Series H) (3):174-81(1973).

66. Westman, R. A., Internl. J. Eng. Sci. 13(4):369-91(1975).

67. Wooley, G. R.; Carver, D. R., J. Aircraft 8(10):817-20(1971).

68. Adams, R. D.; Peppiatt, N. A., J. Strain Analysis 8(2):134-9(1973).

69. Pirvics, J., J. Adhesion 6(3):207-28(1974).

70. Adams, R. D.; Peppiatt, N. A., J. Strain Analysis 9(3):185-96(1974).

71. Williams, M. L., J. Adhesion 4:307-32(1972).

72. Good, R. J., J. Adhesion 4:133-54(1972).

73. De Vries, K. L.; Williams, M. L.; Chang, M. D., Exptl. Mech. 14(3):89-97(1974).

74. Jemian, W. A.; Ventrice, M. B., J. Adhesion 1(3):190-207(1969).

75. Broek, D. Elementary engineering fracture mechanics. p. 115-16. Leyden, Netherlands, Noordhoff International, 1974.

76. Chang, D. J.; Muki, R., Internl. J. Solids Structures 10(5):503-17(1974).

77. Trantina, G. G., J. Composite Materials 6:371-85(1972).

78. Keer, L. M.; Chantaramungkorn, K., J. Appl. Mech. 42(2):353-7(1975).

79. Walsh, P. F.; Leicester, R. H.; Ryan, A., Forest Prod. J. 23(5):30-3 (1973).

80. McClintock, F. A.; Argon, A. S., eds. Mechanical behavior of materials. Reading, MA, Addison-Wesley, 1966.

81. Weiss, V.; Yukawa, S. Critical appraisal of fracture mechanics. p. 1-22. In ASTM Special Publication No. 38, 1964.

82. Inglis, C. E., Trans. Naval Arch. 60:219-30(1913).

83. Broek, D. Elementary Engineering Fracture Mechanics. Leyden, Netherlands, Noordhoff International, 1974.

84. Paris, P. C.; Sih, G. C. M. Stress analysis with cracks. p. 30-81. In ASTM Special Publication No. 381, 1964.

85. Westergaard, H. M., J. Appl. Mech. 6:A49-53(1939).

86. Wu, E. M., J. Appl. Mech. 34(4):967-74(1967).

87. Shih, C. F. Small-scale yielding analysis of mixed mode plane-strain crack problems. p. 187-210. In Fracture analysis. ASTM STP 560, Am. Soc. Testing Materials, 1974.

88. Rice, J. R. Mathematical analysis in the mechanics of fracture. Vol. II. p. 217. In Fracture: an advanced treatise (H. Liebowitz, ed.). New York, Academic Press, 1968.

89. Hein, V. L.; Erdogen, F., Intern. J. Fracture Mech. 7:317-30(1971).

90. Sih, G. C.; Paris, P. C.; Irwin, G. R., Intern. J. Fracture Mech. 1:189-203(1965).

91. Zienkiewicz, O. C., Appl. Mech. Rev. 23:249-56(1970).

92. Argyris, J. H.; Kelsey, S. Energy theorems and structural analysis. London, Butterworths, 1960.

93. Pian, T. H. H.; Tong, P., Intern. J. Numerical Methods Eng. 1:3-28 (1969).

94. Bathe, K. J.; Wilson, E. L.; Peterson, F. E. SAP IV - A structural analysis program for static and dynamic analysis of linear structural systems. EERC Report No. 73-11. Berkeley, CA, College of Engineering, University of California, June 1973. (Revised 1974).

95. Bauer, N.; Lewin, S. Z. In Weissberger's techniques of organic chemistry. Vol. I. Part I. p. 136. New York, Interscience, 1959.

96. Hardacker, K. W., Tappi 45(3):237-46(1962).

97. Nomura, S.; Kawabata, S.; Hiromichi, K.; Yamaguchi, Y.; Fukushima, A.; Takahara, H., J. Polymer Sci. Part A-2, 7:325-55(1969).

98. Jayme, G.; Balser, K., Svensk Papperstid. 70(20):655-67(1967).

99. Takahara, H.; Nomura, S.; Kawai, H.; Yamaguchi, Y.; Okazaki, K.; Fukushima, A., J. Polymer Sci. Part A-2, 6(1):197-221(1968).

100. Hardacker, K. W.; Brezinski, J. P., Tappi 56(4):154-7(1973).

101. Marin, J.; Sauer, J. A. Strength of materials. 2nd Ed. p. 28. New York, MacMillan, 1954.

102. Brezinski, J. P.; Hardacker, K. W., unpublished work, 1973.

103. Mann, R. W. Elastic wave propagation in paper. Doctor's Dissertation. Appleton, WI, The Institute of Paper Chemistry, 1978.

104. Comninou, M., J. Appl. Mech. 44(4):631-6(1977).

105. Anderson, G. P.; Bennett, S. J.; De Vries, K. L. Analysis and testing of adhesive bonds. p. 37-8. New York, Academic Press, 1977.

106. Seth, R. S.; Page, D. H., J. Materials Sci. 9(1):1745-53(1974).

107. Chan, S. K.; Tuba, I. S.; Wilson, W. K., Eng. Fracture Mech. 2:1-17 (1970).

108. Kobayashi, A. S.; Maiden, D. E.; Simon, B. J. Application of the method of finite element analysis to two-dimensional problems in fracture mechanics. ASME Mtg., 69-WA/PVP-12, Los Angeles, CA, 1969.

109. Anderson, G. P.; Ruggles, V. L.; Stibor, F. S., Intern. J. Fracture Mech. 7:63-76(1971).

110. Gallagher, R. H. Survey and evaluation of the finite element method in linear fracture mechanics analysis. p. 637-53. In Proc. of First International Conf. on Structural Mechanics in Reactor Technology. Berlin, 1971; Berlin, West Germany, 1972.

111. Oglesby, J. J.; Lomacky, O., J. Eng. Ind. 95(1):177-85(1973).

112. Rice, J. R., J. Appl. Mech. 35(2):379-86(1968).

113. Bucci, R. J.; Paris, P. C.; Landers, J. D.; Rice, J. R. J-Integral estimation procedures. Part II. ASTM STP514. p. 40-69. In Fracture toughness. Proc. of 1971 Natl. Symp. on Fracture Mechanics. ASTM, 1972.

114. Gallagher, R. H. Large-scale computer programs for structural analysis. In Proc. of symp. on general purpose finite element computer programs (P. Marcal ed.). New York, ASME, 1970.

115. Bushnell, D. A computerized information retrieval system. p. 737-804. In Structural mechanics computer programs (Pilkey, W., Sachzalski, K. and Schaffer, H. eds.). Charlottesville, VA, University Press of Virginia, 1974.

116. Arridge, R. G. C.; Folkes, M. J., Polymer 17:495-500(1976).

117. Parks, D. M., Intern. J. Fracture 10(4):487-502(1974).

118. Wilson, E. L.; Bathe, K.-J.; Doherty, W. P., Computers and Structures 4(2):363-73(1974).

119. Wilson, E. L. SOLID SAP - A static analysis program for three-dimensional solid structures. SESM Report 71-19. Berkeley, CA, Dept. of Civil Engineering, University of California, 1971.

120. Cook, R. D., J. Structural Div., Proc. ASCE 110(ST9):1851-63(1974).

121. Dunder, V.; Ridlon, S., J. Structural Div., Proc. ASCE 104(ST1):9-21 (1978).

122. Timoshenko, S.; Goodier, J. N. Theory of elasticity. 2nd ed. p. 39. New York, McGraw-Hill, 1951.

123. Zienkiewicz, O. C. The finite element method in engineering science, New York, McGraw-Hill, 1971.

124. Wilson, W. K. On combined mode fracture mechanics. Doctor's Dissertation. Pittsburgh, PA, University of Pittsburgh, 1969.

125. Tracy, D. M., Eng. Fracture Mech. 3(3):255-65(1971).

126. Benzley, S. E., Intern. J. Numerical Method Eng. 8(3):537-45(1974).

127. Shames, I. H. Introduction to solid mechanics. p. 116. Englewood Cliffs, N.J., Prentice-Hall, 1975.

128. Stavsky, Y.; Hoff, N. J. Mechanics of composite structures. p. 5-59. In Composite engineering (A. G. H. Dietz ed.). Cambridge, MA, MIT Press, 1960.

APPENDIX I

FINITE ELEMENTS AND THE DIRECT DISPLACEMENT METHOD

FORMULATION OF ELEMENTS IN THE DIRECT DISPLACEMENT METHOD

Two equations presented in this brief review are taken from Chapter 2 of Zienkiewicz's book on the finite element method.[123] The formulation (in-plane stress) for a triangular element (Fig. 72) with nodes i, j, m, will be developed first and then generalized to an assemblage representing an approximation to an elastic continuum body.

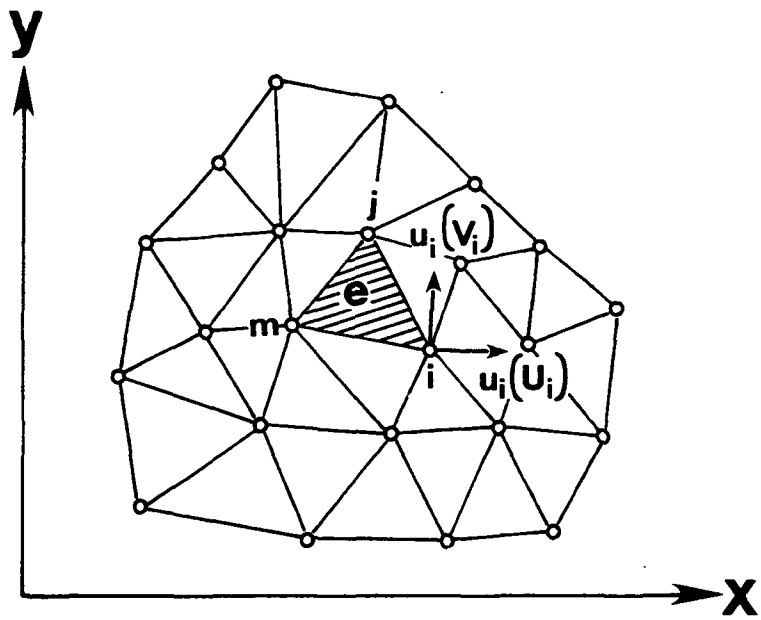

Figure 72. A plane stress finite element in an elastic body.

The displacements $\{f(x,y)\}$ within an element are related to the element nodal point displacements $\{\delta\}^e$ by

$$\{f\} = [N]\{\delta\}^e = [N_i,\ N_j,\ N_m] \begin{Bmatrix} \delta_i \\ \delta_j \\ \delta_m \end{Bmatrix}, \tag{36}$$

where [N] contains components which are general functions of position. In this plane stress case, both $\{f\}$ and $\{\delta\}^e$ have horizontal (u) and vertical (v) movement. The functions [N] are called displacement shape functions. These functions represent the primary distinction between element types and play a central role in the finite element method.

The strains can be determined from the known displacements within the elements. The matrix [B] relates the strains to the displacements matrix as

$$\{\varepsilon\} = [B]\{\delta\}^e \tag{37}$$

The strain-displacement matrix [B] can be obtained easily in the plane stress case from the differential equation relating strain to displacement

$$\varepsilon = \begin{Bmatrix} \varepsilon_x \\ \varepsilon_y \\ \gamma_{xy} \end{Bmatrix} = \begin{Bmatrix} \dfrac{\partial u}{\partial x} \\ \dfrac{\partial v}{\partial y} \\ \dfrac{\partial v}{\partial x} + \dfrac{\partial u}{\partial y} \end{Bmatrix}, \tag{38}$$

and the previously chosen shape functions $[N_i,\ N_j,\ N_m]$ of Eq. (36).

For generality, a possible initial strain (ε_o) and residual stress (σ_o) are assumed, leading (for the elastic case) to the stress-strain equation,

$$\sigma = [D](\{\varepsilon\} - \{\varepsilon_o\}) + \{\sigma_o\}, \tag{39}$$

where [D] is the elasticity matrix. The stress matrix contains the components

$$\{\sigma\} = \begin{Bmatrix} \sigma_x \\ \sigma_y \\ \tau_{xy} \end{Bmatrix} \tag{40}$$

For an isotropic elastic material the matrix [D] is

$$[D] = [E/(1 - \nu^2)] \begin{bmatrix} 1 & \nu & \\ \nu & 1 & \\ 0 & 0 & (1 - \nu)/2 \end{bmatrix} \tag{41}$$

The forces on the element nodes are expressed as

$$\{F\}^e = \begin{Bmatrix} F_i \\ F_j \\ F_m \end{Bmatrix}, \tag{42}$$

and include the boundary stresses and distributed loads on element, e. Each force has a component corresponding to the node displacements, which for the plane stress case is

$$\{F_i\} = \begin{Bmatrix} U_i \\ \\ V_i \end{Bmatrix} \tag{43}$$

The distributed loads {p} act on a volume of the element with directions the same as {f} at that point, as in

$$\{p\} = \begin{Bmatrix} X \\ Y \end{Bmatrix}, \tag{44}$$

where X and Y are the body force components.

To formulate the required equation of equilibrium relating nodal displacements to nodal force, an arbitrary (virtual) nodal displacement is imposed and the external and internal work done by the various forces and stresses resulting from that displacement are equated. If $d\{\delta\}^e$ is the virtual nodal displacement, then Eq. (36) and (37) become

$$d\{f\} = [N]\, d\{\delta\}^e \text{ and } d\{\varepsilon\} = [B]\, d\{\delta\}^e \tag{45}$$

The sum of the products of the nodal forces and their node displacements is

$$d(\{\delta\}^e)^T \{F\}^e \tag{46}$$

the total external work. Per unit volume, the internal work of the stresses and distributed forces is

$$d\{\varepsilon\}^T \{\sigma\} - d\{f\}^T \{p\}, \tag{47}$$

or

$$(d\{\delta\}^e)^T ([B]^T \{\sigma\} - [N]^T \{p\}) \tag{48}$$

Through integrating over the element volume, we obtain the total internal work. Equating this to the total external work gives

$$(d\{\delta\}^e)^T \{F\}^e = (d\{\delta\}^e)^T (\int [B]^T \{\sigma\}\, d(vol) - \int [N]^T \{p\}\, d(vol)) \tag{49}$$

Since, by assumption, they are arbitrary, the equal multipliers are removed and Eq. (37) and (39) are substituted to yield

$$\{F\}^e = (\int [B]^T [D][B]\, d(vol))\, \{\delta\}^e - \int [B]^T [D]\, \{\varepsilon_o\}\, d(vol) + \int [B]^T \{\sigma_o\}\, d(vol) - \int [N]^T \{p\}\, d(vol) \tag{50}$$

This equation is typical of equations for structural elements, since the stiffness matrix can be identified as

$$[k]^e = \int [B]^T [D][B]\, d(vol), \tag{51}$$

the nodal forces from distributed loads are

$$\{F\}_p^e = - [N]^T \{p\}\, d(vol), \tag{52}$$

those from initial strains are

$$\{F\}^e_{\varepsilon_o} = - [B]^T [D]\{\varepsilon_o\}\ d(vol), \tag{53}$$

and from residual stresses

$$\{F\}^e_o = - \int [B]^T \{\sigma_o\}\ d(vol), \tag{54}$$

and in these terms,

$$\{F\}^e = [k]^e \{\delta\}^e + \{F\}^e_a + \{F\}^e_o + \{F\}^e_p$$

In the process of subdividing the continuum into finite elements, each element and its nodes are numbered and the global coordinates of each node are recorded. The stiffness matrix for the discretized continuum is simply constructed by summation of the individual element stiffness matrices

$$[K] = \sum_e [k]^e \tag{55}$$

Concentrated nodal forces {R} and distributed external loading {g} may exist on the external boundaries of the body. These are added to the equilibrium considerations at the nodes in matrix form for the concentrated loads

$$\{R\} = \begin{Bmatrix} R_i \\ R_j \\ R_m \end{Bmatrix} \tag{56}$$

and for the distributed load by

$$\{F\}^e_b = - \int [N]^T \{g\}\ d(area), \tag{57}$$

where the integration is over the external surface of the element. This generalization proceeds under the assumption that displacements (u_i, v_i) are continuous

between adjacent elements. Thus the shape functions N_i must define the displacement field such that only finite strains exist on the element interfaces. Equating the internal and external work for the entire body now gives, in terms of a force balance,

$$[K]\ \{\delta\} + \{F\}_p + \{F\}_b + \{F\}_{\varepsilon_o} + \{F\}_{\sigma_o} - \{R\} = 0 \tag{58}$$

The virtual work principle may be restated to show explicitly the variation of strain energy (U) of the structure and the variation of the potential energy (V) of the external loads.

$$\int d\{\varepsilon\}^T \{\sigma\}\ d(\text{vol}) - [d\{\delta\}^T \{R\} + \int d\{f\}^T \{f\}^T \{p\}\ d(\text{vol}) + \int d\{f\}^T \{g\}\ d(\text{area})] = 0 \tag{59}$$

or

$$d(U + V) = d(\chi) = 0 \tag{60}$$

The total potential energy (χ) of the system must be stationary for variations of admissible displacements for equilibrium to be ensured. Equation (60) can simply be written as the variation with respect to displacements of a limited set of parameters

$$\text{grad}_\delta\ \chi = 0 \tag{61}$$

Typically, a set of simultaneous linear equations, based on Eq. (61), are formulated and solved directly to obtain the minimum total potential energy in terms of a finite number of nodal parameters (i.e., displacements). If a proper shape function is chosen and the elements are formulated correctly, each increase in the number of node points (finite elements) in the continuum approximation will lead to a convergence to an exact solution. A proper shape

function must meet certain convergence criteria and continuity restraints. Many different displacement functions have been developed. A brief survey of the main types of assumed displacement functions follow.

ELEMENT DISPLACEMENT FUNCTIONS

Some of the earliest element formulations involved plane stress triangular elements with assumed linear polynominals as

$$\begin{aligned} u &= \alpha_1 + \alpha_2 x + \alpha_3 y \\ v &= \alpha_4 + \alpha_5 x + \alpha_6 y \end{aligned} \tag{62}$$

These displacement functions produced elements with constant strain characteristics. A similar result occurs for a bilinear rectangular element with the displacement functions

$$\begin{aligned} u &= \alpha_1 + \alpha_2 x + \alpha_3 y + \alpha_4 xy \\ v &= \alpha_5 + \alpha_6 x + \alpha_7 y + \alpha_8 xy \end{aligned} \tag{63}$$

Extension to tetrahedron with the similar constant strain character would employ the displacement function

$$\begin{aligned} u &= \alpha_1 + \alpha_2 x + \alpha_3 y + \alpha_4 z \\ v &= \alpha_5 + \alpha_6 x + \alpha_7 y + \alpha_8 z \\ w &= \alpha_9 + \alpha_{10} x + \alpha_{11} y + \alpha_{12} z \end{aligned} \tag{64}$$

It was soon realized that including more nodes (degrees of freedom) in an element gave better overall solution accuracy with fewer total degrees of freedom. Thus quadratic, cubic, quartic, etc., polynominals came into use as displacement functions for straight-sided elements with appropriate multiple nodes. Unfortunately, a natural limit to the usefulness of these higher order elements

existed, because their straight sides reduced the ability of these larger elements to approximate complex geometries.

This geometric approximation difficulty was reduced when Irons introduced the local curved coordinates, defined by the same shape functions as used in the approximating function.[91] These elements are known as isoparametric elements. Subsequent use of numerical integration, as in the Newton-Cotes or Gaussian quadrature procedures, permitted more efficient solution of both the curved body problems and those with linear boundaries. Isoparametric elements have improved the accuracy of many analyses, but their value for any particular problem requires an examination of the effort to program these complex elements versus the improvement in the solution time required for a given accuracy. Discussion of isoparametric elements is included in the following review of singularity type of finite element used in fracture mechanics.

SINGULARITY ELEMENTS

The fourth approach mentioned by Gallagher[110] was the formulation of special crack tip elements which incorporate the known singularity in the element displacement function. Many different elements have been proposed and no attempt will be made to discuss all of them. Instead, examples of various element formulations will be presented.

Wilson[124] was among the first to formulate these special crack tip elements. In 1969, he presented a circular boundary finite element for Mode III type stress fields in a cracked isotropic elastic body. The assumed displacement field was of the form $u = v = 0$; $w = w(x,y)$, which, in polar coordinates, gives as the first term of the asymptotic expansion about crack tip

$$w\ (r,\theta) = [K_{III}(2r)^{1/2}/\mu]\ \sin(\theta/2) \tag{65}$$

Since this unexpanded displacement field function is appropriate only as r → 0, the radius of the special crack tip element must be arbitrarily restricted to a very small area around the crack tip. The displacement components were discontinuous across the circular boundary with the standard code elements and although the compatibility conditions were violated, this fomulation was convergent. The Mode III stress intensity factor, K_{III}, was obtained from the solution of the equilibrium equations of the finite element formulation. To offset the limitations of the single term displacement functions, a natural extension to the higher order elements with expanded displacement functions followed.

Singularities were soon incorporated into isoparametric finite elements. Tracy[125] formulated a triangular and rectangular element with their displacement functions in terms of the elements' natural coordinates (ξ,η). These coordinates were defined so that each edge of an element had one coordinate constant while the other varied linearly along it. He then obtained the functional relationship between (ξ,η) and the physical coordinates (x,y) by mapping the physical element in a (ξ,η) parameter plane (see Fig. 73). The coordinate transformations were accomplished with the mapping

$$\{X\} = \{X\}_A\ (1-\xi)\eta + \{X\}_B\ (1-\xi)(1-\eta) + \{X\}_C\xi(1-\eta) + \{X\}_D\xi\eta. \tag{66}$$

$\{X\}_A$ represented the position vector of node A in the physical plane. In the case of the triangle, Fig. 73b, $\{X\}_A = \{X\}_B$. For a crack located on $x \leq 0$, a displacement function which included the singular field of Eq. (4) throughout the triangle of Fig. 73b was

$$u(\xi,\eta) = \alpha_1 + \alpha_2 (\xi)^{1/2} + \alpha_3 (\xi\eta)^{1/2}$$
$$v(\xi,\eta) = \alpha_4 + \alpha_5 (\xi)^{1/2} + \alpha_6 (\xi\eta)^{1/2}, \tag{67}$$

where $u,v(\xi,\eta)$ were physical cartesian displacements of a point within the element. Although A and B were thought of as being distinct in the mapping, physically there was only one location (the crack tip) and only one set of displacements for that point. When the crack tip was ringed by triangular elements, and each was radially joined with the quadrilateral isoparametric elements of Fig. 73a with displacement function

$$u(\xi,\eta) = \alpha_1 + \alpha_2 \xi + \alpha_3 \eta + \alpha_4 \xi\eta$$
$$v(\xi,\eta) = \alpha_5 + \alpha_6 \xi + \alpha_7 \eta + \alpha_8 \xi\eta, \tag{68}$$

the singularity was embedded and displacement compatibility on interelement boundaries was assured.

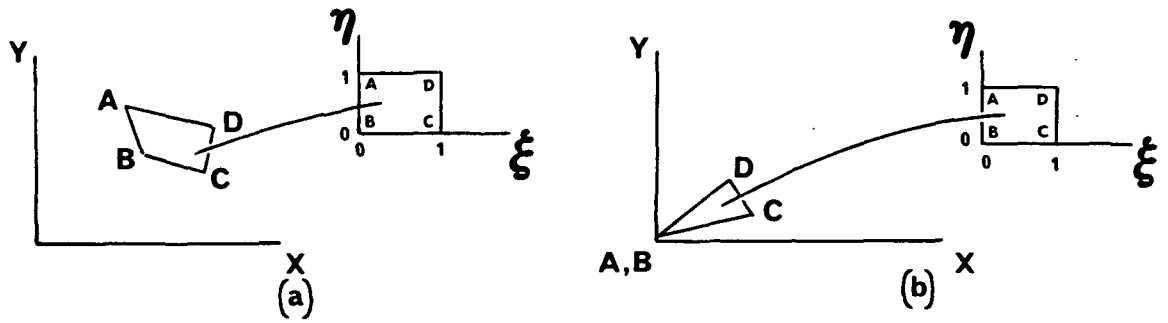

Figure 73. (a) A typical quadrilateral element mapped into a square.
(b) A typical near tip triangle mapped into a square.[125]

More recently, Benzley[126] proposed an isoparametric quadrilateral element with a singularity at one corner node. The arbitrary quadrilateral element, shown in Fig. 74, had singularity effects included by "enriching" a bilinear element displacement assumption [Eq. (63)] with terms that gave the proper singularity at the node i', i.e.,

$$u_i = \alpha_{i1} + \alpha_{i2}\,\xi + \alpha_{i3}\,\eta + \alpha_{i4}\,\xi\eta + K_I Q_{1i}(r,\theta) + K_{II} Q_{2i}(r,\theta), \qquad (69)$$

where $i = 1,2$ the global cartesian coordinate directions

ξ,η = local nondimensional element coordinates

K_I, K_{II} = intensities (unknown coefficients) of singular terms

Q_i = specific singular assumptions

when Eq. (69) was solved for the unknown coefficients α_{ij} in terms of the nodal displacements, $\overline{u}_{ik}$, where $k = 1,2,3,4$ the displacement assumption was written as

$$u_i = \sum_{k=1}^{4} f_k\,\overline{u}_{ik} + K_I\left(Q_{1i} - \sum_{k=1}^{4} f_k\,\overline{Q}_{1ik}\right) + K_{II}\left(Q_{2i} - \sum_{k=1}^{4} f_k\,\overline{Q}_{2ik}\right) \qquad (70)$$

where $\overline{Q}_{ik}$ = the value Q_i at node k

$f_k = 1/4\,(1 - \xi\xi_k)(1 - \eta\eta_k)$

ξ_k,η_k = the coordinates of node k($\pm$ 1)

To avoid incompatibility with the standard bilinear element, an interfacial element was given the following altered displacement formulation:

$$u_i = \sum_{k=1}^{4} f_k\,u_{ik} + R(\xi,\eta)\left[K_I\left(Q_{1i} - \sum_{k=1}^{4} f_k\,\overline{Q}_{1ik}\right) + K_{II}\left(Q_{2i} - \sum_{k=1}^{4} f_k\,\overline{Q}_{2ik}\right)\right] \qquad (71)$$

$R(\xi,\eta)$ was set equal to a function of $1/2(1 + \xi\xi_k)$ and $1/2(1 - \eta\eta_k)$ such that it

equaled 1 on the "enriched" element boundary and 0 on the bilinear element boundaries.

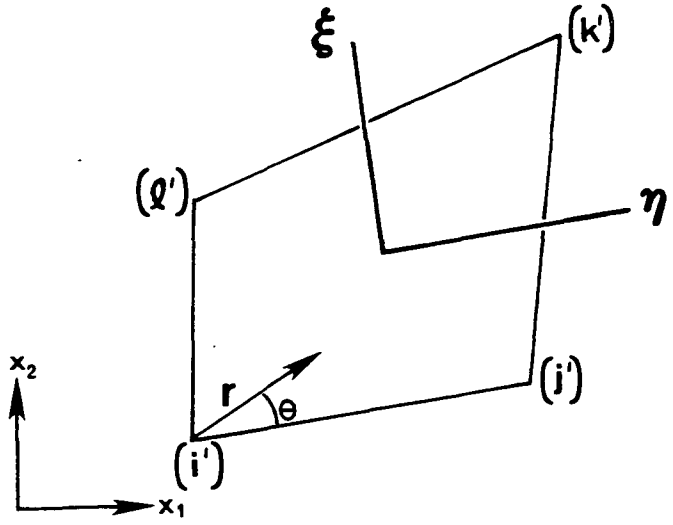

Figure 74. Arbitrary quadrilateral element with singular point at node (i').

This element was found be Benzley[126] to produce more accurate stress intensity factor calculations with fewer degrees of freedom than the direct calculations of Anderson, et al.[109] and singular element of Tracy.[125]

APPENDIX II

EFFECTS OF BONDING PRESSURE AND CLEANING SEQUENCE ON BOND SHEAR STRENGTH

An experiment was performed to determine which of two surface preparations and three pressures would provide the optimum bonding. Three films (134 PUD-O, 193 PUD-O, and 215 PD) were cleaned by two different sequences: (1) Janes'[51] cleaning procedure (CCl_4, 95% C_2H_5OH, H_2O) or (2) H_2O only. Lap joints (47.6 x 12.7 mm) with a 3.175 mm overlap were assembled wet and sandwiched between three layers of Millipore filters which were in turn backed by ten layers of filter paper. This sandwich was pressed between steel platens covered by 150 mesh wire. The steel platens had a center hole intersected by a lateral hole to allow air to pass through the wire when a vacuum was applied to the platen.

Pressure was applied to the desired level (100, 500, and 1500 psi) by the Baldwin Universal testing machine for a minimum of 8 hours. Immediately following press opening, a sword electric hygrometer was inserted into the filter paper of the sandwich to measure the relative humidity, which was found to range from 41 to 52%, indicating attainment of equilibrium. Following separation from the Millipore filters, which was difficult for the 1500 psi samples, the lap joints were conditioned an additional 24 hours at standard conditions (50% RH and 73°F) before measurement and testing.

Specimen width, lap length, and thickness were measured and then the sample was axially strained in tension to failure in the Instron Universal testing machine at a 1.27 mm/minute elongation rate with a 34.9 mm span between line-type clamps. Initial modulus, strain and apparent shear stress at failure were calculated from the load/elongation curves obtained.

Mean bond shear strength and coefficient of variation results for the four replications of each condition are shown in Table 12.

Table 12. Effect of surface preparation and bonding pressure on bond strength.

Film Identification	Cleaning Sequence No.	Bonding Pressure (psi) 100 $\bar{X}$[a]	100 $S/\bar{X}$[b]	500 $\bar{X}$	500 $S/\bar{X}$	1500 $\bar{X}$	1500 $S/\bar{X}$
134 PUD-0	1	0.087	0.215	0.074	--	--	--
	2	0.072	0.138	0.056	0.064	--	--
193 PUD-0	1	0.085	0.038	0.077	0.158	0.084	0.036
	2	0.071	0.079	0.075	0.111	0.069	--
215 PD	1	>0.081	0.051	>0.065	0.033	>0.077	0.064
	2	>0.075	0.032	>0.083	0.153	>0.087	0.133

[a]Mean, bond shear strength [kg/(mm)^2].
[b]Coefficient of variation.

In agreement with the results of Janes'[51] the CCl_4, 95% C_2H_5OH, H_2O cleaning sequence produced higher bond shear strength for virtually all of the test conditions. The effect of varying bonding pressure from 100 to 1500 psi appeared to have small mixed effects. The coefficient of variation, which had no apparent pattern, ranged from about 3 to 21% as compared to Janes'[51] 3% to 11%. Much of this increased variation resulted from variation in the overlap length, misalignment in lap joints, prior debonding, and failures occurring in other than the elastic regime of the load/elongation curve. Strain to failure results followed the shear stress patterns closely, as would be expected. Apparent modulus values (machine-direction only) were unaffected by cleaning and only slightly affected by pressure, tending to decrease with increasing pressure. The indication of shear stresses greater than (>) the amount stated results from adherend tensile failures.

Most lap joint failures could not be characterized as unstable fractures, because partial debonding occurred before complete lap joint failure.

APPENDIX III

CELLOPHANE ELASTIC CONSTANT DETERMINATION

As presented in the model development discussion of the Theoretical Program, cellophane is considered to be approximately orthotropic linear elastic at strains less than 0.5%. From theory of elasticity, outlined below, nine elastic constants are required to describe the elastic properties of such a material. In the program that follows, five independent measurements were combined with four elastic constant estimates from cellophane structure theory[97] to yield the working engineering elastic constants.

CELLOPHANE ELASTIC CONSTANT MEASUREMENT

From the work of Brezinski and Hardacker[102] it appeared that the in-plane Poisson ratios (ν_{yx},ν_{xy}) could be measured using the biaxial load/elongation apparatus (see Fig. 75). Since cellophane film, like paper, is a thin planar material, the z-direction properties are difficult to measure. Usually they are ignored, but in a proper stress analysis they cannot be. Some of the z-direction properties can be measured by ultrasonic techniques.[103] By measuring the shear and compression ultrasonic wave velocities propagated along various material axes, one can apparently obtain additional constants involving z-direction elastic properties.

ORTHOTROPIC ELASTICITY THEORY

According to elasticity theory,[127] a material having elastic symmetry about three mutually perpendicular planes is orthotropic. In matrix form, the stresses in such a body are related to the stiffness matrix and strains as:

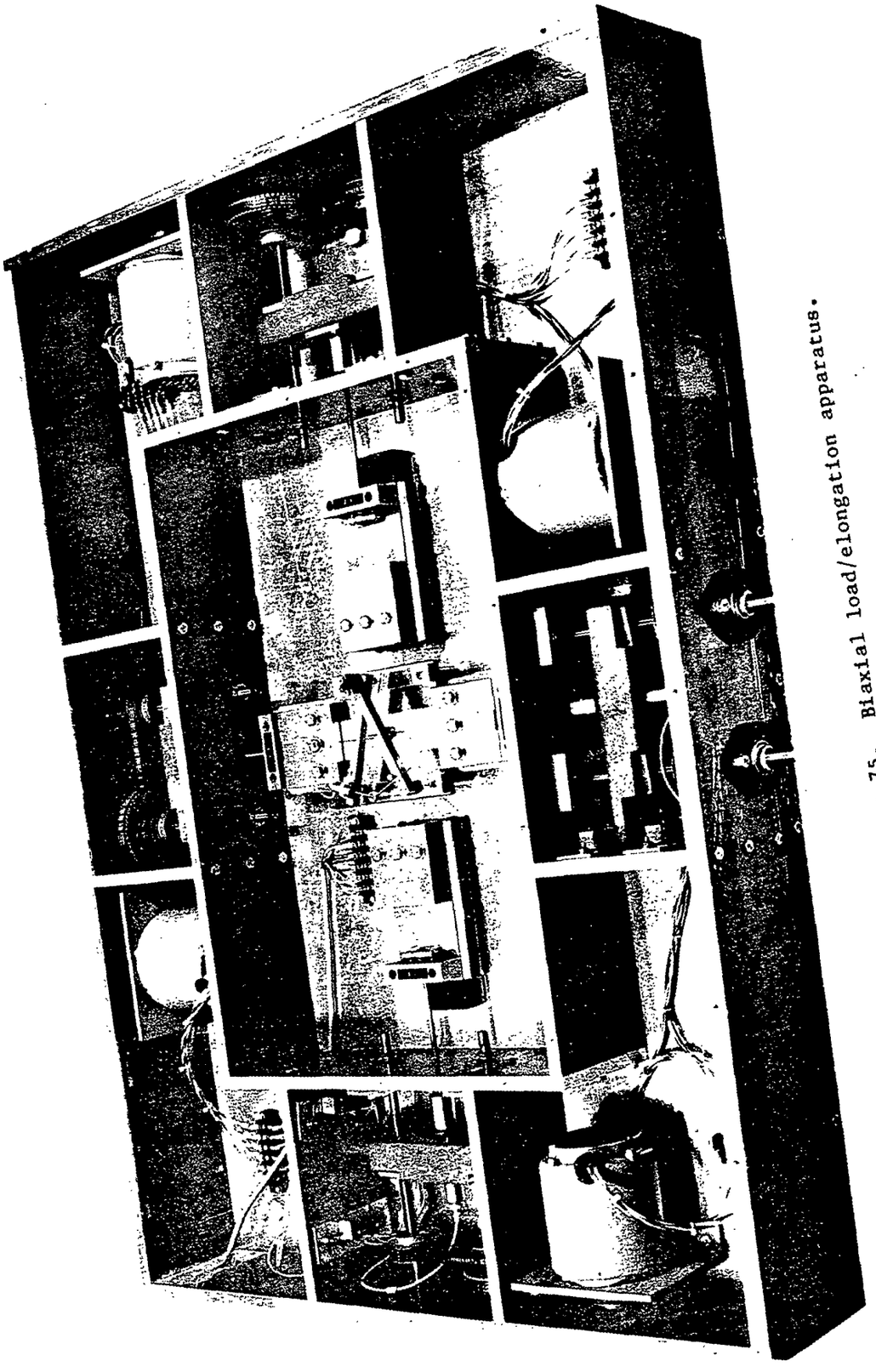

Figure 75. Biaxial load/elongation apparatus.

$$\begin{vmatrix} \sigma_{xx} \\ \sigma_{yy} \\ \sigma_{zz} \\ \sigma_{xy} \\ \sigma_{yz} \\ \sigma_{xz} \end{vmatrix} = \begin{vmatrix} C_{11} & C_{12} & C_{13} & 0 & 0 & 0 \\ C_{21} & C_{22} & C_{23} & 0 & 0 & 0 \\ C_{31} & C_{32} & C_{33} & 0 & 0 & 0 \\ 0 & 0 & 0 & C_{44} & 0 & 0 \\ 0 & 0 & 0 & 0 & C_{55} & 0 \\ 0 & 0 & 0 & 0 & 0 & C_{66} \end{vmatrix} \begin{vmatrix} \varepsilon_{xx} \\ \varepsilon_{yy} \\ \varepsilon_{zz} \\ \varepsilon_{xy} \\ \varepsilon_{yz} \\ \varepsilon_{xz} \end{vmatrix} \qquad (72)$$

where σ_{ii} and σ_{ij} are the normal stresses and shear stress, respectively; and ε_{ii} and ε_{ij} are the corresponding strains. The C_{ij}'s constitute the stiffness coefficients of the stiffness matrix. Only nine independent stiffness coefficients are required for complete description of the material's elastic properties, since $C_{ji} = C_{ij}$, for $i \neq j$.[127]

STIFFNESS COEFFICIENTS BY ULTRASONIC WAVE VELOCITY TECHNIQUES

There is a fairly simple relationship between the stiffness coefficients on the stiffness matrix diagonal (C_{ij}'s, $i = j$), compressional wave velocities (V_{ij}, $i = j$) and shear wave velocities (V_{ij}, $i \neq j$) given for infinite material by:

$$\begin{aligned} \rho V_{xx}^2 &= C_{11} & \rho V_{xy}^2 &= C_{44} \\ \rho V_{yy}^2 &= C_{22} & \rho V_{yz}^2 &= C_{55} \\ \rho V_{zz}^2 &= C_{33} & \rho V_{xz}^2 &= C_{66} \end{aligned} \qquad (73)$$

where ρ is the material density. Equations for the other constants exist, but unfortunately cellophane film cannot be considered an infinite material. Actually, only the z-direction compressional wave velocity, V_{zz}, and the shear wave velocities (V_{xy}, V_{yz}, and V_{xz}) can be obtained directly on planar materials. Utilization of orthotropic plane wave theory has permitted derivation of

equations relating ultrasonic wave velocities, V_{so}, to the stiffness coefficients, C_{ij}, for planar materials.[103] These equations, when used in conjunction with an instrument such as the Morgan Dynamic Modulus Tester which generates compression and shear waves in the sheet plane, provide the following relationships between the stiffness coefficients and the ultrasonic wave velocities:

$$\rho V_{so_{xx}}^2 = C_{11} - C_{13}^2/C_{33}; \quad \rho V_{so_{yy}}^2 = C_{22} - C_{23}^2/C_{33}; \quad \rho V_{so_{xy}}^2 = C_{44} \qquad (74)$$

These techniques provide four independent measurements with the presently available equipment. A fifth independent measurement can be obtained by static experimental measurement of the Poisson ratio, ν_{xy} or ν_{yx}, using the biaxial load/elongation apparatus (Fig. 75).

Both of the acoustic techniques use piezoelectric transducers to generate mechanical waves, which are transmitted to the specimen and through the specimen to a second similar transducer which converts the mechanical disturbance back to an electrical impluse. Ultrasonic velocities are obtained by electronic equipment measuring the transit time between transducers, and a direct measurement of the transducer separation.

POISSON RATIO DETERMINATION BY BIAXIAL STRAINING

By definition a Poisson ratio, ν_{ij}, is the ratio of the strain (ε_{ii}) perpendicular to the direction of loading to that in the loading direction (ε_{jj}).

$$-\nu_{ij} = \varepsilon_{ii}/\varepsilon_{jj}; \quad \text{for } i \neq j \qquad (75)$$

The most direct experimental approach is clearly evident, but for thin film material (i.e., cellophane and most paper) a tensile load along one axis

produces (in addition to the strain of interest) buckling. In most cases this buckling produces lateral contractions greater than the strains, resulting in erroneously high ν_{ij}'s. By loading a thin film material in mutually perpendicular directions simultaneously (biaxial stressing), this buckling phenomenon can largely be eliminated.

The in-plane Poisson ratios (ν_{xy}, ν_{yx}) can be calculated from biaxial straining using the Eq. (72):

$$\begin{aligned} \nu_{yx} &= (\sigma_{yy}/\sigma_{xx})\ (E_x/E_y) - \varepsilon_{yy}\ (E_x/\sigma_{xx}) \\ \nu_{xy} &= (\sigma_{xx}/\sigma_{yy})\ (E_y/E_x) - \varepsilon_{xx}\ (E_y/\sigma_{yy}), \end{aligned} \tag{76}$$

where E_x and E_y and the Young's moduli in the machine-direction (MD) and the cross-direction (CD), respectively. By previously determining these moduli values and recording the loads in both directions (P_x, P_y) against deformation (δ_x, δ_y) the Poisson ratios can be calculated from biaxial straining data. Determination of ν_{xy} and ν_{yx} allows an internal consistency check, since:

$$E_i\ \nu_{ij} = E_j\ \nu_{ji} \tag{77}$$

As can be seen in Fig. 75, the biaxial load/elongation apparatus consists of two mutually perpendicular pairs of line type clamps which move on horizontal precision ball-bearing slides. Each clamp pair movement is produced by two synchronized stepping motors, while the loads applied are sensed by calibrated strain gage type load cells attached in-line with one clamp of each pair. Deformation is recorded through a variable permeance transducer mounted on an A-frame, which is supported by steel balls freely rolling on smooth glass supports (Fig. 76). Two steel pins with fine tungsten wire tips were lowered from the A-frame until they touched the cellophane surface, and then a microdrop of cellulose paste was applied with a blunt needled syringe to attach the film to the

pins. Prior to gluing, these pins were precisely spaced (span = 39.6 mm) and aligned by a removable fixture (not seen in Fig. 76).

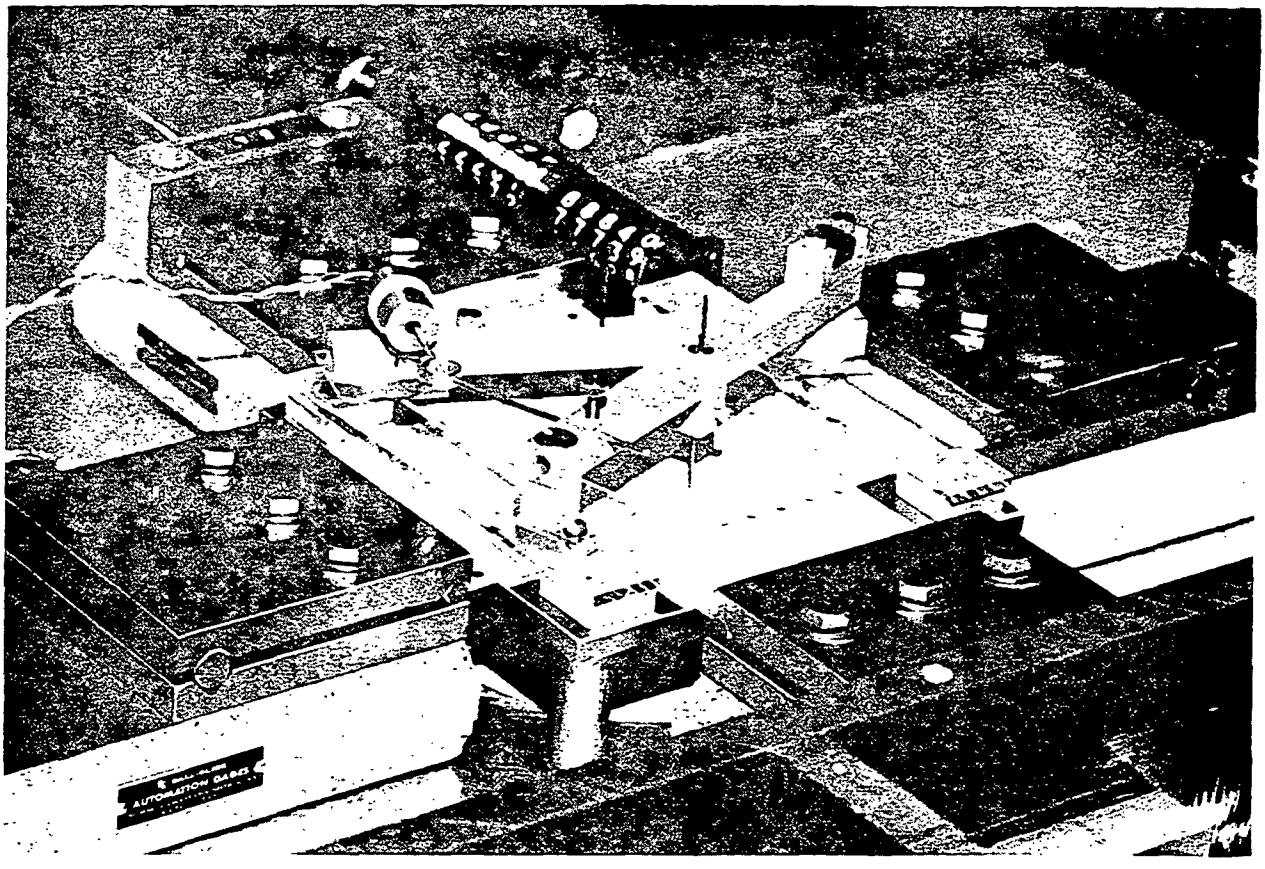

Figure 76. A-frame strain gage and test specimen.

Straining proceeds as a series of stepped pulses. At the beginning a balance reading of the A-frame transducer bridge was recorded for that pulsed strain increment. Several more balance readings were recorded on the curve (Fig. 77) up to the maximum strain level of approximately 0.2%. These balance readings (δ_x, δ_y) and corresponding loads (P_x, P_y) were used to calculate the stress (σ_{xx}, σ_{yy}) and strains (ε_{xx}, ε_{yy}) for different curve segments. This provided an additional internal consistency check.

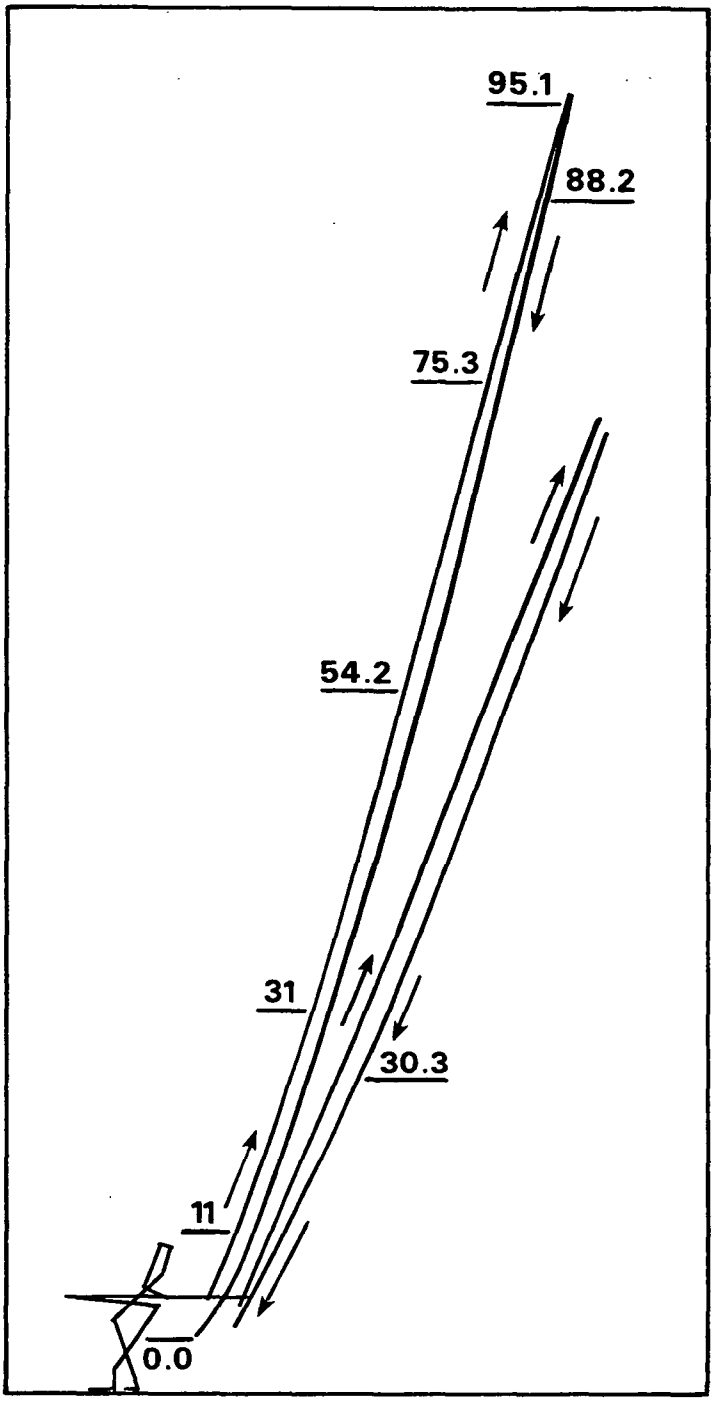

Figure 77. Typical biaxial load/elongation curve.

A special specimen shape (Fig. 78) is used which permits uniform biaxial strain fields to develop in an approximately 50 x 50 mm central region.[102] The deformation measurements take place within this region.

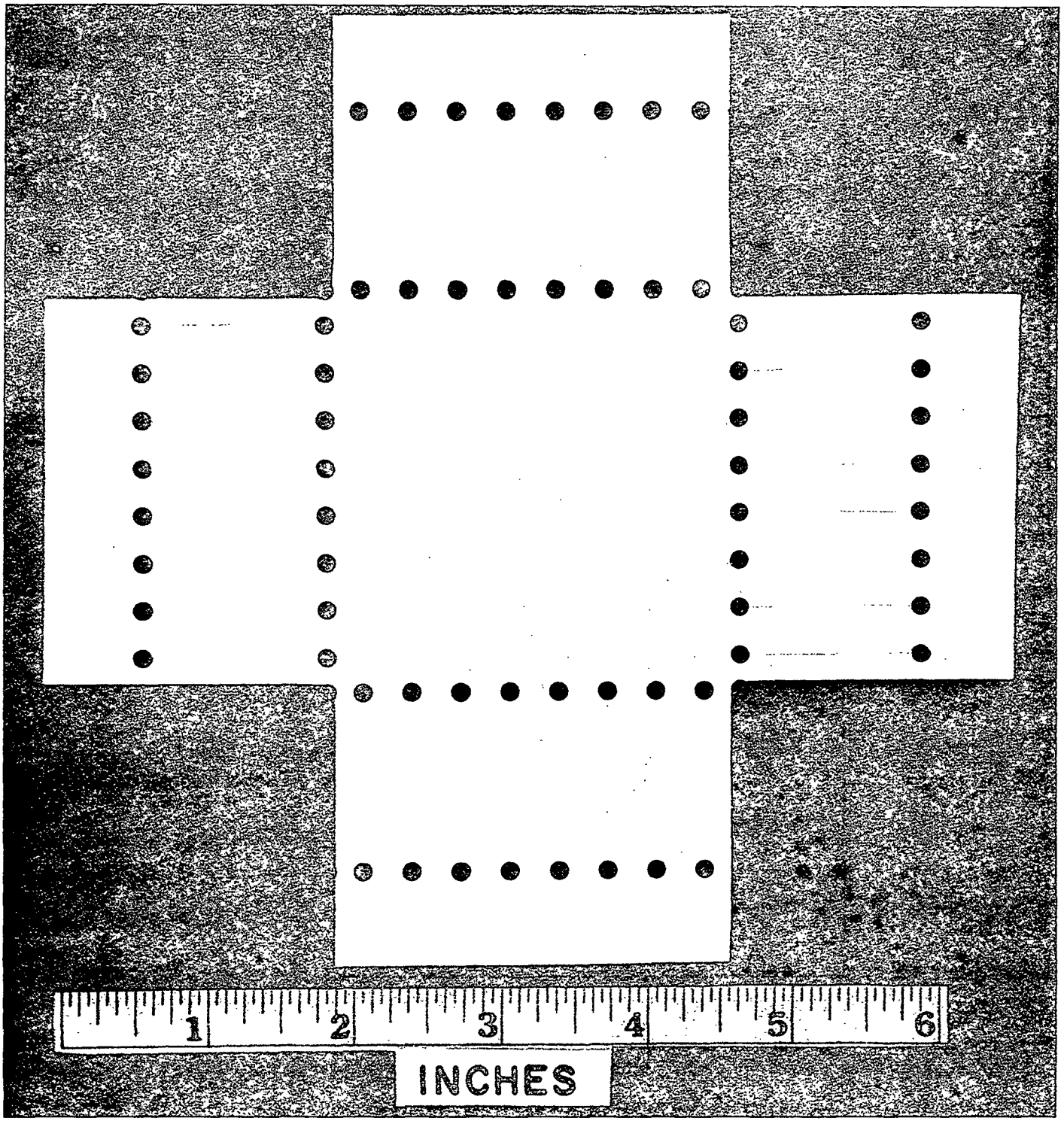

Figure 78. Biaxial test specimen configuration.

CELLOPHANE FILM PREPARATION

Three types of cellophane film (134 PUD-O, 193 PUD-O, 215 PD) were cut to a 178 x 178 mm size, two per film type. Each specimen was given a sequence-one cleaning (CCl_4, 95% ETOH, 3X distilled H_2O) and was maintained in triple-distilled water before pressing at 100 psi for 8 hours according to the procedures given in Appendix II. Following removal from the press, specimens were conditioned at 50% RH and 73°F for a minimum of 48 hours. All testing was conducted under these same conditions. After conditioning, one specimen of each film type was cut into the biaxial specimen shape (Fig. 78) for testing.

BIAXIAL AND ULTRASONIC TEST RESULTS

Specimens were aligned with the MD parallel to the machine x-axis. The x-axis clamps were closed with a 50 inches-pound torque and testing was begun. The sequence of property determinations was E_x, ν_{yx}, ν_{xy}, and finally E_y. A typical curve for ν_{yx} is shown in Fig. 77.

Three of the acoustic measurements ($V_{so_{xx}}$, $V_{so_{yy}}$, and $V_{so_{xy}}$) were made with the Morgan Dynamic Modulus Tester on all of the specimens (two per film type). The z-direction velocity, V_{zz}, was determined on 1-inch squares (unstressed specimens only) layered with petroleum jelly to 9 and 18 layers. The system and coupler delay times were used to correct the transit time to just that in the cellophane film according to the techniques developed by Mann.[103] Cellophane densities were calculated from data supplied by the manufacturer (ρ = 1.434 g/cm^3). The results of both tests are listed in Table 13.

Table 13. Biaxial and ultrasonic test results.

Material	Technique	Elastic Modulus[a] E_x	E_y	E_z	Poisson Ratios ν_{yx}	ν_{xy}[b]	E_y/E_x	ν_{xy}/ν_{yx}	Shear Modulus[a] μ_{xy}
134 PUD-O (press dried)	Biaxial	9.175	6.194	--	0.507	0.348	0.675	0.675	--
193 PUD-O (press dried)	Biaxial	9.175	5.953	--	0.486	0.323	0.650	0.665	--
193 PUD-O (as received)	Biaxial	9.765	5.852	--	0.377	0.274	0.599	0.727	--
215 PD (press dried)	Biaxial	8.552	5.390	--	0.462	0.250	0.630	0.541	--

		$\rho V_{so_{xx}}^2$	$\rho V_{so_{yy}}^2$	$\rho V_{so_{zz}}^2$			$\rho V_{so_{yy_2}}^2 / \rho V_{so_{xx}}^2$		$\rho V_{so_{yy}}^2$
134 PUD-O (press dried)	Acoustic	10.640	7.787	3.444	--	--	0.732	--	2.466
193 PUD-O (stressed)	Acoustic	10.468	7.285	--	--	--	0.696	--	2.237
(press dried)	Acoustic	10.500	7.744	3.186	--	--	0.738	--	2.466
193 PUD-O (as received)	Acoustic	11.386	7.557	--	--	--	0.664	--	2.624
215 PD (press dried)	Acoustic	10.655	7.270	--	--	--	0.682	--	2.553

[a][x 10^{10} dynes/(cm)^2].
[b]Most consistent data.

Only four of the independent elastic parameters ($\rho V_{so_{xx}}^2$, $\rho V_{so_{yy}}^2$, $\rho V_{so_{zz}}^2$, and ν_{xy}) listed in Table 13 are useful for calculating six (C_{11}, C_{22}, C_{33}, C_{12}, C_{13}, and C_{23}) of the nine elastic constants of an orthotropic material. Estimates of two more independent parameters (ν_{xz} and ν_{yz}) were made. As a guide to make these estimates, the theoretical calculations of Nomura, et al.[97] for the uniform stress and uniform strain hypothesis were examined. Neither set of theoretical calculations produced a consistent set of constants, but the

general correspondence of the accumulated data was slanted toward the uniform strain hypothesis. Some slight adjustments away from the uniform strain hypothesis produced a consistent set of constants. The constants were calculated by solving the set of six equations involving the four independent measurements and the two estimated Poisson ratios. The two unknown shear moduli were adjusted relative to the measured μ_{xy} in accordance with the modified data of the uniform strain hypothesis. These stiffness coefficients are listed in Table 14.

Table 14. Calculated stiffness coefficients.[a]

	Cellophane Film			
Stiffness Coefficient	134 PUD-O (press dried)	193 PUD-O (press dried)	193 PUD-O (as received)	215 PD (press dried)
C_{11}	14.946	14.094	13.835	12.415
C_{22}	11.042	9.980	9.326	8.607
C_{33}	3.444	3.186	(3.186) est.	(3.186) est.
C_{12}	7.447	6.507	5.201	4.198
C_{13}	3.851	3.399	2.793	2.368
C_{23}	3.348	2.930	2.374	2.064
C_{44}	2.466	2.237	2.624	2.553
C_{55}	1.260	1.242	--	--
C_{66}	1.388	1.401	--	--

[a][x 10^{10} dynes/(cm)^2].

CALCULATIONS OF STIFFNESS COEFFICIENTS

The equations which related Poisson ratios to the stiffness coefficients are:

$$\nu_{yx} = \frac{C_{12}\,C_{33} - C_{13}\,C_{23}}{C_{22}\,C_{33} - C_{23}^2} \quad ; \quad \nu_{xy} = \frac{C_{12}\,C_{33} - C_{13}\,C_{23}}{C_{11}\,C_{33} - C_{13}^2}$$

$$\nu_{zx} = \frac{C_{13}\,C_{22} - C_{12}\,C_{23}}{C_{22}\,C_{33} - C_{23}^2} \quad ; \quad \nu_{xz} = \frac{C_{13}\,C_{22} - C_{12}\,C_{23}}{C_{11}\,C_{22} - C_{12}^2} \tag{78}$$

$$\nu_{zy} = \frac{C_{23}\,C_{11} - C_{12}\,C_{13}}{C_{11}\,C_{33} - C_{13}^2} \quad ; \quad \nu_{yz} = \frac{C_{23}\,C_{11} - C_{12}\,C_{13}}{C_{11}\,C_{22} - C_{12}^2}$$

The results shown in Table 14 do not indicate any large differences in the elastic constants of 134 PUD-O and 193 PUD-O.

ENGINEERING CONSTANT CALCULATIONS

Using the above equations for Poisson ratios[78] and the following equation for the calculation of Young's moduli (E_x, E_y, E_z),

$$E_i = \begin{bmatrix} C_{11} & C_{12} & C_{13} \\ C_{12} & C_{22} & C_{23} \\ C_{13} & C_{23} & C_{33} \end{bmatrix} (C_{jj}\,C_{kk} - C_{jk}^2)^{-1} \tag{79}$$

where the indices i, j, k are taken in cyclic order, the engineering constants were calculated from the stiffness coefficients shown in Table 14. These results are presented in Table 15.

When these calculations are compared to the statically determined E_x, E_y, films 134 PUD-O and 193 PUD-O have larger calculated E_y's (+ 4.9% and 4.0%, respectively) and smaller E_x's (- 3.2% and 2.8%, respectively). Both other films have considerably higher E's than those measured statically. Overall there is little difference between 193 and 134 press dried for those constants that depend primarily on the acoustic data of one specimen. Since the experimental utilization is a static test situation, not acoustic, all the calculated engineering constants (except ν_{ij}'s) were adjusted, based on the average E_x

values determined for all the static data obtained in this thesis research. The nine working engineering constants are listed in Table 16.

Table 15. Engineering elastic constants.[a]

Engineering Constants	Cellophane Film 134 PUD-0 (press dried)	193 PUD-0 (press dried)	193 PUD-0 (as received)	215 PD (press dried)
E_x	8.879	8.900	10.098	6.679
E_y	6.498	6.193	6.703	6.604
E_z	2.173	2.101	2.384	2.512
ν_{xy}	0.476	0.464	0.413	0.366
ν_{xz}	0.656	0.640	0.569	0.506
ν_{yx}	0.348	0.323	0.274	0.250
ν_{zx}	0.161	0.151	0.134	0.131
ν_{zy}	0.213	0.195	0.180	0.176

[a][x 10^{10} dynes/(cm)^2].

Table 16. Working engineering constants.

Material	Young's Modulii[a] E_x	E_y	E_z	Poisson Ratios ν_{xy}	ν_{zy}	ν_{zx}	Shear Modulii[a] μ_{xy}	μ_{yz}	μ_{xz}
134 PUD-0	9.486	6.960	2.328	0.476	0.583	0.656	2.594	1.350	1.485
193 PUD-0	9.691	6.743	2.288	0.467	0.575	0.640	2.786	1.323	1.487

[a][x 10^{10} dynes/(cm)^2].

No adjustment of film 215 PD has been made because the static data were erratic, probably because this was a plasticized film (21% glycerin), and any difference in the extent of plasticizer removal resulted in different test results. There is some question whether engineering constants obtained on wide specimens (< 12.7 mm) in static testing will be equivalent to the constants

measured on narrow specimens.[102] A comparison of in-plane moduli for 134 PUD-O and 193 PUD-O fibers and 12.7-mm wide strips are presented in Table 17. These results show, in general, lower moduli for the narrow (300 to 500 μm) cellophane fibers than for the wider strip. While no experimental data as complete as that just presented has been discovered in the literature, and it is thus difficult to assess its accuracy, Nomura, et al.[97] reported in-plane Poisson ratios of 0.4. The magnitude of their other results was significantly lower (for acoustic measurements at 1% strain), but the relative E_x, E_y, ν_{xy} values were nearly the same as that reported here.

Table 17. Summary of elastic constant[a] determinations on cellophane fibers and strips.

Test Configuration		134 PUD-O		193 PUD-O	
		MD	CD	MD	CD
MACROC	$\bar{X}$ =	975.3	713.2	997.9	703.4
	S.D. =	20.91	10.32	22.69	50.95
	C.V. =	2.14%	1.45%	2.27%	7.24%
	No. of Tests	4	3	4	4
ALL MACRO	$\bar{X}$ =	948.6	680.8	967.9	670.6
	S.D. =	46.73	45.83	49.66	64.51
	C.V. =	4.93%	6.73%	5.13%	9.62%
	No. of Tests	6	5	6	6
MICRO	$\bar{X}$ =	952.9	597.1	919.2	580.8
FLER low sensitivity	S.D. =	22.88	43.19	97.33	28.44
	C.V. =	2.40%	7.23%	10.6%	4.9%
	No. of Tests	3	3	3	3
FLER high sensitivity	$\bar{X}$ =	869.4	537.3	838.9	510.2
	S.D. =	47.61	11.53	71.09	42.17
	C.V. =	5.48%	2.15%	8.47%	8.26%
	No. of Tests	3	3	3	3
ALL MICRO	$\bar{X}$ =	911.2	567.2	879.1	545.5
	S.D. =	56.67	43.26	88.0	50.28
	C.V. =	6.22%	7.63%	10.0%	9.22%
	No. of Tests	6	6	6	6

$\bar{X}$ = mean[a]; S.D. = standard deviation[a]; C.V. = coefficient of variation.

[a]Units, dynes/(μm)^2.

APPENDIX IV

CELLOPHANE MACROLAP JOINT EXPERIMENTAL RESULTS

Table 18. Cellophane macrolap joint experimental results.

Specimen Identification No.	Lap Length, μm	L/T	W/T	Average Thickness, μm	Total Strain at Failure	Inverse Modulus, μm**2/dyne	Bond Shear Strength, dynes/μm**2	Nominal Axial Stress at Failure, dynes/μm**2
				134 PUD-O MD/MD Experiment C				
C1112	505.4	13.82	356.8	36.58	0.327	0.001084	0.201	2.739
C1113	334.3	9.11	359.6	36.70	0.264	0.001139	0.226	2.057
C1114	412.5	11.44	356.3	36.07	0.276	0.001086	0.209	2.365
C1121	787.5	21.38	350.3	36.83	0.394	0.001117	0.130	2.779
C1122	1068.0	29.61	378.4	36.07	0.389	0.001060	0.114	3.339
C1123	978.3	26.38	347.9	37.08	0.394	0.001163	0.123	3.228
C1124	1421.8	40.13	378.2	35.43	0.564	0.001015	0.127	5.010
C1131	1736.0	47.96	359.2	36.19	0.558	0.001092	0.091	4.290
C1133	1645.0	43.47	340.8	37.85	0.691	0.001144	0.122	5.281
C1134	2338.0	65.28	383.9	35.81	0.645	0.001028	0.086	5.537
C1141	2646.0	72.34	350.0	36.58	0.622	0.001025	0.076	5.480
C1143	2695.0	74.20	363.4	36.32	0.769	0.001102	0.080	5.873
C1144	3164.0	85.91	346.2	36.83	0.644	0.001090	0.063	5.358

Table 19. Cellophane macrolap joint experimental results.

Specimen Identification No.	Lap Length, μm	L/T	W/T	Average Thickness, μm	Total Strain at Failure	Inverse Modulus, μm**2/dyne	Bond Shear Strength, dynes/μm**2	Nominal Axial Stress at Failure, dynes/μm**2
				134 PUD-0 CD/CD Experiment C				
C1211	606.5	16.47	336.7	36.83	0.454	0.001570	0.167	2.754
C1214	598.4	16.59	345.2	36.07	0.471	0.001517	0.178	2.940
C1213	823.4	22.75	344.0	36.19	0.560	0.001654	0.140	3.150
C1221	880.5	23.66	335.9	37.21	0.574	0.001528	0.146	3.454
C1223	1188.6	32.27	338.0	36.83	1.573	0.001670	0.187	6.004
C1224	1182.1	32.77	347.9	36.07	3.138	0.001642	0.204	6.605
C1231	1946.0	51.59	326.1	37.72	0.820	0.001514	0.090	4.671
C1232	1764.0	47.90	334.0	36.83	2.754	0.001703	0.139	6.653
C1233	3262.0	90.44	343.8	36.07	8.105	0.001691	0.076	6.851
C1234	2219.0	64.00	359.1	34.67	7.654	0.001638	0.110	7.012
C1241	3024.0	80.72	328.3	37.46	3.191	0.001544	0.086	6.946
C1242	3185.0	85.89	334.4	37.08	2.145	0.001668	0.077	6.582
C1244	2954.0	81.61	342.6	36.19	5.538	0.001572	0.088	7.160

Table 20. Cellophane macrolap joint experimental results.

Specimen Identification No.	Lap Length, μm	L/T	W/T	Average Thickness, μm	Total Strain at Failure	Inverse Modulus, μm**2/dyne	Bond Shear Strength, dynes/μm**2	Nominal Axial Stress at Failure, dynes/μm**2
				134 PUD-O MD/CD Experiment C				
C1311	604.9	16.26	337.3	37.21	0.351	0.001518	0.129	2.053
C1313	836.4	22.87	348.6	36.58	0.311	0.001474	0.084	1.869
C1314	671.8	18.69	353.4	35.94	0.260	0.001426	0.090	1.637
C1321	921.2	24.51	331.2	37.59	0.364	0.001580	0.090	2.153
C1323	1607.7	44.42	348.1	36.19	0.398	0.001455	0.058	2.567
C1324	932.6	25.32	339.4	36.83	0.293	0.001385	0.080	2.002
C1331	1974.0	54.54	356.4	36.19	0.300	0.001369	0.039	2.028
C1344	2541.0	69.47	347.2	36.58	0.394	0.001332	0.040	2.762
C1333	2975.0	83.66	350.1	35.56	0.804	0.001467	0.058	4.839
C1341	2884.0	76.98	331.0	37.46	0.858	0.001418	0.068	5.173
C1343	4956.0	137.41	354.9	36.07	4.173	0.001439	0.050	6.827

Table 21. Cellophane macrolap joint experimental results.

Specimen Identification No.	Lap Length, μm	L/T	W/T	Average Thickness, μm	Total Strain at Failure	Inverse Modulus, μm**2/dyne	Bond Shear Strength, dynes/μm**2	Nominal Axial Stress at Failure, dynes/μm**2
				193 PUD-O MD/MD Experiment C				
C2112	482.6	18.54	507.0	26.03	0.416	0.001061	0.193	3.588
C2114	590.2	23.01	510.6	25.65	0.458	0.001079	0.180	4.113
C2111	500.6	18.77	487.4	26.67	0.538	0.001202	0.205	3.844
C2113	1058.2	40.65	508.9	26.03	1.745	0.001123	0.200	8.088
C2121	971.8	37.51	509.5	25.91	0.909	0.001183	0.171	6.410
C2122	1090.8	42.95	519.7	25.40	1.265	0.001016	0.190	8.172
C2123	1125.0	44.29	519.7	25.40	1.651	0.001094	0.185	8.210
C2124	1141.3	44.94	519.7	25.40	1.876	0.001055	0.193	8.655
C2131	1482.1	56.38	494.5	26.29	2.316	0.001000	0.161	9.074
C2132	1345.2	52.96	519.7	25.40	1.871	0.001045	0.165	8.730
C2133	1459.3	54.72	494.9	26.67	2.351	0.001120	0.152	8.314
C2134	2023.0	79.65	515.8	25.40	1.120	0.001013	0.099	7.861
C2141	2058.0	77.91	488.3	26.42	2.982	0.001005	0.124	9.649
C2142	1869.0	72.95	518.4	25.65	2.520	0.001036	0.127	9.272
C2143	1869.0	72.85	514.5	25.65	2.478	0.001075	0.120	8.717

Table 22. Cellophane macrolap joint experimental results.

Specimen Identification No.	Lap Length, μm	L/T	W/T	Average Thickness, μm	Total Strain at Failure	Inverse Modulus, μm**2/dyne	Bond Shear Strength, dynes/μm**2	Nominal Axial Stress at Failure, dynes/μm**2
193 PUD-O CD/CD Experiment C								
C2211	655.5	25.55	479.5	25.65	2.453	0.001511	0.270	6.907
C2212	751.7	29.59	488.2	25.40	7.660	0.001547	0.259	7.672
C2213	541.3	21.31	488.2	25.40	5.834	0.001681	0.325	6.920
C2214	622.8	24.52	488.2	25.40	6.465	0.001515	0.302	7.395
C2221	1157.6	45.13	483.4	25.65	11.173	0.001500	0.179	8.065
C2222	927.8	35.99	484.8	25.78	8.276	0.001578	0.212	7.614
C2223	1193.5	44.75	461.2	26.67	10.909	0.001657	0.165	7.404
C2224	997.9	38.33	480.1	26.03	9.204	0.001592	0.198	7.538
C2231	1547.3	58.58	469.4	26.42	7.236	0.001568	0.130	7.605
C2232	1573.4	60.44	487.8	26.03	10.113	0.001586	0.124	7.496
C2233	1252.2	48.33	480.5	25.91	11.654	0.001650	0.162	7.724
C2234	1988.0	78.27	484.3	25.40	10.873	0.001555	0.101	7.933
C2241	2065.0	79.71	474.8	25.91	13.622	0.001489	0.105	8.403
C2242	1806.0	71.10	488.2	25.40	8.113	0.001538	0.110	7.790
C2243	1890.0	73.31	484.8	25.78	9.131	0.001616	0.101	7.380

Table 23. Cellophane macrolap joint experimental results.

Specimen Identification No.	Lap Length, μm	L/T	W/T	Average Thickness, μm	Total Strain at Failure	Inverse Modulus, μm**2/dyne	Bond Shear Strength, dynes/μm**2	Nominal Axial Stress at Failure, dynes/μm**2
				193 PUD-O MD/CD Experiment C				
C2312	96.2	3.71	497.9	25.91	0.389	0.001457	0.673	2.421
C2313	596.8	23.03	497.9	25.91	0.376	0.001437	0.113	2.533
C2314	583.7	22.75	495.0	25.65	0.460	0.001456	0.119	2.637
C2323	1100.6	43.33	505.9	25.40	0.436	0.001422	0.068	2.862
C2324	1097.3	42.35	488.3	25.91	0.433	0.001390	0.069	2.850
C2331	1680.3	62.99	476.2	26.67	0.473	0.001391	0.051	3.159
C2332	1729.0	65.77	486.9	26.29	0.489	0.001398	0.054	3.441
C2334	1420.2	55.36	497.0	25.65	0.442	0.001388	0.054	2.893
C2322	1361.5	53.07	510.6	25.65	0.549	0.001423	0.071	3.631
C2333	1603.0	63.11	505.9	25.40	0.518	0.001253	0.055	3.396
C2341	2191.0	84.16	493.6	26.03	0.600	0.001405	0.048	3.907
C2342	2107.0	81.33	490.2	25.91	0.847	0.001334	0.069	5.371
C2343	2275.0	90.02	508.4	25.27	0.940	0.001396	0.064	5.598

Table 24. Cellophane macrolap joint experimental results.

Specimen Identification No.	Lap Length, μm	L/T	W/T	Average Thickness, μm	Total Strain at Failure	Inverse Modulus, μm**2/dyne	Bond Shear Strength, dynes/μm**2	Nominal Axial Stress at Failure, dynes/μm**2
				215 PD MD/MD Experiment C				
C3111	326.1	14.51	578.3	22.48	0.482	0.001111	0.270	3.921
C3112	531.5	24.48	598.6	21.72	0.684	0.001109	0.227	5.559
C3113	355.4	16.86	626.1	21.08	0.440	0.001154	0.210	3.536
C3114	753.3	35.31	602.3	21.34	2.234	0.001151	0.241	8.404
C3121	277.2	12.54	588.3	22.10	0.382	0.001191	0.252	3.165
C3123	869.1	40.73	618.7	21.34	2.727	0.001151	0.212	8.624
C3131	322.8	14.95	611.4	21.59	0.384	0.001113	0.216	3.234
C3133	671.8	30.75	599.7	21.84	1.073	0.001170	0.225	6.920
C3134	1472.3	69.01	604.6	21.34	4.247	0.001081	0.143	9.775
C3141	1561.0	72.30	597.5	21.59	3.953	0.001069	0.134	9.659
C3143	1764.0	80.29	591.7	21.97	4.278	0.001167	0.119	9.244
C3144	1002.8	45.91	595.1	21.84	2.194	0.001111	0.190	8.509

Table 25. Cellophane macrolap joint experimental results.

Specimen Identification No.	Lap Length, μm	L/T	W/T	Average Thickness, μm	Total Strain at Failure	Inverse Modulus, μm**2/dyne	Bond Shear Strength, dynes/μm**2	Nominal Axial Stress at Failure, dynes/μm**2
				215 PD CD/CD Experiment C				
C3211	635.9	27.97	554.3	22.73	13.447	0.001639	0.274	7.653
C3212	657.1	30.08	572.2	21.84	9.133	0.001644	0.262	7.571
C3213	342.3	15.68	567.7	21.84	0.607	0.001631	0.217	3.403
C3214	365.2	17.12	576.5	21.34	1.469	0.001561	0.372	6.311
C3221	1010.9	47.38	595.2	21.34	12.207	0.001604	0.159	7.538
C3222	1268.5	56.75	559.2	22.35	11.351	0.001689	0.129	7.311
C3224	565.8	25.60	563.4	22.10	1.396	0.001605	0.236	5.930
C3232	1680.0	76.91	574.5	21.84	8.851	0.001646	0.095	7.182
C3233	1348.4	61.73	576.8	21.84	11.698	0.001577	0.123	7.512
C3234	1953.0	92.08	589.4	21.21	12.522	0.001537	0.077	8.080
C3241	2366.0	104.08	538.9	22.73	10.865	0.001726	0.071	7.335
C3242	1960.0	89.73	567.7	21.84	12.654	0.001615	0.085	7.633
C3244	2191.0	99.72	555.3	21.97	13.164	0.001610	0.081	8.038

Table 26. Cellophane macrolap joint experimental results.

Specimen Identification No.	Lap Length, μm	L/T	W/T	Average Thickness, μm	Total Strain at Failure	Inverse Modulus, μm**2/dyne	Bond Shear Strength, dynes/μm**2	Nominal Axial Stress at Failure, dynes/μm**2
				215 PD MD/CD Experiment C				
C3321	828.3	37.70	575.8	21.97	0.507	0.001416	0.092	3.361
C3323	900.0	42.18	599.9	21.34	0.684	0.001355	0.107	4.378
C3324	834.8	37.35	570.4	22.35	0.524	0.001489	0.090	3.321
C3331	1652.0	76.52	588.2	21.59	0.894	0.001397	0.066	4.950
C3332	1596.0	73.92	595.2	21.59	0.676	0.001431	0.060	4.260
C3333	1593.0	72.93	586.0	21.84	0.800	0.001407	0.069	4.903
C3334	1384.3	63.74	587.1	21.72	0.736	0.001427	0.073	4.586
C3341	1946.0	91.21	611.6	21.34	5.214	0.001382	0.087	7.604
C3342	1890.0	86.02	584.9	21.97	0.754	0.001478	0.054	4.543
C3343	2023.0	94.82	592.9	21.34	3.907	0.001363	0.080	7.476
C3311	244.6	10.76	554.3	22.73	0.396	0.001418	0.228	2.391
C3312	663.6	31.10	595.2	21.34	0.494	0.001422	0.107	3.263
C3313	355.4	16.66	599.9	21.34	0.413	0.001504	0.164	2.644
C3314	753.3	35.52	601.2	21.21	0.447	0.001354	0.082	2.855
C3322	798.9	37.45	595.2	21.34	0.411	0.001323	0.082	3.034
C3344	854.4	38.01	571.6	22.48	0.444	0.001373	0.080	2.978

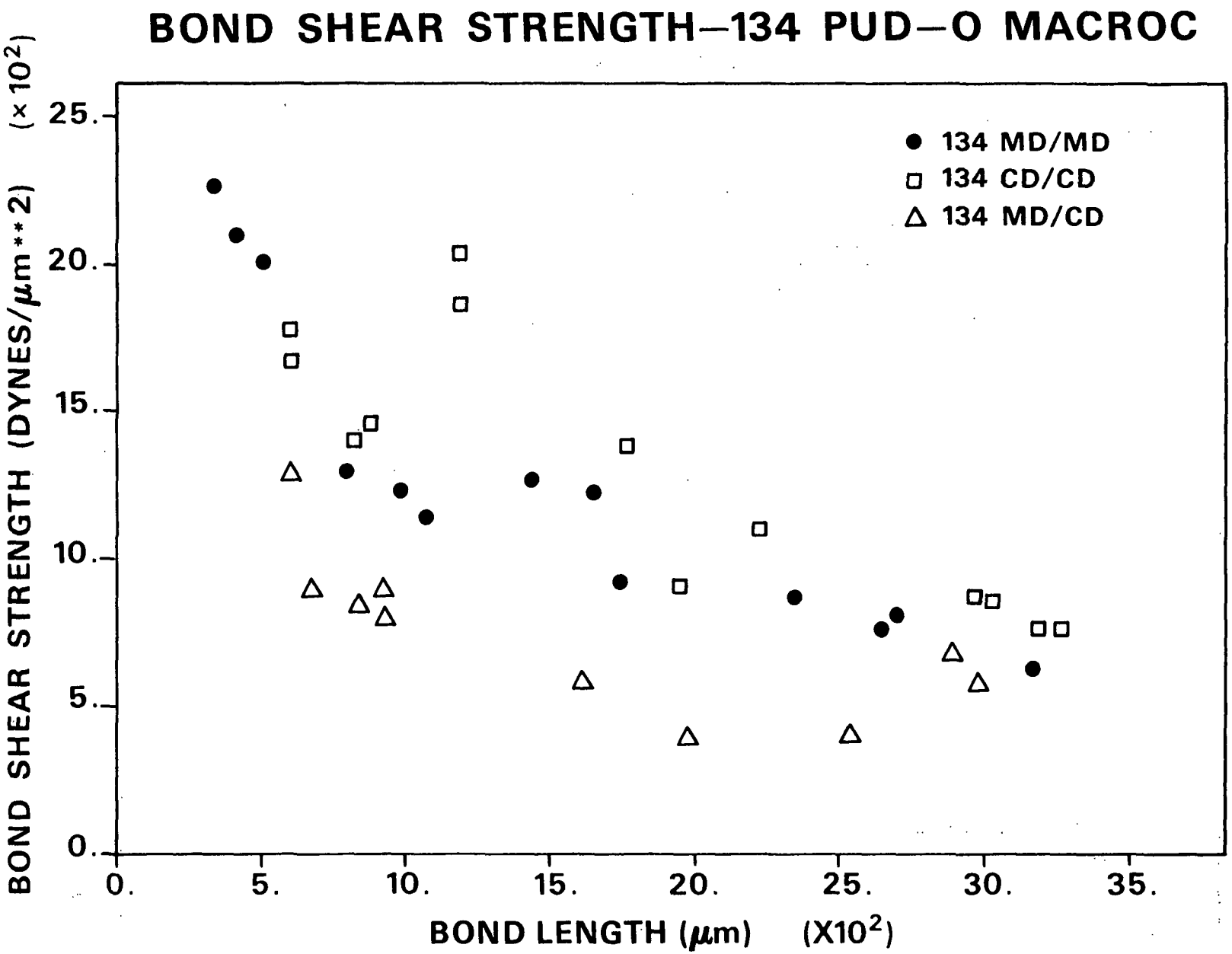

Figure 79. Effect of bond length on the bond shear strength of 134 PUD-O cellophane macrolap joints (MD/MD, CD/CD, MD/CD configurations).

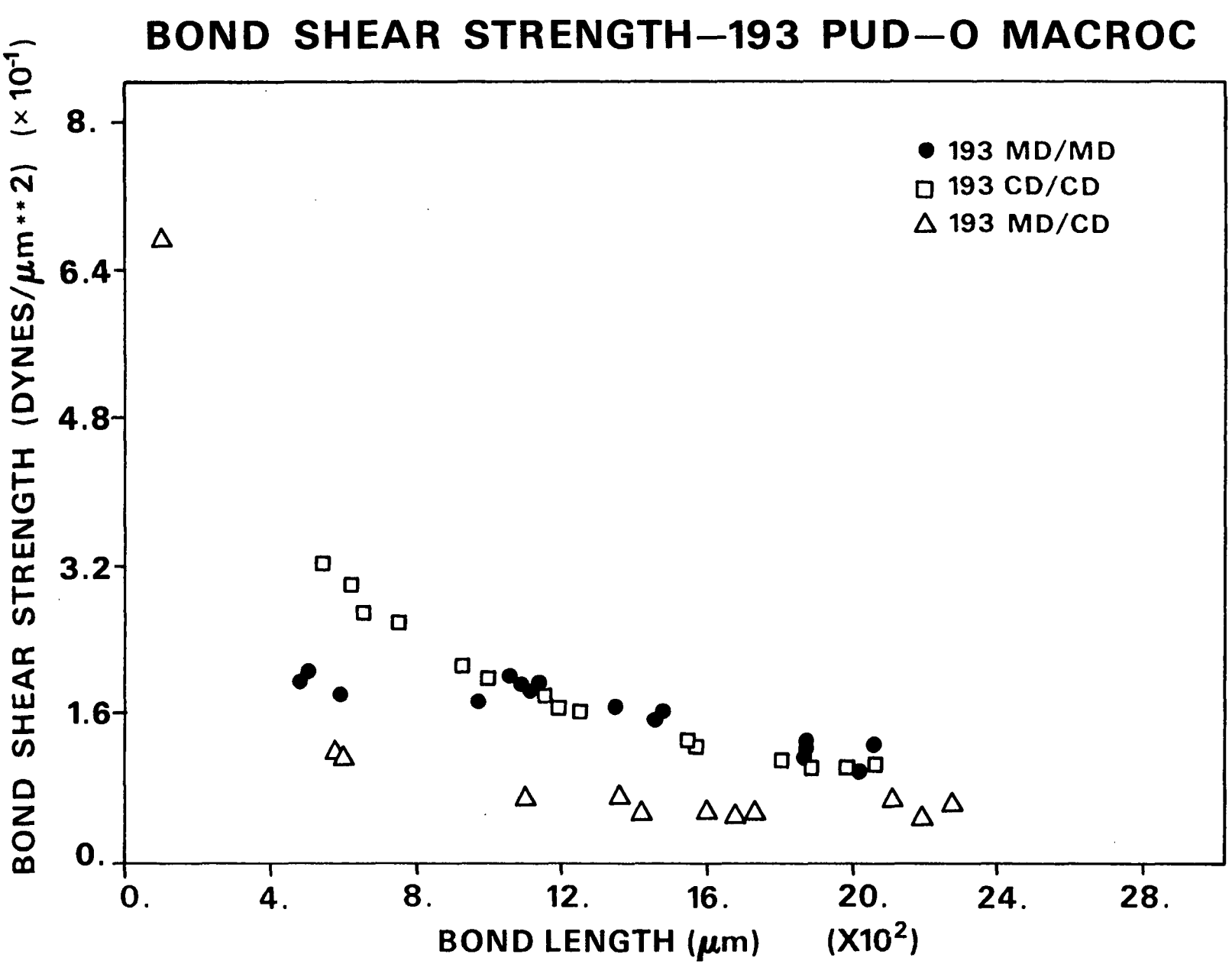

Figure 80. Effect of bond length on the bond shear strength of 193 PUD-O cellophane macrolap joints (MD/MD, CD/CD, MD/CD configurations).

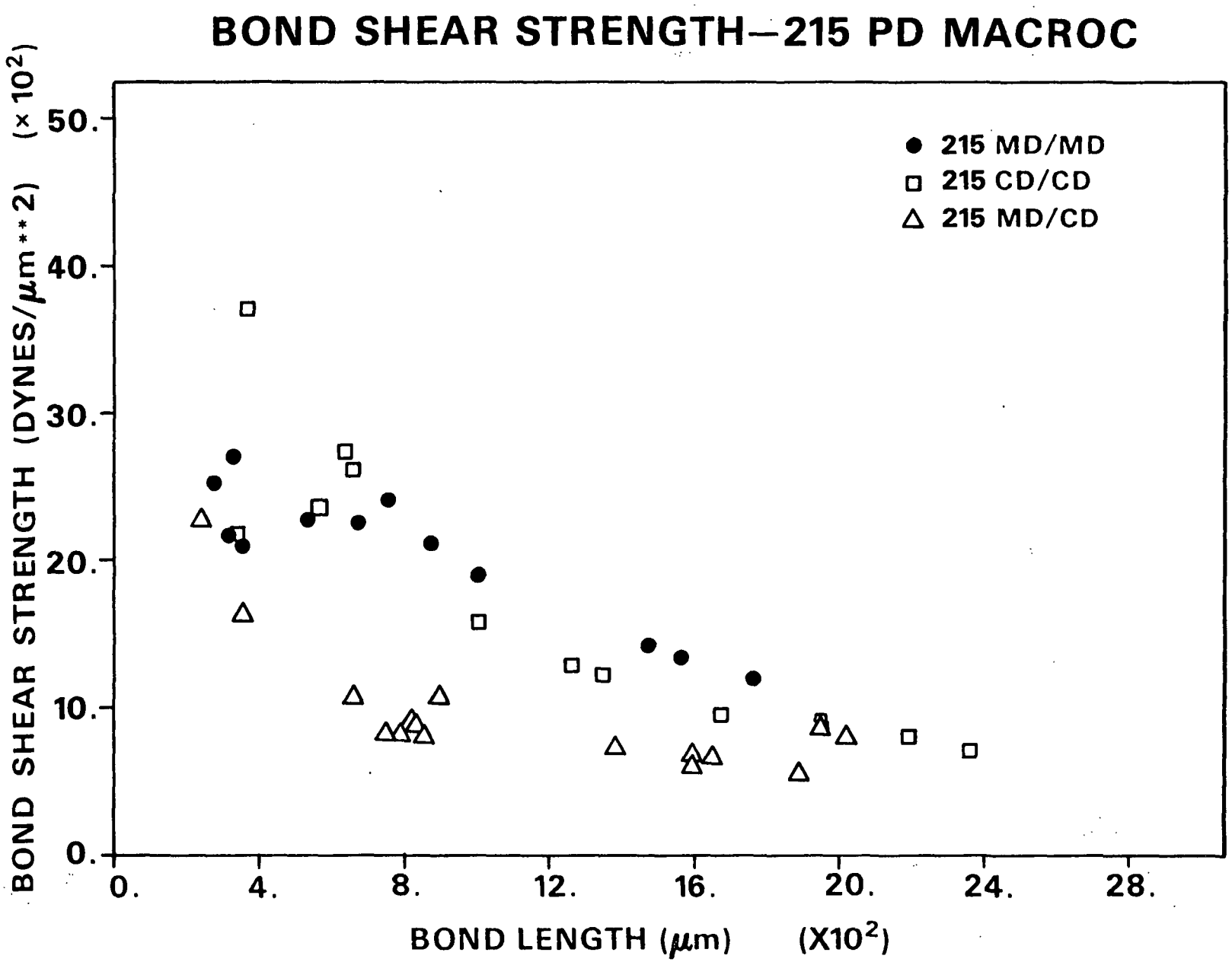

Figure 81. Effect of bond length on both bond shear strength of 215 PD cellophane macrolap joints (MD/MD, CD/CD, MD/CD configurations).

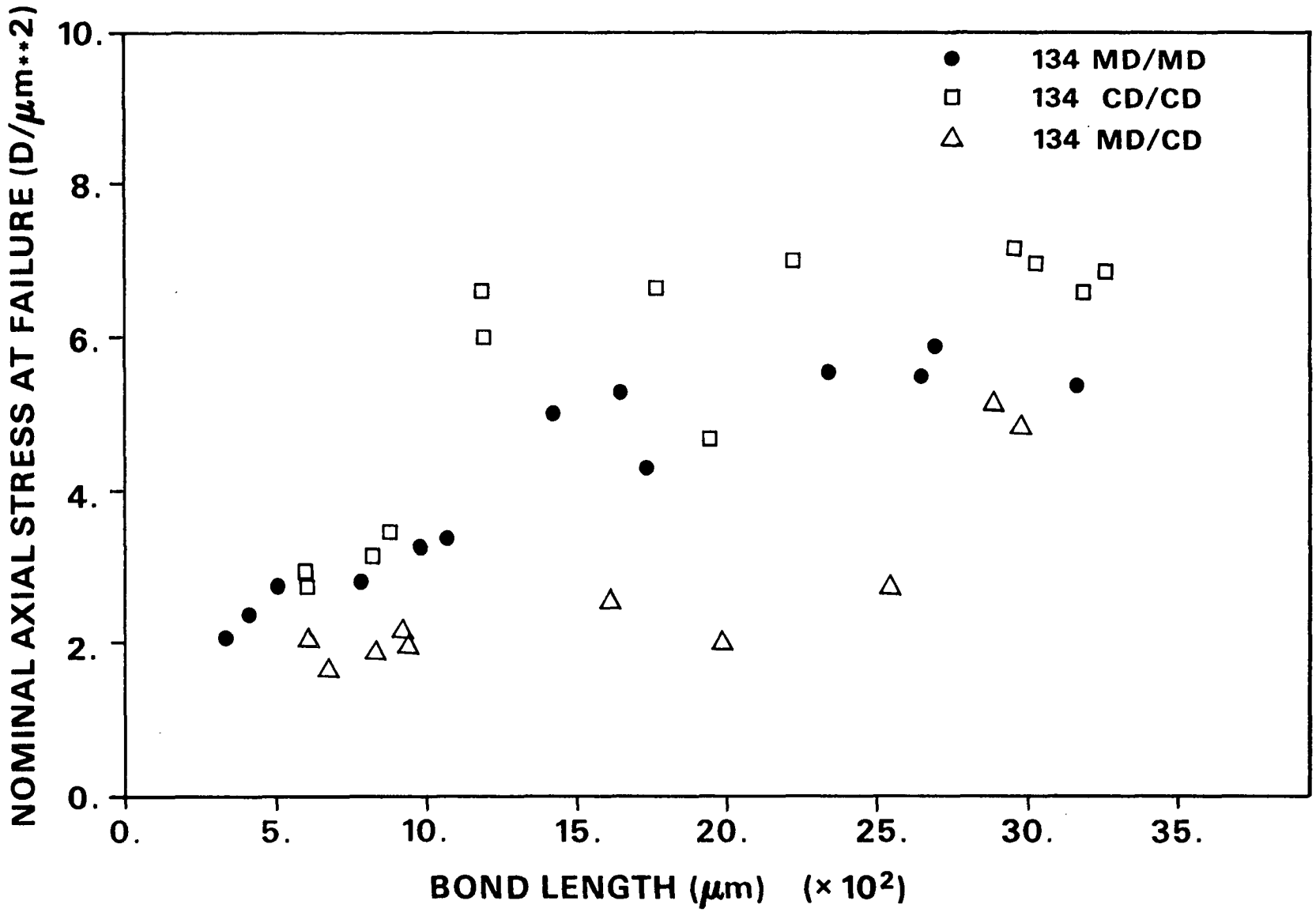

Figure 82. Effect of bond length on the nominal axial stress at failure of 134 PUD-O cellophane macrolap joints (MD/MD, CD/CD, MC/DC configurations).

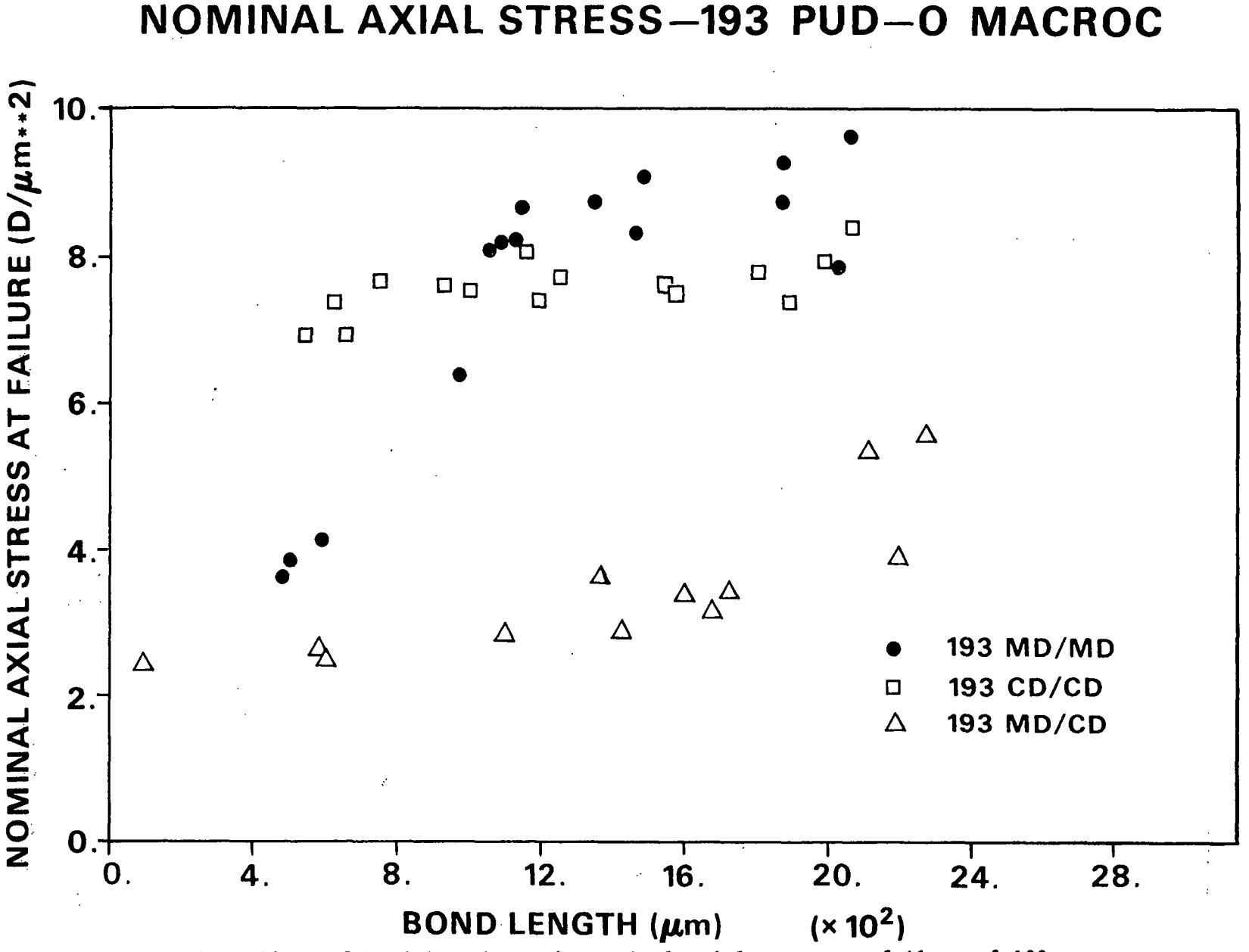

Figure 83. Effect of bond length on the nominal axial stress at failure of 193 PUD-O cellophane macrolap joints (MD/MD, CD/CD, MD/CD configurations).

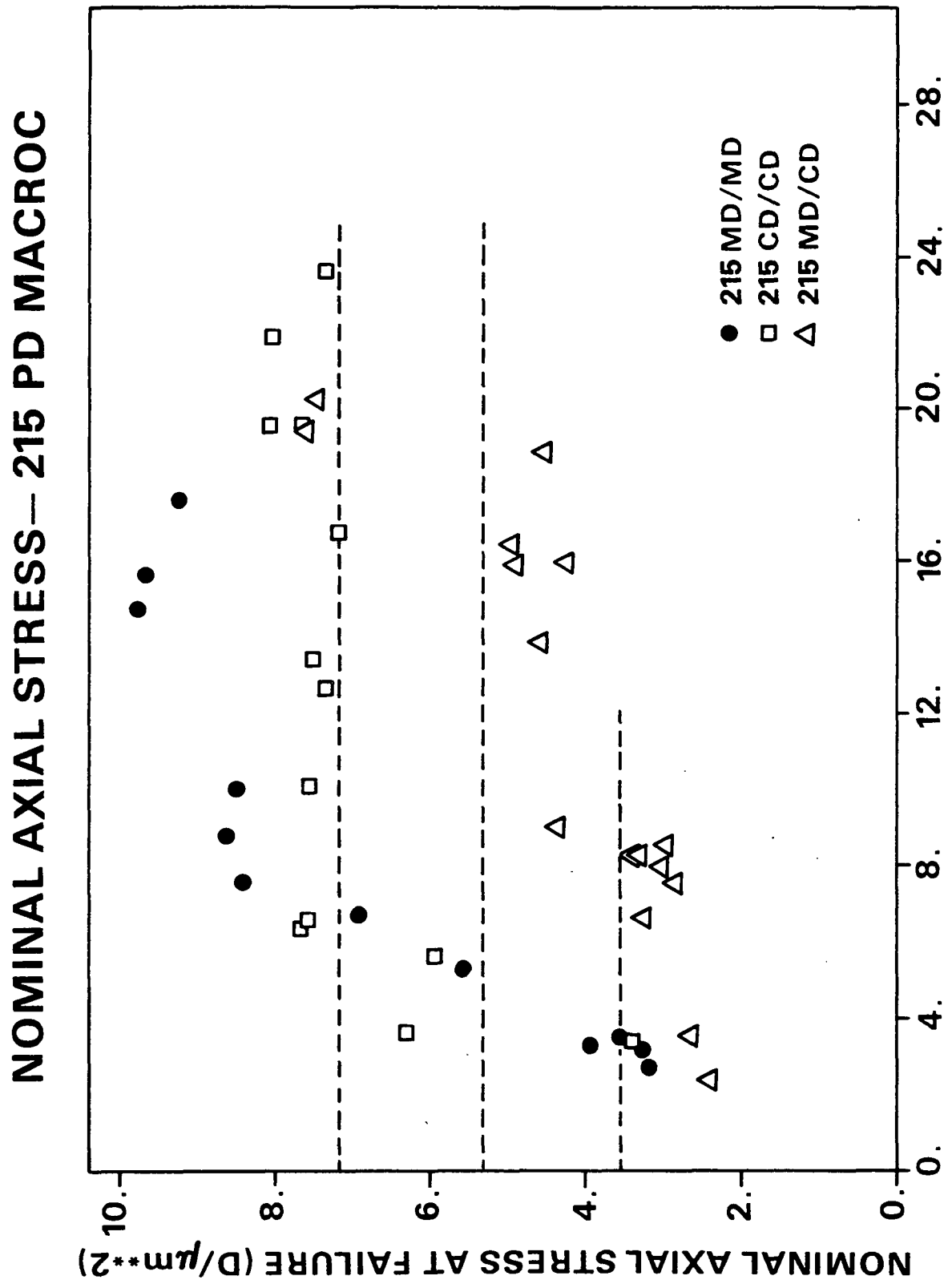

Figure 84. Effect of bond length on the nominal axial stress at failure of 215 PD cellophane macrolap joints (MD/MD, CD/CD, MD/CD configurations).

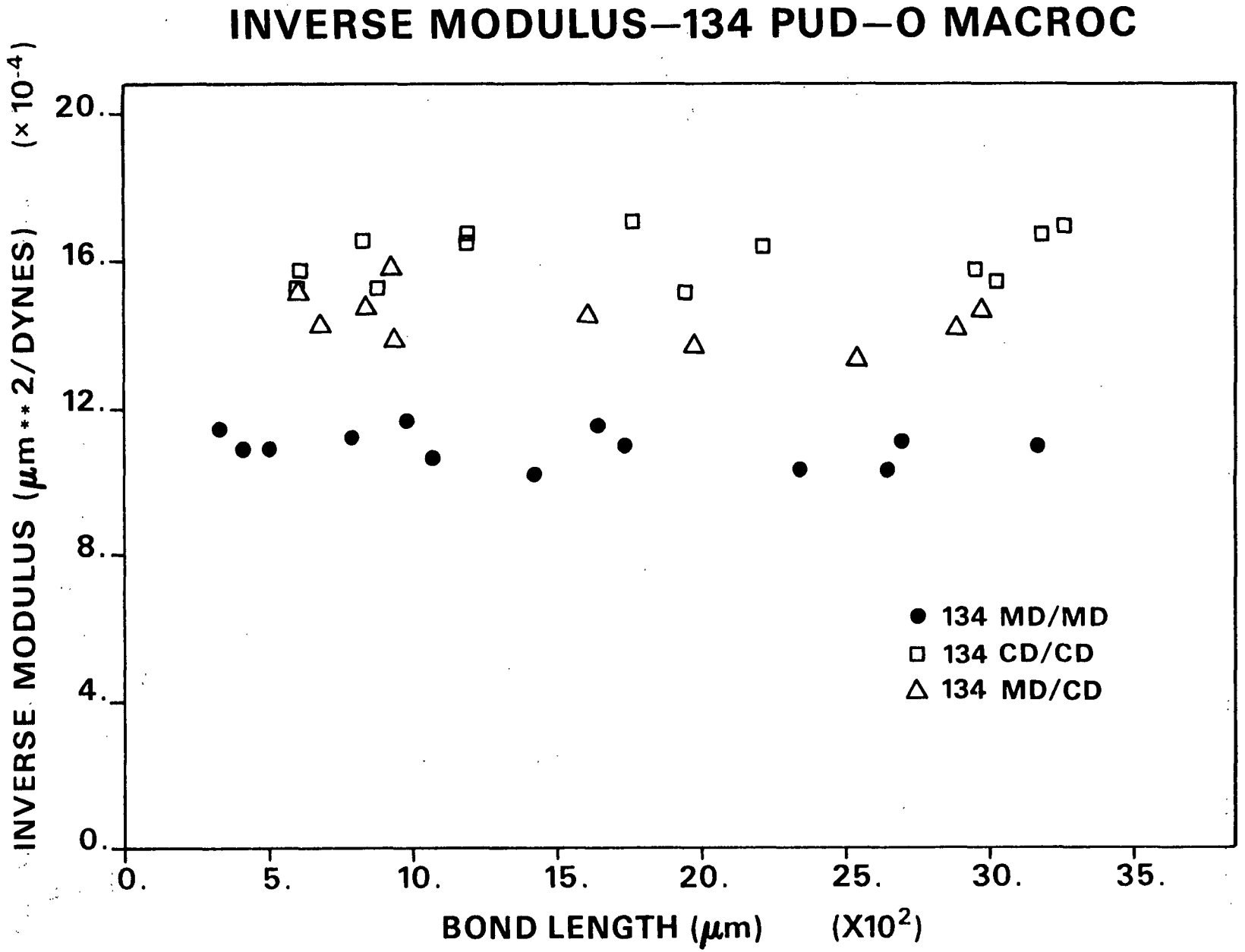

Figure 85. Effect of bond length on the inverse modulus of 134 PUD-O cellophane macrolap joints (MD/MD, CD/CD, MD/CD configurations).

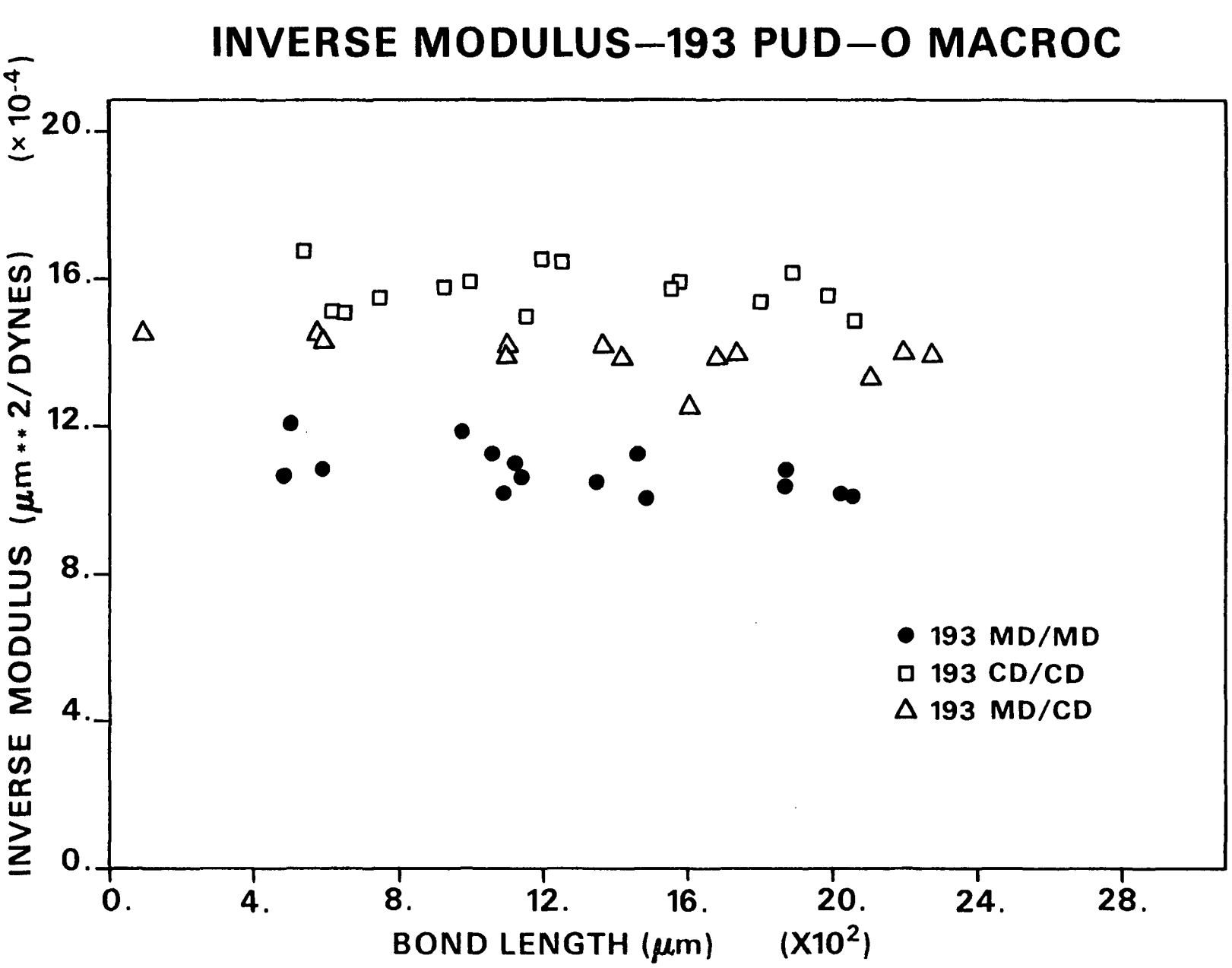

Figure 86. Effect of bond length on the inverse modulus of 193 PUD-O cellophane macrolap joints (MD/MD, CD/CD, MD/CD configurations).

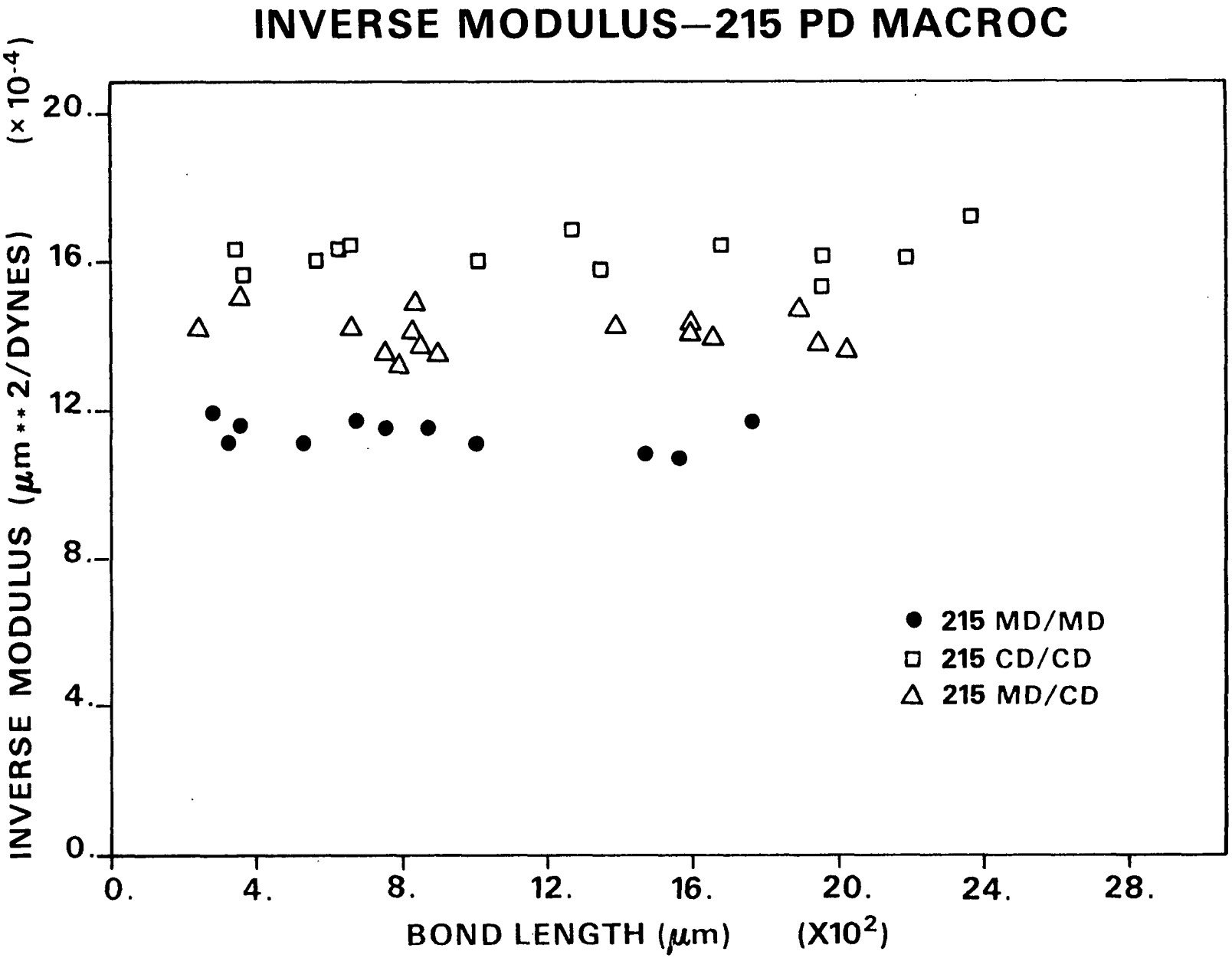

Figure 87. Effect of bond length on the inverse modulus of 215 PD cellophane macrolap joints (MD/MD, CD/CD, MD/CD configurations).

APPENDIX V

CELLOPHANE MICROLAP JOINT EXPERIMENTAL RESULTS

Table 27. Cellophane microlap joint experimental results.

FLER Curve No.	Total Span, μm	Bond Length, μm	L/T	W/T	Total Crack Length, μm	Total Strain at Failure	Critical Displacement, μm	Inverse Modulus, μm**2/dyne	Bond Shear Strength, dynes/μm**2	Nomimal Axial Stress at Failure, dynes/μm**2
					193 PUD-0 MD/MD Experiment D-1					
K-989	3511.9	256.0	9.48	11.67	109.0	0.336	11.80	0.001067	0.276	2.743
K-992	3555.1	422.9	14.96	11.33	69.0	0.368	13.08	0.000954	0.207	3.288
L-001	3598.3	218.3	7.99	10.81	21.0	0.417	15.00	0.001112	0.386	3.203
L-006	3555.1	468.1	17.79	13.02	2.0	0.667	23.70	0.001055	0.275	5.180
					193 PUD-0 MD/MD Experiment D-2					
K-998	3598.3	291.9	11.69	12.83	0.0	0.421	15.14	0.000996	0.307	3.743
K-991	3569.5	273.2	10.07	10.65	0.0	0.320	11.41	0.001006	0.292	2.987
L-003	3569.5	261.5	9.30	10.26	0.0	0.406	14.51	0.001003	0.333	3.309
L-002	3641.4	253.2	9.23	10.64	0.0	0.408	14.85	0.001015	0.342	3.607
K-997	3569.5	164.4	6.08	11.60	0.0	0.357	12.73	0.001056	0.508	3.099
K-999	3598.3	142.8	5.51	12.76	0.0	0.309	11.11	0.001002	0.462	2.721
K-994	3569.5	1040.0	37.82	11.92	0.0	2.730	97.45	0.001269	0.220	8.849
K-996	3555.1	1003.0	37.76	12.28	0.0	2.871	102.07	0.001632	0.241	9.174
L-007	3555.1	535.0	19.92	11.21	0.0	1.386	49.27	0.000973	0.350	7.973
L-011	3569.5	666.0	23.91	10.53	0.0	5.506	196.53	0.001213	0.378	10.819
L-012	3569.5	767.0	27.11	10.14	0.0	6.939	247.70	0.001137	0.357	11.829

Table 27 (Contd.). Cellophane microlap joint experimental results.

FLER Curve No.	Total Span, μm	Bond Length, μm	L/T	W/T	Total Crack Length, μm	Total Strain at Failure	Critical Displacement, μm	Inverse Modulus, μm**2/dyne	Bond Shear Strength, dynes/μm**2	Nomimal Axial Stress at Failure, dynes/μm**2
					134 PUD-0 MD/MD Experiment J-1					
L-080	3598.3	816.2	19.57	12.05	0.0	0.443	15.93	0.001085	0.185	3.871
L-081	3555.1	579.9	13.82	11.94	0.0	0.450	15.99	0.001172	0.234	3.361
L-082	3598.3	390.4	9.43	12.27	0.0	0.339	12.19	0.001185	0.270	2.730
L-115	3569.5	230.5	5.59	12.12	0.0	0.416	14.85	0.001091	0.512	3.157
L-083	3555.1	163.2	3.96	12.05	0.0	0.468	16.64	0.001237	0.716	3.102
L-116	3583.9	115.7	2.91	12.24	0.0	0.443	15.88	0.001136	1.093	3.442
					193 PUD-0 MD/MD Experiment J-2					
L-102	3583.9	249.0	8.33	3.75	0.0	0.440	15.77	0.001050	0.385	3.411
L-103	3713.4	141.0	4.77	3.90	0.0	0.464	17.23	0.001110	0.724	3.679
L-104	3555.1	196.7	6.64	3.69	0.0	0.430	15.28	0.001042	0.545	3.939
					193 PUD-0 MD/CD Experiment J-3					
L-090	4030.0	587.0	19.03	10.46	0.0	0.397	15.99	0.001495	0.133	2.577
L-091	3598.3	301.9	10.13	10.75	81.2	0.349	12.57	0.001392	0.230	2.392
L-093	3555.1	233.7	7.99	10.94	0.0	0.343	12.19	0.001176	0.303	2.530
L-094	3497.5	94.9	3.28	11.07	0.0	0.404	14.14	0.001417	0.794	2.652
L-095	3598.3	88.6	2.95	10.73	0.0	0.372	13.38	0.001511	0.786	2.365

Table 27 (Contd.). Cellophane microlap joint experimental results.

FLER Curve No.	Total Span, μm	Bond Length, μm	L/T	W/T	Total Crack Length, μm	Total Strain at Failure	Critical Displacement, μm	Inverse Modulus, μm**2/dyne	Bond Shear Strength, dynes/μm**2	Nomimal Axial Stress at Failure, dynes/μm**2
193 PUD-O/134 PUD-O MD/MD Experiment J-4										
L-084	3598.3	565.9	16.55	13.73	0.0	0.417	15.01	0.001183	0.173	3.043
L-086	3555.1	282.8	7.94	13.55	0.0	0.369	13.11	0.001180	0.362	2.933
L-087	3540.7	173.0	4.79	13.43	0.0	0.324	11.49	0.001268	0.459	2.426
L-088	3526.3	166.6	4.60	13.07	0.0	0.401	14.14	0.001292	0.574	2.899
L-089	3555.1	92.4	2.66	13.73	0.0	0.375	13.33	0.001408	0.903	2.452
193 PUD-O CD/CD Experiment J-5										
L-098	3526.3	45.6	1.53	10.41	0.0	0.470	16.58	0.001715	1.683	2.633
L-099	3540.7	78.5	2.61	10.57	0.0	0.493	17.45	0.001767	1.001	2.671
L-096	3511.9	288.6	9.52	10.25	0.0	0.964	33.87	0.001947	0.455	4.359
L-097	3483.1	92.5	3.04	10.20	0.0	0.723	25.20	0.001865	1.042	3.276

Table 27 (Contd.). Cellophane microlap joint experimental results.

FLER Curve No.	Total Span, μm	Bond Length, μm	L/T	W/T	Total Crack Length, μm	Total Strain at Failure	Critical Displacement, μm	Inverse Modulus, μm**2/dyne	Bond Shear Strength, dynes/μm**2	Nomimal Axial Stress at Failure, dynes/μm**2
					193 PUD-O Experiment K					
L-105	3713.4	461.4	15.36	9.19	0.0	0.607	22.54	0.000985	0.332	5.312
L-106	3511.9	383.8	12.42	9.59	0.0	0.475	16.69	0.001162	0.292	3.847
L-108	3555.1	275.9	8.93	9.28	0.0	0.396	14.09	0.001039	0.369	3.561
L-078	3555.1	189.8	6.46	9.19	0.0	0.369	13.11	0.001128	0.463	3.109
L-109	3511.9	187.0	6.19	9.51	0.0	0.367	12.90	0.001043	0.472	3.241
L-110	3583.9	169.8	5.63	9.91	0.0	0.396	14.20	0.001152	0.550	3.190
L-111	3569.5	169.6	5.66	9.19	0.0	0.483	17.23	0.001063	0.607	3.818
L-112	3569.5	25.8	0.86	9.14	81.7	0.328	11.70	0.001162	2.696	2.847
L-113	3569.5	106.1	3.57	8.97	0.0	0.439	15.66	0.000964	0.955	3.709
L-114	3569.5	68.2	2.31	9.04	0.0	0.437	15.61	0.001056	1.451	3.661

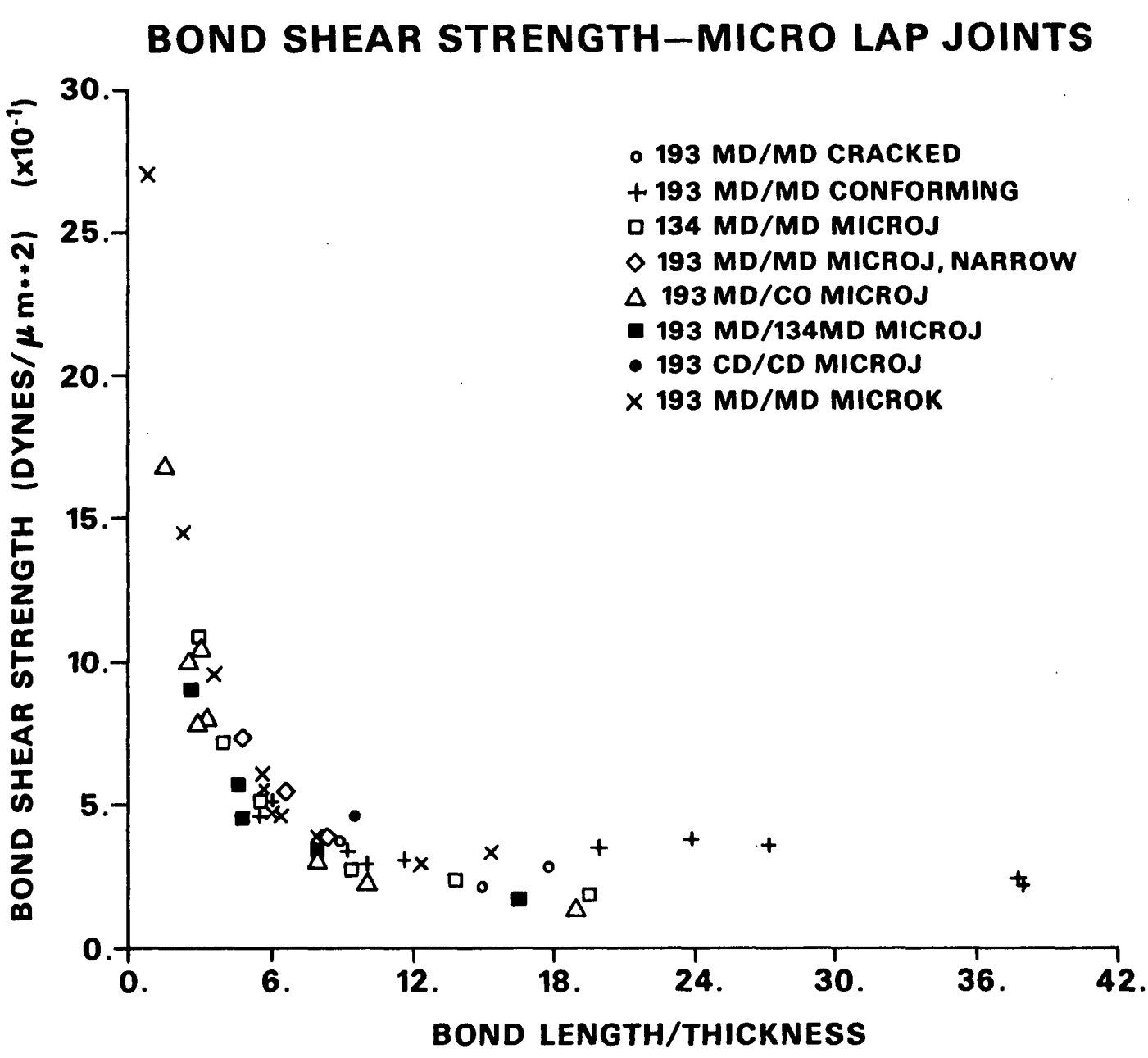

Figure 88. Effect of bond length on the bond shear strength of cellophane microlap joints.

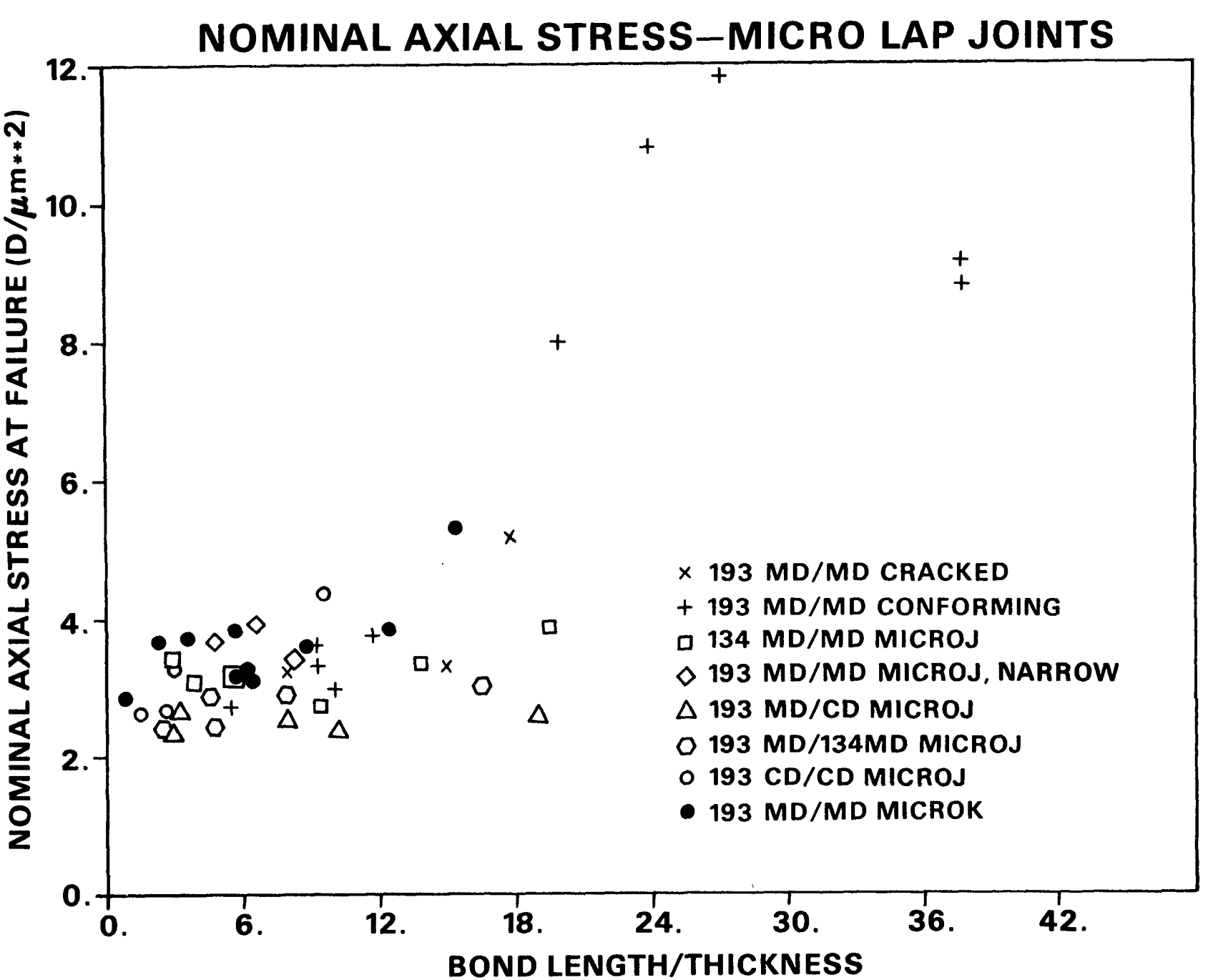

Figure 89. Effect of bond length on the nominal axial stress at failure of cellophane microlap joints.

APPENDIX VI

WOOD FIBER LAP JOINTS - PRELIMINARY RESULTS AND DISCUSSION

PROCEDURE

A crude apparatus was constructed for forming single lap joints from dried wood pulp fibers. This allowed a fiber, which had previously been attached to pins with epoxy adhesive, as shown in Fig. 43, to be cut into two parts with a razor blade. The holocellulose loblolly pine tracheids (prepared by acid chlorite method, with three caustic extractions to a 58% yield[26]) were press dried at 100 to 1000 psi before being mounted on the metal pins. The pins were then pushed closer together to give the desired amount of overlap. Following wetting with a drop of water, a glass anvil was lowered onto the overlap area. Proper alignment of the two segments was attained by manipulation with a dissecting needle. The fiber was allowed to dry for at least three hours, after which the anvil was removed. Testing was completed after a minimum of 18 hours conditioning at 50% RH and 23°C. Fiber and bond dimensions of the lap joint were measured with the Cook image-splitting eyepiece.

Tensile testing was performed with the Fiber Load/Elongation Recorder at a loading rate of 0.35 g/sec. The results of this testing are contained in Table 31.

RESULTS AND DISCUSSION

From these data it is evident that each bond had substantial strength (2.9 to 17.0 g). The bond shear strength ranged from 0.502 to 2.049 kg/mm^2. The lower value is equal to most bond shear strength results in the literature, and the other value is substantially higher. Approximately 1.3 kg/mm^2 was the highest value previously reported for holocellulose.[40] Thorpe's[40] recent data showed an average value of 0.408 kg/mm^2 for holocellulose fibers.

Table 28. Holocellulose wood fiber lap joint experimental results.

FLER Curve No.	Fiber Thickness, μm	Fiber Width, μm	Bond Length, μm	L/T	Bond Area, μm^2	Bonding Pressure, psi	Breaking Load, g	Average Bond Shear Strength, kg/mm^2	Strain at Failure, %	Apparent Modulus, kg/mm^2	Nominal Axial Stess at Failure, kg/mm^2
					Latewood						
K-952	11.4	41.4	118	10.4	4,755	431	9.44	1.985	--	--	16,440
K-950	7.5	42.1	64	≈30.0	6,380	321	6.59	1.033	1.03	1,600	16,236
K-951	13.1	34.0	321	24.5	12,776	822	14.56	1.140	1.11	2,387	27,473
K-944	11.6	56.9	65	5.65	3,710	--	2.88	0.777	0.33	3,791	4,382
K-956	9.1	39.3	72	8.0	2,851	719	5.84	2.049	0.89	1,835	14,823
					Earlywood						
K-949	6.1	55.2	219	36.1	8,507	241	6.67	0.784	2.54	680	17,425
K-943	5.5	62.4	92	16.7	5,729	--	2.88	0.502	1.16	695	8,392
K-942	3.9	82.4	65	16.6	5,348	--	6.80	1.270	1.06	1,738	21,053
K-948	9.5	63.4	57	6.1	3,967	516	3.17	0.799	2.99	144	4,845
K-947	10.0	41.6	128	12.9	7,090	289	7.95	1.122	1.54	658	13,780
					(fiber failures)						
K-946	5.5	73.2	215	39.4	15,953	128	13.92	>0.873	2.24	997	>29,779
K-945	7.6	60.9	182	23.9	11,961	--	>17.0	>1.421	>2.54	862	>33,921

The fact that these were single lap joints of previously dried fibers (whose bonding strength is thought to be substantially reduced from never-dried fibers) is intriguing. Undoubtedly the single lap joint configuration produces stress distributions which are different from the 90° crossing angle configuration. One expects layered orthotropic materials in which two adjacent layers cross at some angle greater than 0° to experience increased shear stress between the adjacent layers as compared to the parallel configuration.[128] If this analogy holds for the wood pulp fibers, bond shear strength will be dependent upon the crossing angle of the bond and the fibril angles of the cell-wall layers.

To the variability evident in the bond strength data, one attempts to attribute (from known behavior of lap joints) the variation in such variables as the ratio of lap length to fiber thickness (L/T). A multiple linear regression analysis was performed on the combined data and separately on solely earlywood and latewood data to examine these parameters. The results of this analysis, in light of the apparent variability of the experimental results, are quite surprising. As can be seen in Table 32, the correlation of σ_{nom_c} with structural parameters is very good (R^2 = 0.83 for the combined data group).

As might be expected from the particular configuration of these lap joints, the load/elongation curves are similar to those of single fibers, being essentially linear along most of the curve. In virtually every case the curves gave no indication of the impending failure. Except for one lap joint, observation with a stereomicroscope of the bond during stressing indicated that the failure proceeded in an unstable manner.

Table 29. Regression analysis results for wood fiber lap joints.

Fiber Type	Dependent Variable	Coefficient of Independent Variables T	L/T	T/W	Intercept	R^2	F	DF1/DF2
Early and latewood	σ_{nom_c}	-2.81	0.332	125.9	12.75	0.83	11.23	3/7
Latewood	σ_{nom_c}	-0.86	0.927	--	15.48	0.87	10.21	2/3
Earlywood	σ_{nom_c}	-1.18	0.363	--	13.59	0.66	0.66	2/2

Scanning electron microscopic examination of the failure regions has shown failures which appear to occur only in the interfacial region, agreeing with Thorpe's observation on holocellulose 90° crossing bonds.[40]

These results provide evidence that the strength of lap joint structures, composed of wood fibers, will be dependent on the same factors as the cellophane lap joints of this thesis. The coefficients of the structural parameter L/T are much greater than those obtained for the cellophane microlap joints. This may indicate that high hemicellulose (~ 20%) fiber-fiber bonds will have a stronger dependence on bond length as a result of viscous effects. The intercept values (12.75 to 15.42) for the regression analysis are, however, good indicators of a substantial stress intensification and a linear elastic type fracture behavior.

APPENDIX VII

FORTRAN IV LISTING: PRESAP - COMPUTER PROGRAM FOR GENERATING SAP IV INPUT

```
C*********************************************************************
C*
C*                        ******* PRESAP *******
C*
C*              A PREPROCESSOR PROGRAM FOR THE GENERATION OF SINGLE
C*             FIBER,  SINGLE LAP AND CONFORMING LAP JOINT STRUCTURES
C*             WITH  EXPERIMENTAL GLUE CONNECTIONS,2/D GLUE SIMULATIONS
C*             OR DIRECT UNIFORM, PERIMETER, OR CANTILEVER LOADS.
C*             PROBLEMS ARE GENERATED FOR SAP IV FINITE ELEMENT STRESS
C*             ANALYSIS PROGRAM.  OTHER OPTIONS ALLOW THE SAVING OF
C*             ELEMENT CENTROIDS FOR STRESS PLOTTING, CRACK TIP RADIUS
C*             VECTORS FOR FRACTURE PARAMETER CALCULATIONS,AND OUTPUT
C*             DECK FOR  STRUCTURE PLOTTING OF SELECTED PORTIONS OF THE
C*             OF THE  GENERATED STRUCTURE.  BOTH 2/D PLANE STRAIN AND
C*             STRESS  AND 3/D VARIABLE 8-21 NODE SOLID ELEMENTS MAY BE
C*             DESIGNATED.
C*                    BY  ALAN F. BUTTON , MAY 18,1978
C*
C*********************************************************************
      DOUBLE PRECISION PROB
      DIMENSION CARD(20),INODE( 5),JNODE( 5),KNODE( 5),HDRIPL(20),
     1 HDRIFR(20),HDRIST(20),PROHED(10)
      COMMON NELSX,NELSY,NELSZ,NELSL,SRD,LRD,IDEL(2),ZFACT
      COMMON MODEL,LODMOD,MATAXS,IPLOT,IFRACT,ISTRES,IPL,IFR,IST,IO
      COMMON L,T1,T2,W1,W2,S1,S2,A1,A2
      COMMON LOADPT(250)
      REAL L,L2T
      INTEGER SRD,RUNEND,ELTYPE,ELMENT,ZFACT
C
C
      IO =1
      IPL = 2
      IFR = 3
      IST = 4
      NDLS = 0
      INTRS=3
      INTT=2
      NUMELT=1
      G=980.7
      INCOMP=0
   10 READ (5,1002) PROHED,PROB
 1002 FORMAT(10A4,35X,A5)
      READ(5,1001) ELMENT,MODEL,LODMOD,L,T1,T2,W1,W2,S1,S2,A1,A2,
     1 CRITLD,NELSX,NELSY,NELSZ,NELSL,SRD,LRD,LL,MATAXS,IPLOT,IFRACT,
     2 ISTRES,ZFACT
 1001 FORMAT (2X,3I1,10F7.2,5X/12I5)
      IF(MODEL - 4) 20,15,15
   15 IPL = 1
      IO = 2
   20 MODL = (ELMENT*100) + (MODEL*10) + LODMOD
      REWIND 9
      N=0
      IDEL(1) = 0
      IDEL(2) = 0
      NPPLOT = 0
```

```
      NEPLOT = 0
      NPGLU = 0
      NEGLU = 0
      NPLAP = 0
      NELAP =0
      NPLCK = 0
      NELCK = 0
      NPRCK = 0
      NERCK = 0
      L2T = (L - A1 - A2)/((T1 + T2)/2)
      CRITLD=CRITLD*G
      SIGMA=CRITLD/(T2*W2)
      IF(SIGMA - 0.0001) 96,98,98
   96 SIGMA = 10.0
   98 CONTINUE
      IF(ELMENT-2) 100,105,110
  100 CONTINUE
      CRITLD=(CRITLD*2)/(W1+W2)
C
C-----PLANE STRAIN-------------------------------------------------
C
      ELTYPE=4
      NEX=1
      GO TO 200
  105 CONTINUE
C
C-----PLANE STRESS-------------------------------------------------
C
      ELTYPE=4
      NEX=1
      GO TO 200
  110 CONTINUE
C
C---3/D 21-NODE SUB/ISOPARAMETRIC ELEMENTS, 1/2 OF FULLWIDTH-----------
C
      CRITLD=CRITLD/2
      ELTYPE=8
      MAXNOD=21
      NOPSET=1
      NEX = NELSX
  200 CONTINUE
C
C-----CHECKS FOR CRACKED LAP JOINTS AND ASSIGNS DEGREE OF REFINEMENT---
C
      IF(MODEL - 2) 300,202,202
  202 A = A1
      T = T1
      IJ = 0
      RESLL = L - (A1 + A2)
  204 IJ = IJ + 1
      GRID = T/LRD
      IDEL(IJ) = 0
      IF(RESLL - (T1 + T2)) 206,206,208
  206 GRID = RESLL/(2 * LRD)
  208 IF(A) 230,230,212
  212 IF(A - GRID) 214,214,216
```

```
  214 IDEL(IJ) = 1
      GO TO 230
  216 IF(A - (2 *GRID)) 218,218,220
  218 IDEL(IJ) = 2
      GO TO 230
  220 IF(A - (GRID * 3)) 222,222,224
  222 IDEL(IJ) = 3
      GO TO 230
  224 IF(A - (GRID * 4)) 226,226,228
  226 IDEL(IJ) = 4
      GO TO 230
  228 IDEL(IJ) = 5
  230 A = A2
      T = T2
      IF(IJ - 2) 204,300,300
  300 IF(NELSX) 301,301,316
C
C-----CALCULATION OF NODAL POINTS AND ELEMENTS OF EACH 2/D STRUCTURAL
C
  301 IF(MODEL - 2) 302,302,309
  302 NEADJ1= NELSZ
      NEADJ = NELSZ
      GO TO 311
  309 NEADJ = NELSZ + 1
      NEADJ1 = NELSZ
  311 IF(LODMOD - 4) 305,303,303
  303 NPGLU = 6 * (NELSZ + 3)
      NEGLU = 5 * (NELSZ + 2)
      NGLUAJ = NELSZ + 1
  305 IF(MODEL - 2) 314,307,307
  307 NPLAP = (((2 * NELSZ) + 1) * (1 + NELSL + (2 * LRD))) +
     1 ((2 * (NELSZ + 1)) * (IDEL(1) + IDEL(2) + SRD - 1))
      NELAP = (2 * (SRD + IDEL(1) + IDEL(2) + (2 * LRD) + NELSL)) *
     1 NELSZ
      IF(MODEL - 3) 306,304,304
  304 NELAP = NELAP + (2 * SRD)
  306 NPLCK = ((NELSZ + 1) * ((IDEL(1) * 2) + SRD - 1)) +
     1 (((2 * NELSZ) + 1) * (LRD + 1))
      NELCK = NELSZ * (SRD + (2 * (IDEL(1) + LRD)))
      IF(MODEL -3) 310,308,308
  308 NELCK = NELCK + SRD
  310 NPRCK = ((NELSZ + 1) * ((IDEL(2) * 2) + SRD - 1)) +
     1 (((2 * NELSZ) + 1) * (LRD + 1))
      NERCK = NELSZ * (SRD + (2 * (IDEL(2) + LRD)))
      IF(MODEL - 3) 314,312,312
  312 NERCK = NERCK + SRD
  314 NPSPN = (NELSY + 1) * (NELSZ + 1)
      NESPN = NELSY * NELSZ
      GO TO 318
C
C-----CALCULATION OF NODAL POINTS AND ELEMENTS OF 3/D STRUCTURAL PARTS-
C
  316 SECTN1 = (3 * NELSX * NELSZ) + (2 * (NELSX + NELSZ)) + 1
      SECTN2 = (2 * NELSX * NELSZ) + NELSZ + NELSX + 1
      SECTN3 = (6 * NELSX * NELSZ) + (2 * NELSX) + (4 * NELSZ) + 1
      SECTN4 = (4 * NELSX * NELSZ) + (2 * NELSZ) + NELSX + 1
```

```
      NEADJ1 = NELSX * NELSZ
      NEADJ = NELSX * NELSZ
      IF(LODMOD-4) 317,315,315
  315 NPGLU = (9 * (NELSX + 2)) + ((NELSX + 2) * 3 * (NELSZ + 3))
      NEGLU = (5 * (1 + NELSX)) + (2 * ((NELSZ + 2) * (NELSX + 1)))
      NGLUAJ = SECTN1
  317 IF(MODEL - 2) 321,319,319
  319 NPLAP = (2 * ((SRD - 1) + IDEL(1) + IDEL(2))*(SECTN1+SECTN2))+
     1 (2 * SECTN2) +(((2 * LRD) + NELSL) * (SECTN3 + SECTN4))+SECTN3
      NELAP = 2*(SRD+IDEL(1)+IDEL(2)+(2*LRD)+NELSL)* NELSZ*NELSX
      NPLCK = SECTN2+SECTN3+((SRD-1+(2*IDEL(1))) * (SECTN1+SECTN2))
     1 + (LRD * (SECTN3 + SECTN4))
      NELCK = (SRD + (2 * (IDEL(1) + LRD))) * NELSZ * NELSX
      NPRCK = SECTN2+SECTN3+((SRD-1+(2*IDEL(2))) * (SECTN1+SECTN2))
     1 + (LRD * (SECTN3 + SECTN4))
      NERCK = (SRD + (2 * (IDEL(2) + LRD))) * NELSZ * NELSX
  321 NPSPN = (NELSY * (SECTN1 + SECTN2)) + SECTN1
      NESPN = NELSY * NELSZ * NEX
C
C-----CALCULATION OF THE TOTAL NODAL POINTS, ELEMENTS, MATERIALS, AND--
C-----Z-DIRECTION POSITION OF NSPAN=1 FOR ALL STRUCTURES--------------
C
  318 IF(LODMOD - 6) 322,320,350
  320 NUMNP = NPGLU + NPSPN - NGLUAJ
      NUMEL = NEGLU + NESPN
      NMAT = 3
      CRITLD = -CRITLD
      GO TO 337
  322 IF(LODMOD - 3) 332,332,324
  324 NUMNP = NPSPN + NPGLU - NGLUAJ
      NUMEL =  NESPN + NEGLU
      IF(MODEL - 2) 326,328,328
  326 NMAT = 3
      GO TO 337
  328 NUMNP = NUMNP + NPLAP + NPSPN
      NUMEL = NUMEL + NELAP + NESPN
      NMAT = 4
      IF(NELSX) 329,329,331
  329 IF(MODEL - 3) 331,330,330
  330 NMAT = 6
  331 IF(MODEL - 2) 337,337,362
  332 IF(MODEL - 2) 334,338,340
  334 NUMNP = NPSPN
      NUMEL = NESPN
      NMAT = 1
      IF(LODMOD - 1) 336,337,335
  335 IF(LODMOD - 2) 337,336,337
  336 CRITLD = -CRITLD
  337 ZPOS = 0.0
      GO TO 370
  338 ZPOS = 0.0
      NMAT = 2
      GO TO 348
  340 IF(NELSX) 342,342,344
  342 NMAT = 4
      GO TO 346
```

```
  344 NMAT = 2
  346 ZPOS = -T1/2
  348 NUMNP = (2 * NPSPN) + NPLAP
      NUMEL = (2 * NESPN) + NELAP
      GO TO 370
  350 IF(MODEL - 2) 352,354,356
  352 NUMNP = (2 * (NPGLU - NGLUAJ)) + NPSPN
      NUMEL = (2 * NEGLU) + NESPN
      NMAT = 3
      ZPOS = 0.0
      GO TO 370
  354 NMAT = 4
      ZPOS = 0.0
      GO TO 360
  356 NMAT = 6
      ZPOS = -T1/2
      IF(NELSX) 360,360,358
  358 NMAT = 4
  360 NUMNP = (2 * (NPGLU + NPSPN - NGLUAJ))+ NPLAP
      NUMEL = (2 * (NEGLU + NESPN)) + NELAP
      GO TO 370
  362 ZPOS = -T1/2
C
C-----WRITES PROBLEM AND PARAMETERS(DIMENSIONS,LOAD,AND MODEL GENERATION
C-----SPECIFICATIONS),SAVES GENERATED SAPIV PROBLEMS ON FILE = IO, AND
C-----PUNCHES HEADER CARDS TO BE USED IN POSTPROCESSOR PROGRAMS---------
C
  370 WRITE (6,1010) PROB,PROHED,MODL,SIGMA,NUMNP,NUMEL,L,T1,T2,W1,W2,
     1 S1,S2,A1,A2,CRITLD,NELSX,NELSY,NELSZ,NELSL,SRD,LRD,LL,MATAXS,
     2 IPLOT,IFRACT,ISTRES,ZFACT
      WRITE (IO,1012) PROHED,MODL,SIGMA,PROB,NUMNP,NUMELT,LL
 1010 FORMAT ('1PROBLEM NO.  ',A5///' ',10A4,'  MODEL=',I3,' SIGMA=',
     1 F5.2,'D/UM2'///' NUMNP=',I5/' NUMEL=',I5//' L=',F7.1/' T1=',F6.2/
     2 ' T2=',F6.2/' W1=',F7.1/' W2=',F7.1/' S1=',F7.1/' S2=',F7.1/
     3 ' A1=',F6.2/' A2=',F6.2/' CRITLD=',F8.2//' NX=',I3/' NY=',I3/
     4 ' NZ=',I3/' NL=',I3/' SRD=',I3/' LRD=',I3/' LL=',I3/' MATAXS=',
     5 I3//' IPLOT=',I3/' IFRACT=',I3/' ISTRES=',I3/' ZFACTOR=',I3)
 1011 FORMAT (10A4,'  MODEL=',I3,' SIGMA=',F5.2,'D/UM2',7X,A5)
 1012 FORMAT (10A4,'  MODEL=',I3,' SIGMA=',F5.2,'D/UM2',7X,A5/3I5,F7.1)
C
C-----CALCULATION OF TOTAL POINTS AND ELEMENTS OF  STRUCTURES FOR
C
      IF(IPLOT - 1) 401,372,374
  372 NPPLOT = NUMNP
      NEPLOT = NUMEL
      GO TO 400
  374 IF(IPLOT - 3) 376,384,386
  376 IF(LODMOD - 4) 372,380,378
  378 IF(LODMOD - 6) 380,380,382
  380 NPPLOT = NUMNP - NPGLU
      NEPLOT = NUMEL - NEGLU - NEADJ1
      GO TO 400
  382 NPPLOT = NUMNP - (2 * NPGLU)
      NEPLOT = NUMEL - (2 * (NEGLU + NEADJ1))
      GO TO 400
  384 NPPLOT = NPSPN + NPLCK
```

```
      NEPLOT = NESPN + NELCK
      IF(LODMOD - 6) 400,387,387
  386 IF(IPLOT - 5) 385,388,390
  385 NPPLOT = NPSPN + NPRCK
      NEPLOT = NESPN + NERCK
      IF(LODMOD - 3) 400,387,387
  387 NPPLOT = NPPLOT - NGLUAJ
      NEPLOT = NEPLOT - NEADJ1
      GO TO 400
  388 NPPLOT = NPGLU
      NEPLOT= NEGLU
      GO TO 400
  390 IF(IPLOT- 7) 388,392,394
  392 NPPLOT = NPLAP
      NEPLOT = NELAP - (NEADJ * 2)
      GO TO 400
  394 IF(IPLOT - 9) 396,398,400
  396 NPPLOT = NPLCK
      NEPLOT = NELCK - NEADJ
      GO TO 400
  398 NPPLOT = NPRCK
      NEPLOT = NERCK - NEADJ
C-----READS AND WRITES (UNIT=IPL) SAPLOT TITLE CARD-------------------
  400 READ(5,1040) HDRIPL
      WRITE (IPL,1012) PROHED,MODL,SIGMA,PROB,NPPLOT,NUMELT,LL
      WRITE(6,9011) HDRIPL,NPPLOT,NEPLOT
C-----READS AND WRITES(UNIT=IFR) FRACTURE PARAMETERS TITLE-------------
  401 IF(IFRACT) 404,404,402
  402 READ(5,1040) HDRIFR
      WRITE (IFR,1012) PROHED,MODL,SIGMA,PROB,NELSX,NMAT,MATAXS,W2
      WRITE(6,9011) HDRIFR
C-----READS AND WRITES(UNIT=IST) STRESS PLOT TITLE CARD----------------
  404 IF(ISTRES) 407,407,406
  406 READ(5,1040) HDRIST
      WRITE (IST,9010) PROHED,MODL,SIGMA,PROB,NELSX,NELSZ,NELSL,SRD,LRD,
     1 IDEL(1),IDEL(2),L,T1,T2
      WRITE(6,9011) HDRIST,NELSX,NELSZ,NELSL,SRD,LRD,IDEL(1),
     1 IDEL(2),L,T1,T2
 9010 FORMAT(10A4,'  MODEL=',I3,' SIGMA=',F5.2,'D/UM2',7X,A5/7I5,3F10.3)
 9011 FORMAT('0',20A4,/,(7I5,3F10.3))
 1040 FORMAT(20A4)
  407 CONTINUE
C
C---GENERATES NODAL POINTS, BOUNDARY CONDITIONS, AND MATERIAL AXES-----
C
      CALL SPAN (N,ZPOS,LOADPT,INODE,JNODE,KNODE)
      IF(MODEL - 2) 408,408,414
  408 IF(MATAXS-1) 410,412,412
  410 NORTHO=0
      GO TO 420
  412 NORTHO=1
      GO TO 420
  414 IF(MATAXS - 1) 412,416,418
  416 NORTHO = 2
      GO TO 420
  418 NORTHO = 3
```

```
  420 CONTINUE
C
C---WRITES ELEMENT CONTROL CARD-----------------------------------------
C
      IF(ELMENT-3) 500,505,505
  500 WRITE(IO,1020) ELTYPE,NUMEL,NMAT,ELMENT,INCOMP
      IF(IPLOT - 1) 502,501,501
  501 WRITE(IPL,1020) ELTYPE,NEPLOT,NMAT,ELMENT,INCOMP
  502 CONTINUE
 1020 FORMAT(3I5,5X,2I5)
      LIMIT=(3*NMAT)+4
      GO TO 510
  505 WRITE(IO,1021) ELTYPE,NUMEL,NMAT,NORTHO,NDLS,MAXNOD,NOPSET,
     1 INTRS,INTT
      IF(IPLOT - 1) 507,506,506
  506 WRITE(IPL,1021) ELTYPE,NEPLOT,NMAT,NORTHO,NDLS,MAXNOD,NOPSET,
     1 INTRS,INTT
  507 CONTINUE
 1021 FORMAT(3I5,5X,6I5)
      LIMIT=(3*NMAT)+NOPSET+5 +(2 * NDLS)
  510 CONTINUE
C
C  READS MODEL/MATERIAL SPECIFIC PROPERTY,ORIENTATION AXES, AND STRESS
C---LOCATIONS FROM LIBRARY----------------------------------------------
C
      DO 525 M=1,LIMIT
      CALL GET(CARD,80,8)
      CALL PUT(CARD,80,IO)
      IF(IFRACT) 514,514,512
  512 IF(M -(3 * NMAT)) 513,513,514
  513 CALL PUT(CARD,80,IFR)
  514 IF(IPLOT) 518,518,517
  517 CALL PUT(CARD,80,IPL)
  518 IF(NELSX) 525,525,515
  515 CONTINUE
      IF(M-(3*NMAT)) 525,516,525
  516 WRITE(IO,1022) (II,INODE(II),JNODE(II),KNODE(II),II=1,NORTHO)
      IF(IPLOT ) 525,525,520
  520 WRITE (IPL,1022) (II,INODE(II),JNODE(II),KNODE(II),II = 1,NORTHO)
 1022 FORMAT(4I5)
  525 CONTINUE
C
C---GENERATES ELEMENT CARDS---------------------------------------------
C
      CALL ELGENR (NODE1)
C
C---GENERATES LOAD SPECIFICATIONS---------------------------------------
C
      CALL LOAD (LOADPT,LL,CRITLD)
C
      READ(5,1030) RUNEND
 1030 FORMAT (I5)
      IF(RUNEND) 900,910,900
  900 WRITE(6,1032)
 1031 FORMAT(80X/80X)
 1032 FORMAT(' ',80X/80X)
```

```
      GO TO 10
  910 WRITE (IO,1031)
      END FILE IO
      END FILE IPL
      END FILE IFR
      END FILE IST
      STOP
      END
      SUBROUTINE SPAN (N,ZPOS,LOADPT,INODE,JNODE,KNODE)
C
C*********************************************************************
C*
C*    THIS SUBROUTINE GENERATES THE NODAL POINTS FOR ALL FREE SPANS,AND
C*    CALLS SUBROUTINES GLUED AND OVRLAP, WHICH GENERATE THE GLUE
C*    CONNECTIONS AND OVERLAP STRUCTURES OF MODELS 2 AND 3.
C*
C*********************************************************************
C
C
      DIMENSION NPN(25),NXT(25),NYT(25),NZT(25),NXR(25),NYR(25),NZR(25)
     1X(25),Y(200),Z(50),TEMP(25),LOADPT(1),INODE( 5),JNODE( 5),
     2KNODE( 5)
      COMMON NELSX,NELSY,NELSZ,NELSL,SRD,LRD,IDEL(2),ZFACT
      COMMON MODEL,LODMOD,MATAXS,IPLOT,IFRACT,ISTRES,IPL,IFR,IST,IO
      COMMON L,T1,T2,W1,W2,S1,S2,A1,A2
      REAL L
      INTEGER SRD
C
C
      RESLL = L - (A1 + A2)
      ST = S1 + S2 + L
      SLOPE = (T1 + T2)/(2 * ST)
      ALPHA = ATAN(SLOPE)
      YORIG = S1 + A1 + (RESLL/2)
      ROTAPT = (ST *T1) / (T1 + T2)
      RPOINT = ROTAPT - YORIG
      IF(NELSX) 1,1,2
    1 NNX=1
      NNZ=NELSZ+1
      NNY=NELSY+1
      GO TO 3
    2 NNX=(NELSX*2)+1
      NNZ=(NELSZ*2)+1
      NNY=(NELSY*2)+1
    3 CONTINUE
      LOADPT(2)=0
      N=0
      S=S1
      T=T1
      W=W1
      NSPAN=1
      GO TO 6
    5 CONTINUE
      S=S2
      NSPAN=2
      T=T2
```

```
      W=W2
    6 CONTINUE
C*********************************************************************
      DO 400 I=1,NNY
C*********************************************************************
      IF(NSPAN-2) 20,40,40
C
C--CHECKS FOR RIGHT AND LEFT GLUE CONNECTIONS-------------------------
C
   20 YPOS = - (S + A1 + (RESLL/2))
      IF(I - 1) 22,22,24
   22 IF(LODMOD - 6) 100,90,90
   24 IF(MODEL - 2) 26,100,100
   26 IF(I - NNY) 100,28,28
   28 IF(LODMOD - 4) 100,90,30
   30 IF(LODMOD - 6) 90,100,90
   40 YPOS = ((RESLL + T)/2) + A2
      IF(MODEL - 3) 42,44,44
   42 ZPOS = -T
      GO TO 26
   44 ZPOS = -T/2
      GO TO 26
   90 CONTINUE
C
      CALL GLUED (N,S,T,W,LOADPT,NSPAN)
C
      IF(I-NNY)   98,400,400
   98 CONTINUE
      IF(I-1) 305,305,100
  100 CONTINUE
C
C---CALCULATES Y-COORD. FOR SPAN=1, OR SPAN=2, AND FOR 2/D, OR 3/D IN--
C---REGULAR RECTANGLES WITH VERTICAL COLUMNS (SECTIONS) FOR XZ PLANE---
C
      Y(I)= YPOS+(((S-(T/2))/(NNY-1))*(I-1))
      IF(MODEL-2) 104,105,105
  104 CONTINUE
      Y(I)= YPOS+((S/(NNY-1))*(I-1))+(L/2)
  105 M=0
C*********************************************************************
      DO 300 J=1,NNZ
C*********************************************************************
      IF(NELSX) 115,115,106
C-----SETS NNX LIMITS FOR 3/D ELEMENTS-------------------------------
  106 CONTINUE
      IF(I-1) 102,102,110
  102 CONTINUE
      IF(J-1) 115,115,110
  110 CONTINUE
      IF(NNX-(NELSX+1)) 113,111,113
  111 CONTINUE
      KI=I/2
      KK=KI*2
      IF(KK-I) 112,114,112
  112 CONTINUE
      NNX=(NELSX*2)+1
```

```
      GO TO 115
  113 CONTINUE
      NNX=NELSX+1
      GO TO 115
  114 CONTINUE
      NNX=NELSX
  115 CONTINUE
      Z(J)= T-((T/(NNZ-1))*(J-1))+ZPOS
C*********************************************************************
      DO 200 K=1,NNX
C*********************************************************************
      N=N+1
      NPN(K)=N
      NXT(K)=0
      NYT(K)=0
      NZT(K)=0
      NXR(K)=1
      NYR(K)=1
      NZR(K)=1
      TEMP(K)=0.0
      IF(NELSX) 120,120,121
C
C   CALCULATION OF X-COORDS. FOR 2/D
C
  120 CONTINUE
      X(K)=0.0
      NXT(K)=1
      GO TO 125
  121 CONTINUE
C
C---CALCULATION OF X-COORDS. FOR 3/D-----------------------------------
C
      IF(NSPAN - 2) 107,118,118
  107 IF(I - 2) 109,108,118
  108 IF(LODMOD-5) 118,118,109
  109 IF(J - 1) 118,116,118
  116 INCRE1=2+(3*(NELSX+NELSZ)+(5*NELSX*NELSZ))
      IF(MATAXS-1) 118,117,117
  117 INODE(1) =NPN(1)
      JNODE(1) =NPN(1) +  INCRE1
      KNODE(1) = NPN(1) + 1
  118 CONTINUE
      KI=I/2
      KK=KI*2
      IF(KK-I) 122,123,122
  122 CONTINUE
      X(K)=(W/2)-((W/((NNX-1)*2))*(K-1))
      IF(K-NNX) 125,119,119
  119 NXT(K)=1
      GO TO 125
  123 CONTINUE
      KJ=J/2
      JK=KJ*2
      IF(JK-J) 122,124,122
  124 CONTINUE
      X(K)=(W/2)-(W/(2*NNX))*(K-1)-(W/(4*NELSX))
```

```
      GO TO 200
C
C---BEGIN CHECKING FOR SPECIAL END CONDITIONS-------------------------
C
  125 CONTINUE
      IF(NSPAN-2) 126,136,136
  126 CONTINUE
      IF(I-1) 127,127,134
  127 CONTINUE
      IF(LODMOD-2) 130,128,128
  128 CONTINUE
      IF(LODMOD-5) 129,130,200
C
C---SETS SPECIFIC RESTRAINT CONDITION DF'S (PERIMETER,TOTAL)-----------
C
  129 CONTINUE
      IF(J-1) 130,130,131
  130 CONTINUE
      NXT(K)=1
      NYT(K)=1
      NZT(K)=1
      GO TO 200
  131 CONTINUE
      IF(J-NNZ) 132,130,130
  132 CONTINUE
      IF(NELSX) 200,200,133
  133 CONTINUE
      IF(K-1) 130,130,200
C
C
  134 CONTINUE
C---CHECK FOR NSPAN=1-------------------------------------------------
      IF(I-NNY) 200,135,135
  135 CONTINUE
      IF(MODEL-2) 137,200,200
  136 CONTINUE
C---CHECK FOR NSPAN=2-------------------------------------------------
      IF(I-NNY) 200,137,137
  137 CONTINUE
      IF(LODMOD-1) 139,147,138
  138 CONTINUE
      IF(LODMOD-3) 139,142,139
C
C---CANTILEVER LOADING------------------------------------------------
C
  139 CONTINUE
      IF(K-NNX) 200,140,140
  140 CONTINUE
      IF(J-1) 141,141,200
  141 CONTINUE
      M=M+1
      LOADPT(M)=N
      GO TO 200
C
C---PERIMETER LOADING-------------------------------------------------
C
```

```
  142 CONTINUE
      IF(J-1) 147,147,144
  144 CONTINUE
      IF(K-1) 145,145,146
  145 CONTINUE
      IF(NELSX) 146,146,147
  146 CONTINUE
      IF(J-NNZ) 200,147,147
C
C---TOTAL RESTRAINT, EXCEPT Y-FREE-----------------------------------
C
  147 CONTINUE
      NXT(K)=1
      NZT(K)=1
      NYT(K)=0
      M=M+1
      LOADPT(M)=N
  200 CONTINUE
C*********************************************************************
C-----ADJUSTMENT OF THE INCLINATION OF CONFORMING LAP JOINTS THROUGH AN
C-----ANGLE,ALPHA, ABOUT THE CENTERLINE POINT,RPOINT.-----------------
C
      IF(MODEL - 2) 206,206,205
  205 RADIUS = Y(I) - RPOINT
      YTEMP = (RADIUS * COS(ALPHA)) + (Z(J) * SIN(ALPHA)) + RPOINT
      ZTEMP = -((RADIUS * SIN(ALPHA)) - (Z(J) * COS(ALPHA)))
      GO TO 210
  206 YTEMP = Y(I)
      ZTEMP = Z(J)
  210 CONTINUE
C
C-----SAVES NODAL POINT DATA FOR SAPLOT, FILE = IPL-------------------
C
      IF(IPLOT - 1) 222,220,212
  212 IF(NSPAN - 2) 214,216,222
  214 IF(IPLOT - 3) 220,220,222
  216 IF(IPLOT - 3) 220,222,218
  218 IF(IPLOT - 4) 222,220,222
  220 WRITE(IPL,1001)(NPN(K),NXT(K),NYT(K),NZT(K),NXR(K),NYR(K),
     1 NZR(K),X(K),YTEMP,ZTEMP,TEMP(K),K = 1,NNX)
  222 IF(NPN(1) - 1) 201,201,202
  201 WRITE (IO,1000) NPN(1),NXT(1),NYT(1),NZT(1),NXR(1),NYR(1),
     1NZR(1),X(1),YTEMP,ZTEMP,TEMP(1)
 1000 FORMAT (I5,'A',I4,5I5,3F10.3,5X,F10.5)
      INDENT=2
      IF(NELSX) 300,300,203
  202 INDENT=1
  203 WRITE(IO,1001)(NPN(K),NXT(K),NYT(K),NZT(K),NXR(K),NYR(K),NZR(K),
     1X(K),YTEMP,ZTEMP,TEMP(K),K = INDENT,NNX)
 1001 FORMAT (7I5,3F10.3,5X,F10.5)
  300 CONTINUE
C*********************************************************************
  305 CONTINUE
  400 CONTINUE
      IF(NSPAN - 2) 402,500,500
  402 IF(MODEL - 2) 500,404,404
```

```
  404 CONTINUE
C
      CALL OVRLAP (N,ALPHA,RPOINT,INODE,JNODE,KNODE)
C
      GO TO 5
  500 CONTINUE
      RETURN
      END
C
C
      SUBROUTINE GLUED (N,S,T,W,LOADPT,NSPAN)
C
C
C  THIS SUBROUNTINE GENERATES THE NODAL POINTS FOR THE 3/D GLUE
C  AND THE 2/D GLUE SIMULATION.
C
C
      DIMENSION NPN(25),NXT(25),NYT(25),NZT(25),NXR(25),NYR(25),NZR(25)
     1X(25),Y(25),Z(25),TEMP(25),LOADPT(1)
      COMMON NELSX,NELSY,NELSZ,NELSL,SRD,LRD,IDEL(2),ZFACT
      COMMON MODEL,LODMOD,MATAXS,IPLOT,IFRACT,ISTRES,IPL,IFR,IST,IO
      COMMON L,T1,T2,W1,W2,S1,S2,A1,A2
      REAL L
C
C
      M=0
      INPN=N
      A=400.0
      RESLL = L - (A1 + A2)
      IF(NELSX) 15,15,10
C
C  GLUE CONNECTION=> 3/D
C
   10 CONTINUE
      NNY=8
      NNX=NELSX+2
      LOADPT(2)=0
      GO TO 19
C
C  GLUE CONNECTION=> 2/D
C
   15 NNY=6
      LOADPT(2)=0
      NNZ=NELSZ+3
      NNX=1
   19 CONTINUE
C*********************************************************************
      DO 600 I=1,NNY
C*********************************************************************
      IF(NELSX) 60,60,18
   18 CONTINUE
      IF(INPN) 20,20,35
   20 II=NNY-(I-1)
      IF(II-4) 28,22,24
   22 II=5
      GO TO 28
```

```
   24 CONTINUE
      IF(II-6) 26,28,28
   26 II=4
   28 MIRROR=-1
      YPOS = S + A1 + (RESLL/2)
   30 INVERT=1
      GO TO 50
   35 CONTINUE
      II=I
      IF(MODEL - 2) 36,41,41
   36 IF(II - 2) 37,39,41
   37 II=2
      GO TO 41
   39 II=1
   41 CONTINUE
      IF(MODEL - 2) 43,45,45
   43 MIRROR=1
      YPOS=0.0
      GO TO 30
   45 MIRROR=1
      YPOS = S + A2 + (RESLL/2)
      INVERT=-1
      IF(II - 4) 124,47,48
   47 II = 5
      GO TO 124
   48 IF(II - 6) 49,124,124
   49 II = 4
   50 CONTINUE
      GO TO 124
C
C  2/D PARAMETERS
C
   60 CONTINUE
      IF(INPN) 62,62,65
   62 II=NNY-(I-1)
      MIRROR=-1
      YPOS = S + A1 + (RESLL/2)
   64 INVERT=1
      GO TO 80
   65 II=I
      IF(MODEL - 2) 67,69,69
   67 MIRROR=1
      YPOS=0.0
      GO TO 64
   69 MIRROR=1
      YPOS = S + A2 + (RESLL/2)
      INVERT=-1
   80 CONTINUE
      IF(II-4) 82,90,92
   82 CONTINUE
      IF(II-2) 84,86,88
   84 Y(I)=YPOS*MIRROR
      GO TO 150
   86 Y(I)=(YPOS+600)*MIRROR
      GO TO 150
   88 Y(I)=(YPOS+1200)*MIRROR
```

```
      GO TO 150
   90 Y(I)=(YPOS+1535)*MIRROR
      GO TO 150
   92 CONTINUE
      IF(II-5) 90,94,96
   94 Y(I)=(YPOS+4200)*MIRROR
      GO TO 150
   96 Y(I)=10750*MIRROR
      GO TO 150
C
C  3/D PARAMETERS
C
  124 CONTINUE
      IF(II-2) 126,128,130
  126 NNZ=NELSZ+2
      ELIPSE=1.0
      Y(I)=(YPOS*MIRROR)
      GO TO 150
  128 NNZ=1
      ELIPSE=0.4145
      Y(I)=(YPOS+100)*MIRROR
      GO TO 150
  130 CONTINUE
      IF(II-4) 132,144,134
  132 NNZ=NELSZ+3
      Y(I)=(YPOS+600)*MIRROR
      GO TO 150
  134 CONTINUE
      IF(II-6) 146,136,138
  136 NNZ=3
      ELIPSE=1.0
      Y(I)=(YPOS+1535)*MIRROR
      GO TO 150
  138 CONTINUE
      IF(II-8) 140,142,142
  140 NNZ=3
      ELIPSE=1.0
      Y(I)=(YPOS+4200)*MIRROR
      GO TO 150
  142 NNZ=3
      ELIPSE=1.0
      Y(I)=10750*MIRROR
      GO TO 150
  144 NNZ=1
      ELIPSE=0.4145
      Y(I)=(YPOS+1100)*MIRROR
      GO TO 150
  146 NNZ=NELSZ+2
      ELIPSE=1.0
      Y(I)=(YPOS+1200)*MIRROR
  150 CONTINUE
C
C  2/D PARAMETERS
C
C*****************************************************************************
      DO 550 J=1,NNZ
```

```
C
      DO 500 K=1,NNX
C*********************************************************************
      Y(K)=Y(I)
      N=N+1
      NPN(K)=N
      TEMP(K)=0.0
      NXT(K)=0
      NYT(K)=0
      NZT(K)=0
      NXR(K)=1
      NYR(K)=1
      NZR(K)=1
      IF(K-NNX) 154,152,152
  152 NXT(K)=1
      IF(NELSX) 300,300,154
C
C  GLUE CONNECTOR=> 3/D
C
  154 CONTINUE
      IF(II-5) 190,196,156
  156 CONTINUE
      IF(J-2) 158,164,170
  158 CONTINUE
      IF(K-2) 160,162,162
  160 X(K)=SQRT(A*A/2)
      GO TO 172
  162 X(K)=(W/2)-(W/(2*NELSX))*(K-2)
      GO TO 172
  164 CONTINUE
      Z(K)=0.0
      IF(K-2) 166,168,168
  166 X(K)=A
      GO TO 180
  168 X(K)=(W/2)-(W/(2*NELSX))*(K-2)
      GO TO 180
  170 CONTINUE
      IF(K-2) 171,158,158
  171 ELIPSE=-ELIPSE
      GO TO 158
  172 Z(K)=SQRT(A*A-(X(K)*X(K)))*ELIPSE
  180 CONTINUE
      IF(II-7) 250,182,182
  182 NXT(K)=1
      NZT(K)=1
      GO TO 250
  190 CONTINUE
      IF(II-3) 192,220,194
  192 CONTINUE
      IF(II-2) 196,194,194
  194 IF(K - 2) 195,158,158
  195 ELIPSE = ELIPSE * INVERT
      GO TO 158
  196 CONTINUE
      JJ=J
      IF(INVERT) 198,250,210
```

```
  198 CONTINUE
      IF(J-2) 158,200,200
  200 CONTINUE
      IF(K-2) 202,204,204
  202 X(K)=A
      GO TO 206
  204 X(K)=(W/2)-(W/(2*NELSX))*(K-2)
  206 CONTINUE
      IF(INVERT) 208,250,212
  208 Z(K)=(-T/NELSZ)*(J-2)
      GO TO 250
  210 CONTINUE
      IF(J-NNZ) 200,170,170
  212 Z(K)=T-(T/NELSZ)*(JJ-1)
      GO TO 250
  220 CONTINUE
      IF(INVERT) 222,250,226
  222 ELIPSE=1.0
      IF(J-NNZ) 198,224,224
  224 ELIPSE=-0.75
      GO TO 158
  226 ELIPSE=0.75
      JJ=J-1
      IF(J-2) 158,228,228
  228 ELIPSE=-1.0
      IF(J-NNZ) 200,158,158
  250 CONTINUE
      IF(II-NNY) 500,252,252
  252 CONTINUE
      IF(INPN) 254,254,256
  254 CONTINUE
      NYT(K)=1
      GO TO 500
  256 CONTINUE
      IF(J-2) 500,258,500
  258 CONTINUE
      IF(K-NNX) 500,259,259
  259 LOADPT(1)=N
      GO TO 500
  300 CONTINUE
C
C  GLUE SIMULATOR=> 2/D
C
      X(K)=0.0
      IF(J-2) 302,304,304
  302 Z(K)=A
      GO TO 350
  304 CONTINUE
      IF(J-NNZ) 305,310,310
  305 CONTINUE
      IF(INVERT) 306,500,308
  306 Z(K) = (-T/NELSZ) * (J - 2)
      GO TO 350
  308 Z(K)=T-(T/NELSZ)*(J-2)
      IF((J-2)-NELSZ) 350,309,350
  309 Z(K)=0.0
```

```
      GO TO 350
  310 Z(K)=-A
  350 CONTINUE
      IF(II-5) 500,355,352
  352 CONTINUE
      IF(INPN) 354,354,356
  354 NYT(K)=1
  355 NZT(K)=1
      GO TO 500
  356 NZT(K)=1
      IF(J-2) 364,358,358
  358 CONTINUE
      IF(Z(K)) 362,364,362
  362 CONTINUE
      IF(J-NNZ) 500,364,364
  364 M=M+1
      LOADPT(M)=N
  500 CONTINUE
C*********************************************************************
C-----SAVES NODAL POINT DATA FOR SAPLOT,FILE = IPL--------------------
      IF(IPLOT - 1) 498,496,490
  490 IF(NSPAN - 2) 492,494,498
  492 IF(IPLOT - 5) 498,496,498
  494 IF(IPLOT - 6) 498,496,498
  496 WRITE(IPL,1001) (NPN(K),NXT(K),NYT(K),NZT(K),NXR(K),NYR(K),NZR(K)
     1 X(K),Y(K),Z(K),TEMP(K),K = 1,NNX)
  498 CONTINUE
      IF(NPN(1)-1) 502,502,504
  502 WRITE(IO,1000) NPN(1),NXT(1),NYT(1),NZT(1),NXR(1),NYR(1),NZR(1),
     1X(1),Y(1),Z(1),TEMP(1)
 1000 FORMAT(I5,'A',I4,5I5,3F10.3,5X,F10.5)
      INDENT=2
      IF(NELSX) 550,550,506
  504 INDENT=1
  506 WRITE(IO,1001) (NPN(K),NXT(K),NYT(K),NZT(K),NXR(K),NYR(K),NZR(K),
     1X(K),Y(K),Z(K),TEMP(K),K=INDENT,NNX)
 1001 FORMAT (7I5,3F10.3,5X,F10.5)
  550 CONTINUE
C*********************************************************************
  600 CONTINUE
      RETURN
      END
C*********************************************************************
C
C   THIS SUBROUTINE GENERATES ALL THE ELEMENT GRID FOR THE CONTINUOUS
C   OF THE SINGLE FIBER MODELS AND THE LAP JOINTS.  THE OVERLAP REGION
C   LAP JOINTS ARE GENERATED BY A SECOND ROUTINE (LAPEL).  GLUE
C   MODELS ARE PRODUCED BY THE SUBROUTINE GLUEL.  BOTH OF THESE ARE
C   THIS SUBROUTINE (ELGENR).
C
C*********************************************************************
C
C
      SUBROUTINE ELGENR (NODE1)
C
C
```

```
      DIMENSION NN(20,21),NUMEL(20)
      COMMON NELSX,NELSY,NELSZ,NELSL,SRD,LRD,IDEL(2),ZFACT
      COMMON MODEL,LODMOD,MATAXS,IPLOT,IFRACT,ISTRES,IPL,IFR,IST,IO
      COMMON L,T1,T2,W1,W2,S1,S2,A1,A2
      INTEGER SRD
C
C
      NEL=0
      NODE1 = 1
      INTRS = 3
      INTT = 2
      LSA =0
      LSB =0
      LSC = 0
      LSD = 0
      NSPAN = 1
      NNX=NELSX
      NNZ=NELSZ
      NNY=NELSY
      W=W1
      NMAT=1
      GO TO 6
    5 CONTINUE
      NSPAN=2
      NMAT=2
      IF(LODMOD - 4) 6,4,4
    4 NMAT = 4
C
C  CHECK FOR ORTHOTROPIC MATERIAL ORIENTATION (MD,CD)
C
    6 CONTINUE
      NODEA=NODE1
      IF(MATAXS - 1) 1,2,3
    1 MAXES = 0
      GO TO 8
    2 MAXES = 1
      GO TO 8
    3 IF(NSPAN - 2) 2,1,1
    8 CONTINUE
C*********************************************************************
      DO 250 I=1,NNY
C*********************************************************************
      IF(I-1) 9,9,20
    9 CONTINUE
      IF(NSPAN-2) 10,20,20
   10 CONTINUE
      IF(LODMOD-5) 20,20,12
   12 CONTINUE
C
      CALL GLUEL (NEL,NODE1,W,MAXES)
C
      IF(I - NNY) 20,18,18
   18 IF(NNY - 1) 19,19,250
   19 IF(NSPAN - 2) 20,250,250
   20 CONTINUE
      IF(NELSX) 22,22,40
```

```
C
C   GENERATES 2/D ELEMENT GRID
C
   22 CONTINUE
      INCZ=NNZ+1
      IOP=0
C*********************************************************************
      DO 27 J=1,NNZ
C*********************************************************************
      NEL=NEL+1
      NN(J,4)=NODE1+(INCZ*(I-1))+(J-1)
      NN(J,1)=NN(J,4)+1
      NN(J,3)=NN(J,4)+INCZ
      NN(J,2)=NN(J,3)+1
      NUMEL(J)=NEL
      IF(I-1) 23,23,28
   23 CONTINUE
      IF(NSPAN-2) 24,32,32
   24 CONTINUE
      IF(LODMOD-5) 32,32,33
   28 CONTINUE
      IF(NSPAN - 2) 26,21,21
   26 IF(MODEL - 2) 21,32,32
   21 IF(I - NNY) 32,29,29
   29 CONTINUE
      IF(LODMOD-6) 30,32,31
   30 CONTINUE
      IF(LODMOD-3) 32,32,31
   33 CONTINUE
      IF(J-NNZ) 31,34,34
   34 NODE1=NODE1+1
   31 NN(J,3)=NN(J,3)+1
      NN(J,2)=NN(J,2)+1
   32 CONTINUE
      IF(NN(J,4)-1) 25,25,27
   25 WRITE (6,1000) NUMEL(1),(NN(1,M),M=1,4),NMAT,IOP,W
 1000 FORMAT('0',9X,'DELIMITING 2/D ELEMENT CARDS'//6I5,20X,I5,5X,F10.2
   27 CONTINUE
C*********************************************************************
      WRITE(IO,1001) (NUMEL(K),(NN(K,M),M=1,4),NMAT,IOP,W,K=1,NNZ)
 1001 FORMAT (6I5,20X,I5,5X,F10.2)
C-----SAVES 2/D ELEMENTS FOR SAPLOT,FILE = IPL-----------------------
      IF(IPLOT - 1) 200,39,41
   41 IF(LODMOD - 6) 42,46,45
   42 IF(LODMOD - 3) 35,35,43
   43 IF(NSPAN - 2) 44,49,49
   44 IF(MODEL - 2) 49,35,35
   45 IF(NSPAN - 2) 46,49,49
   46 IF(I - 1) 200,200,47
   47 IF(LODMOD - 6) 48,35,48
   48 IF(MODEL - 2) 49,35,35
   49 IF(I - NNY) 35,200,200
   35 IF(NSPAN - 2) 36,37,200
   36 IF(IPLOT - 3) 39,39,200
   37 IF(IPLOT - 3) 39,200,38
   38 IF(IPLOT - 4) 200,39,200
```

```
   39 WRITE(IPL,1001)(NUMEL(K),(NN(K,M),M=1,4),NMAT,IOP,W,K=1,NNZ)
      GO TO 200
C
C    GENERATES 3/D ELEMENT GRID
C
   40 CONTINUE
      IOP=1
      NDIS=21
      NXYZ=8
C*********************************************************************
      DO 120 J=1,NNZ
C
      DO 112 K=1,NNX
C*********************************************************************
      IREUSE = 0
      NEL=NEL+1
      NUMEL(K)=NEL
      INCRE1 = 2 + (3 *(NELSX + NELSZ) + (5 * NELSX * NELSZ))
      IF(I-1) 50,50,60
   50 CONTINUE
      IF(NSPAN - 2) 52,51,51
   51 IF(NNY - 1) 65,65,100
   52 CONTINUE
      IF(LODMOD-5) 100,100,54
C
C  17-NODE 3/D ELEMENT AT BEGINNING OF FREE SPAN FOLLOWING GLUE
C
   54 NDIS=17
      INCRE3=((NELSX+2)*(NELSZ+1))+((1+NELSX)*(NELSZ+2))+(NELSX*NELSZ)
      NN(K,4)=NODE1+(K-1)+((J-1)*(2+NELSX))
      NN(K,3)=NN(K,4)+1
      NN(K,1)=NN(K,4)+INCRE3+(K-1)+(2*NELSX)*(J-1)
      NN(K,2)=NN(K,1)+2
      NN(K,8)=NN(K,4)+(2+NELSX)
      NN(K,7)=NN(K,8)+1
      NN(K,5)=NN(K,1)+(2+(3*NELSX))
      NN(K,6)=NN(K,5)+2
      NN(K,9)=NN(K,1)+1
      NN(K,12) = NN(K,4) + ((NELSX + 2) * (NELSZ+1))+J*(NELSX-1) + 2
      NN(K,11)=0
      NN(K,10)=NN(K,12)+1
      NN(K,16)=NN(K,12)+1+(2*NELSX)
      NN(K,15)=0
      NN(K,14)=NN(K,16)+1
      NN(K,13)=NN(K,5)+1
      NN(K,17)=NN(K,1)+(2*NELSX)+1-(K-1)
      NN(K,18)=NN(K,17)+1
      NN(K,19)=0
      NN(K,20)=0
      NN(K,21)=NN(K,12)+NELSX+1
      GO TO 108
   60 CONTINUE
      IF(I-NNY) 100,62,62
   62 IF(NSPAN - 2) 63,65,65
   63 IF(MODEL - 2) 65,100,100
   65 IF(LODMOD - 6) 64,100,66
```

```
   64 CONTINUE
      IF(LODMOD-3) 100,100,66
   66 NDIS=17
C
C  17-NODE 3/D ELEMENT AT END OF FREE SPAN->GLUE CONNECTION
C
      INCRE4=((2*NELSX)+1)*(NELSZ+1)+(NELSZ*(NELSX+1))
      NN(K,4)=(2*(K-1))+NODEA+((2+(NELSX*3))*(J-1))
      NN(K,3)=NN(K,4)+2
      NN(K,1)=INCRE1+NN(K,4)-(K-1)-((J-1)*(2*NELSX))+3+NELSX
      NN(K,2)=NN(K,1)+1
      NN(K,8)=NN(K,4)+2+(3*NELSX)
      NN(K,7)=NN(K,8)+2
      NN(K,5)=NN(K,1)+2+NELSX
      NN(K,6)=NN(K,5)+1
      NN(K,9)=0
      NN(K,11)=NN(K,4)+1
      NN(K,12)=NN(K,4)+INCRE4-(K-1)-((J-1)*(NELSX+1))
      NN(K,10)=NN(K,12)+1
      NN(K,13)=0
      NN(K,15)=NN(K,8)+1
      NN(K,16)=NN(K,12)+(2*NELSX)+1
      NN(K,14)=NN(K,16)+1
      NN(K,17)=0
      NN(K,18)=0
      NN(K,20)=NN(K,4)+(2*NELSX)+1-(K-1)
      NN(K,19)=NN(K,20)+1
      NN(K,21)=NN(K,12)+NELSX+1
      GO TO 108
  100 CONTINUE
      IF(K-1) 106,106,101
  101 CONTINUE
      IF(K-NNX) 102,106,106
  102 IREUSE=1
      IF(I-1) 104,104,105
  104 IREUSE=0
      GO TO 106
  105 CONTINUE
      IF(I-NNY) 106,104,104
  106 CONTINUE
C
C-----STANDARD 21-NODE 3/D ELEMENT-----------------------------------
C
      INCRE2=(3*NELSX*NELSZ)+(2*(NELSX+NELSZ))-(K-2)-((NELSX+1)*(J-1))
      NN(K,4)=NODEA+(2*(K-1))
      NN(K,3)=NN(K,4)+2
      NN(K,1)=NN(K,4)+INCRE1
      NN(K,2)=NN(K,1)+2
      NN(K,5)=NN(K,1)+(2+(NELSX*3))
      NN(K,6)=NN(K,5)+2
      NN(K,7)=NN(K,6)-INCRE1
      NN(K,8)=NN(K,7)-2
      NN(K,9)=NN(K,1)+1
      NN(K,12)=NN(K,4)+INCRE2
      NN(K,11)=NN(K,4)+1
      NN(K,10)=NN(K,12)+1
```

```
      NN(K,13)=NN(K,5)+1
      NN(K,14)=NN(K,10)+1+(2*NELSX)
      NN(K,15)=NN(K,13)-INCRE1
      NN(K,16)=NN(K,14)-1
      NN(K,17)=NN(K,1)+(2*NELSX)+1-(K-1)
      NN(K,18)=NN(K,17)+1
      NN(K,19)=NN(K,18)-INCRE1
      NN(K,20)=NN(K,19)-1
      NN(K,21)=NN(K,10)+NELSX
      IF(NSPAN - 2) 117,108,108
  117 IF(NN(K,4) - NODE1) 107,107,108
  107 WRITE(6,1020) NUMEL(1),NDIS,NXYZ,NMAT,MAXES,IOP,INTRS,INTT,
     1 IREUSE,LSA,LSB,LSC,LSD,(NN(1,M),M=1,21)
 1020 FORMAT('0',9X,'DELIMITING 3/D ELEMENT CARDS'//6I5,15X,3I5,4I2/
     1 16I5/5I5)
  108 CONTINUE
      IF(K-1) 109,109,112
  109 CONTINUE
      IF(J-1) 140,140,112
  140 CONTINUE
      IF(I-1) 111,111,110
  110 CONTINUE
      IF(I-NNY) 112,111,111
  111 CONTINUE
      NODE=NN(1,1)
  112 CONTINUE
C*************************************************************************
      DO 129 KK=1,NNX
C*************************************************************************
      IF(KK-NNX) 115,113,113
  113 IREUSE=0
  115 WRITE(IO,1021) NUMEL(KK),NDIS,NXYZ,NMAT,MAXES,IOP,INTRS,INTT,
     1 IREUSE,LSA,LSB,LSC,LSD,(NN(KK,M),M=1,21)
      IF(IPLOT - 1) 129,128,130
  130 IF(LODMOD - 6) 131,135,134
  131 IF(LODMOD - 3) 124,124,132
  132 IF(NSPAN - 2) 133,138,138
  133 IF(MODEL - 2) 138,124,124
  134 IF(NSPAN - 2) 135,138,138
  135 IF(I - 1) 129,129,136
  136 IF(LODMOD - 6) 137,124,137
  137 IF(MODEL - 2) 138,124,124
  138 IF(I - NNY) 124,129,129
  124 IF(NSPAN - 2) 125,126,129
  125 IF(IPLOT - 3) 128,128,129
  126 IF(IPLOT - 3) 128,129,127
  127 IF(IPLOT - 4) 129,128,129
  128 WRITE(IPL,1021) NUMEL(KK),NDIS,NXYZ,NMAT,MAXES,IOP,INTRS,INTT,
     1 IREUSE,LSA,LSB,LSC,LSD,(NN(KK,M),M=1,21)
 1021 FORMAT (6I5,15X,3I5,4I2/16I5/5I5)
  129 CONTINUE
      IF(NDIS - 17) 114,120,114
  114 NODEA = NODEA + (3 * NELSX) + 2
      IF(J-NNZ) 120,116,116
  116 CONTINUE
      NODEA=NODE+(INCRE1*(I-1))
```

```
  120 CONTINUE
C*********************************************************************
      IF(NDIS-17) 200,122,200
  122 NODEA=NODE
C
C   CHECKS RIGHT END SPECIFICATIONS: RETURNS GLUE SPECS TO STATEMENT 12
C
  200 CONTINUE
      IF(I-NNY) 250,210,210
  210 CONTINUE
      IF(NELSX) 211,211,212
  211 CONTINUE
      NODE1=NN(NNZ,1)+1
      IF(LODMOD-6) 219,217,213
  219 CONTINUE
      IF(LODMOD-3) 217,217,213
  217 CONTINUE
      WRITE(6,1002) NUMEL(NNZ),(NN(NNZ,M),M=1,4),NMAT,IOP,W
 1002 FORMAT ('0',6I5,20X,I5,5X,F10.2)
      GO TO 213
  212 CONTINUE
      NODE1=NODE
      IF(LODMOD - 6) 220,218,213
  220 IF(MODEL - 2) 224,222,222
  222 IF(NSPAN - 2) 213,224,224
  224 IF(LODMOD - 3) 218,218,213
  218 WRITE(6,1022) NUMEL(NNX),NDIS,NXYZ,NMAT,MAXES,IOP,INTRS,INTT,
     1 IREUSE,LSA,LSB,LSC,LSD,(NN(NNX,M),M=1,21)
 1022 FORMAT ('0',6I5,15X,3I5,4I2/16I5/5I5)
  213 CONTINUE
      IF(NSPAN-2) 214,215,215
  214 CONTINUE
      IF(MODEL-2) 215,250,250
  215 CONTINUE
      IF(LODMOD-6) 216,250,12
  216 CONTINUE
      IF(LODMOD-3) 250,250,12
  250 CONTINUE
C
C   CHECKS FOR LAP JOINT MODELS, GENERATES THE OVERLAP ELEMENT GRID, AND
C   RETURNS TO STATEMENT 5 WITH NSPAN=2
C
      IF(MODEL-2) 260,251,251
  251 CONTINUE
      IF(NSPAN-2) 252,260,260
  252 CONTINUE
C
      CALL LAPEL (NEL,NODE1)
C
      GO TO 5
  260 CONTINUE
      RETURN
      END
      SUBROUTINE OVRLAP (N,ALPHA,RPOINT,INODE,JNODE,KNODE)
C
C
```

```
C
      DIMENSION NPN(50),NXT(50),NYT(50),NZT(50),NXR(50),NYR(50),NZR(50)
     1 X(50),Y(50),Z(50),TEMP(50),INODE( 5),JNODE( 5),KNODE( 5),
     2 ANGLR(4,7),RAVECT(20,7,4),NPVECT(20,7,4),IJ(4,7),CY1(50),CZ1(50),
     3 NTIP(4)
      COMMON NELSX,NELSY,NELSZ,NELSL,SRD,LRD,IDEL(2),ZFACT
      COMMON MODEL,LODMOD,MATAXS,IPLOT,IFRACT,ISTRES,IPL,IFR,IST,IO
      COMMON L,T1,T2,W1,W2,S1,S2,A1,A2
      COMMON LOADPT(250)
C
      INTEGER SRD,ZDIVR,SRT,ZFACT
      REAL L
C
C
      EPS = 0.0001
      RADIAN = 57.2957795
      JC = 0
      SRT = SRD
      JPOS = SRD + IDEL(1)
      KPOS = JPOS + LRD
      LPOS = KPOS + NELSL
      MPOS = LPOS + LRD
      NPOS = MPOS + IDEL(2)
C-----ZEROS OUT THE FRACTURE AND CENTROID VECTORS----------------------------
      DO 10 LI= 1,20
      DO 10 M = 1,7
      DO 10 IK = 1,4
      IJ(IK,M) = 0
      RAVECT(LI,M,IK) = 0.0
   10 NPVECT(LI,M,IK) = 0
      RESLL = L - (A1 + A2)
C-----CHECKS FOR SHORT RESIDUAL LAP LENGTHS AND PROPER SPECIFICATION---
      IF(RESLL-(T1+T2)) 80,80,90
   80 CONTINUE
      IF(NELSL) 88,88,82
   82 WRITE(6,1000)
 1000 FORMAT('0 **ERROR** RESIDUAL LAP LENGTH .LE. (T1+T2) & NELSL ',
     1'.GT. ZERO')
      STOP
C
C
C
   88 CONTINUE
C-----SETS GRID SIZE IF SHORT OVERLAP----------------------------------
      GRID = RESLL/(2*LRD)
      GRIT = GRID
      GO TO 93
   90 CONTINUE
      IF(NELSL) 91,91,92
   91 NELSL = 1
C-----SETS GRID SIZE FOR NORMAL OVERLAPS AND CALCULATES FRACTURE VECTOR
C-----ANGLES IN RADIANS FOR LATER COMPARISON TO NODE COORDINATES-------
   92 GRID = T1/LRD
      GRIT = GRID
   93 SLOPG1 = GRID/(T1/NELSZ)
      SLOPG2 = GRID/(T2/NELSZ)
```

```
      SLOP1G = 1.0/SLOPG1
      SLOP2G = 1.0/SLOPG2
      ANGLR(1,1) = ATAN (SLOPG1) +  90.0/RADIAN
      ANGLR(1,2) = ATAN (SLOP2G) + 180.0/RADIAN
      ANGLR(1,3) = 90.0/RADIAN
      ANGLR(1,4) = 270.0/RADIAN
      ANGLR(1,5) = ATAN (SLOP1G)
      ANGLR(1,6) = 0.0
      ANGLR(1,7) = ATAN (SLOPG2) + 270.0/RADIAN
C-----CHECKS FOR 2/D AND SETS Y-COORDINATE LOOP LIMITS FOR 2&3/D'S-----
      IF(NELSX) 136,136,140
  136 IF(SRD -(NELSZ/2)) 137,138,137
  137 WRITE (6,2010)
 2010 FORMAT('0','**ERROR**  SRD .NE. NELSZ/2')
      STOP
  138 NNY = IDEL(1) + IDEL(2) + (2 * (SRD + LRD)) + NELSL - 1
      NNX = 1
      LRT = LRD
      NELST = NELSL
      GO TO 148
  140 CONTINUE
C-----3/D CONSTRUCTION PARAMETERS-------------------------
      NNX = (2*NELSX) +1
      NNY = ((NPOS+SRD)*2) - 1
      SRT = 2 * SRD
      JPOS = 2*JPOS
      KPOS = 2*KPOS
      LPOS = 2*LPOS
      MPOS = 2*MPOS
      NPOS = 2*NPOS
      LRT = LRD*2
      GRIT = GRID/2
      NELST = NELSL*2
  148 CONTINUE
C*********************************************************************
      DO 800 I = 1,NNY
C*********************************************************************
C
C-----CALCULATES THE Y-COORDINATES OF 2&3/D'S AND SETS Z-COORDINATE
C-----LIMITS FOR 2/D LAP JOINTS---------------------------------------
      IM = I - 1
      IF(I - SRT) 151,153,154
  153 NNZ = 2*(NELSZ + 1)
      IF(A1) 150,150,152
  150 NNZ = (2*NELSZ) + 1
      GO TO 152
  151 NNZ = NELSZ + 1
  152 Y(I) = -((RESLL/2) + A1 + ((T1/(2*SRT)) * (SRT - I)))
      GO TO 200
  154 CONTINUE
      IF(I - JPOS) 156,159,159
  156 Y(I) = -((RESLL/2) + (GRIT * (JPOS - I)))
      IF(Y(IM) - Y(I)) 158,157,157
  157 Y(I) = Y(IM) + ((A1 - ((IDEL(1) -1) * GRID))/2)
  158 NNZ = 2 * (NELSZ + 1)
      GO TO 200
```

```
  159 CONTINUE
      IF(I - KPOS) 160,160,166
  160 Y(I) =(-(RESLL/2) + (GRIT * (I - JPOS)))
      NNZ = (2 * NELSZ) + 1
      GO TO 200
  166 CONTINUE
      IF(I - LPOS) 168,170,170
  168 Y(I) = -(RESLL/2) + T1 + ((RESLL - (T1 + T2))/NELST) * (I -KPOS)
      NNZ = (2*NELSZ) + 1
      GO TO 200
  170 CONTINUE
      IF(RESLL - (T1 + T2)) 174,174,172
  172 GRID = T2/LRD
      GRIT = GRID
      IF(NELSX) 174,174,173
  173 GRIT = GRID/2
C-----CALCULATES FRACTURE VECTOR ANGLES FOR RIGHT CRACK TIP----------
  174 SLOPG1 = GRID/(T1/NELSZ)
      SLOPG2 = GRID/(T2/NELSZ)
      SLOP1G = 1.0/SLOPG1
      SLOP2G = 1.0/SLOPG2
      ANGLR(2,1) = ATAN (SLOPG1) + 90.0/RADIAN
      ANGLR(2,2) = 180.0/RADIAN
      ANGLR(2,3) = ATAN (SLOP2G) + 180.0/RADIAN
      ANGLR(2,4) = 90.0/RADIAN
      ANGLR(2,5) = 270.0/RADIAN
      ANGLR(2,6) = ATAN (SLOP1G)
      ANGLR(2,7) = ATAN (SLOPG2) + 270.0/RADIAN
      IF(I - MPOS) 176,176,179
  176 NNZ = (2*NELSZ) + 1
  177 Y(I) =  (RESLL/2) + (GRIT * (I - MPOS))
      IF(A2) 200,200,175
  175 IF(Y(I) - ((RESLL/2) + A2)) 200,178,178
  178 Y(I) = Y(IM) + ((A2 - ((IDEL(2) - 1) * GRID))/2)
      GO TO 200
  179 CONTINUE
      IF(I-NPOS) 180,182,184
  180 NNZ = 2*(NELSZ + 1)
      GO TO 177
  182 Y(I) = (RESLL/2) + A2
      NNZ = 2*(NELSZ + 1)
      GO TO 200
  184 Y(I) = (RESLL/2) + A2 + ((T2/(2*SRT))*(I-NPOS))
      NNZ = NELSZ + 1
  200 CONTINUE
      IF(NELSX) 220,220,210
  210 IF(I-SRT) 216,212,212
  212 IF(I-NPOS) 214,214,216
  214 NNZ = NNZ + (NELSZ* 2)
      GO  TO  220
  216 NNZ = NNZ + NELSZ
  220 CONTINUE
C*********************************************************************
      DO 700 J = 1,NNZ
C*********************************************************************
      IF(NELSX) 304,304,300
```

```
C
C-----CALCULATES Z-COORDINATES FOR 2&3/D ELEMENTS---------------------
C
  300 ZDIVR = NELSZ*2
      GO TO 306
  304 ZDIVR = NELSZ
  306 IF(NNZ - ((2*ZDIVR) + 1)) 310,350,330
  310 IF(I -SRT) 312,312,320
  312 T = T1
      II = I
      IF(MODEL - 3) 314,316,316
  314 ZINCR = 0.0
      ZPOS = 0.0
      GO TO 318
  316 ZINCR = T/LRT
      IF(I - SRT) 315,317,317
  315 ZINCR = T/(2* SRT)
  317 ZPOS = -T/2
  318 Z(J) = T + ZPOS + (ZINCR * II) - ((T/ZDIVR) * (J - 1))
      GO TO 355
  320 T = T2
      II = I - NPOS
      IF(MODEL - 3) 322,324,324
  322 ZINCR = 0.0
      ZPOS = -T
      GO TO 318
  324 ZINCR = T/LRT
      IF(I - NPOS) 326,326,325
  325 ZINCR = T/(2 * SRT)
  326 ZPOS = -T
      GO TO 318
  330 CONTINUE
      IF(J - (ZDIVR + 2)) 332,334,336
  332 Z(J) = T1 - (DBLE(T1)/ZDIVR) * (J - 1)
      GO TO 355
  334 Z(J) = 0.0
      GO TO 355
  336 Z(J) = -(DBLE(T2)/ZDIVR) * (J - (ZDIVR + 2))
      GO TO 355
  350 CONTINUE
      IF(J - (ZDIVR + 1)) 332,332,352
  352 Z(J) = -(DBLE(T2)/ZDIVR) * (J - (ZDIVR + 1))
  355 CONTINUE
C
C-----SETS NNX LIMITS FOR 3/D ELEMENTS--------------------------------
C
      IF(NELSX) 380,380,360
  360 KJ = I/2
      JK = KJ*2
      IF(I - JK) 362,368,362
  362 JM = J/2
      MJ = JM*2
C-----CHECKS FOR CRACKED LAP JOINT------------------------------------
      IF(NNZ - ((2 * ZDIVR) + 1)) 365,365,363
  363 IF(J - (ZDIVR + 2)) 365,374,374
  365 IF(J - MJ) 364,366,364
```

```
  364 NNX = NELSX + 1
      GO TO 380
  366 NNX = NELSX
      GO TO 380
  368 JL = J/2
C-----CHECKS FOR CRACKED LAP JOINT-----------------------------------
      LJ = JL*2
      IF(NNZ - ((2 * ZDIVR) + 1)) 371,371,369
  369 IF(J - (ZDIVR + 2)) 371,376,376
  371 IF(J - LJ) 370,364,370
  370 NNX = (NELSX * 2) + 1
      GO TO 380
  374 IF(J - MJ) 366,364,366
  376 IF(J - LJ) 364,370,364
  380 CONTINUE
C*********************************************************************
      DO 470 K = 1,NNX
C*********************************************************************
      N = N + 1
      NPN(K) = N
      NXT(K) = 0
      NYT(K) = 0
      NZT(K) = 0
      NXR(K) = 1
      NYR(K) = 1
      NZR(K) = 1
      TEMP(K) = 0.0
      IF(NELSX) 390,390,394
C
C-----2/D ELEMENT COORDINATES---------------------------------------
C
  390 X(K) = 0.0
      NXT(K) = 1
      GO TO 430
C
C-----GENERATION OF THE MATERIAL AXES ORIENTATION PARAMETERS---------
C
  394 IF(I - 2) 396,420,420
  396 IF(J - 2) 398,420,420
  398 IF(K - 2) 400,420,420
  400 JI = 0
      INCRE1 = (2 * NELSX * NELSZ) + NELSX + NELSZ + 2
      IF(MODEL - 3) 420,404,404
  404 IF(MATAXS - 1) 406,408,408
  406 JI = JI + 1
      INODE(JI) = NPN(1) + 1
      JNODE(JI) = INODE(JI) + INCRE1
      KNODE(JI) = NPN(1)
      GO TO 420
  408 JI = 2
      INODE(JI) = NPN(1)
      JNODE(JI) = NPN(1) + INCRE1 - 1
      KNODE(JI) = NPN(1) + 1
      IF(MATAXS - 1) 420,420,406
  420 CONTINUE
C
```

```
C-----GENERATION OF 3/D X-COORDINATES----------------------------------
C
      W = W1
      IF(W1 - W2) 423,421,423
  421 KI = I/2
      KK = KI*2
      IF(KK - I) 426,422,426
  423 WRITE(6,2000)
 2000 FORMAT(' **ERROR** W1 .NE. W2')
      STOP
  422 X(K) = (W/2) - ((W/((NNX-1) * 2)) * (K - 1))
      IF(K - NNX) 430,424,424
  424 NXT(K) = 1
      GO TO 430
  426 CONTINUE
      KJ = J/2
      JK = KJ*2
C-----CHECKS FOR CRACKED LAP JOINT-------------------------------------
      IF(NNZ - ((2 * ZDIVR) + 1)) 427,427,425
  425 IF(J -(ZDIVR + 2)) 427,429,429
  427 IF(JK - J) 422,428,422
  428 CONTINUE
      X(K) = (W/2) -((W/(2*NNX)) * (K -1))- (W/(4 * NELSX))
C
C-----SAVES 3/D ELEMENT CENTROID COORDINATES FOR STRESS PLOTTING-------
C
      WRITE (9,3000) X(K),Y(I),Z(J)
 3000 FORMAT (3A4)
      GO TO 430
  429 IF(JK - J) 428,422,428
  430 CONTINUE
C
C-----THIS SECTION OF THE PROGRAM SAVES 2/D ELEMENT NODAL POINTS WHICH-
C-----LIE ON 1 OF 7 RADII  VECTORS AROUND EITHER OF THE TWO CRACK TIPS
C-----CONVERTS THEM TO AN 'R' VALUE TO BE USED IN FRACTR---------------
C-----RADIUS VECTORS ARE SAVED FOR K = 1 AND NNX FOR THE 3/D LAP JOINTS-------
C
      IF(IFRACT) 470,470,432
  432 IF(I-JPOS) 434,438,440
  434 MF = 1
      ML = 2
  436 YORIG = -(RESLL/2)
      IK = 1
      GO TO 460
  438 MF =3
      ML =4
      GO TO 436
  440 IF(I - KPOS) 442,442,444
  442 MF = 5
      ML = 7
      GO TO 436
  444 IF(I - LPOS) 470,446,448
  446 MF = 1
      ML = 3
  447 YORIG = RESLL/2
      IK = 2
```

```
      GO TO 460
  448 IF(I - MPOS) 446,450,452
  450 MF = 4
      ML = 5
      GO TO 447
  452 MF = 6
      ML = 7
      GO TO 447
  460 CONTINUE
      MAXIK = 2
      IF(NELSX) 461,461,454
  454 IF(NNX - NELSX) 470,470,456
  456 IF(K-NNX) 458,459,470
  458 IF(K - 1) 461,461,470
  459 IK = IK + 2
      MAXIK = 4
  461 CONTINUE
      IF(MODEL - 4) 457,455,455
  455 MAXIK = 1
  457 CONTINUE
C*********************************************************************
      DO 470 M = MF,ML
C*********************************************************************
      YDIF = Y(I) - YORIG
      ANGLR(3,M) = ANGLR(1,M)
      ANGLR(4,M) = ANGLR(2,M)
      IF(YDIF) 464,462,464
  462 IF(Z(J)) 466,473,467
  464 CTAN = SIN(ANGLR(IK,M))/COS(ANGLR(IK,M))
      IF(ABS(CTAN - (Z(J)/YDIF)) - EPS) 465,465,470
  465 IF(Z(J)) 466,468,467
  466 IF(M -ML) 470,469,469
  467 IF(M - MF) 469,469,470
  468 IF(M - MF) 470,470,463
  463 IF(M - ML) 469,470,470
  469 IJ(IK,M) = IJ(IK,M) + 1
      IJM = IJ(IK,M)
      RAVECT(IJM     ,M,IK) = SQRT((Z(J)*Z(J)) + (YDIF*YDIF))
      NPVECT(IJM     ,M,IK) = NPN(K)
      GO TO 470
  473 NTIP(IK) = NPN(K)
C
  470 CONTINUE
C*********************************************************************
      IF(NELSX) 471,471,550
  471 IF(ISTRES) 550,550,472
C
C-----CALCULATES 2/D ELEMENT CENTROID COORDINATES FOR STRESS PLOTTING--
C
  472 IF(I - 1) 500,500,474
  474 IN = I - 1
      IF(J - 1) 500,500,476
  476 JN = J - 1
      CXVECT = 0.0
      DY =  ABS(CY1(IN) - Y(I))
      DZ =  ABS(CZ1(JN) - Z(J))
```

```
      CFACT = (SQRT((DY * DY) + (DZ * DZ)))/2
      IF(I -SRT) 480,480,478
  478 IF(I - NPOS) 488,488,480
  480 IF(MODEL - 2) 550,484,482
  482 IF(J-2) 500,496,486
  484 IF(J - (NELSZ + 1)) 494,494,500
  486 IF(J - (NELSZ + 1)) 494,498,500
  488 IF(I - JPOS) 492,494,490
  490 IF(I - MPOS) 494,494,492
  492 IF(J - ((NNZ/2) + 1))494,500,494
  494 CYVECT = (CY1(IN) + Y(I))/2
      CZVECT = (CZ1(JN) + Z(J))/2
      GO TO 499
  496 CZVECT = CZ1(JN) - CFACT
      CYVECT = CY1(IN) + CFACT
      WRITE (9,3000) CXVECT,CYVECT,CZVECT
      GO TO 506
  498 CYVECT = (CY1(IN) + Y(I))/2
      CZVECT = (CZ1(JN) + Z(J))/2
      WRITE (9,3000) CXVECT,CYVECT,CZVECT
      CZVECT = Z(J) - (DY - CFACT)
      CYVECT = Y(I) - CFACT
  499 WRITE (9,3000) CXVECT,CYVECT,CZVECT
  500 IF(I - NPOS) 506,502,506
  502 IF(J - (NNZ - NELSZ)) 506,504,504
  504 JC = JC + 1
      CZ1(JC) = Z(J)
      GO TO 508
  506 CZ1(J) = Z(J)
  508 CY1(I) = Y(I)
  550 CONTINUE
C
C-----ADJUSTMENT OF THE INCLINATION OF CONFORMING LAP JOINTS THROUGH AN
C-----,ALPHA, ABOUT THE CENTERLINE POINT,RPOINT.----------------------
C
      IF(MODEL - 2) 574,574,572
  572 RADIUS = Y(I) - RPOINT
      YTEMP = (RADIUS * COS(ALPHA)) + (Z(J) * SIN(ALPHA)) + RPOINT
      ZTEMP=-((RADIUS * SIN(ALPHA)) - (Z(J) * COS(ALPHA)))
      GO TO 580
  574 YTEMP = Y(I)
      ZTEMP = Z(J)
  580 CONTINUE
C
C-----SAVES NODAL POINT INFORMATION FOR SAPLOT, FILE = IPL-------------
C
      IF(IPLOT - 1) 670,668,652
  652 IF(IPLOT - 2) 668,668,654
  654 IF(IPLOT - 4) 659,660,656
  656 IF(IPLOT - 7) 670,668,658
  658 IF(IPLOT - 8) 668,659,660
  659 IF(I - KPOS) 668,668,670
  660 IF(I - LPOS) 670,668,668
  668 WRITE(IPL,1010) (NPN(K),NXT(K),NYT(K),NZT(K),NXR(K),NYR(K),NZR(K)
     1 X(K),YTEMP,ZTEMP,TEMP(K),K = 1,NNX)
 1010 FORMAT(7I5,3F10.3,5X,F10.5)
```

```
  670 WRITE(IO,1010) (NPN(K),NXT(K),NYT(K),NZT(K),NXR(K),NYR(K),NZR(K),
     1 X(K),YTEMP,ZTEMP,TEMP(K),K = 1,NNX)
  700 CONTINUE
  800 CONTINUE
C
C-----SORTS RADIUS VECTORS TO GIVE SMALLEST TO LARGEST 'R' VALUES,-----
C-----AND WRITES VECTORS ON UNIT = IFR-------------------------------
C
C**********************************************************************
      DO 820 M = 1,7
      DO 820 IK = 1,MAXIK
C**********************************************************************
      IF(IJ(IK,M) - 1) 820,820,804
  804 IKM = IJ(IK,M)
      CALL REORDR(RAVECT(1,M,IK),NPVECT(1,M,IK),IKM)
  820 CONTINUE
      IF(IFRACT) 840,840,825
  825 CONTINUE
      DO 850 IK = 1,MAXIK
      MAXIJK = 0
      DO 828 J = 1,7
  828 MAXIJK = MAX0(IJ(IK,J),MAXIJK)
      WRITE (IFR,1022) IK,MAXIJK,NTIP(IK),RESLL
 1022 FORMAT(3I5,F10.3)
      WRITE(IFR,1020) (ANGLR(IK,M),M = 1,7)
 1020 FORMAT(7(F9.6,2X))
      DO 830 K = 1,MAXIJK
  830 WRITE(IFR,1021) (NPVECT(K,M,IK),RAVECT(K,M,IK),M = 1,7)
 1021 FORMAT(7(I4,F7.3))
  850 CONTINUE
  840 CONTINUE
      ENDFILE 9
      REWIND 9
      RETURN
      END
C
C
      SUBROUTINE GLUEL (NEL,NODE1,W,MAXES)
C
C
C**********************************************************************
C
C  THIS SUBROUTINE GENERATES THE ELEMENTS FOR THE 3/D GLUE CONNECTIONS
C  AND 2/D GLUE SIMULATORS
C
C**********************************************************************
C
C
      DIMENSION NN(20,21),NUMEL(20)
      COMMON NELSX,NELSY,NELSZ,NELSL,SRD,LRD,IDEL(2),ZFACT
      COMMON MODEL,LODMOD,MATAXS,IPLOT,IFRACT,ISTRES,IPL,IFR,IST,IO
      INTEGER AXES
C
C
      INTRS = 3
      INTT = 2
```

```
      LSA = 0
      LSB = 0
      LSC = 0
      LSD = 0
      INEL=NEL
      DO 5 I = 1,20
      DO 5 K = 1,21
    5 NN(I,K) = 0
      IF(NELSX) 250,250,10
   10 NNY=5
      NNX=NELSX+1
      NDIS=8
      NXYZ=8
      IOP=1
      IREUSE=0
      IF(INEL) 15,15,12
   12 NODE1=NODE1-(3+NELSX)
   15 NODEA=NODE1
C*********************************************************************
      DO 150 I=1,NNY
C*********************************************************************
      IF(INEL) 20,20,30
C-----SELECTS PROPER NODE NUMBER INCREMENTS-------------------------
   20 II=NNY-(I-1)
      GO TO 40
   30 II=I
   40 CONTINUE
      IF(II-3) 42,44,46
   42 NNZ=NELSZ+2
      IF(II-2) 50,41,50
   41 CONTINUE
      IF(INEL) 43,43,50
   43 NODEA=NODEA-(NELSZ+1)*(2+NELSX)
      GO TO 50
   44 NNZ=1
      IF(INEL) 45,45,50
   45 NODEA=NODEA+(2+NELSX)
      GO TO 50
   46 NNZ=2
      INCRE1=6+(3*NELSX)
      GO TO 55
   50 INCRE1=(NELSX+2)*(NELSZ+3)
   55 CONTINUE
C
C-----GENERATES 3/D GLUE CONNECTION STRUCTURES AND ASSIGNS MATERIAL AND
C-----AXES ORIENTATIONS---------------------------------------------
C
C*********************************************************************
      DO 140 J=1,NNZ
C
      DO 130 K=1,NNX
C*********************************************************************
      NEL=NEL+1
      NN(K,4)=NODEA+(K-1)+((J-1)*(2+NELSX))
      NN(K,3)=NN(K,4)+1
      NN(K,2)=NN(K,3)+INCRE1
```

```
      NN(K,1)=NN(K,2)-1
      NN(K,5)=NN(K,1)+(2+NELSX)
      NN(K,6)=NN(K,5)+1
      NN(K,8)=NN(K,4)+(2+NELSX)
      NN(K,7)=NN(K,8)+1
      NUMEL(K)=NEL
      IF(INEL) 60,60,100
   60 CONTINUE
      IF(II-2) 64,64,62
   62 NMAT=2
      AXES=0
      GO TO 74
   64 NMAT=3
      AXES=0
      IF(J-2) 74,66,70
   66 CONTINUE
      IF(K-2) 74,68,68
   68 NMAT=1
      AXES=MAXES
      GO TO 74
   70 CONTINUE
      IF(J-NNZ) 66,62,62
   74 CONTINUE
      IF(II-1) 76,76,82
   76 CONTINUE
      IF(K-1) 78,78,82
   78 CONTINUE
      IF(J-1) 80,80,82
   80 NODE2=NN(K,6)
   82 CONTINUE
      IF(INEL) 85,85,115
   85 CONTINUE
      IF(NN(K,4)-NODE1) 95,95,128
   95 WRITE(6,1000) NUMEL(1),NDIS,NXYZ,NMAT,AXES,IOP,INTRS,INTT,
     1 IREUSE,LSA,LSB,LSC,LSD,(NN(1,M),M=1,21)
 1000 FORMAT('0',9X,'DELIMITING 3/D ELEMENT CARDS'//6I5,25X,I5/16I5/5I5
      GO TO 128
  100 CONTINUE
      IF(MODEL-2) 60,102,102
  102 IF(II - 3) 103,62,62
  103 IF(J - 2) 62,104,110
  104 NMAT=3
      AXES=0
      IF(K-2) 128,108,108
  108 NMAT=4
      AXES=MAXES
      GO TO 128
  110 CONTINUE
      IF(J-NNZ) 104,112,112
  112 NMAT=3
      AXES=0
  115 CONTINUE
      IF(I-NNY) 128,122,122
  122 CONTINUE
      IF(K-NNX) 128,124,124
  124 CONTINUE
```

```
      IF(J-NNZ) 128,126,126
  126 WRITE(6,1002) NUMEL(K),NDIS,NXYZ,NMAT,AXES,IOP,INTRS,INTT,
     1 IREUSE,LSA,LSB,LSC,LSD,(NN(K,M),M=1,21)
  128 CONTINUE
      WRITE(IO,1001) NUMEL(K),NDIS,NXYZ,NMAT,AXES,IOP,INTRS,INTT,
     1 IREUSE,LSA,LSB,LSC,LSD,(NN(K,M),M=1,21)
C-----SAVES 3/D ELEMENTS FOR SAPLOT,FILE = IPL-------------------------
      IF(IPLOT - 1) 130,135,132
  132 IF(INEL) 133,133,134
  133 IF(IPLOT - 5) 130,135,130
  134 IF(IPLOT - 6) 130,135,130
  135 WRITE(IPL,1001) NUMEL(K),NDIS,NXYZ,NMAT,AXES,IOP,INTRS,INTT,
     1 IREUSE,LSA,LSB,LSC,LSD,(NN(K,M),M=1,21)
 1001 FORMAT(6I5,15X,3I5,4I2/16I5/5I5)
 1002 FORMAT('0',6I5,15X,3I5,4I2/16I5/5I5)
  130 CONTINUE
C*************************************************************************
  140 CONTINUE
C*************************************************************************
      NODEA=NODEA+INCRE1
  150 CONTINUE
C*************************************************************************
      GO TO 465
  250 CONTINUE
C
C  GLUE SIMULATOR=> 2/D
C
      IOP=0
      NNY=5
      NNZ=NELSZ+2
C*************************************************************************
      DO 460 I=1,NNY
C*************************************************************************
      IF(INEL) 252,252,260
  252 II=NNY-(I-1)
      GO TO 270
  260 II=I
  270 CONTINUE
C*************************************************************************
      DO 450 J=1,NNZ
C*************************************************************************
      NEL=NEL+1
      NN(J,4)=NODE1+(J-1)+(NELSZ+3)*(I-1)
      NN(J,1)=NN(J,4)+1
      NN(J,3)=NN(J,4)+(NELSZ+3)
      NN(J,2)=NN(J,3)+1
      NUMEL(J)=NEL
      IF(II-3) 304,304,302
  302 NMAT=2
      GO TO 400
  304 CONTINUE
      IF(MODEL-2) 306,324,324
  306 CONTINUE
      IF(J-2) 308,310,310
  308 NMAT=3
      GO TO 400
```

```
  310 CONTINUE
      IF(J-NNZ) 314,312,312
  312 NMAT=2
      GO TO 401
  314 CONTINUE
      IF(II-2) 318,318,316
  316 NMAT=3
      GO TO 401
  318 NMAT=1
      GO TO 401
  324 CONTINUE
      IF(INEL) 306,306,326
  326 CONTINUE
      IF(J-2) 328,330,330
  328 NMAT=2
      GO TO 401
  330 CONTINUE
      IF(J-NNZ) 334,332,332
  332 NMAT=3
      GO TO 401
  334 IF(II - 3) 338,336,302
  336 NMAT = 3
      GO TO 401
  338 NMAT = 4
  400 CONTINUE
      NODE2=NN(J,2)
  401 CONTINUE
      IF(NN(J,4)-1) 402,402,404
  402 WRITE(6,1010) NUMEL(1),(NN(1,M),M=1,4),NMAT,IOP,W
 1010 FORMAT('0',9X,'DELIMITING 2/D ELEMENT CARDS'//6I5,20X,I5,5X,F10.2
  404 CONTINUE
      WRITE(IO,1011) NUMEL(J),(NN(J,M),M=1,4),NMAT,IOP,W
C-----SAVES 2/D ELEMENTS FOR SAPLOT,FILE = IPL-------------------------
      IF(IPLOT - 1) 409,408,405
  405 IF(INEL) 406,406,407
  406 IF(IPLOT - 5) 409,408,409
  407 IF(IPLOT - 6) 409,408,409
  408 WRITE (IPL,1011) NUMEL(J),(NN(J,M),M = 1,4),NMAT,IOP,W
  409 IF(INEL) 450,450,410
 1011 FORMAT(6I5,20X,I5,5X,F10.2)
 1012 FORMAT('0',6I5,20X,I5,5X,F10.2)
      IF(INEL) 450,450,410
  410 CONTINUE
      IF(I-NNY) 450,412,412
  412 CONTINUE
      IF(J-NNZ) 450,414,414
  414 WRITE(6,1012) NUMEL(J),(NN(J,M),M=1,4),NMAT,IOP,W
  450 CONTINUE
C*****************************************************************************
  460 CONTINUE
  465 NODE1=NODE2
      RETURN
      END
C
C
C
```

```
      SUBROUTINE LAPEL(NEL,NODE1)
C
C
C
      DIMENSION NN(20,21),NUMEL(20)
      COMMON NELSX,NELSY,NELSZ,NELSL,SRD,LRD,IDEL(2),ZFACT
      COMMON MODEL,LODMOD,MATAXS,IPLOT,IFRACT,ISTRES,IPL,IFR,IST,IO
      COMMON L,T1,T2,W1,W2,S1,S2,A1,A2
      INTEGER SRD,ZFACT
      REAL L
C
C
      JJ = 0
      LSA = 0
      LSB = 0
      LSC = 0
      LSD = 0
      NODEA = NODE1
      W = W1
      NNY = 2*(SRD + LRD) + IDEL(1) + IDEL(2) + NELSL
      JPOS = SRD + IDEL(1)
      KPOS = JPOS + LRD
      LPOS = KPOS + NELSL
      MPOS = LPOS + LRD
      NPOS = MPOS + IDEL(2)
C*********************************************************************
      DO 600 I = 1,NNY
C*********************************************************************
      IF(NELSX) 112,112,300
  112 IF(I - SRD) 120,120,116
  116 IF(I - NPOS) 124,124,118
  118 W = W2
  120 NNZ = NELSZ
      INCZ = NELSZ + 1
      IF(MODEL - 3) 126,122,122
  122 NNZ = NELSZ + 1
      GO TO 126
  124 NNZ = 2 * NELSZ
      INCZ = (NELSZ * 2) + 1
  126 IOP = 0
C
C-----GENERATES 2/D ELEMENTS-----------------------------------------
C
C*********************************************************************
      DO 230 J = 1,NNZ
C*********************************************************************
      NEL = NEL + 1
      NUMEL(J) = NEL
C-----SPECIFIC MATERIAL ASSIGNMENTS----------------------------------
      NMAT = 1
      IF(I - SRD) 130,130,136
  130 IF(MODEL - 3) 156,132,132
  132 NMAT = NMAT + 2
      IF(LODMOD - 4) 140,134,134
  134 NMAT = NMAT + 2
      GO TO 140
```

```
  136 IF(I - NPOS) 150,150,138
  138 NMAT = 2
      IF(MODEL - 3) 152,132,132
C-----FREE SPAN CONNECTOR GRID FOR CONFORMING LAP JOINT GENERATED------
  140 NN(J,1) = NODEA + (J - 1)
      NN(J,3) = NN(J,1) + INCZ
      NN(J,2) = NN(J,3) + 1
      NN(J,4) = NN(J,1) - 1
      IF(J - 1) 144,144,142
  142 IF(J - NNZ) 148,146,146
  144 NN(J,4) = NN(J,3)
      GO TO 194
  146 NN(J,2) = NN(J,3)
      NN(J,3) = NN(J,4)
      GO TO 194
  148 NN(J,4) = NODEA + (J - 2)
      NN(J,1) = NN(J,4) + 1
      NN(J,3) = NN(J,1) + INCZ
      NN(J,2) = NN(J,3) + 1
      GO TO 194
  150 IF(J - NELSZ) 156,156,152
  152 NMAT = 2
      IF(LODMOD - 4) 156,154,154
  154 NMAT = 4
C-----GENERATION OF OVERLAP 2/D ELEMENT GRID--------------------------
  156 IF(I - SRD) 190,190,158
  158 IF(I - NPOS) 160,160,190
  160 IF(I -(MPOS + 1)) 162,168,164
  162 IF(I - JPOS) 164,164,190
  164 INCZ = 2 * (NELSZ + 1)
  168 IF(J - NELSZ) 190,190,170
  170 NN(J,4) = NODEA + J
      IF(I - JPOS) 192,174,172
  172 IF(I - (MPOS + 1)) 190,176,192
  174 INCZ = (2 * NELSZ) + 1
      GO TO 192
  176 INCZ = 2 * (NELSZ + 1)
  190 NN(J,4) = NODEA + (J - 1)
  192 NN(J,1) = NN(J,4) + 1
      NN(J,3) = NN(J,4) + INCZ
      NN(J,2) = NN(J,3) + 1
  194 CONTINUE
C
C-----SAVES 2/D ELEMENTS FOR SAPLOT-----------------------------------
C
      IF(IPLOT - 1) 210,206,195
  195 IF(IPLOT - 3) 206,202,196
  196 IF(IPLOT - 5) 204,210,197
  197 IF(IPLOT - 7) 210,198,198
  198 IF(I - 1) 210,210,199
  199 IF(I - NNY) 200,210,210
  200 IF(IPLOT - 8) 206,202,204
  202 IF(I - KPOS) 206,206,210
  204 IF(I - LPOS) 210,210,206
  206 WRITE(IPL,9010) NUMEL(J),(NN(J,M),M = 1,4),NMAT,IOP,W
 9010 FORMAT(6I5,20X,I5,5X,F10.2)
```

```
C
C-----SAVES 2/D ELEMENT CENTROID COORDINATES FOR STRESS PLOTTING,FILE =
C
  210 IF(ISTRES - 1) 220,212,212
  212 IF(I - 1) 220,220,214
  214 IF(I - NNY) 216,220,220
  216 READ(9,3000) CXVECT,CYVECT,CZVECT
 3000 FORMAT (3A4)
      WRITE (IST,9030) NUMEL(J),CXVECT,CYVECT,CZVECT
 9030 FORMAT (I5,3F15.5)
  220 WRITE(IO,9010) NUMEL(J),(NN(J,M),M = 1,4),NMAT,IOP,W
  230 CONTINUE
C*********************************************************************
      IF(I - NPOS) 236,232,236
  232 NPZ = NELSZ + 1
      NODEA = NN(NPZ,3)
      GO TO 240
  236 NODEA = NN(1,3)
  240 NODSAV = NODEA
      GO TO 550
  300 CONTINUE
C
C-----21-NODE 3/D ELEMENT GENERATION-------------------------------
C
      NNX = NELSX
      IF(I - SRD) 312,312,310
  310 IF(I - NPOS) 314,314,312
  312 NNZ = NELSZ
      GO TO 316
  314 NNZ = 2 * NELSZ
  316 IREUSE = 0
      IOP = 1
      NDIS = 21
      NXYZ = 8
      INTRS = 3
      INTT = 2
C*********************************************************************
      DO 540 J = 1,NNZ
C
      DO 500 K = 1,NNX
C*********************************************************************
      NEL = NEL + 1
      NUMEL(K) = NEL
      IREUSE = 0
      IF(K - 1) 330,330,322
  322 IF(K - NNX) 324,330,330
  324 IREUSE = 1
      IF(I - 1) 330,326,326
  326 IF(I - NNY) 330,328,328
  328 IREUSE = 0
  330 CONTINUE
      INCRE1 = 2 + (3 * (NELSX + NELSZ)) + (5 * NELSX * NELSZ)
      INCRE2 = (3 * NELSX * NELSZ) + (2 * (NELSX + NELSZ)) - (K - 2) -
     1 ((NELSX + 1) * (J - 1))
C-----SPECIFIC MATERIAL ASSIGNMENT---------------------------------
      IF(I - SRD) 332,332,334
```

```
  332 NMAT = 1
      IF(MODEL - 3) 370,372,372
  334 IF(I - NPOS) 350,350,336
  336 NMAT = 2
      IF(LODMOD - 4) 340,338,338
  338 NMAT = 4
  340 IF(MODEL - 3) 374,376,376
  350 INCRE1 = 2 + (3 * (NELSX + (2 * NELSZ))) + (10 * NELSX * NELSZ)
      INCRE2 = (6 * NELSX * NELSZ) + (2 * (NELSX + (2 * NELSZ))) -
     1 (K - 2) - ((NELSX + 1) * (J -1))
      IF(J - NELSZ) 352,352,354
  352 NMAT = 1
      IF(I - (MPOS + 1)) 355,366,360
  354 NMAT = 2
      IF(LODMOD - 4) 358,356,356
  355 IF(I - JPOS) 360,360,370
  356 NMAT = 4
  358 IF(I - JPOS) 362,364,359
  359 IF(I -(MPOS + 1)) 374,362,362
  360 INCRE1 = INCRE1 + (3 * NELSX)  + 2
      INCRE2 = INCRE2 + (2 * NELSX) + 1
      GO TO 370
  362 INCRE1 = INCRE1 + (3 * NELSX) + 2
      INCRE2 = INCRE2 + NELSX + 1
      GO TO 374
  364 INCRE1 = INCRE1 + NELSX + 1
      INCRE2 = INCRE2 + NELSX + 1
      GO TO 374
  366 INCRE1 = INCRE1 + NELSX + 1
C-----SELECTS MATERIAL AXIS ORIENTATIONS-------------------------------
  370 IF(MATAXS -1) 382,384,384
  372 IF(MATAXS - 1) 384,386,386
  374 IF(MATAXS - 1) 382,384,382
  376 IF(MATAXS - 1) 384,386,388
  382 MAXES = 0
      GO TO 390
  384 MAXES = 1
      GO TO 390
  386 MAXES = 2
      GO TO 390
  388 MAXES = 3
  390 IF(I - SRD)410,410,392
  392 IF(I - NPOS) 394,394,410
  394 IF(J - NELSZ) 410,410,396
  396 IF(I - JPOS) 400,400,398
  398 IF(I - (MPOS + 1)) 410,410,400
C-----CALCULATES NODE NO.'S ASSOCIATED WITH EACH 3/D ELEMENT-----------
  400 NN(K,4) = NODEA + (2 * (K - 1)) + (2 * NELSX) +1
      GO TO 412
  410 NN(K,4) = NODEA + (2 * (K -1))
  412 NN(K,3) = NN(K,4) + 2
      NN(K,1) = NN(K,4) + INCRE1
      NN(K,2) = NN(K,1) + 2
      NN(K,5) = NN(K,1) + (2 + (NELSX * 3))
      NN(K,6) = NN(K,5) + 2
      NN(K,7) = NN(K,6) - INCRE1
```

```
      NN(K,8) = NN(K,7) - 2
      NN(K,9) = NN(K,1) + 1
      NN(K,12) = NN(K,4) + INCRE2
      NN(K,11) = NN(K,4) + 1
      NN(K,10) = NN(K,12) + 1
      NN(K,13) = NN(K,5) + 1
      NN(K,14) = NN(K,10) + 1 + (2 * NELSX)
      NN(K,15) = NN(K,13) - INCRE1
      NN(K,16) = NN(K,14) - 1
      NN(K,17) = NN(K,1) + (2 * NELSX) + 1 - (K - 1)
      NN(K,18) = NN(K,17) + 1
      NN(K,19) = NN(K,18) - INCRE1
      NN(K,20) = NN(K,19) - 1
      NN(K,21) = NN(K,10) + NELSX
      IF(I - NPOS) 418,416,418
  416 IF(J - (NELSZ + 1)) 418,422,424
  418 IF(J - 1) 424,420,424
  420 IF(K - 1) 424,422,424
  422 NODSAV = NN(1,1)
  424 CONTINUE
C
C-----SAVES 3/D ELEMENTS FOR SAPLOT-----------------------------------
C
      IF(IPLOT - 1) 475,470,450
  450 IF(IPLOT - 3) 470,466,452
  452 IF(IPLOT - 5) 468,475,454
  454 IF(IPLOT - 7) 475,456,456
  456 IF(I - 1) 475,475,458
  458 IF(I - NNY) 464,475,475
  464 IF(IPLOT - 8) 470,466,468
  466 IF(I - KPOS) 470,470,475
  468 IF(I - LPOS) 475,475,470
  470 WRITE(IPL,9020) NUMEL(K),NDIS,NXYZ,NMAT,MAXES,IOP,INTRS,INTT,
     1 IREUSE,LSA,LSB,LSC,LSD,(NN(K,M),M=1,21)
 9020 FORMAT(6I5,15X,3I5,4I2,/,16I5)
C-----SAVES 3/D ELEMENT CENTROID COORDINATES FOE STRESS PLOTTING,FILE
  475 IF(ISTRES - 1) 480,478,478
  478 READ(9,3000) CXVECT,CYVECT,CZVECT
      WRITE (IST,9030) NUMEL(K),CXVECT,CYVECT,CZVECT
  480 WRITE(IO,9020) NUMEL(K),NDIS,NXYZ,NMAT,MAXES,IOP,INTRS,INTT,
     1 IREUSE,LSA,LSB,LSC,LSD,(NN(K,M),M=1,21)
  500 CONTINUE
C*********************************************************************
      IF(J - NNZ) 510,540,540
  510 NODEA = NODEA + (3 * NELSX) + 2
  540 CONTINUE
      NODEA = NODSAV
  550 CONTINUE
  600 CONTINUE
      NODE1 = NODSAV
      RETURN
      END
C*********************************************************************
C
C   THIS SUBROUTINE DISTRIBUTES THE LOAD TO INDIVIDUAL NODAL POINTS
C   THE VALUE OF LODMOD.  DISTRIBUTION IS DETERMINED ON THE BASIS OF
```

```
C   LOAD BEING DIVIDED INTO NELSX VERTICAL STRIPS AND THEN THE NODES
C   A LOAD VALUE PROPORTIONAL TO THEIR PART OF THIS VERTICAL STRIP LOAD
C
C*********************************************************************
C
      SUBROUTINE LOAD (LOADPT,LL,CRITLD)
      DIMENSION LOADPT(1),YZLOAD(10),LCASE(10),X(10),Y(10),Z(10)
      COMMON NELSX,NELSY,NELSZ,NELSL,SRD,LRD,IDEL(2),ZFACT
      COMMON MODEL,LODMOD,MATAXS,IPLOT,IFRACT,ISTRES,IPL,IFR,IST,IO
      COMMON L,T1,T2,W1,W2,S1,S2,A1,A2
C
C   LODMOD IS THE LOAD MODEL TYPE: WHERE0,2,6=CANTILEVER; 1=UNIFORM
C    3=PERIMETER LOAD; 4,5,7=GLUE CONNECTION; 8,9=GLUE SIMULATOR.  IF
C   2/D MODEL IS ASSUMED.
C
      JJ=0
      NNZ=NELSZ+1
      NNX=(NELSX*2)+1
      IF(LOADPT(2)) 1,1,2
    1 NNZ=1
      NNX=1
    2 CONTINUE
      IF(CRITLD) 6,5,6
    5 READ(5,1000) (YZLOAD(M),M=1,8)
 1000 FORMAT(8F10.0)
      GO TO 7
    6 CONTINUE
      YZLOAD(1)=CRITLD
    7 CONTINUE
      IF(NELSX) 9,9,8
    9 CONTINUE
      IF(LODMOD-6) 12,14,13
   12 CONTINUE
      IF(LODMOD-3) 14,14,13
   13 NNZ=3
      GO TO 14
    8 CONTINUE
      NNZ=(2*NELSZ)+1
      IF(LOADPT(2)) 11,11,14
   11 NNZ=1
   14 CONTINUE
C*********************************************************************
      DO 930 I=1,NNZ
C
      DO 920 J=1,NNX
C
      DO 920 K=1,LL
C*********************************************************************
      LCASE(K)=K
      IF(LODMOD-6) 15,10,25
   15 CONTINUE
      IF(LODMOD-3) 20,400,200
   20 CONTINUE
      IF(LODMOD-1) 10,100,10
   25 CONTINUE
      IF(LODMOD-8) 200,300,300
```

```
C
C    CANTILVER BEAM WITH CENTERLINE POINT END LOAD
C
   10 CONTINUE
      X(K)=0.0
      Y(K)=0.0
      Z(K)=YZLOAD(K)
      GO TO 900
C
C    2/D MODELS
C
  100 CONTINUE
      IF(NELSX) 110,110,500
  110 CONTINUE
      X(K)=0.0
      Z(K)=0.0
C
C    MODELS WITH UNIFORM LOAD
C
      Y(K)=YZLOAD(K)/NELSZ
      IF(I-1) 122,122,123
  122 CONTINUE
      Y(K)=Y(K)/2
      GO TO 900
  123 CONTINUE
      IF(I-NNZ) 900,122,122
  200 CONTINUE
      IF(NELSX) 210,210,600
C
C    MODELS WITH GLUE CONNECTION
C
  210 CONTINUE
      Z(K)=0.0
      X(K)=0.0
      Y(K)=YZLOAD(K)/2
      IF(I-2) 212,900,212
  212 Y(K)=Y(K)/2
      GO TO 900
  300 CONTINUE
      IF(NELSX) 310,310,700
C
C    MODELS WITH GLUE SIMULATION
C
  310 CONTINUE
  400 CONTINUE
      IF(NELSX) 410,410,800
C
C    MODELS WITH PERIMETER LOAD
C
  410 CONTINUE
      IF(I-1) 413,413,412
  412 CONTINUE
      IF(I-NNZ) 920,413,413
  413 CONTINUE
      X(K)=0.0
      Z(K)=0.0
```

```
      Y(K)=YZLOAD(K)/2
      GO TO 900
C
C   3/D MODELS
C
  500 CONTINUE
C
C   MODELS WITH UNIFORM LOAD
C
      X(K)=0.0
      Z(K)=0.0
      Y(K)=YZLOAD(K)/((NELSX*2)*NELSZ)
      IK=I/2
      KK=IK*2
      IF(KK-I) 511,520,511
  511 CONTINUE
      JK=J/2
      KK=JK*2
      IF(KK-J) 520,530,520
  520 CONTINUE
      IF(J-1) 521,521,522
  521 CONTINUE
      Y(K)=Y(K)/4.0
      GO TO 530
  522 CONTINUE
      IF(J-NNX) 523,521,521
  523 CONTINUE
      Y(K)=Y(K)/2.0
  530 CONTINUE
      IF(I-1) 532,532,531
  531 CONTINUE
      IF(I-NNZ) 900,532,532
  532 CONTINUE
      Y(K)=Y(K)/2.0
      GO TO 900
  600 CONTINUE
C
C   MODELS WITH GLUE CONNECTION
C
      X(K)=0.0
      Y(K)=YZLOAD(K)
      Z(K)=0.0
      GO TO 900
  700 CONTINUE
C
C   MODELS WITH GLUE SIMULATION
C
  800 CONTINUE
C
C   MODELS WITH PERIMETER LOAD
C
      Y(K)=YZLOAD(K)/(2*NELSX*NELSZ)
      IF(I-1) 801,801,805
  801 CONTINUE
      IF(J-1) 802,802,803
  802 Y(K)=Y(K)/8
```

```
      GO TO 810
  803 IF(J-NNX) 810,804,804
  804 Y(K)=Y(K)/2
      GO TO 810
  805 IF(I-NNZ) 806,801,801
  806 CONTINUE
      IF(J-1) 807,807,920
  807 Y(K)=Y(K)/4
  810 CONTINUE
      X(K)=0.0
      Z(K)=0.0
  900 CONTINUE
      JJ=JJ+1
      IF(JJ-1) 901,901,902
  901 WRITE(6,1010)
 1010 FORMAT('0',15X,'NODE LOADS')
  902 CONTINUE
      WRITE(6,1013)  LOADPT(JJ),LCASE(K),X(K),Y(K),Z(K)
      WRITE(IO,1011) LOADPT(JJ),LCASE(K),X(K),Y(K),Z(K)
      WRITE (IFR,1011) LOADPT(JJ),LCASE(K),X(K),Y(K),Z(K)
      WRITE(IFR,1012)
 1011 FORMAT(2I5,3F10.4)
 1013 FORMAT('0',2I5,3F10.4)
  920 CONTINUE
C*********************************************************************
C
C   REDEFINITION OF NNX
C
      IK=I/2
      KK=IK*2
      IF(KK-I) 921,922,921
  921 CONTINUE
      NNX=NELSX+1
      GO TO 930
  922 CONTINUE
      NNX=(NELSX*2)+1
  930 CONTINUE
C
C   INSERTION OF LL+1  BLANK CARDS AT PROBLEM END
C
      LLAD1=LL+1
      DO 940 L=1,LLAD1
  940 WRITE(IO,1012)
 1012 FORMAT (80X)
      RETURN
      END
C-----REORDR SORT ROUTINE TO SORT A REAL VECTOR & CARRY AN INTEGER-----
C-----VECTOR ALONG FOR A LENGTH OF N-----------------------------------
      SUBROUTINE REORDR(INTARY,NNTARY,N)
      REAL      INTARY(1)
      DIMENSION NNTARY(1)
      M=N
200   M=M/2
      IF(M) 300,40,300
300   K=N-M
      J=1
```

```
41    I=J
49    LL=I+M
      IF(INTARY(I)-INTARY(LL)) 60,60,50
50     S=INTARY(I)
      NS = NNTARY(I)
      NNTARY(I) = NNTARY(LL)
      INTARY(I)=INTARY(LL)
      INTARY(LL)=S
      NNTARY(LL) = NS
      I=I-M
      IF(I-1) 60,49,49
60    J=J+1
      IF(J-K) 41,41,200
40    RETURN
      END
```

APPENDIX VIII

FORTRAN IV LISTING: FRACTR - COMPUTER PROGRAM FOR CALCULATING FRACTURE PARAMETERS

```
/JOB GO,TIME=99
C     ************************************************************************
C     *                    ********  FRACTR  ********                         *
C     *     PROGRAM FOR CALCULATING FRACTURE PARAMETERS THROUGH APPLI-  *
C     *     CATION OF EXPANDED DISPLACEMENT FIELD EQUATIONS TO DIS-     *
C     *     PLACEMENT CALCULATION ON LAP JOINT STRUCTURES UTILIZING A   *
C     *     GENERAL PURPOSE FINITE ELEMENT STRUCTURAL ANALYSIS PROGRAM, *
C     *     SAP IV (A STATIC, LINEAR ELASTIC MODEL ASSUMED).            *
C     *             7/5/78, BY  ALAN F. BUTTON                          *
C     ************************************************************************
C
      COMMON A(10,10),A1(22),A2(22)
      COMMON  HED(10),HEDIFR(20),DHED(20),PLTHED(20),IFR
      COMMON  MAXIJK(4),ANGL(4,7),D(4,3),E(2,9),C(3),SVAL(10)
      COMMON XX(22),Y1(22),Y2(22),YG(22),LX(6),LY1(6),LY2(6),LYG(10)
C
      DIMENSION NTIP(4),NP(4,7,20),RADIUS(4,7,20),LOADPT(100),
     1 DX(4,7,20),DR(4,7,20),DT(4,7,20),YLOAD(100),HEDSP(10)
C
      DOUBLE PRECISION A
      INTEGER ELMENT
      REAL LAMBDA,MU,KA
C
      RADIAN = 57.29578
      PI = 3.1415927
      ETOUGH = 5465.8
      IFR = 2
      IDSP = 1
C
      DO 10 I = 1,4
      DO 10 J = 1,3
   10 D(I,J) = 0.0
      DO 20 I = 1,6
      DO 20 J = 1,7
   20 A(I,J) = 0.0
C
      READ (5,1200) HEDSP
C     WRITE (6,1101) HEDSP
  100 READ (5,1100) HED,ELMENT,MODEL,LODMOD
 1100 FORMAT(10A4,8X,3I1)
      IF(ELMENT)600,600,102
  102 WRITE (6,1101) HED,ELMENT,MODEL,LODMOD
 1101 FORMAT(' ',10A4,8X,3I5)
      ENER = ENERJ
      ENERJ = 0.0
      RESL = RESLL
  103 READ (IFR,1110) HEDIFR
 1110 FORMAT(20A4)
      IF(ICOMP(HEDIFR,1,HED,1,40)) 103,118,103
  118 READ (IFR,1120) NELSX,NMAT,MATAXS,W
C     WRITE(6,1111) HEDIFR,NELSX,NMAT,MATAXS,W
C1111 FORMAT(' ',20A4,3I5,F7.1)
 1120 FORMAT(3I5,F7.1)
      M = 0
      IF(NELSX) 105,105,107
```

```
  105 MAXIK = 2
      GO TO 110
  107 MAXIK = 4
  110 CONTINUE
C*******************************************************************************
      DO 125 K = 1,MAXIK
C*******************************************************************************
      READ (IFR,1130) IK,MAXN,NPN,RESLL
C     WRITE(6,1131) IK,MAXN,NPN,RESLL
C1131 FORMAT(' ',3I5,F10.3)
      MAXIJK(IK) = MAXN
      NTIP(IK) = NPN
 1130 FORMAT(3I5,F10.0)
      READ (IFR,1140) (ANGL(IK,I),I = 1,7)
C1141 FORMAT(' ',7(F7.5,4X))
 1140 FORMAT(7(F7.5,4X))
      READ (IFR,1150) ((NP(IK,L,J),RADIUS(IK,L,J),L = 1,7),J = 1,MAXN)
C     WRITE(6,1151) ((NP(IK,L,J),RADIUS(IK,L,J),L=1,7),J=1,MAXN)
C1151 FORMAT(' ',7(I4,F7.3))
 1150 FORMAT(7(I4,F7.3))
  125 CONTINUE
      READ (5,1160) JINT,MATMOD,IPLOT,LAMBDA,(SVAL(I),I = 1,6)
 1160 FORMAT(3I3,1X,7F10.0)
C     WRITE(6,1161) JINT,MATMOD,IPLOT,LAMBDA,(SVAL(I),I = 1,6)
C1161 FORMAT(' ',3I3,1X,7F10.2)
C
      CALL ELAST (NELSX,MATAXS,LODMOD,MATMOD,ELMENT,MU,KA)
C
      M = 0
      IF(NELSX) 126,126,130
  126 IF(MODEL - 2) 130,130,127
  127 CONTINUE
      DO 128 I = 1,4
  128 READ(IFR,1110) CRD
  130 READ (IFR,1170) LPT,LL,YL
      IF(LPT) 140,140,135
  135 M = M + 1
      LOADPT(M) = LPT
      YLOAD(M) = YL
C     WRITE(6,1171) LPT,LL,YL
C1171 FORMAT(' ',2I5,10X,F10.4)
      IF(M-3) 130,140,140
  140 CONTINUE
 1170 FORMAT(2I5,10X,F10.4)
  200 READ(IDSP,1200) HED
 1200 FORMAT(10A4)
      IF(ICOMP(HED,2,HEDIFR,1,39)) 200,215,200
  215 READ (IDSP,1110) DHED
      NT = 0
      IF(ICOMP(HEDSP,1,DHED,1,28)) 215,220,215
C 218 WRITE(6,1211) N,X,Y,Z
C1211 FORMAT(' ',1X,I6,8X,3E14.5)
  220 NT = NT + 1
      IF(LOADPT(M) - NT) 270,222,222
  222 READ (IDSP,1210) N,X,Y,Z
 1210 FORMAT(1X,I6,8X,3E14.5)
```

```
C*************************************************************************
      DO 230 MM = 1,M
C*************************************************************************
C-----SELECTS DISPLACEMENTS FROM IDSP (SAP IV OUTPUT) CORRESPONDING TO----
C-----THE NODES TO WHICH LOADS  WERE APPLIED.  USED TO CALCULATE STORED---
C-----ELASTIC ENERGY (ENERJ).                                          ----
C-----------------------------------------------------------------------
      IF(ICOMP(N,1,LOADPT(MM),1,4)) 230,225,230
  225 ENERJ = ENERJ + (Y * YLOAD(MM))/2
      IF(MM - 2) 220,226,220
  226 IF(JINT) 220,227,220
  227 DISPCL = Y
      GO TO 220
  230 CONTINUE
C*************************************************************************
      DO 260 II = 1,MAXIK
C*************************************************************************
C-----SELECTS DISPLACEMENTS FROM IDSP CORRESPONDING TO THE NODE LOCATED---
C-----AT THE CRACK(NOTCH) TIP. USED TO CALCULATE THE DISPLACEMENTS     ---
C-----RELATIVE TO THE CRACK TIP.                                      ---
C-----------------------------------------------------------------------
      IF(ICOMP(N,1,NTIP(II),1,4)) 240,235,240
  235 D(II,1) = X
      D(II,2) = Y
      D(II,3) = Z
      GO TO 220
  240 CONTINUE
C*************************************************************************
      DO 260 JJ = 1,7
C
      IJK = MAXIJK(II)
C
      DO 260 KK = 1,IJK
C*************************************************************************
C-----SELECTS DISPLACEMENTS FROM IDSP CORRESPONDING TO THE NODES LOCATED--
C-----ALONG EACH OF 7 RADII AT EACH CRACK TIP. USED IN CONJUNCTION WITH --
C-----NTIP ABOVE.                                                      --
C-----------------------------------------------------------------------
      IF(NP(II,JJ,KK)) 260,260,242
  242 IF(ICOMP(N,1,NP(II,JJ,KK),1,4)) 260,245,260
  245 DX(II,JJ,KK) = X
      DR(II,JJ,KK) = Y
      DT(II,JJ,KK) = Z
      IF(II - 1) 252,252,220
  252 IF(JJ - 1) 254,254,220
  254 JK = KK + 1
      IF(NP(II,JJ,JK)) 270,270,220
  260 CONTINUE
      GO TO 220
  270 CONTINUE
      SLOPE = (D(2,3) - D(1,3))/RESLL
      ROTA = ATAN(SLOPE)
      RO   = ROTA * RADIAN
      WRITE (6,3040) RO
 3040 FORMAT(' DEGREES OF ROTATION =',F8.2)
      ROTA = 0.0
```

```
      ORIG = ANGL(2,2)
      DO 300 J = 1,7
      IF(ANGL(2,J) - ORIG) 275,280,285
  275 ANGL(2,J) = ANGL(2,J) + ORIG + ROTA
      GO TO 290
  280 ANGL(2,J) = 0.0 + ROTA
      GO TO 290
  285 ANGL(2,J) = ANGL(2,J) - ORIG + ROTA
  290 ANGL(1,J) = ANGL(1,J) + ROTA
      ANGL(3,J) = ANGL(1,J)
      ANGL(4,J) = ANGL(2,J)
  300 CONTINUE
C*******************************************************************************
      DO 500 I = 1,MAXIK
C
      WRITE(6,2001) I
 2001 FORMAT(' CRACK TIP =',I3/80X)
C
      DO 450 J = 1,7
C
      NN = 0
      IJK = MAXIJK(I)
C
      DO 400 K = 1,IJK
C*******************************************************************************
      M = 0
      KK = K
  310 IF(NP(I,J,KK)) 400,400,315
C-----DX IS A TEMPORARY SETUP PENDING RESOLUTION OF THE 3/D MODELS--------
  315 Y =      DR(I,J,KK)- D(I,2)
      Z =      DT(I,J,KK)- D(I,3)
      DXTEMP     = DX(I,J,KK) - D(I,1)
      DRTEMP     = (COS(ANGL(I,J)) * Y) + (SIN(ANGL(I,J)) * Z)
      DTTEMP     = (-SIN(ANGL(I,J)) * Y) + (COS(ANGL(I,J)) * Z)
C     WRITE(6,3020) DXTEMP,DRTEMP,DTTEMP
C3020 FORMAT(' ',3E15.5)
      COEFR1 = ((RADIUS(I,J,KK)/(2 * PI)) ** LAMBDA)/(4 * MU)
      COEFR2 = RADIUS(I,J,KK)/(2 * MU)
      COEFR3 = RADIUS(I,J,KK)/MU
      M = M + 1
      A(M,1) = COEFR1 * (((2 * KA) - 1) * COS(ANGL(I,J)/2)
     1 - (COS((3 * ANGL(I,J))/2)))
      A(M,2) = -COEFR1 * (((2 * KA) - 1) * SIN(ANGL(I,J)/2)
     1 -3 * SIN((3 * ANGL(I,J))/2))
      A(M,3) = COEFR2 * (KA - 1 + 2 * COS(2 * ANGL(I,J)))
      A(M,4) = 0.0
      A(M,5) = DRTEMP
      N = M + 2
      A(N,1) = COEFR1 * (SIN(3 * (ANGL(I,J)/2))
     1 - (1 + (2 * KA)) * SIN(ANGL(I,J)/2))
      A(N,2) = -COEFR1 * (((2 * KA) + 1) * COS(ANGL(I,J)/2)
     1 - 3 * COS((3 * ANGL(I,J))/2))
      A(N,3) = -COEFR3 * SIN(2 * ANGL(I,J))
      A(N,4) =  COEFR3 * (KA + 1)
      A(N,5) = DTTEMP
      KK = K + 1
```

```
      IF(M - 1) 310,310,325
  325 CONTINUE
C     WRITE(6,3000) J,K,((A(IJ,JJ),JJ=1,5),IJ=1,4)
C3000 FORMAT(' A MATRIX =',2I2/(5E15.5))
C
      CALL SIMEQ(A,4,5)
C
      THETA =(ANGL(I,J) - ROTA) * RADIAN + 0.1
      XX(K) = ((RADIUS(I,J,K) + RADIUS(I,J,KK))/2)
      YG(K)=(C(1)*A(1,5)* A(1,5) + C(2) * A(2,5) * A(2,5)) * PI
      Y1(K) =DABS(A(1,5))
      Y2(K) =DABS(A(2,5))
      A1(K) =DABS(A(3,5))
      A2(K) =DABS(A(4,5))
      NN = NN + 1
  400 CONTINUE
      IF(NP(I,J,2)) 445,445,405
  405 IF(IPLOT) 420,420,410
C
  410 CALL GRAFIT(I,J,NN,THETA,MAXIK)
C
  420 CONTINUE
      DO 442 JK = 1,NN
      IF(JK - 1) 442,430,440
  430 WRITE(6,2000) THETA,XX(1),Y1(1),Y2(1),A1(1),A2(1),YG(1)
 2000 FORMAT('1    ANGLE  RADIUS(AV.)',5X,'K1',13X,'K2',11X,'ALPHA1',
     1 9X,'ALPHA2',12X,'G'//F10.0,F10.3,5E15.5)
      GO TO 442
  440 WRITE(6,2010) XX(JK),Y1(JK),Y2(JK),A1(JK),A2(JK),YG(JK)
 2010 FORMAT(' ',9X,F10.3,5E15.5)
  442 CONTINUE
  445 CONTINUE
  450 CONTINUE
  500 CONTINUE
      IF(ELMENT - 2) 530,550,540
  530 ENERJ = ENERJ * W
      GO TO 550
  540 ENERJ = ENERJ * 2
  550 WRITE(6,3010) ENERJ
 3010 FORMAT('0  STORED ELASTIC ENERGY =',E15.5/)
      IF(JINT) 100,100,555
  555 FTOUGH =((ENERJ - ENER)/((RESL - RESLL) * W)) * 10000.0
      SRATIO = SQRT(ETOUGH/FTOUGH)
      WRITE (7,4000) DISPCL,FTOUGH,SRATIO
 4000 FORMAT (3F10.4)
      WRITE (6,3110) FTOUGH,SRATIO
 3110 FORMAT('0  FRACTURE TOUGHNESS =',E15.5,'ERGS/CM**2'///'   STREN',
     1 'GTH RATIO ='E15.5////)
      GO TO 100
  600 CONTINUE
      STOP
      END
      SUBROUTINE  ELAST(NELSX,MATAXS,LODMOD,MATMOD,ELMENT,MU,KA)
C
C     *  THIS SUBROUTINE GENERATES THE COMPLIANCE MATRIX FOR USE         *
C     *  IN THE EXPANDED DISPLACEMENT FIELD EQUATIONS AND THE STRAIN     *
```

```
C      *  ENERGY RELEASE RATE CALCULATIONS OF ** FRACTR ** .              *
C
       COMMON A(10,10),A1(22),A2(22)
       COMMON HED(10),HEDIFR(20),DHED(20),PLTHED(20),IFR
       COMMON MAXIJK(4),ANGL(4,7),D(4,3),E(2,9),C(3),SVAL(10)
C
       DOUBLE PRECISION A
       INTEGER ELMENT
       REAL MU,KA,NU
C
       DIMENSION S(2,6,6)
C
       DO 10 I = 1,2
       DO 10 J = 1,6
       DO 10 K = 1,6
    10 S(I,J,K) = 0.0
       M = 0
       IF(NELSX) 100,100,150
   100 M = M + 1
       READ (IFR,1100)(E(M,I),I = 1,7)
C      WRITE(6,1101) (E(M,I),I=1,7)
C1101 FORMAT(' ',10X,3E12.4,3E9.4,E12.4)
  1100 FORMAT(80X/10X,7F10.0)
       IF(M - 1) 110,110,170
   110 IF(LODMOD - 4) 100,115,115
   115 CONTINUE
       DO 120 J = 1,4
   120 READ (IFR,1110) CRD
  1110 FORMAT(20A4)
       GO TO 100
   150 M = M + 1
       READ (IFR,1120)(E(M,I),I = 1,9)
  1120 FORMAT(80X,/,10X,6F10.0/3F10.0)
       IF(M - 1) 155,155,170
   155 IF(LODMOD - 4) 150,160,160
   160 CONTINUE
       DO 165 K = 1,6
   165 READ (IFR,1110) CRD
       GO TO 150
   170 CONTINUE
C-----FORMATION OF THE COMPLIANCE MATRIX FOR 2/D STRUCTURAL MODELS-------------
       DO 225 M=1,2
       S(M,1,1) = 1/E(M,1)
       S(M,2,2) = 1/E(M,2)
       S(M,3,3) = 1/E(M,3)
       S(M,1,2) = -E(M,4)/E(M,2)
       S(M,1,3) = -E(M,5)/E(M,3)
       S(M,2,3) = - E(M,6)/E(M,3)
       S(M,4,4) = 1/E(M,7)
       S(M,2,1) = S(M,1,2)
       S(M,3,1) = S(M,1,3)
       S(M,3,2) = S(M,2,3)
       IF(NELSX) 230,230,200
C-----ADDITIONAL CONSTANTS FOR 3/D-------------------------------------------
   200 S(M,5,5) = 1/E(M,9)
       S(M,6,6) = 1/E(M,8)
```

```
      IF(MATAXS - 1) 230,220,210
  210 IF(M - 1) 220,220,230
C-----REARRANGE COMPLIANCE MATRIX FOR 3/D MATERIAL AXIS ORIENTATIONS-----------
  220 STEMP = S(M,1,1)
      S(M,1,1) = S(M,2,2)
      S(M,2,2) = STEMP
      STEMP = S(M,2,3)
      S(M,2,3) = S(M,1,3)
      S(M,3,2) = S(M,1,3)
      S(M,1,3) = STEMP
      S(M,3,1) = S(M,1,3)
      STEMP = S(M,5,5)
      S(M,5,5) = S(M,6,6)
      S(M,6,6) = STEMP
  225 CONTINUE
  230 IF(MATMOD - 2) 235,245,270
C-----ISOTROPIC, PLANE STRAIN CASE-------------------------------------------
  235 M = M + 1
      C(1) =  (1 - (E(1,4) * E(1,4)))/E(1,1)
      C(2) = C(1)
      C(3) = (1 - E(1,4))/E(1,1)
      MU = E(1,7)
      KA = 3 - 4 * E(1,5)
      IF(ELMENT - 2) 300,240,280
C-----ISOTROPIC, PLANE STRESS CASE-------------------------------------------
  240 C(1) = 1/E(1,1)
      C(2) = C(1)
      KA = (3 - E(1,5))/(1 + E(1,5))
      GO TO 300
  245 CONTINUE
C-----ORTHOTROPIC ELASTICITY CASE (PLANE STRESS, 0 DEGREES ONLY)  ---------
      CT = SQRT(SQRT(S(1,2,2)/S(1,1,1))
     1 +((2*S(1,1,2) + S(1,4,4))/(2*S(1,1,1))))
      C(1) = SQRT(S(1,1,1) * S(1,2,2)/2) * CT
      C(2) = (S(1,1,1)/1.4142136) * CT
      NU = E(1,5)
      KA = 3 - 4 * NU
      MU = E(1,7)
C     WRITE (6,3000) CT,C(1),C(2)
C3000 FORMAT ('0    CT=',E15.5//'    C(1)='E15.5//'    C(2)=',E15.5//)
      IF(ELMENT - 2) 250,300,300
C-----ORTHOTROPIC (PLANE STRAIN CASE)-----------------------------------
  250 CONTINUE
      GO TO 300
C-----BIMATERIAL CASE--------------------------------------------------------
  270 CONTINUE
C-----3/D CASE---------------------------------------------------------------
  280 CONTINUE
  300 CONTINUE
C     WRITE(6,2000) MU,KA,(((S(I,J,K),K=1,6),J=1,6),I=1,2)
C2000 FORMAT(' ',2F10.5//,(6F15.10))
      RETURN
      END
```

```
      SUBROUTINE SIMEQ(A,NR,NC)
C******      SOLUTION OF SIMULTANEOUS LINEAR EQUATIONS
C******          MATRIX OF COEFFICIENTS = A
C******          NR = NUMBER OF ROWS IN A
C******          NC = NUMBER OF COLUMNS IN A
      DIMENSION A(10,10),R(100)
      DOUBLE PRECISION A,R,D,T
      IF(NR - NC) 4,4,3
    3 NCT = NC
      GO TO 5
    4 NCT = NR
    5 K = 1
      D = 1.
    7 IF(A(K,K)) 12,8,12
C******    DIAGONAL=0, FIND A ROW WITH A NON-ZERO ELEMENT
C******    AND INTERCHANGE THE ROWS
    8 DO 9 I = K,NR
      IF(A(I,K)) 10,9,10
    9 CONTINUE
C******   IF THERE IS NO NON-ZERO ELEMENT, PROBLEM IS COMPLETE
      GO TO 17
C******   INTERCHANGE ROW I AND ROW K
   10 DO 11 J = 1,NC
      T = A(I,J)
      A(I,J) = A(K,J)
   11 A(K,J) = T
C******    CORRECT THE SYSTEM OF EQUATIONS FOR ROW K
   12 DO 16 I = 1,NR
      IF(I - K) 13,16,13
   13 DO 14 J = 1,NC
   14 R(J) = (A(I,J)*A(K,K) - A(I,K)*AIK,J))/D
      DO 15 J = 1,NC
   15 A(I,J) = R(J)
   16 CONTINUE
      D = A(K,K)
      K = K + 1
      IF(K - NCT) 7,7,17
C***     DIVIDE EACH ROW BY THE DIAGONAL ELEMENT
   17 DO 20 I = 1,NR
      DIV = A(I,I)
      IF(DIV) 18,20,18
   18 DO 19 J = 1,NC
   19 A(I,J) = A(I,J)/DIV
   20 CONTINUE
      RETURN
      END
      SUBROUTINE GRAFIT(I,J,NN,THETA,MAXIK)
C
      COMMON A(10,10),A1(22),A2(22)
      COMMON HED(10),HEDIFR(20),DHED(20),PLTHED(20),IFR
      COMMON MAXIJK(4),ANGL(4,7),D(4,3),E(2,9),C(3),SVAL(10)
      COMMON XX(22),Y1(22),Y2(22),YG(22),LX(6),LY1(6),LY2(6),LYG(10)
```

```
C
      DOUBLE PRECISION
C
      DIMENSION ISYM(7)
C
      ISYM(1) = 170
      ISYM(2) = 183
      ISYM(3) = 175
      ISYM(4) = 176
      ISYM(5) = 181
      ISYM(6) = 182
      ISYM(7) = 185
      IF(J - 1) 100,5,20
    5 IF(I - 1) 100,10,15
   10 CALL ITLZ
      CALL DPT (1,4)
      READ (5,1000) LX,LY1
      READ (5,1010) LY2,LYG
      READ (5,1020) PLTHED,DHED
 1000 FORMAT(6A4,6X,6A4)
 1010 FORMAT(6A4,6X,10A4)
 1020 FORMAT(20A4/20A4)
   15 CALL PLOT(0.,-11.,-2)
      CALL PLOT(2.5,1.5,-3)
      CALL AXIS(0.,0.,LX,-24,4.,0.,SVAL(1),SVAL(2))
      CALL AXIS(0.,0.,LY2,24,4.,90.,SVAL(1),SVAL(5))
C----ESTABLISH NEW ORIGIN FOR K1 PLOT, DRAWS AND LABELS AXES-----------
      CALL PLOT(0.,5.,-3)
      CALL AXIS(0.,0.,LX,-24,4.,0.,SVAL(1),SVAL(2)
      CALL AXIS(0.,0.,LY1,24,4.,90.,SVAL(1),SVAL(4))
C----ESTABLISHES NEW ORIGIN FOR G PLOT, DRAWS AND LABELS AXES----------
      CALL PLOT(8.,-4.,-3)
      CALL AXIS(0.,0.,LX,-24,6.,0.,SVAL(1),SVAL(3))
      CALL AXIS(0.,0.,LYG,40,6.,90.,SVAL(1),SVAL(6))
C     REESTABLISHES THE ORIGINAL ORIGIN
      CALL PLOT(-8.,-1.,-3)
      CALL SYMBOL(-1.,-.8,.1225,PLTHED,0.,80)
      CALL SYMBOL(.44,-1.05,.1225,HEDIER,0.,52)
      CALL SYMBOL(7.,.2,.12,DHED,0.,80)
      CALL SYMBOL(8.44,-.05,.12,HEDIFR,0.,52)
C     CALL SYMBOL(9.,10.5,.14,'LEGEND',0.,6)
C     CALL SYMBOL(8.64,10.2,.14,'SYMBOL ANGLE",0.,12)
   20 CONTINUE
      XX(NN + 1) = SVAL(1)
      Y1(NN + 1) = SVAL(1)
      Y2(NN + 1) = SVAL(1)
      YG(NN + 1) = SVAL(1)
      XX(NN + 2) = SVAL(2)
      Y1(NN + 2) = SVAL(4)
      Y2(NN + 2) = SVAL(5)
      YG(NN + 2) = SVAL(6)
      MM = J/2
```

```
      MI = MM * 2
      IF(MI - J) 35,30,35
   30 II = 8 - J
      GO TO 40
   35 II = J
   40 CALL LINE(XX,Y2,NN,1,+1,II)
C---_ESTABLISHES PLOT FROM ORIGIN OF K1 PLOT, DRAWS CURVE FOR RADIUS TH
      CALL PLOT(0.,5.,-3)
      CALL LINE(XX,Y1,NN,1,+1,II)
C----ESTABLISHES PLOT FROM ORIGIN OF G GRAPH, DRAWS CURVE FOR RADIUS TH
      CALL PLOT(8.,-4.,-3)
      XX(NN + 2) = SVAL(3)
      CALL LINE(XX,YG,NN,1,+1,II)
      XX(NN + 2) = SVAL(2)
C----DRAWS SYMBOL AND WRITES ANGLE THETA FOR LEGEND--------------------
      YL = 7.05 - .25 * J
      YN = YL + 0.07
      CALL DRAW(.82,YN,0.,ISYM(II),0.,1.,.35)
      CALL NUMBER(1.12,YL,.14,THETA,0.,-1)
C----REESTABLISHES THE PLOT FROM THE ORIGINAL ORIGIN-------------------
      CALL PLOT(-8.,-1.,-3)
C----MOVES PEN INTO POSITION FOR NEW PROBLEM PLOTTING------------------
      IF(J - 7) 100,50,50
   50 CALL PLOT(15.5,9.5,-3)
      IF(MAXIK - I) 55,55,100
   55 CALL FINAL
  100 RETURN
      END
```

APPENDIX IX

FORTRAN IV LISTING: SAPLOT - COMPUTER PROGRAM FOR PLOTTING FINITE ELEMENT GRID

```
C      SAPLOT MODIFIED 4/24/78 BY ALAN F. BUTTON TO PROCESS STATIC LOADS
C      ONLY, UP TO 1500 NODES OF ELEMENTS INCLUDING 8-21 VARIABLE NODE
C      3/D TYPE IN REVISED SAP IV. DEFORMED STRUCTURES ARE SCALED TO FIT
C      EITHER 8.5X11.0 OR 11.0X14.0 PAPER.
C
       COMMON SINA,COSA,SINB,COSB
       COMMON NPAR(14),NUMNP
       COMMON NP(1000),X(1000),Y(1000),Z(1000)
       COMMON IG(1000,5)
       COMMON XMIN,XMAX,YMIN,YMAX,PSF,LL,NF,IAXIS,IDR,IPRT
       COMMON HED(13),PLTHED(20),HEDIPL(20),DHED(20),NHED,IHED
       DIMENSION NBLK(2)
       INTEGER*2 IG,IDUM
C
C      READ MASTER CONTROL CARD (2F10.0,4I5)
C
C         CC     1-10  ALPHA   VERTICAL INCLINATION (DEG)
C               11-20  BETA    ROTATION ABOUT VERTICAL AXIS (DEG)
C               21-25  IAXIS   VERTICAL AXIS
C                              =1  X AXIS
C                              =2  Y AXIS
C                              =3  Z AXIS
C               26-30  IDR     FLAG FOR DRAWING FOR THESIS PAPER SIZE
C                              =0  NO, 11 X 14
C                              =1  YES, 8.5 X 11
C               31-35  IDEF    FLAG FOR DEFORMED SHAPE OR MODE SHAPE
C                              =0  NO
C                              =1  YES
C               36-40  IPRT    FLAG FOR PRINT DETAIL
C                              =0  NORMAL PRINT
C                              =1  EXTRA PRINT
C               40-45  NMODE   NUMBER OF MODES TO BE READ FROM FILE 7
C               51-52
C                THRU          MODE NUMBERS, MODE(I),I=1,NMODE
C               69-70
C
     5 CALL ITLZ
       CALL DPT (1,4)
       READ(5,1000)ALPHA,BETA,IAXIS,IDR,IDEF,IPRT,NMODE
C
C      READ SAP TITLE CARD AND CONTROL CARD
C
       IPL = 2
       REWIND 1
       READ(5,1030) PLTHED
       READ(5,1040) HED
     7 READ(IPL,1030)HEDIPL
  1030 FORMAT(20A4)
  1040 FORMAT(13A4)
       IF(ICOMP(HED,1,HEDIPL,1,52)) 7,8,7
     8 READ(IPL,1010) NUMNP,NELTYP,LL,NF,NDYN,MODEX,NAD,XEQB,N10SV
  1010 FORMAT(9I5)
       WRITE(6,2000)HEDIPL,NUMNP,NELTYP,LL,NF,NDYN,MODEX,NAD,XEQB,N10SV
       WRITE (6,2010)     IAXIS ,ALPHA,BETA,IDR,IDEF,IPRT,NMODE
```

```
C
C     CHECK THE NUMBER OF CHARACTERS IN THE TITLE
C
      CALL INIT(NBLK,1,8,64)
      NHED=52
      IHED = 80
      DO 17 I = 1,20
      IF(ICOMP(PLTHED(I),1,NBLK,1,8)) 16,15,16
   15 IHED = (I - 1) * 4
      GO TO 17
   16 CONTINUE
   17 CONTINUE
      WRITE (6,2080) IHED
      ALPHA=ALPHA/57.29578
      BETA=BETA/57.29578
      SINA=SIN(ALPHA)
      SINB=SIN(BETA)
      COSA=COS(ALPHA)
      COSB=COS(BETA)
      IF (NUMNP-1000) 20,20,18
   18 WRITE (6,1020) NUMNP
      STOP
C
C     USE INPUTJ FROM SAP 4 TO READ NODAL CARDS
C
   20 CALL INPUTJ(NP,X,Y,Z,NUMNP,NEQ)
C
C     ZERO OUT THE NODAL CONNECTIVITY MATRIX
C
      DO 10 I = 1,NUMNP
      DO 10 J = 1,5
   10 IG(I,J)=0.
C
C     CONVERT X,Y,Z TO X',Y' SYSTEM
C
      DO 200 N=1,NUMNP
      IF(IAXIS-2) 100,120,140
C
C     X AXIS VERTICAL
C
  100 X1=XP(Y(N),Z(N))
      Y1=YP(Y(N),Z(N),X(N))
      X(N)=X1
      Y(N)=Y1
      GO TO 200
C
C     Y AXIS VERTICAL
C
  120 X1=XP(Z(N),X(N))
      Y1=YP(Z(N),X(N),Y(N))
      X(N)=X1
      Y(N)=Y1
      GO TO 200
C
C     Z AXIS VERTICAL
C
```

```
  140 X1=XP(X(N),Y(N))
      Y1=YP(X(N),Y(N),Z(N))
      X(N)=X1
      Y(N)=Y1
  200 CONTINUE
      IF(IPRT) 201,201,199
  199 WRITE(6,2050)(N,X(N),Y(N),N=1,NUMNP)
C
C     SCALE THE ARRAYS
C
  201 CALL MINMAX(X,Y,NUMNP,DELP,XMIN,YMIN,IDR,XMAX,YMAX,XC,YC)
C
      CALL PLOT (0.,-11.,-2)
      CALL PLOT (1.5,1.,-3)
      IF (IDR) 205,205,202
  202 CONTINUE
C
C     DRAW THE BOUNDARY FOR THE THESIS PAPER
C
      CALL PLOT (0.,0.,3)
      CALL PLOT (6.,0.,2)
      CALL PLOT (6.,9.,2)
      CALL PLOT (0.,9.,2)
      CALL PLOT (0.,0.,2)
      XA = 6.2
      XB = 6.45
      YA = 0.0
      YB = 1.32
      XSP = 8.0
      ANGL = 90.0
      GO TO 206
  205 XA = 0.0
      XB = 1.32
      YA = -0.2
      YB = -0.45
      XSP = 13.5
      ANGL = 0.0
  206 PSF = 1.0/DELP
      WRITE (6,2040) XMAX,XMIN,YMAX,YMIN,DELP,PSF
      DO 210 N=1,NUMNP
      X(N)=((X(N)-XMIN)*PSF)+ XC
      Y(N)=((Y(N)-YMIN)*PSF)+ YC
  210 CONTINUE
      IF(IPRT) 213,213,211
  211 WRITE (6,2020)
      WRITE (6,2030) (N,X(N),Y(N),N=1,NUMNP)
  213 CONTINUE
C
C     WRITE THE PLOT TITLE AND RESET THE ORIGIN
C
      CALL SYMBOL (XA,YA,0.14,PLTHED,ANGL,IHED)
      CALL SYMBOL (XB,YB,0.14,HED,ANGL,NHED)
      CALL PLOT(0.,0.,-3)
C
C     DRAW THE AXES
C
```

```
C
C     READ THE ELEMENT CARDS
C
  300 DO 310 I=1,NELTYP
      READ (IPL,1020) NPAR
      MTYPE=NPAR(1)
      CALL ELTYPE(MTYPE)
  310 CONTINUE
C
C     ORDER & PRINT THE CONNECTIVITY MATRIX
C
      CALL PRNTIG
C
C     PLOT THE STRUCTURE
C
      CALL STPLOT
      CALL PLOT (XSP,10.,-3)
      IF (IDEF) 315,330,315
  315 CONTINUE
C
C     PUT THE X' AND Y' COORDINATES ON FILE 1
C
      WRITE (1) (X(I),Y(I),I=1,NUMNP)
      ENDFILE 1
C     IF (NMODE .GT. 0) GO TO 326
C     IF (NDYN .GT. 0) GO TO 320
C
C     PLOT THE DEFORMED SHAPE DUE TO STATIC LOADS
C
      CALL DEFPLT(1)
C
C     PLOT THE MODE SHAPES
C
C 320 CALL DEFPLT(2)
C     GO TO 330
C
C     PLOT THE MODE SHAPES USING FILE 7
C
C 326 REWIND 2
C     READ (2) NEQ,NBLOCK,NEQB,MBAND,N1,NF1
C     IF (PRT) WRITE (6,2070) NEQ,NBLOCK,NEQB,MBAND,NF1
C     N1=1
C     N2=N1+6*NUMNP
C     N3=N2+(NEQB*NF1)*2
C     N4=N3+6*NF1
C     IF (MTOT .GE. N4) GO TO 328
C     WRITE (6,2060) N4,MTOT
C     STOP
C 328 CALL FILSHP(A(N1),A(N2),NEQB,NUMNP,NF1,NBLOCK,NEQ,IPRT,MODE,NMODE
C    1             A(N3))
  330 CALL FINAL
      GO TO 5
 1000 FORMAT (2F10.0,5I5,5X,10I2)
 1020 FORMAT (14I5)
 2000 FORMAT ('1SAP 3-D PLOT PACKAGE',///,1X,20A4,///,
     1  38H C O N T R O L   I N F O R M A T I O N, // 4X,
```

```
     2  27H NUMBER OF NODAL POINTS   =, I5 / 4X,
     3  27H NUMBER OF ELEMENT TYPES  =, I5 / 4X,
     4  27H NUMBER OF LOAD CASES     =, I5 / 4X,
     5  27H NUMBER OF FREQUENCIES    =, I5 / 4X,
     6  27H ANALYSIS CODE (NDYN)     =, I5 / 4X,
     7  16H    EQ.0,  STATIC,                / 4X,
     8  26H    EQ.1,  MODAL EXTRACTION,      / 4X,
     9  25H    EQ.2,  FORCED RESPONSE,       / 4X,
     A  27H    EQ.3,  RESPONSE SPECTRUM,     / 4X,
     *  28H    EQ.4,  DIRECT INTEGRATION,    / 4X,
     B  27H SOLUTION MODE (MODEX)    =, I5 / 4X,
     C  19H    EQ.0,  EXECUTION,             / 4X,
     D  20H    EQ.1,  DATA CHECK,            / 4X,
     E  19H NUMBER OF SUBSPACE,              / 4X,
     F  27H ITERATION VECTORS (NAD)  =, I5 / 4X,
     G  27H EQUATIONS PER BLOCK      =, I5 / 4X,
     H  27H TAPE10 SAVE FLAG (N10SV) =, I5 / 4X<
 2010 FORMAT (///,' PLOT INFORMATION:',//,5X,
     1        'VERTICAL AXIS = ',I1,/,5X,
     2        'ANGLE OF INCLINATION OF VERTICAL AXIS (DEG)=',F7.3,/,5X,
     3        'ROTATION ABOUT VERTICAL AXIS (DEG)         =',F7.3,/,5X,
     4        'FLAG FOR DRAWING OF THE COORDINATE AXES    =',I3,/,5X,
     5        'FLAG FOR DEFORMED SHAPE PLOT               =',I3,/,5X,
     6        'PRINT FLAG                                 =',I3,/,5X,
     7        'NUMBER OF MODES READ FROM FILE 7           =',I3)
 2020 FORMAT ('1X-Y VALUES FOR PLOT OF UNDEFORMED STRUCTURE',/,
     1        '  NODE',10X,'X',14X,'Y')
 2030 FORMAT ((I5,2F15.4))
 2040 FORMAT ('1XMAX=',F12.5,/,
     1        ' XMIN=',F12.5,/,
     2        ' YMAX=',F12.5,/,
     3        ' YMIN=',F12.5,/,
     4        ' DELP=',F12.5,/,
     7        ' PSF =',F12.5)
 2050 FORMAT ('1X-Y LOCATIONS OF NODES BEFORE SCALING:',/,
     1        '  NODE',10X,'X',14X,'Y',/,(I5,2F15.4))
C2060 FORMAT ('0REQUIRED STORAGE=',I10,/,
C    1        ' AVAILABLE STORAGE=',I10)
C2070 FORMAT ('0INFORMATION AS READ FROM FILE 2:',///,
C    1        ' NEQ   =',I5,/,
C    2        ' NBLOCK=',I5,/,
C    3        ' NEQB  =',I5,/,
C    4        ' MBAND =',I5,/,
C    5        ' NF    =',I5)
 2080 FORMAT ('     NUMBER OF CHARACTERS IN THE TITLE          =',I3)
      STOP
      END
      SUBROUTINE ELTYPE (MTYPE)
      COMMON SINCOS(4)
      COMMON NPAR(14)
      DIMENSION           LC(4),ILC(4)
      DIMENSION IX(7),IY(7),EL(4),IE(5),NP(21),INP(21),IS(2),ISP(2),
     1          MLD(4),KLD(4),MULT(4)
      IPL = 2
      IK = 0
      GO TO (100,200,300,300,500,600,700,800,1900,1900,1900,1200),MTYPE
```

```
C
C     TRUSS ELEMENT (FROM RUSS IN SAP IV)
C
  100 WRITE (6,2000)
      STOP
C
C     BEAM ELEMENT (FROM TEAM IN SAP IV)
C
  200 WRITE (6,2020)
      STOP
C
C     PLANE STRESS MEMBRANE & 2-D ELEMENT (FROM PLNAX IN SAP IV)
C
  300 WRITE (6,2090)
      NUME=NPAR(2)
      NUMMAT=NPAR(3)
      DO 320 M=1,NUMMAT
      READ (IPL,1010) N,NT
      DO 310 I=1,NT
      READ (IPL,1000) CRD
      READ (IPL,1000) CRD
  310 CONTINUE
  320 CONTINUE
      DO 330 I=1,4
  330 READ (IPL,1000) CRD
      N=0
  340 READ (IPL,1050) M,(IE(I),I=1,5),REFT,PRESS,NS,KG,THICK
      MAT=IE(5)
      IF (KG) 342,341,342
  341 KG = 1
  342 IF (NPAR(5) - 1) 344,343,344
  343 THICK = 1.0
  344 IF (NS) 346,345,346
  345 NS = 4
  346 IF (NS - 4) 347,348,348
  347 NS = 1
  348 IF (IE(3) - IE(4)) 350,349,350
  349 IF (NS - 20) 350,351,350
  351 NS = 16
  350 N=N+1
      IF(IK) 352,352,370
  352 MN = M - N
      IF(N - 1) 356,353,356
  353 IF(MN) 356,356,354
  354 IK = 1
      MN = 0
      GO TO 370
  356 IF(MN) 355,370,355
  355 CONTINUE
      DO 360 I=1,4
  360 IX(I)=IX(I)+KG
      GO TO 390
  370 DO 380 I=1,4
  380 IX(I)=IE(I)
  390 WRITE(6,2100) M,(IX(I),I = 1,4),MAT,REFT,PRESS,NS,KG,THICK
      CALL SETIG(IX(2),IX(3))
```

```
      CALL SETIG(IX(1),IX(2))
      CALL SETIG(IX(1),IX(4))
      IF (IX(3) - IX(4)) 395,400,395
  395 CONTINUE
      CALL SETIG(IX(3),IX(4))
  400 IF (N - NUME) 405,450,405
  405 IF(MN) 350,340,350
  450 CONTINUE
      RETURN
C
C     8 NODE BRICK (FROM BRICK8 IN SAP IV)
C
  500 WRITE (6,2110)
      NUME=NPAR(2)
      NCRD=6+NPAR(3)+NPAR(4)
      DO 510 I=1,NCRD
  510 READ (IPL,1000) CRD
      NEL=0
  520 READ (IPL,1060) INEL,(INP(I),I=1,8),ININT,IMAT,IINC,MLD,ISP,TTEMP
      DO 522 I=1,4
  522 MULT(I)=0.
      IF (IINC) 524,523,524
  523 IINC=1
  524 IF (IMAT) 530,525,530
  525 IMAT=1
  530 NEL=NEL+1
      ML=INEL-NEL
      IF (ML) 535,540,560
  535 WRITE (6,2120) INEL
      STOP
  540 DO 542 I=1,8
  542 NP(I)=INP(I)
      NINT=ININT
      MAT=IMAT
      INC=IINC
      REFT=TTEMP
      IS(1)=ISP(1)
      IS(2)=ISP(2)
      SKIP=99999.
      IF (NINT) 545,546,550
  545 NINT=IABS(NINT)
      SKIP=1.
      GO TO 550
  546 SKIP=0.
  550 CONTINUE
      DO 555 I=1,4
      KLD(I)=IABS(MLD(I))
      IF (MLD(I)) 552,552,555
  552 MULT(I)=0
  555 CONTINUE
      GO TO 570
  560 DO 562 I=1,8
  562 NP(I)=NP(I)+INC
      DO 564 I=1,4
  564 KLD(I)=KLD(I)*MULT(I)
  570 WRITE (6,2130) NEL,(NP(I),I=1,8),NINT,MAT     ,KLD,REFT,IS
```

```
      CALL SETIG(NP(1),NP(2))
      CALL SETIG(NP(1),NP(4))
      CALL SETIG(NP(1),NP(5))
      CALL SETIG(NP(2),NP(3))
      CALL SETIG(NP(2),NP(6))
      CALL SETIG(NP(3),NP(4))
      CALL SETIG(NP(3),NP(7))
      CALL SETIG(NP(4),NP(8))
      CALL SETIG(NP(5),NP(6))
      CALL SETIG(NP(5),NP(8))
      CALL SETIG(NP(6),NP(7))
      CALL SETIG(NP(7),NP(8))
      IF (NUME-NEL) 535,580,590
  580 RETURN
  590 IF (ML) 520,520,530
C
C     PLATE/SHELL ELEMENT (FROM TPLATE IN SAP IV)
C
  600 WRITE (6,2060)
      STOP
C
C     BOUNDARY ELEMENT (FROM CLAMP IN SAP IV)
C
  700 WRITE (6,2140)
      NUME=NPAR(2)
      READ (IPL,1000) CRD
      NE=0
  710 KG=0
      MARK=0
  720 READ (IPL,1070)NP1,NI,NJ,NK,NL,KD,KR,KN,SD,SR,TRACE
      IF (TRACE .EQ. 0.) TRACE=1.0E+10
      IF (KG) 725,725,730
  725 KG=KN
      NN=NP1
      NNI=NI
      NNJ=NJ
      NNK=NK
      NNL=NL
      NKD=KD
      NKR=KR
      SSD=SD
      SSR=SR
      TTR=TRACE
      GO TO 750
  730 MARK=1
  740 NN=NN+KG
      NNI=NNI+KG
  750 KEL=NE+1
      WRITE (6,2150) KEL,NN,NNI,NNJ,NNK,NNL,NKD,NKR,KN,SSD,SSR,TTR
      CALL SETIG(NNI,NNJ)
      NE=NE+1
      IF (NE - NUME) 755,780,755
  755 IF (NN - NP1) 740,760,760
  760 IF (MARK - 1) 720,710,720
  780 CONTINUE
      RETURN
```